# Enhancement of Functionality of Structures Using Isolation and Semi-Active Control in Consideration of Performance of Furniture and Appliances

September 2013

Yundong SHI

# TABLE OF CONTENTS

# CHAPTER 1

# Introduction

## 1.1 Background

The most current earthquake standards lead to the design of structural elements so that they can resist earthquake loads without collapse. This approach, however, does not regard the performance of non-structural elements and building contents. Even if the structure is undamaged, damage to the non-structural elements and contents may temporarily affect the functionality of structures. For critical structures such as hospitals, immediate functionality of the structure is of utmost importance. The cost associated with the loss of functionality due to damage to contents can be considerable.

Various techniques have been proposed to improve the performance and enhance the functionality of structures. Among them, base isolation is one of the most successful and widely-applied techniques. Base isolation can protect both the structure and non-structural elements and contents so as to maintain the functionality of the structure during and immediately after the earthquake. A few base isolation responses during earthquakes have been recorded, indicating the advantage of the base-isolated structures [1.1, 1.2] over fixed-base structures. Ref [1.1] shows an investigation into the performance of few hospitals after the January 17, 1994 Northridge earthquake. The USC Hospital investigated was an isolated steel frame building. The building remained operational throughout the 1994 Northridge Earthquake. There was no damage to the USC Hospital. In contrast, the Los Angeles County Medical Center located less than a mile away suffered serious damage and was not operational after the earthquake.

Base isolation has become very popular around the world, particularly in Japan. The number of isolated buildings in Japan increased rapidly after the 1995 Kobe earthquake. The construction number per year before 1995 remained less than 10, while it increased drastically to more than 150 afterward. At present, there are over 2,500 base-isolated buildings in Japan [1.3], and the applications are extensively applied to hospitals and medical facilities, because these facilities are the first ones that need to function right after a damaging earthquake event.

Floor isolation is a cost effective alternative to base isolation [1.4] to enhance the functionality. It is installed in a single floor or room in the fixed-base structure to protect a group of appliances placed on the isolation. It provides a more flexible solution to isolate appliances in some cases,

including for retrofit.

Although the isolation technology has been used for many years [1.5, 1.6], several aspects are worth investigating. First, the actual performance has not been fully understood in large earthquakes, especially under some types of ground motion, such as long-period ground motions. Long-period ground motion is considered to be a threat to the isolated systems [1.7, 1.8]. Because the natural period of the isolated system is designed to be long in the horizontal directions to decouple the system from the ground, the long-period motion has the potential to resonate with the isolated system and cause a large response.

Majority of the current research on isolation technology has focused on the structural response. However, the behavior of the non-structural element and contents in the isolated system is not explored extensively. The functionality of a structure is not only related to the structural behavior, but more directly related to the behavior of non-structural element and contents in the structure, especially in today's performance based design. A few studies are available for the performance of free standing appliance or that anchored to the structure [1.4]. However, little information about the behavior of the appliances with mobile conditions, such as casters, in an isolated system is available. Such kinds of mobile appliances are widely used in a hospital to promote its mobility in the daily use. Research efforts including the experimental work are needed in this field.

The primary target of the isolated system is to reduce the acceleration in an earthquake event [1.9]. However, it is also necessary to limit the displacement, especially under long-period motions. Large displacement will necessitate large clearance for the isolated system and increase the cost of the structure. This requirement is more critical for floor isolation because of the smaller space available.

Adding damping to the system by employing passive dampers is an effective way to reduce the displacement under long-period motion, but at the expense of increasing the acceleration response of the structure, which is against the objective of designing isolated system. To design an isolated system which can effectively reduce the acceleration to protect the appliances in it, and also limit the displacement to save usable space, is another subject worth investigating.

Applying semi-active control technology to the isolated system has the potential to reduce both the acceleration and displacement responses of the isolated system [1.10, 1.11]. Semi-active control is proved quite promising in controlling the structural response [1.10]. However, due to the complexity of the control system, it is yet not widely accepted in the engineering field. Effectiveness of semi-active control with isolated system will depends not only on the hardware (e.g., damper device), but also on software (e.g., control algorithm). Regarding the application of control to the isolated system, several challenging tasks exist, including the modeling of control device, algorithm design, and force tracking system, among others.

As ground motion has high variability, the isolated system may be subjected to motions with different frequency components. Motions with high frequencies tend to cause large acceleration of the isolated system because of the high amplitude, while motions with low frequencies tend to cause large displacement because of resonance. The control algorithm should consider the variability of motion and guarantee the efficiencies under different types of motions, i.e., short-period and

long-period motions. A control strategy that has the ability to adapt to the change in motion type had better be established. Relevant studies in the control field with base/floor isolation need further investigation before being accepted for practical application.

## 1.2 Objective

The objective of this dissertation is to examine the functionality of base/floor isolated systems under large earthquakes, particularly those with long-period. A full scale shaking table test was conducted on a base-isolated hospital building, in which hundreds of non-structural elements and contents including furniture and medical appliance with different fixing conditions, were installed. The performance of both the structure and the contents were observed and evaluated based on the test results to obtain insight into the performance of functionality of the base-isolated building in large earthquakes.

A floor isolation system with semi-active control was designed and studied to find the solution toward improving the performance of isolated system and furniture placed on the system under both short and long-period motions. The study aims at controlling both the acceleration and displacement of the floor isolation system. A series of shaking table test was conducted to validate the designed system.

To summarize, the following issues are the focus of this dissertation:

(1) Examining the structural response of base-isolated building against large earthquakes;

(2) Examining the behavior of associated medical appliances, particularly those with mobile conditions under long-period ground motions;

(3) Developing a semi-active controlled floor isolation system to provide protection for a group of appliances; and

(4) Developing control algorithms that can handle different types of earthquakes, i.e., short-period and long-period motions, so as to improve the functionality of the floor isolation system.

In addition, a motion capture technique was developed for measuring large displacement motions and estimate velocity responses of sliding appliances in the shaking table test.

## 1.3 Organization

This dissertation consists of eight chapters. Chapter 1 is the background of this study, and Chapter 8 is the summary and conclusions. Chapters 2 to 7 constitute the main part of the dissertation. The respective focuses of those chapters are: (1) a literature review of the study focusing on the enhancement of functionality and operability of structures; (2) development of motion capture technique to trace the appliance behavior in the shaking table test; (3) the E-Defense full scale shaking table test on base-isolated and fixed-base hospital conducted to study the behavior of structure and non-structural elements as well as the contents inside of the room; (4) development of

control strategies for a semi-active controlled floor isolation system; and (5) shaking table test to evaluate the performance of the floor isolation system to protect the equipment. The contents of the six chapters are summarized as follows.

In Chapter 2, functionality of the structure is defined first. Technologies developed to enhance the functionality of structures are reviewed for base isolation, floor isolation, and structural control. Their principles and the advantages and disadvantages of each technology together with associated applications are summarized. Reviewed also in this chapter are the control algorithms working with semi-active control technology as well as dynamic and inverse dynamic models for semi-active control devices. The review covers theory, simulation, and experiment.

In Chapter 3, a motion capture technique is described for the measurement of the appliance's movement in shaking table test. The basic issues, such as the influence of the angles between cameras, number of cameras needed, and accuracy of measured displacements and estimated velocities are examined through a series of shaking table test. The influence of camera vibration to the measuring accuracy is also discussed. An easy yet effective and fast method is developed to correct the errors caused by camera vibration.

In Chapter 4, the full scale shaking table test of the hospital structure is introduced, including the design of the specimen, base isolator and damping system, and placement of medical appliance. The test is conducted using different types of ground motions including short-period and long-period motions. The test results are examined in terms of the horizontal responses of the structure and appliance with the aid of hundreds of sensors attached to the specimen and the motion capture technique described in Chapter 3.

In Chapter 5, a semi-active controlled floor isolation system is designed to protect a group of sensitive and valuable appliances in a building. The designed floor isolation system utilizes a magnetorheological fluid damper (MR damper) that is controllable by varying the input current. Dynamic loading test is carried out to examine the dynamic property of the MR damper. A Bouc-Wen model is adopted to describe the MR damper behavior for the simulation in developing the control algorithm introduced in the next chapter. A PI controller is also developed to track the force calculated from the control algorithm as close as possible.

In Chapter 6, different control strategies are formulated including passive control and semi-active control. The control algorithms adopted for the semi-active control are LQR control, $H_\infty$ control, and LQR control with frequency-dependent scheduled gain (LQRSG). The LQRSG is developed based on the LQR control but the control gain is adapted according to the frequency characteristics of the input motion. To develop this program, simulation work is carried out with the Bouc-Wen model developed in Chapter 5. A window method is designed to detect the dominant frequency of the input excitation in real time, without knowing any information of the excitation *a priori*. The $H_\infty$ control is also adopted and a new shaping filter is designed to consider the influence of input motion in the frequency domain. The test program of each control strategy is described.

In Chapter 7, a series of shaking table tests are performed to validate the performance of the proposed floor isolation system for different control strategies. Different types of motion including short and long-period motions, ground motion, and recorded floor motions are adopted. Both the

responses of the floor isolation and the appliances on the floor isolation are examined. Comparison between the semi-active controlled floor isolation system and the passive controlled system as well as the comparison between different control algorithms including LQR control, $H_\infty$ control and the newly developed LQRSG control are presented.

# REFERENCES


[1.1] Schiff AJ. Northridge earthquake: lifeline performance and post-earthquake response. *Amer Society of Civil Engineers*. 1995.

[1.2] Higashino M., and Okamoto S., Response Control and Seismic Isolation of Buildings. Taylor & Francis, 2006.

[1.3] Tanaka Y., Fukuwa N., Tobita, J., and Mori M., Present Situation of Isolation Building in Japan Base on Establishing a Database on Technical Evaluation Sheet. *The 13th Japan Earthquake Engineering Symposium, Japan Association for Earthquake Engineering* 2010, 569-576 (Japanese).

[1.4] Lambrou V, Constantinou MC. Study of seismic isolated systems for computer floors. Rep. No. NCEER-94-0020, State University of New York at Buffalo, Buffalo, N.Y., 1994.

[1.5] Becker TC, Furukawa S, Mahin SA, Nakashima M. Comparison of US and Japanese Codes and Practices for Seismically Isolated Buildings. *Structures Congress, Structural Engineering Institute of ASCE*, 2010.

[1.6] Otani S. and Kani N., Japanese state of practice in design of seismically isolated buildings. 4th US-Japan workshop on performance-based earthquake engineering methodology for reinforced concrete building structures. Toba, Japan 2002.

[1.7] Heaton TH, Hall JF, Wald DJ, Halling MW. Response of high-rise and base-isolated buildings to a hypothetical Mw 7.0 blind thrust earthquake. *Science* 1995; 267: 206–211.

[1.8] Structural Response and Performance for Long-period Seismic Ground Motions. AIJ, 2007 (Japanese).

[1.9] Kelly JM. The role of damping seismic isolation. *Earthquake Engineering and Structural Dynamics* 1999; 28:3-20.

[1.10] Housner GW, Bergman LA, Caughey TK, Chassiakos AG, Claus RO, Masri SF, Skelton RE, Soong TT, Spencer BF and Yao TP. Structural control: past, present and future. *Journal of Engineering Mechanics* 1997; 123(9):897:971.

[1.11] Spencer BF, Nagarajaiah S. State of the art of structural control. *Journal of Structural Engineering* 2003; 129:845-856.

# LIST OF PUBLICATIONS

## *Referred journal papers:*

[1] Furukawa S, Sato E, **Shi Y**, Becker TC, Nakashima M. Full-scale shaking table test of a base-isolated medical facility subjected to vertical motions. Earthquake Engineering and Structural Dynamics. Available on line.

[2] **Shi Y**, Becker TC, Kurata M, Nakashima M. $H_\infty$ control in the frequency domain for a semi-active floor isolation system. Frontiers of Structural and Civil Engineering. (Accepted for publication)

[3] **Shi Y**, Becker TC, Furukawa S, Sato E, Nakashima M. LQR control with frequency-dependent scheduled gain for a semi-active floor isolation system. Earthquake Engineering and Structural Dynamics. (Accepted for publication)

[4] **Shi Y**, Kurata M, Nakashima M. Disorder and damage of base-isolated medical facilities when subjected to large ground motions. Engineering Structures. (under review)

## *Referred conference papers:*

[5] **Shi Y**, Sato E, Hoki K, Nakashima M. Test on hybrid floor isolation system with semi-active control. 9th International Conference on Urban Earthquake Engineering/4th Asia Conference on Earthquake Engineering, March 2012; 1459-1464.

[6] **Shi Y**, Sato E, Enokida R, Nakashima M. Development of hybrid floor isolation system with semi-active control. Proceeding of 15th World Conference on Earthquake Engineering, September 2012, ID: 2786.

[7] Furukawa S, Sato E, **Shi Y**, Nakashima M. Structural and appliance performance of base-isolated medical facility subjected to strong vertical ground motions. Proceeding of 15th World Conference on Earthquake Engineering September 2012, ID: 1664.

[8] **Shi Y**, Tracy BC, Masahiro K, Nakashima M. Design of A PI controller for MR dampers using damper force feedback. Proceedings of the First International Symposium on Earthquake Engineering, November 2012, ID: 38, pp. 311-316.

## *Domestic conference papers:*

[1] **Shi Y**, Enokida R, Nagae T , Kajiwara K, Yamazaki T, Nakashima M. Proposal of shaking table test technique to enhance the reproducible frequency ranges of tables : Part2. Experimental validation of the shaking table test technique. Proceeding of the Annual Meeting Kinki Branch 2010; ID: 2019, pp. 73-76. [in Japanese]

[2] Enokida R, Kajiwara K, Nagae Takuya, **Shi Y**, Yamazaki T, Nakashima M. Proposal of shaking table test technique to enhance the reproducible frequency ranges of tables: Part1: proposal of pounding shaking table test technique. Proceeding of the Annual Meeting Kinki Branch 2010; ID: 2018, pp. 69-72. [in Japanese]

[3] Furukawa S, Sato E, **Shi Y**, Nakashima M. Examination into Functionality of Base-Isolated

Buildings under Vertical Ground Motion. Proceeding of the Annual Meeting Kinki Branch 2010; ID: 2014, pp. 53-56.

[4] **Shi Y**, Enokida R, Kajiawara K, Nagae T, Yamazaki T, Nakashima M. Proposal on shaking table test technique to promote high frequency response : Part3. Comparisons with simulation and experimental results. Summaries of technical papers of Annual Meeting Architectural Institute of Japan. B-2, 2010; ID: 21024, pp. 47-48. [in Japanese]

[5] Yamazaki T, Enokida R, Nagae T, **Shi Y**, Kajiwara K, Nakashima M. Proposal on shaking table test technique to promote high frequency response: Part2. Experimental validation. Summaries of technical papers of Annual Meeting Architectural Institute of Japan. B-2, 2010; ID: 21023, pp. 45-46. [in Japanese]

[6] Enokida R, Kajiwara K, Nagae T, **Shi Y**, Yamazaki T, Nakashima M. Proposal on shaking table test technique to promote high frequency response : Part1. Concept of pounding shaking table test technique. Summaries of technical papers of Annual Meeting Architectural Institute of Japan. B-2, 2010; ID: 21022, pp. 43-44. [in Japanese]

[7] **Shi Y**, Sato E, Furukawa S, Nakashima M, Application of motion capture technique for measurement of furniture behavior in shaking table tests. Proceeding of the Annual Meeting Kinki Branch 2011; ID: 2025. pp. 97-100.

[8] Furukawa S, **Shi Y**, Sato E, Nakashima M. Vertical Dynamic Response Characteristics of Base-isolated Building: Result of Full-scaled Shaking Table Test. Proceeding of the Annual Meeting Kinki Branch 2011; ID: 2024. pp. 93-96.

[9] **Shi Y**, Sato E, Furukawa S, Nakashima M, Application of motion capture technique for measurement of furniture behavior in shaking table tests, Summaries of technical papers of Annual Meeting Architectural Institute of Japan. B-2, 2011. ID: 21211, pp. 421-422.

[10] Furukawa S, Sato E, Sakai H, **Shi Y**, Fukuyama K, Inoue T, Nakashima M. Research project on assessment of functionality in medical and telecommunication facilities. Part 23: Vertical dynamic response characteristics of base-isolated system against vertical ground motions. Summaries of technical papers of Annual Meeting Architectural Institute of Japan. B-2, 2011; ID:21215, pp. 429-430. [in Japanese]

[11] **Shi Y**, Sat E, Hoki K, Kurata M, Nakashima M. Semi-active control of floor isolation systems for furniture protection. Proceeding of the Annual Meeting Kinki Branch 2012.

[12] **Shi Y**, Sat E, Hoki K, Kurata M, Nakashima M. Development of semi-active controlled floor isolation system for appliance protection. Summaries of technical papers of Annual Meeting Architectural Institute of Japan. B-2, 2012; ID: 21268, pp. 535-536.

## *Referred journal papers at graduate course:*

[1] **Shi Y**, Chen Y. Experimental study on connection of beam to side column in steel gabled frames. *Building structure* 2012; 11:114-118.

# CHAPTER 2

# Review of previous research

## 2.1 Introduction

### 2.1.1 Background

In recent years the earthquake engineering community pays much attention on performance-based design. In this context, a number of innovative control technologies have been developed to achieve enhanced functionality and operability. Those technologies include passive control, active control, hybrid control and semi-active control [2.1].

Base isolation system is a type of passive control and has been successfully applied in practical application for many years around the world, particularly in Japan. It is designed not only to maintain the safety of the structure but also to improve the performance of nonstructural elements and contents in the structure. Floor isolation, as an alternative to base isolation, is adopted to isolate a group of important and valuable equipment.

Various efforts have been undertaken in the last three decades on active control and semi-active control [2.1, 2.2]. Many types of control devices have been developed, and a number of the devices have been applied to practical applications, mainly in Japan. In conjunction with those active and semi-active control devices, various control algorithms have been developed. The combination of passive control and active/semi-active control (the combined system is termed as hybrid system) is also investigated to adapt to changing demands for the sake of structural response reduction.

Behavior of the contents (e.g., equipment) in the building is of a great concern in the context of performance design. Their behavior will directly influence functionality of the structure, especially for some critical structures such as a hospital [2.3]. Structural control technologies to improve the contents behavior are needed through analytical and experimental work.

### 2.1.2 Organization

This chapter summarizes various technologies developed to improve the functionality of critical structures. Section 2 introduces the concept of functionality and summarizes four different types of systems to enhance the functionality. Researches on two types of isolation systems, i.e., base isolation and floor isolation, are reviewed in Sections 2.3 and 2.4. Section 2.5 reviews the implementation of

control design for semi-active control with MR dampers, including the MR damper modeling, control algorithms, and force tracking design.

## 2.2 Functionality of structure

### 2.2.1 Functionality

Functionality of a structure is the ability of the structure to perform its intended use. For example, the functionality of a hospital is the hospital's ability to provide medical service to the public. For critical structures such as the hospital facility or computer center, immediate functionality of the structure is of upmost importance. The cost of losing functionality after an earthquake is known to be considerable.

In recent years the earthquake engineering community has been focusing on performance-based design. Performance-based design is an approach with the goal to incorporate a pre-defined level of post-earthquake performance into the design of the structure such that the damage is kept to 'acceptable' levels, with the definition of acceptable varying on the type and use of the structure [2.4]. The functionality of the structure will relate to the performance of different targets, including the structure, nonstructural elements, and contents (furniture and equipment) in the structure. Within the scope of this dissertation, functionality of the structure is relevant to the structure and contents inside of the structure.

Vision 2000 [2.5] defines four performance levels in terms of damage to the structure and nonstructural components and in terms of consequences to the occupants and functions carried on within the facility. The four levels are: (i) fully operational; (ii) operational; (c) life safe; and (d) near collapse. Table 2.1 shows the permissible damage of some typical contents in the structure at different performance levels. For the critical structures, the damage to the contents inside of the building at life safe level is significant, and may considered to be not acceptable. Figure 2.1 shows the contents damage in an office building, in the 2011 Tohoku earthquake, Japan. The performance level can be classified as the life safe level; however, the disordered contents inside of building will cause significant influence on the functionality of the building.

Table 2.1 Vision 200 performance levels and permissible damage for typical contents

| | Furniture | Office equipment | Computer systems | Storage racks and cabinets |
|---|---|---|---|---|
| Fully operational | Negligible effects | Negligible effects | Operational | Negligible damage, overturning restrained; |
| Operational | Minor damage; some sliding and overturning | Minor damage; some sliding and overturning | Minor damage; some sliding and overturning; mostly | Minor damage; overturning restrained; some |

| | | | | |
|---|---|---|---|---|
| | | | functional | spilling |
| Life safe | Extensive damage from sliding, overturning, leaks, falling debris, etc. | Extensive damage from sliding, overturning, leaks, falling debris, etc. | Extensive damage from sliding, overturning, leaks, falling debris, etc. | Extensive damage from leaks, falling debris, overturning, spilling, etc. |
| Near collapse | Extensive damage from sliding, overturning, leaks falling debris, etc. | Extensive damage from sliding, overturning, leaks falling debris, etc. | Extensive damage from sliding, overturning, leaks falling debris, etc. | Extensive damage from leaks, falling debris, overturning, spilling, etc. |

Figure 2.1 Contents damage inside the structure

### 2.2.2 Technologies to enhance functionality of structure

The most current earthquake standards lead to the design of structural elements so that the structure's capacity including strength, ductility is increased, and they can resist earthquake loads without collapse. This approach, however, does not reduce the structural response. Consequently such a method does not explicitly regard the performance of building contents, which are sensitive to the structural response. Even if the structure survives earthquakes by good design practice with enhanced strength and ductility, the vibration sensitive equipment located in the structure may still lose the functionality due to large floor accelerations.

On the other hand, many innovations have been proposed to reduce the structure response. Many of them have been used successfully in the real practice, while some of them are still under research. Those innovations include base isolation and energy dissipation devices operating in either a passive or active (or semi-active) mode which, enlarge the structure's capacity to absorb input energy, hence enhancing its functionality and safety [2.6].

Generally, the structures with control can be categorized into four different groups [2.1]: (1) passive control system; (b) active control system; (c) hybrid control system; and (d) semi-active control system.

(1) *Passive control system*

A passive control system does not require an external power source. Passive control devices impart forces that are developed in response to the motion of the structure. Passive control has been widely adopted in different types of structures [2.1]. The passive control dissipates energy inserted by the earthquake by stiffening, strengthening and adding damping to structures with mechanical devices. Typical passive systems are those with base isolation, mass dampers, friction devices, metallic yield devices, viscous-elastic damper, viscous fluid dampers and others.

Since there is no energy inserted to the structure, the structure is inherently stable. Passive control technique does not need sophisticate controller design, which makes it easily accepted by engineers in real practice. In addition, passive control is usually relatively inexpensive [2.1]. The disadvantage of passive system is that the system is only effective for a limited frequency band [2.1].

Isolation system is regarded as one type of passive control system. The associated research work is separately reviewed in Section 2.3 and 2.4.

(2) *Active control system*

Many limitations of passive control can be overcome by active control. Active control system is one in which an external source powers control actuators that apply forces to the structure in a prescribed manner, which is designed with various available control algorithms. The active controller is designed based on the feedback signals and/or feedforward signals fed to the control system.

In comparison with passive system, a number of advantages associated with active system can be cited [2.6]. Effectiveness in motion control is limited primarily by the capacity of control device. It can apply to different site conditions and ground motions. Also it is possible to select the control objectives, for example, human comfort over other aspects. However, since an active control system requires external source powers from the actuators to apply the control force, availability of a large amount of power during an earthquake event is a great concern. In addition, the force from the actuators can be used to dissipate energy or add energy in the structure. It has a potential to destabilize the system with an improper controller design.

Most of the practical applications of active control to civil structures are found in Japan. The first full scale application of active control to the structure was accomplished by the Kajima Corp. in 1989 [2.7] to a 10 storey building. An overview paper [2.8] lists the practical application of active control to buildings in Japan between 1989 and 2007. Most of the systems are with AMD actuators.

(3) *Hybrid control system*

The common usage of the term “hybrid control” implies the combined use of active and passive control systems [2.1]. Such a combination can sometimes alleviate some of the limitations that exist for either a passive or an active control acting alone, thus leading to an improved solution. Additionally, the resulting hybrid control system can be more reliable than a fully active system, although it is often more complicated.

Hybrid control has been investigated by many researchers to exploit their potential to increase the overall reliability and efficiency of the controlled structure [2.6, 2.8-2.10]. Research in the hybrid

control systems mainly focus on two classifications of systems [2.1]: (i) hybrid mass damper (HMD) system, and (ii) active base isolation system. The HMD is the most common control device employed in full-scale civil engineering applications [2.2, 2.9]. In the 52 practical applications of active/hybrid controls listed in [2.8], the vast majority are hybrid control system using HMD. The HMD integrates certain active control operation into passive mass damper movement. The energy used to operate a typical HMD is far less than those with a fully active mass driver system. Most of the applications are for high rise buildings.

(4) *Semi-active control system*

Semi-active control system is a class of active control system for which the external energy requirements are orders of magnitude smaller than typical active control system [2.1, 2.11]. Typically, semi-active devices do not add mechanical energy to the structural system.

Semi-active control devices [2.2] have received a great deal of attention in recent years. The semi-active control combines the best features of passive control and semi-active control. On one side, since the semi-active device does not inject energy to the structure, the stability of the system in a bounded-input bounded-output sense is guaranteed. On the other side, semi-active devices can also vary the control force based on the control algorithm adopted. It has the potential to achieve or even surpass the performance of an active control system [2.12].

Within the field of structural engineering, the first application of semi-active structural control for systems subjected to environmental loads appears to have been proposed by Hrovat et al. [2.13] in 1983. Reference [2.8] shows an overview of the practical applications of semi-active control to buildings in Japan, which were constructed between 1990 and 2006. Among those semi-active control devices, controllable fluid dampers, especially those using magnetorheological (MR) fluids, have gained a particular interest. The first full scale implementation of MR dampers for civil engineering was achieved for the Tokyo National museum of Emerging Science and Innovation, using two 30 ton MR dampers manufactured by Sanwa Tekki [2.2]. For practical application with semi-active control base isolation, 40 ton MR dampers were installed in a residential building in Japan along with laminated rubber bearings [2.14]. More detail research reviews on MR damper and MR damper model are shown in Section 2.5.

## 2.3 Base isolation system

To achieve enhanced functionality and operability, base isolation has become very popular around the world. The number of isolated buildings in Japan increased rapidly after the 1995 Kobe earthquake. The construction number per year before 1995 remained less than 10, while it increased drastically to 150 afterward. At present, there are over 2500 base-isolated buildings in Japan, and the applications are extensively applied to hospitals and medical facilities, because these facilities are the first ones that need to function right after a damaging earthquake event [2.3]. New developments on the base-isolation are still active [2.3, 2.15, 2.16] by employing new technology.

### 2.3.1 Passive base isolation system

Base isolation is a technology that protects the structure from the destructive effects of an earthquake. It decouples the structure from the ground [2.17] and this decoupling allows the building to behave more flexibility laterally to improve its response to an earthquake.

One of the main objectives of designing the base isolation is to reduce the structural response, which will benefit the structure safety. Historical reviews of passive structural isolation devices [2.18-2.20] have shown that these devices have great potential to prevent earthquake damage to buildings. The peak transmitted accelerations and the deflections generated in the structure are dramatically reduced by using properly designed base isolation systems.

The protection of the building contents is another favorable feature of seismic isolation [2.21, 2.22]. Different levels of protection for different classes of contents can be expected, according to the type of isolation system and the flexibility of the superstructure. Relevant researches [2.22, 2.23] show that each type of isolation system reduced considerably the seismic effects on internal equipment in wide frequency regions.

Nowadays, the usage of equipment with casters has become common in facilities such as hospitals to provide convenient mobility to the working stuffs. In such a situation, the behavior of equipment is a great concern which will influence the structure functionality significantly. A study [2.27] shows the influence of low frequency energy content in the earthquake to the secondary systems with the floor response spectra method.

Reference [2.24] shows an investigation of the performance of hospital functionality after the January 17, 1994 Northridge earthquake for few hospitals. The USC Hospital is an isolated steel frame building. The building remained operational throughout the 1994 Northridge Earthquake. There was no damage to the USC Hospital. In contrast, the Los Angeles County Medical Center located less than a mile away suffered $400 million of damage and was not operational after the earthquake. Such a comparison clearly shows the advantage of using isolation technique over the base-fixed building.

While passive base isolation system performed successfully during the 1994 Northridge earthquake, studies [2.25] show that the near filed earthquakes, which contain strong velocity pulses with long-periods, may result in excessive isolator drifts. A solution to this is to increase the passive damping in the isolation system. However, such a solution will increase the interstorey drifts and superstructure accelerations at high frequencies [2.26].

Nonetheless, the passive base isolation is a great success in improving the functionality of the building, because of its simplicity, reliability and effectiveness [2.1]. More research, however, is needed to further improve the functionality of the base isolation, especially its performance under large earthquakes and the behavior of the contents in the structure.

### 2.3.2 Active/semi-active base isolation system

Active and semi-active base isolation systems are classified as hybrid control system. The passive base isolation system tends to have large displacement response under long-period earthquake

motions. Therefore, a large clearance between the structure and retaining wall is required, which will not only cause potential failure to the isolators, but also increase the cost of the entire building. One approach to addressing the limitations of passive isolation systems is to develop a hybrid isolation system by replacing the passive control devices with active/semi-active devices. Numerous researchers have studied hybrid base isolation systems for seismic protection of buildings. A majority of the hybrid isolation systems that have been proposed employ active control devices at the isolation level to control the structural response [2.28-2.30]. Alternatively, semi-active control devices [2.1, 2.2] that require only a relatively small power supply have been investigated recently for use in isolation systems [2.31-2.37].

The combination of a base isolation system with active/semi-active control has potential to improve the performance of a passive base isolation system by achieving a balanced level of control performance in reduction of both floor accelerations and base displacements. Researches [2.33, 2.38] claim that the hybrid isolation system reduces the isolator displacement without significantly increasing the acceleration response.

The control performance depends on the control device used, type of excitation to the structure, and the control algorithm adopted. It is a challenging task to design a satisfactory hybrid control which can guarantee good performance of the structure and contents in the structure under different loadings. Perhaps this is the reason why there is no clear guideline for designing a hybrid control isolation system.

In summary, the passive isolation system is a simple yet effective way to keep the post-earthquake functionality of the structure. However, passive systems are only effective for a limited frequency band. Hybrid control has the potential to overcome those problems, but the effectiveness will depend on various aspects. Further research is needed to develop high performance controllers.

## 2.4 Floor isolation system

Base isolation of an entire building may not be practical or economical in some cases including retrofit. In such situations, a floor isolation system, designed for one floor or room of the structure for particularly sensitive or expensive equipment, is a cost-effective alternative [2.16, 2.39-2.43]. Unlike equipment isolation systems which are designed for a particular piece of equipment or base isolation systems which are designed for an entire building, floor isolation systems protect a group of equipment, such as important and expensive medical devices in a hospital.

### 2.4.1 Unique features of floor isolation system

Compared with base isolation, floor isolation offers some unique features. (i) The weight on a floor isolation system is considerably lighter than that of a base isolation system. This makes the use of rubber bearings difficult because of the large axial loads needed to ensure flexibility with the use of rubber bearings. As an alternative, spherical friction bearings, which do not require large axial

loads, can be used [2.43]. (ii) Since the space of a floor isolation system is limited, small clearance distances between the floor isolation system and surrounding walls are preferred. (iii) Rearrangement or moving in and out of equipment on the floor is sometimes necessary. In these situations, the mass of the system may change which cannot be accommodated by passively control. (iv) Unless a floor isolation system is located on the ground floor level, the input motion to the floor isolation system is not the same as the input motion to the structure. Usually the structural motion is larger than the ground motion [2.40]. In addition, the frequency components of the motion are physically filtered by the structure, leaving relatively low frequency components.

As ground motion has high variability, the floor isolation may be subjected to motions with different frequency components. Motions with high frequency tend to cause large acceleration of the floor isolation system because of the high amplitude, while motions with low frequency tend to cause large displacement because of resonance. The acceleration of the floor isolation must be mitigated to protect the appliance; however, the displacement also needs to be suppressed in order to maximize the usable floor isolation area.

### 2.4.2 Previous research

Fujita [2.41] in 1985 reviewed the application of floor isolation systems in Japan. They were mainly designed for banking systems, air-traffic control and chemical process control. Shaking table tests and analysis results showed that the floor isolation system was effective in reducing acceleration response, while the displacement was considerably larger.

Since the floor isolation and base isolation share the same concept, i.e., to decouple the structure from the ground (base isolation) or floor (floor isolation), some of the conclusions derived from base isolation also applies to floor isolation. Effective reduction in acceleration with passive system is achieved with the expense of increasing the displacement of the floor isolation system, which sometimes is not preferred. Increasing the damping to the system will reduce the displacement response; however, this would increase the acceleration response [2.42,]. In addition, as stated earlier, the load on the floor may vary due to the rearrangement of equipment (moving in/out of equipment) and it will cause significant change in the structural characteristics, including the natural period and damping ratio, for the passive floor isolation system.

In order to reduce the acceleration to protect the appliance as well as to limit the displacement in order to maximize the usable floor isolation area, semi-active control can be used. Fan et al [2.16] studied the semi-active control of a floor isolation system with an MR damper. The floor isolation was placed on the second floor of a 3-story steel frame. Different control algorithms have been tested. Experimental results illustrate the effectiveness of the performance of a decentralized sliding mode control in protecting the vibration-sensitive equipment from earthquakes.

In summary, research on floor isolation is not as extensive as on the base isolation system yet. Although both systems share similar design concept, they have differences as described in Section 2.4.1. In addition, most of researches for floor isolation are using a passive control system. Therefore, it is desirable to study the behavior of floor isolation with semi-active control which has

the potential to suppress both the floor acceleration and displacement.

## 2.5 Semi-active control with MR damper

As described in the previous sections, effectiveness of the active/semi-active control system will depends on several aspects. For semi-active control, they include, but not limit to, control device modelling, control algorithm and force tracking system to realize the desired force.

### 2.5.1 MR damper modeling

MR dampers are widely used in semi-active control. MR fluids contained in the MR damper are the magnetic analogs of electrorheological fluids and typically consist of micron-sized, magnetically polarizable particles dispersed in a carrier medium such as mineral or silicone oil. When a magnetic field is applied to the fluids, particle chains form, and the fluid becomes a semi-solid and exhibits viscoplastic behavior. Transition to rheological equilibrium can be achieved in a few milliseconds [2.44].

Figure 2.2 shows a MR damper manufactured by Sanwa Tekki Corp. The magnetic field of the MR damper is adjusted by the current applied to the coil. The power needed for such a damper can be readily provided by batteries.

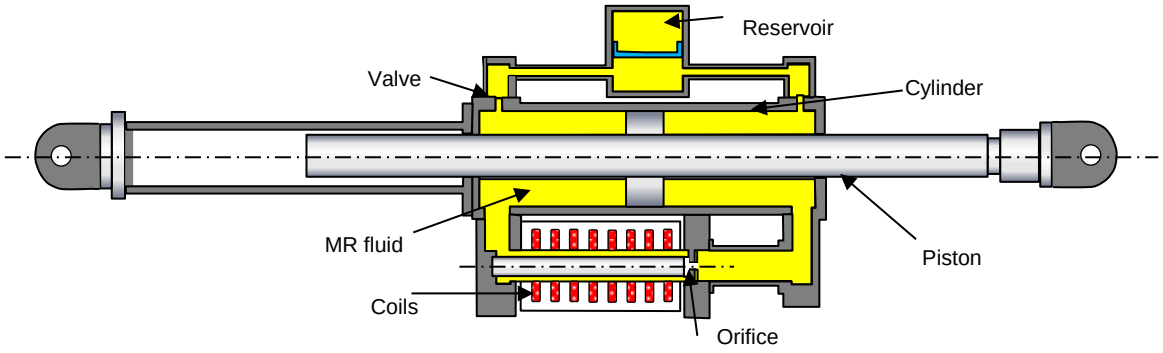


Figure 2.2 An example of MR damper (by Sanwa Tekki Corp.)

To develop a control algorithm that takes the maximum advantage of the unique features of the MR damper, an appropriate model must be established to describe the relationship between the input current and the output force. In such a model, the velocity and current are known parameters while the force is unknown. To the present, various models have been developed including parametric and non-parametric models. Ref. [2.45] reviewed modeling of MR dampers using parametric modeling based on mechanical idealizations. Those models include the Bingham model-based dynamic models, biviscous models, and Bouc-Wen hysteresis operator-based dynamic models, among others. The non-parametric modeling uses analytical expressions to describe the characteristics of the modeled device. Those models include the polynomial model [2.46], neural network model [2.45], fuzzy model [2.17], etc.

One of the main purposes of designing the MR damper model is to carry out simulation work for control strategy design. Therefore, the model should be accurate enough to capture the main

characteristics of the MR damper, yet as simple as possible. To calibrate many parameters in a complicated model is a challenging task. Simulation with a complicate model usually takes a longer time, and the results are sensitive to the parameter change and the time interval in the simulation. Three frequently used models, the Bingham model, Bouc-Wen model, and phenomenological model [2.44], are reviewed.

(1) *Bingham model*

The Bingham model combines a Coulomb friction element in parallel with a viscous dashpot. The governing equation is

$$u = \operatorname{sign}(\dot{x})\, f_c + c_0 \dot{x} + f_0 \tag{2.1}$$

where $u$ is the MR damper force; $\dot{x}$ denotes the velocity across the MR damper; $c_0$ is the damping coefficient, $f_c$ is the frictional force related to the field-dependent yield stress and $f_0$ is the offset in the force. The three parameters $c0$, $f_c$, and $f_0$ may be current-dependent, and usually the dependency can be expressed as a linear or quadratic equation.

The advantage of using Bingham model is that it is easy to establish the model by calibrating a smaller number of parameters. It can describe the behavior of MR damper reasonably when the velocity is large. In addition, the current can be easily solved from Equation (2.1). A disadvantage of it is that the Bingham model cannot account for the hysteretic behavior of the MR damper in the small velocity zone.

(2) *Bouc-Wen model*

The schematic of a Bouc-Wen model is shown in Figure 2.3 and the equation governing the MR damper force $u$ is given by

$$\begin{aligned} u &= c_0 \dot{x} + k_0 (x - x_0) + \alpha z \\ \dot{z} &= -\gamma |\dot{x}| z |z|^{n-1} - \beta \dot{x} |z|^n + A\dot{x} \end{aligned} \tag{2.2}$$

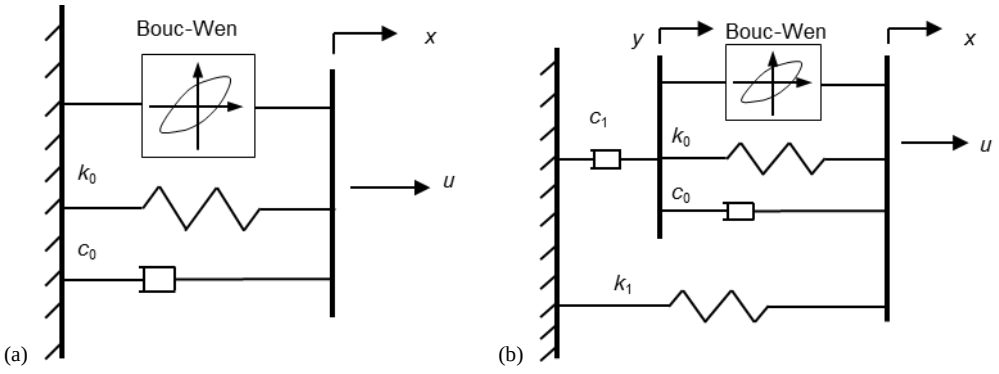


Figure 2.3 Schematic of (a) Bouc-Wen model; (b) Phenomenological model

where $z$ is an evolutionary variable. By adjusting $\alpha$, $\beta$, $\gamma$, and $n$, it is possible to control the force-velocity characteristic shape for MR damper. The eight parameters $c_0$, $k_0$, $x_0$, A, $\alpha$, $\beta$, $\gamma$ and $n$ should be identified. Typically, the relationship between the eight parameters and the input current to the MR damper should be established. Finally, more than eight parameters need to be calibrated. By carefully tuning the parameters [2.47], the Bouc-Wen model is able to reasonably describe the relationship between force, and velocity and input current. Compared with the Bingham model, it is more accurate, but also more challenging to calibrate the parameters involved.

(3) *Phenomenological model*

The phenomenological model is proposed by Spencer et al. [2.44] by modifying the Bouc-Wen model. Figure 2.3 shows the schematic of this model. The MR damper force is governed by the equations:

$$u = c_1\dot{y} + k_1(x - x_0) \tag{2.3}$$

where $y$ is the internal displacement of the MR damper ruled by

$$\dot{y} = \frac{1}{c_0 + c_1}\left(\alpha z + c_0\dot{x} + k_0\left(x - y\right)\right) \tag{2.4}$$

where $z$ is the evolutionary variable ruled by

$$\dot{z} = -\gamma\left|\dot{x} - \dot{y}\right| z\left|z\right|^{n-1} - \beta\left(\dot{x} - \dot{y}\right)\left|z\right|^{n} + A\left(\dot{x} - \dot{y}\right) \tag{2.5}$$

There are ten parameters in Equations (2.3) to (2.5). Similar to the Bouc-Wen model, some of the parameters have to be related to the current. In Ref [2.44], $\alpha$, $c_0$, and $c_1$ are assumed to vary linearly with the applied voltage. A total of fourteen parameters must be determined.

Simulation results [2.44] show that the phenomenological model improves the accuracy of the Bouc-Wen model. However, the model complexity increases unavoidably by an extended number of model parameters. Therefore, this model can be used in applications where a very accurate model is required [2.45].

.

### 2.5.2 Control algorithm

Figure 2.4 shows the diagram of design for semi-active control. There are two challenging tasks in the design. The first one is to select an algorithm for the controller to calculate the desired active force with the feedback or feedforward signals from the measurement. The other task is to design a force tracking system which can calculate control signals to the semi-active device so as to track the desired force as close as possible. Some types of algorithms, including the control based on Lyapunov stability theory and Bang-bang control [2.48] switch the control signals to the semi-active device

between zero and the maximum (on-off type), depending on a predefined criterion obtained from the control algorithm. Such algorithms combined the two tasks as one.

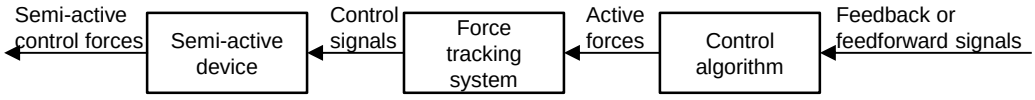


Figure 2.4 Design of two controllers

Effectiveness of the semi-active control significantly depends on the control algorithm. Numerous control algorithms have been developed for active and semi-active control in various structural systems including base isolation. A proper selection of the control algorithm depends on many factors, including the control devices type, characteristics of the structure and excitation, available feedbacks, nonlinearity presented in the control system, and the readiness of implementation of the algorithm.

Among those algorithms, the linear quadratic regulator (LQR) control [2.31, 2.49], LQG control [2.12, 2.34, 2.50], $H_\infty$ control [2.32, 2.35, 2.38], sliding mode control [2.30, 2.33] and Lyapunov control algorithm [2.36] are mostly frequently used in base-isolation system. The so called Clipped optimal control [2.12] is widely used for MR damper controlling, which employs the LQG control strategies and an on-off type force tracking system.

For the floor isolation system studied in this research, the acceleration of the floor isolation must be mitigated to protect the appliance; however, the displacement also needs to be suppressed in order to maximize the usable floor isolation area. As ground motion has high variability, the isolation system may be subjected to motions with different frequency components. Motions with high frequency tend to cause large acceleration of the floor isolation system because of the high amplitude, while motions with low frequency tend to cause large displacement because of resonance. To deal with the motion variability, semi-active control with $H_\infty$ control is adopted in this study due to its efficiency in accounting for the frequency characteristics of the input motion.

$H_\infty$ control is designed in the frequency domain. It allows the designer to directly deal with the characteristics of the input excitation and specify disturbance attenuation over a desired frequency range, as well as to roll off the control action at high frequencies that will not influence the overall behavior significantly [2.51].

The optimal linear control LQR method based on the linear quadratic form of performance index is the core of control. However, it ignores the characteristics of the input excitation. To extend its application to deal with the motion variability, improvement of the control algorithm is needed. This is part of the research in this dissertation, which is presented in Chapter 6. The two algorithms, LQR control and $H_\infty$ control, are briefly reviewed.

(1) *LQR control*

LQR control has been widely used for semi-active or active controlled structures. It is carried out in the time domain. Figure 2.5 shows the diagram of LQR control.

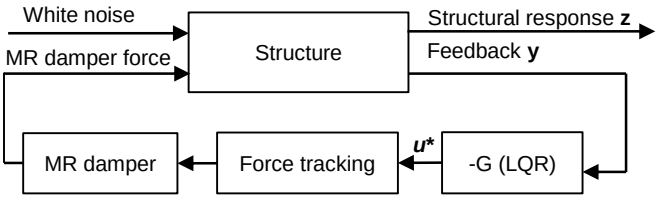


Figure 2.5 Diagram of LQR control design

The dynamic equation of motion for the *n*-DOF structure subjected to the excitation $\ddot{x}_{\text{in}}$ can be expressed as

$$\mathbf{M}\ddot{\mathbf{x}} + \mathbf{C}\dot{\mathbf{x}} + \mathbf{K}\mathbf{x} + \mathbf{\Gamma}_1\mathbf{U}^* = -\mathbf{M}\mathbf{\Gamma}_2\ddot{x}_{\text{in}} \tag{2.6}$$

where **M**, **C**, and **K** are mass, damping and stiffness matrices of the structure, respectively; **x** is an *n*-vector displacements of the structure relative to ground; $\mathbf{U}^*$ is the control force vector and $\mathbf{\Gamma}_1$ denotes the location of dampers; $\mathbf{\Gamma}_2$ is the vector of ones.

Equation (2.6) can be expressed in the state space as

$$\dot{\mathbf{X}} = \mathbf{A}\mathbf{X} + \mathbf{B}\mathbf{U}^* + \mathbf{H}\ddot{x}_{\text{in}} \tag{2.7}$$

where

$$\mathbf{X} = \begin{bmatrix} \mathbf{x} \\ \dot{\mathbf{x}} \end{bmatrix}, \quad \mathbf{A} = \begin{bmatrix} \mathbf{0} & \mathbf{1} \\ \mathbf{-M^{-1}K} & \mathbf{-M^{-1}C} \end{bmatrix}, \quad \mathbf{B} = \begin{bmatrix} 0 \\ -\mathbf{M}^{-1}\Gamma_1 \end{bmatrix}, \quad \mathbf{H} = -\begin{bmatrix} \mathbf{0} \\ \mathbf{\Gamma_2} \end{bmatrix} \tag{2.8}$$

The control force for LQR control is obtained by minimizing a predefined performance function. The following performance function has been used by many researchers [2.31, 2.49]

$$J = \int_0^t \left( \mathbf{X}^T\mathbf{Q}\mathbf{X} + \mathbf{U}^{*\mathbf{T}}\mathbf{R}\mathbf{U}^* \right) dt \tag{2.9}$$

where **Q** is a $2n \times 2n$ semi-positive definite weighting matrix for the structure responses, i.e., displacement and velocity, and **R** is a positive weighting scalar for the control force. Displacement and velocity, i.e., the state vector, are used as the feedback signal **y**. By minimizing the performance function *J* the optimal control force can be obtained

$$u^* = -\mathbf{Gy} = \mathbf{G}\begin{bmatrix}\mathbf{x} & \dot{\mathbf{x}}\end{bmatrix}^{\mathbf{T}} \tag{2.10}$$

where **G** is the feedback gain. It can be solved by computing the solution **P** of the algebraic Riccati equation [2.52]

$$\begin{aligned}&\mathbf{A}^T\mathbf{P} + \mathbf{PA} - \mathbf{PB}R^{-1}\mathbf{B}^T\mathbf{P} + \mathbf{Q} = 0\\&\mathbf{G} = R^{-1}\mathbf{B}^T\mathbf{P}\end{aligned} \tag{2.11}$$

There are two drawbacks in LQR control. One is that the excitation is assumed to white noise process, which is not true for non-stationary excitations. Therefore, the characteristics of input motion are not taken into account in LQR control. The other is that the weight matrices **Q** and **R** are usually taken to be constant, and the control gain by using constant weighting matrices is fixed. Such a constant gain makes the LQR control be equivalent to a passive system (Chapter 6).

A previous study [2.13] indicates that an active designed TMD system with LQR control using a group of constant weightings only increase the damping of the original structure while slightly altering the natural frequencies. Another study [2.31] shows that the semi-active control system is only comparable to a high damping passive control system. For a suite of motion, that share similar frequency characteristics, the LQR control is effective. However, for motions with different frequency characteristics, the classical LQR control will cause the problem similar to in the passive control. This is particularly true during seismic disturbances, when the stiffness and damping of the building structure may change due to inelastic deformation.

Nagashima et al. [2.53] proposed a variable feedback gain designed to adjust the control performance with respect to the variation in the intensity level of the external excitation. The control gain is calculated with a time varying weighting matrix **Q,** which indicates a trade-off control between the control target and control effort. However, such a design does not consider the frequency characteristics of earthquake excitation.

(2) *$H_\infty$ control*

The schematic of $H_\infty$ control is shown in Figure 2.6. $H_\infty$ is one control in the frequency domain which aims at reducing the RMS value of the system response.

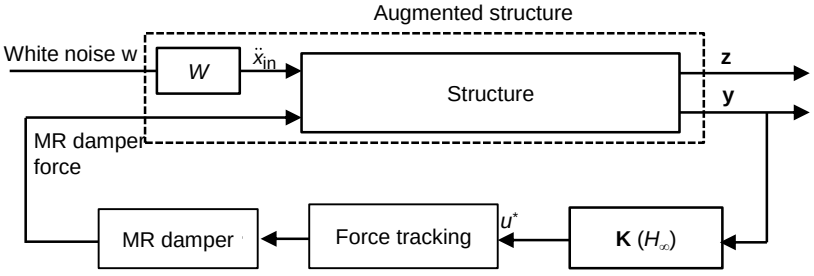


Figure 2.6 Diagram of $H_\infty$ controller design

$H_\infty$ control can also implement a shaping filter to account for the frequency characteristics of the excitation. The control gain **K** of $H_\infty$ control is obtained by minimizing the $\infty$ norm of the transfer function matrix, $\mathbf{H}_{zw}$, from the input excitation $w$ to the regulated responses of **z**.

$$\left\|\mathbf{H}_{zw}\right\| = \sup_{w}\left[\bar{\sigma}\left(\mathbf{H}_{zw}(s)\right)\right] < \bar{\gamma} \tag{2.12}$$

where sup denotes the supremum and $\bar{\sigma}$ stands for the maximum singular value of the transfer function; $\bar{\gamma}$ is a positive bound for the norm.

The control force $u^*$ is calculated by

$$u^* = \mathbf{K}\mathbf{y} \tag{2.13}$$

### 2.5.3 Force tracking system

For the dynamic model (Section 2.5.1), the MR damper forces are related to the velocity and voltage/current to the MR dampers, i.e., the velocity and voltage/current is known, while the force is unknown. On the contrary, the voltage/current signal is unknown in the practical application, since the desired force of the MR damper is designed first. This task can be done with a force tracking system aiming at calculating voltage/current to the MR damper to realize the desired force calculated from the adopted algorithm, such as LQR control.

The design of force tracking system depends on the control algorithm and the semi-active device significantly. For example, for the Bang-bang type control [2.36, 2.48] the control signal (voltage/current) switches between the minimum and maximum values. Another example shows that an approximate linear relationship between the command signal and damping coefficient can be used for the semi-active fluid damper [2.31], which acts as the force tracking law.

The MR damper is featured with its nonlinear behavior as described in Section 2.5.1. Several force tracking methods have been developed and used in both simulation and experiment work, including inverse dynamic models [2.46, 2.54], clipped methods [2.12, 2.34, 2.47], and force feedback controllers [2.55, 2.57], among others.

(1) *Inverse dynamic models*

As discussed in the dynamic modeling of the MR damper, the reversibility of the MR damper model is preferred since such a model can be easily used to calculate the control signal. The inverse dynamic models include: inverse Bingham mode [2.45], inverse polynomial model [2.46], and inverse Bouc-Wen model [2.54], among others. The advantage of such inverse dynamic models is that the force can change continuously and no feedback signals are needed. However, since the inverse dynamic models are derived from the dynamic model directly, the accuracy of the inverse model depends on the dynamic model significantly. Generally, a simple model is difficult to catch all the features of the MR damper. For example, although the Bingham model is simple, it cannot describe the hysteretic behavior. Consequently, the accuracy of the corresponding inverse Bingham

model is relatively low. On the other hand, it is difficult to derive the inverse dynamic model from a complicated dynamic model, although it normally gives better accuracy.

(2) *Clipped-optimal controller*

The clipped optimal control proposed by Dyke et al. [2.12] combines an $H_2$/LQG algorithm and an on-off type method to determine the control force. The on-off control method in the clipped-optimal control is widely used in the semi-active control with MR damper because of its simplicity. The on-off switching rule of the voltage to the MR damper is expressed as

$$v = V_{\max} H\left\{\left(f_{\text{des}} - f_{\text{mea}}\right) f_{\text{mea}}\right\} \tag{2.14}$$

where $V_{\max}$ is the maximum voltage for the MR damper; $f_{\text{des}}$ and $f_{\text{mea}}$ are the desired force and actual measured force, respectively; $H(\cdot)$ is the Heaviside step function.

The advantage of this method is that the dynamic features of MR damper are not involved. However, the on-off switching law has the potential to increase the floor accelerations and inter-storey drifts [2.15]. A proper low pass filter is necessary in the real application [2.47, 2.56].

(3) *Continuous force feedback controller*

Since the on-off control for clipped-optimal control may cause large acceleration and inter-story drift, there is a need to develop a method that can change the MR damper voltage slowly and smoothly, such that all voltages between zero and the maximum can be covered [2.55].

The PI (or PID) controller [2.56, 2.57] can be used to calculate the control signal to the MR damper to track the desired control force. Figure 2.7 shows the diagram for a PI controller. The feedback of actual measured force is used to compare with the desired force. The PI controller can be express as

$$\begin{aligned} I &= K_{\text{p}} e + K_{\text{i}} \int e dt \\ e &= f_{\text{des}} - f_{\text{mea}} \end{aligned} \tag{2.15}$$

where $I$ is the input current to the MR damper; $f_{\text{des}}$ and $f_{\text{mea}}$ are the desired force and actual measured force. $K_{\text{p}}$ and $K_{\text{i}}$ are the proportional and integral gains to be determined.

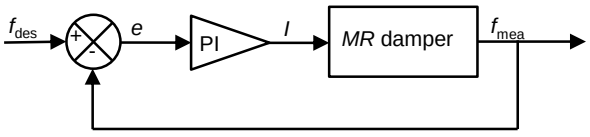


Figure 2.7 PI controller design

Except for the PI controller, the fuzzy logical control is also used to calculate a continuously changing input signal to the MR damper in some researches [2.55].

Generally, the determination of a force tracking system needs to consider the accuracy, simplicity, available data, etc. The PI controller was designed for the MR damper used in this research. Detail is shown in Chapter 5.

## 2.6 Summary

This chapter reviews the techniques to improve the structural functionality and the semi-active control for structure. The major contents are summarized as follows:

(1) The passive base isolation system can significantly reduce the acceleration response of the structure and improve the functionality of the building. However, the displacement response under long-period motions is large. Simply adding damping to the system will decrease the displacement but at the expense of increased acceleration. Active and semi-active base isolation systems have the potential to overcome the problem in passive isolation system under long-period motion. The effectiveness of the control design will depend on the device and control algorithms.

(2) Floor isolation system is an alternative to base isolation. It is necessary to reduce the acceleration to protect the appliance as well as to limit the displacement in order to maximize the usable floor isolation area. Different from the base isolation, the input motion to the floor isolation that is installed on a higher floor, is normally amplified from the ground motion, and filtered by the structure.

(3) In both the base isolation and floor isolation systems, there is little information from the past research on the behavior of appliance equipped with casters to enhance the mobility, under different types of earthquakes with different frequency characteristics.

(4) Different control algorithms, including LQR and $H_\infty$ have been reviewed. LQR cannot account for the frequency characteristic of the input motion. To extend its application, modification is needed. The $H_\infty$ consider the frequency characteristics of the input motion by implementing a shape filter to the controller in the frequency domain.

(5) A model to describe the MR damper behavior is necessary. Three different models, Bingham model, Bouc-Wen model and modified Bouc-Wen model are reviewed. The Bingham model is not able to describe the hysteretic behavior of the MR damper. Bouc-Wen mode can reasonably describe the MR damper behavior with less number of parameters than the modified Bouc-Wen model, although the latter one has higher accuracy. Force tracking system is needed to calculate the control signal to MR damper. The on-off type clipped optimal controller is widely used for MR damper, but the abrupt switch law has the potential to cause large response to the structure.

# REFERENCES

[2.1] Housner GW, Bergman LA, Caughey TK, Chassiakos AG, Claus RO, Masri SF, Skelton RE, Soong TT, Spencer BF and Yao TP. Structural control: past, present and future. *Journal of Engineering Mechanics* 1997; 123(9):897:971.

[2.2] Spencer BF, Nagarajaiah S. State of the art of structural control. *Journal of Structural Engineering* 2003; 129:845-856.

[2.3] Sato E, Furukawa S, Kakehi A, Nakashima M. Full shaking table test for examination of safety and functionality of base-isolated medical facilities. *Earthquake Engineering and Structural Dynamics* 2011; 40: 1435-1453.

[2.4] Lee WK, Billlington SL. Performance-based earthquake engineering assessment of a self-centering, post-tensioned concrete bridge system. *Earthquake Engineering and Structural Dynamics* 2011; 40:887-902.

[2.5] SEAOC. Performance based seismic engineering of buildings, Vision 2000 Report. *Structural Engineers Association of California*. Volumes I and II, Sacramento, California.

[2.6] Soong TT, Reinhorn. An overview of active and hybrid structural control research in the U.S. *The Structural Design of Tall buildings* 1993; 2:193-209

[2.7] Kobori T, Koshika, Yamada N, Ikeda Y. Seismic response controlled structure with active mass driver system. Part 1: design. *Earthquake Engineering and Structural Dynamic* 1991;20:133-139.

[2.8] Ikeda Y. Active and semi-active vibration control of buildings in Japan-practical applications and verification. *Structural Control and Health Monitoring* 2009; 16:703-723.

[2.9] Nishitani A, Inoue Y. Overview of the application of active/semiactive control to building structures in Japan. *Earthquake Engineering and Structural Dynamics* 2001; 30: 1565-1574.

[2.10] Lee-Glauser GJ, Ahmadi G, Horta LG. Integrated passive/active vibration absorber for multistory buildings. *Journal of Structural Engineering 1997*; 123(4):499-504.

[2.11] Yang G, Spencer BF, Carlson JD, Sain MK. Large-scale MR fluid dampers: modeling and dynamic performance considerations. *Engineering structures* 2002; 24:309-323.

[2.12] Dyke SJ, Spencer BF, Sain MK, Carlson JD. Modeling and control of magnetorheological dampers for seismic response reduction. *Smart Materials and Structures*, 5(5):565-575.

[2.13] Hrovat D, Barak P, Rabins M. Semi-active versus passive or active tuned mass dampers for structural control. *Journal of Engineering Mechanics* 1983;109(3):691–705.

[2.14] Fujitani H, Sodeyama H, Tomura T, Hiwatashi T, Shiozaki Y, Hata K, Sunakoda K, Morishita S, Soda S. Development of 400kN magnetorheological damper for a real base-isolated building. Proc., SPIE Conf. Smart Structures and Materials 2003; 5057. SPIE—International Society for Optical Engineering, Bellingham, Wash.

[2.15] Nagarajaiah S, Narasimhan. Seismic control of smart base isolated buildings with new semiactive variable damper. *Earthquake Engineering and Structural Dynamics* 2007; 36:729-749.

[2.16] Fan YC, Loh CH, Yang JN, Lin PY. Experimental performance evaluation of an equipment isolation using MR dampers. *Earthquake Engineering and Structural Dynamics* 2009; 38(3):285–305.

[2.17] Schurter KC, Roschke PN. Neuro-fuzzy control of structures using acceleration feedback. Smart Material and Structures 2011; 10: 770–779.

[2.18] Kelly JM. A seismic base isolation: review and bibliography. *Soil Dynamics and Earthquake*

*Engineering* 1986; 5(3):202-216.

[2.19] Su L, Ahmadi G, Tadjbakhsh IG. A comparative study of performances of various base isolation systems. *Earthquake Engineering and Structural Dynamics 1989,* 18, 11-32.

[2.20] Fan FG, Ahmadi G, Mostaghel N, Tadjbakhsh IG. Performance analysis of seismic base isolation systems for a multistory building. *Soil Dynamics and Earthquake Engineering* 1991; 10: 152-171.

[2.21] Dolce M, Cardone D, Ponzo FC. Shaking table tests on reinforced concrete frames with different isolation systems. *Earthquake Engineering and Structural Dynamics* 2007; 36:573-596.

[2.22] Dolce M, Cardone D. Seismic protection of light secondary systems through different base isolation systems. *Journal of Earthquake Engineering* 2003; 7(2):223–250.

[2.23] Yongqi C, Soong TT. State of the art review seismic response of secondary systems. *Engineering Structures* 1988; 10(4):2118-228.

[2.24] Schiff AJ. Northridge earthquake: lifeline performance and post-earthquake response. *Amer Society of Civil Engineers*. 1995.

[2.25] Heaton TH, Hall JF, Wald DJ, Halling MW. Response of high-rise and base-isolated buildings to a hypothetical Mw 7.0 blind thrust earthquake. *Science* 1995; 267: 206–211.

[2.26] Kelly JM. The role of damping seismic isolation. *Earthquake Engineering and Structural Dynamics* 1999; 28:3-20.

[2.27] Fan FG, Ahamadi G. Floor response spectra for base-isolated multi-storey structures. *Earthquake Engineering and Structural Dynamics* 1990; 19:377-388.

[2.28] Kelly JM, Leitmann G, Soldatos AG. Robust control of base-isolated structures under earthquake excitation. *Journal of optimization theory and applications* 1987; 53(2):159-180.

[2.29] Yang JN, Wu JC, Reinhorn AM, Riley M. Control of sliding isolated buildings using sliding mode control. *Journal of structural Engineering* 1994; 122(2):179-186.

[2.30] Yang JN, Wu JC, Reinhorn AM, Riley M. Control of sliding-isolated buildings using sliding-mode control. *Journal of Structural Engineering* 1996; 122(2):179-186.

[2.31] Symans MD, Constantinou MC. Seismic testing of a building structure with a semi-active fluid damper control system. *Earthquake engineering and structural dynamics* 1997. 26:759-777.

[2.32] Wongprasert N, Symans MD. Experimental evaluation of adaptive elastomeric base-isolated structures using variable-orifice fluid dampers. *Journal of Structural Engineering* 2005; 131(6):867-877.

[2.33] Madden GJ, Wongprasert N. Analytical and numerical study of a smart sliding base isolation system for seismic protection of buildings. *Computer Aided Civil and Infrastructure Engineering* 2003; 18:19-30.

[2.34] Yoshioka H, Ramallo JC, Spencer BF. Smart base isolation strategies employing magnetorheological dampers. *Journal of Engineering Mechanics* (ASCE) 2002; 128(5):540–551.

[2.35] Narasimhan S, Nagarajaiah S. Smart base isolated buildings with variable friction systems:

$H_\infty$ controller and novel SAIVF device. *Earthquake Engineering and Structural Dynamics* 2006; 35(8):921–942.

[2.36] Sahasrabudhe SS, Nagarajaiah S. Semi-active control of sliding isolated bridges using MR dampers: an experimental and numerical study. *Earthquake Engineering and Structural Dynamics* 2005; 34:965-983.

[2.37] Ramallo JC, Johnson EA, Spencer BF. Smart base isolation systems. *Journal of Engineering Mechanics* 2002. 128(10): 1088-1100.

[2.38] Alhan C, Gavin HP, Aldemir U. Optimal control: basis for performance comparison of passive and semiactive isolation systems. *Journal of Engineering Mechanics* 2006; 132(7):705-713.

[2.39] Cui S, Bruneau M, Kasalanati A. Behavior of bidirectional spring unit in isolated floor systems. *Journal of Structural Engineering* 2010; 136(8): 944-952.

[2.40] Liu S, Warn GP. Seismic performance and sensitivity of floor isolation systems in steel plate shear wall structures. *Engineering Structures* 2012; 42: 115-126.

[2.41] Fujita T. Earthquake isolation technology for industrial facilities-research, development and applications in Japan. *Bulletin of the New Zealand national society for earthquake engineering* 1983. 18(3):224-249.

[2.42] Hamidi M, Naggar MHE. On the performance of SCF in seismic isolation of the interior equipment of buildings. *Earthquake Engineering and Structural Dynamics* 2007; 36:1581-1604.

[2.43] Lambrou V, Constantinou MC. Study of seismic isolation systems for computer floors. Rep. No. NCEER-94-0020, State University of New York at Buffalo, Buffalo, N.Y., 1994.

[2.44] Spencer BF, Dyke SJ, Sain MK, Carlson JD. Phenomenological model of a magnetorheological damper. *Journal of Engineering Mechanics* 1997; 123(3):230-238.

[2.45] Wang DH, Liao WH. Magnetorheological fluid dampers: a review of parametric modeling. *Smart Materials and Structures* 2011; 20:1-34.

[2.46] Choi SB, Lee SK. A hysteresis model for the field-dependent damping force of a magnetorheological damper. *Journal of Sound and Vibration* 2001; 245(2):375-383.

[2.47] Nagarajaiah S, Narasimhan S. Smart base-isolated benchmark building. Part II: phase I sample controllers for linear isolation systems. *Earthquake Engineering and Structural Dynamics* 2006; 13:589-604.

[2.48] Dyke SJ, Spencer BF. A comparison of semi-active control strategies for the MR damper. Proc. of the IASTED international conference, *Intelligent Information system* 1997. The Bahamas.

[2.49] Li H, Ou J. A design approach for semi-active and smart base-isolated buildings. *Structural Control and Health Monitoring* 2006; 13: 660-681.

[2.50] Xu Zhou, Agrawal AK. Semi-active control of seismically excited base-isolated building model with friction pendulum systems. *Structural Control and Health Monitoring* 2008; 15:769-784.

[2.51] Spencer BF, Suhardjo J, Sain MK. Frequency domain optimal control strategies for aseismic

protection. *Journal of Engineering Mechanics* 1994; 120(1): 135-158.

[2.52] Arnold WF, Laub AJ. Generalized eigenproblem algorithms and software for algebraic Riccati equations. *proc. IEEE* 1984; 72: 1746-1754.

[2.53] Nagashima I, Maseki R, Asami Y, Hirai J, Abiru H. Performance of hybrid mass damper system applied to a 36-storey high-rise building. *Earthquake Engineering and Structural Dynamics* 2001; 30(11) :1615-1637.

[2.54] Tsang HH, Su RKL, Chandler AM. Simplified inverse dynamics models for MR fluid dampers. *Engineering Structures* 2006; 28:327-341.

[2.55] Ali SF, Ramaswmy A. Hybrid structural control using magnetorheological dampers for base isolated structures. *Smart Material and Structures* 2009; 18:1-16.

[2.56] Ubaidillah, Hudha K, Kadir FAA. Modeling, characterization and force tracking control of a magnetorheological damper under harmonic excitation. *International Journal of Modeling, Identification and Control* 2011. 13(1/2): 9-21.

[2.57] Yang G, Spencer BF, Carlson JD, Sain MK. Large-scale MR fluid dampers: modeling and dynamic performance considerations. *Engineering Structures* 2002; 24: 309-323.

# CHAPTER 3

# Motion capture technique for measurement of equipment behavior

## 3.1 Introduction

### 3.1.1 Background

The response of the nonstructural elements and contents in the structure is an important index in the performance based design. This dissertation will focus on the behavior of the contents including the furniture item and appliances inside the building. One type of commonly used furniture item and appliances is the one equipped with casters at the bottom to enhance its mobility. Compared with the structural response, several features are notable of this kind of furniture item: (i) it has small friction coefficient and the movement is much larger which can reach to meters in an earthquake event [3.1]; (ii) the rotation behavior is significant; (iii) since it is difficult to predict the movement of sliding equipment, measurement of multi targets are required in a test.

A most common and traditional approach to measure the furniture and appliance's response is to mount accelerometers on each appliance and perform double integration of the acceleration data to obtain the corresponding displacement. This procedure is known to bring bias particularly for low frequency domains data [3.2]. Furthermore, at least three accelerometers are required to measure the 2D motion (including rotation) of each appliance. In the test which will be reported in Chapter 4, nearly two hundreds of appliances were installed in the shaking table test, meaning that at least 573 (= 191×3) accelerometers had to be installed to cover the measurement of them all. Another approach is to use displacement transducers such as LVDTs. In that case, a fixed reference for each transducer is needed, and the LVDT has to be physically connected to the measured target by wires. The environment in which many appliances in congestion moved with wires would be extremely messy, and such measurement was naturally impractical.

Recently, quite a few advanced sensors have been made available, for example, the eddy-current sensor [3.3] and the laser Doppler vibrometer [3.4]. First, they are free from contact, and high resolutions are ensured. These new sensors are candidates suited for recording and measurement in the concerned test environment. Drawbacks do exist, however, in these new sensors; some of them cannot cover a large displacement such as 3 m measured for the appliance with casters; and, on top of all they are yet very expensive [3.5]. It is again impractical to apply such sensors for the measurement of so many appliances.

Another alternative is to use the motion capture technique [3.4] with video cameras. This technique is widely used in the measurement of human body's motion [3.6]. It has also been used in the research of civil engineering field [3.4, 3.5, 3.7-3.11]. The cameras adopted in those studies were commonly designed with high recording speed capacity [3.10, 3.11] or with telephoto lenses to ensure high accuracy [3.9], but covered a limited displacement range [3.4, 3.5, 3.7-3.11]. To summarize, the current motion capture technique is characterized primarily by the high accuracy but small coverage of displacement. As easily suspected, the cameras tend to be costly as special devices have to be installed.

In this study, a motion capture technique using readily available commercial video cameras is adopted. The accuracies to measure and estimate the displacement and velocity are validated. Furthermore, when the cameras are installed inside the specimen, the cameras are subjected to vibration. The vibration becomes a source of errors in the displacement estimation. Influence of such vibration and method to mitigate the associated error is investigated.

### 3.1.2 Organization

The methodology of motion capture technique is introduced in Section 3.2. Shaking table tests were conducted to examine the accuracies of the motion capture technique with different camera angles, number of cameras, maximum displacement and frequency in the movement, among others, with a setup in which the cameras were free from vibration in Section 3.3. Section 3.4 discusses the influence of the camera's vibration to the measuring accuracy, and a method is proposed to correct the results obtained from the video subjected to vibration. Further insight into the influence of serious vibration problem is reported in Section 3.5. The idea of designing a rubber isolated camera system is described.

## 3.2 Methodology of motion capture technique

### 3.2.1 Projective mapping

When extracting the motion recorded in the video camera, the image in the camera has to be translated into digitized displacement data. Techniques for the translation have been established (e.g., [3.12]), and commercial software has been made available (e.g., [3-6]). As presented in detail at next section, this study calculates the real displacement of the target with a correction method to consider the vibration problem of the camera. A code using MATLAB [3.13] to translate the image data into the corresponding displacement data is developed. In what follows, the translation procedure that formed the basis of the code is outlined briefly.

A general projective camera can be described using a pinhole camera model [3.12] shown in Figure 3.1. To reconstruct a scene from the image, the relationship between coordinates of point $P$ in the world coordinate system with the coordinates of its corresponding image point $p$ in the image plane, must be established. The task to estimate the relationship for a single camera or a set of

multiple cameras is termed “camera calibration”.

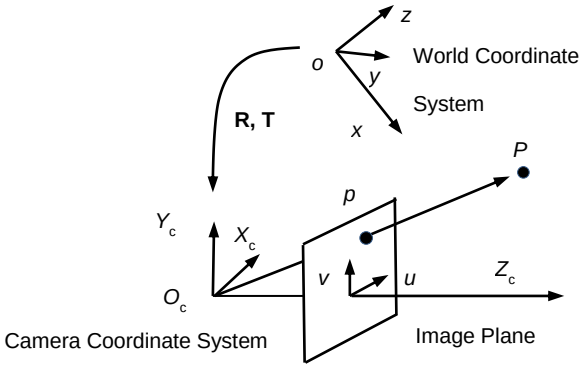


Figure 3.1 Pinhole model

There are three coordinate systems in the pinhole camera model shown in Figure 3.1. First, the relationship between the image plane and the camera coordinate system can be described in Equation (3.1)

$$w\begin{pmatrix} u \\ v \\ 1 \end{pmatrix} = \mathbf{A}\begin{pmatrix} X_c \\ Y_c \\ Z_c \end{pmatrix} \tag{3.1}$$

In which, $(u, v, 1)^T$ is the homogeneous vector of the 2D space point $p$ in the image plane coordinate system, $w$ is a scale factor, and $(X_c, Y_c, Z_c)^T$ is the vector of the 3D space point $P$ in the camera coordinate system. **A** is called the intrinsic matrix, which contains five parameters when nonlinear intrinsic parameters including lens distortion are ignored [3.8].

Second, the relationship between the world coordinate system and camera coordinate system can be determined by the rotation matrix **R** with a dimension of 3×3, and the translation vector **T** with a dimension of 3×1

$$\begin{pmatrix} X_c \\ Y_c \\ Z_c \end{pmatrix} = \mathbf{R}\begin{bmatrix}\mathbf{I} & \mathbf{T}\end{bmatrix}\begin{pmatrix} x \\ y \\ z \\ 1 \end{pmatrix} \tag{3.2}$$

In which, $(x, y, z, 1)^T$, is the homogeneous vector of the 3D space point $P$ in the world coordinate system; **R[I T]** contains six parameters to describe the six degrees of freedom of the camera; and **I** is a unity matrix with a dimension of 3×3. For easy understanding, Equations (3.1) and (3.2) yield Equation (3.3) by combining the intrinsic matrix, rotation matrix and translation vector

$$C_{11}x + C_{12}y + C_{13}z + C_{14} - C_{31}xu - C_{32}yu - C_{33}zu = u$$
$$C_{21}x + C_{22}y + C_{23}z + C_{24} - C_{31}xv - C_{32}yv - C_{33}zv = v \quad (3.3)$$

To determine the eleven parameters, $C_{ij}$, which are referred to as the camera parameters, it is necessary to provide at least six pairs of correspondence between the points in the world coordinate system whose positions (in the 3D coordinates) are known and the 2D coordinates of their images in the image plane. Each world coordinate and image plane coordinate pair gives one equation set (Equation (3.3)) in terms of the camera parameters ($C_{ij}$).

Given the proceeding camera parameters, the unknown values $(x, y, z)^T$ of a sequence of images can be solved from two sets of Equation (3.3), assuming the 2D image plane coordinates of the target are known. This means that at least two cameras are needed to solve the 3D position. For some specific cases, including when the target moves on the ground without overturning or jumping, an additional condition exists

$$z = const. \quad (3.4)$$

where $z$ represents the vertical movement of the target, and it is constant. With this condition, by combining one set of Equations (3.3) and (3.4), it is possible to solve the position of the target. For such a condition, only one camera is needed for the measurement.

For calibration of the two cameras system, a calibration reference with known geometry in the 3D space is required. A reference with a regular shape such as a cuboid is a good candidate, and a total of six markers glued on six corners of the cuboid are needed. On the other hand, four markers are sufficient for the calibration of the one camera system by assuming $z = 0$ in Equation (3.4). In this case, the calibration markers should be placed at the same height ($z$) with the target to track. A planar board with known geometry is sufficient to this end.

### 3.2.2 Marker detection

Data acquisition is traditionally implemented using markers mounted on the target of interest. The markers need to be visible on every frame of the acquired image sequence. The markers can be either active or passive. Passive markers are usually coated with a retro-reflective material to reflect the light back that is generated near the cameras lens. The camera's threshold can be adjusted so that only the bright reflective markers will be sampled, ignoring other details [3.11]. Active markers generally utilize light-emitting diodes (LEDs), mounted on a specific location in the test space.
Rather than reflecting the light back that is generated externally, the markers themselves are powered to emit their own light.

Algorithms have been developed to track the marker position, i.e., the marker coordinates in the image plane (see Figure 3.1). In this study, a commercial program [3.6] capable of extracting the positions of the markers in the image plane was adopted.

## 3.3 Accuracy of motion capture technique

A series of shaking table tests were performed to calibrate the effectiveness and accuracy of the motion capture technique adopted in this study, i.e., the technique using commercial grade digital video cameras. Motion of the furniture that moved in 2D in the horizontal plane including rotation was examined with the three by five meter shaking table facility in Kyoto University.

### 3.3.1 Test program

(1) *Test setup*

Figure 3.2 shows the test setup in the DPRI test. A wagon shown in Figure 3.3 with the sizes of 900×600×880 mm and mass of 50 kg was used as the moving target to be tracked. It was supported by casters, which was of a furniture type commonly used in the hospital. A wooden panel was placed on the surface of the shaking table to reproduce a realistic surface. The rolling friction of the wagon was 0.04 which was very similar to that observed in the E-Defense test. A steel frame was built outside the shaking table, and four steel beams were set at a height of 3 m from the shaking table. Five cameras were clamped at various locations of the beams, with their respective positions noted in parentheses in Figure 3.2 (a). The cameras were located at different positions to fully capture the markers attached on the furniture which moved with rotation.

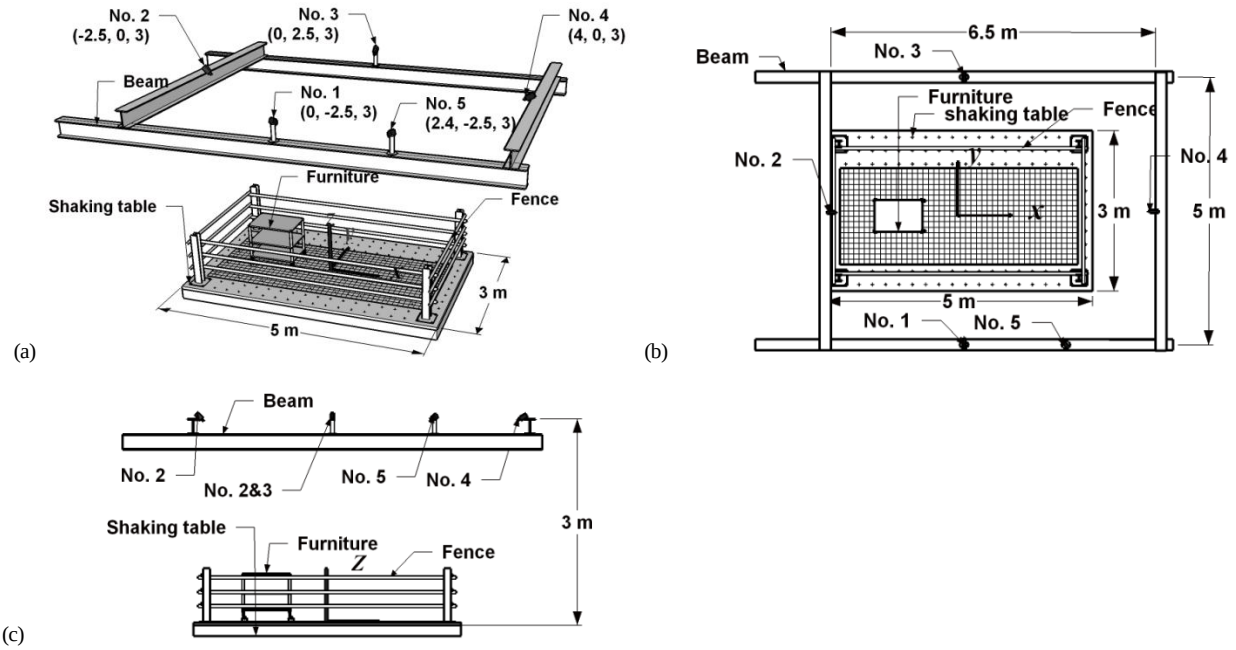


Figure 3.2 Test setup: (a) bird view; (b) layout plan; (c) elevation

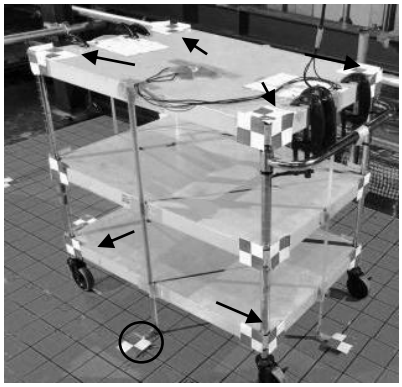

Figure 3.3 Tested wagon

(2) *Input motions*

The four story RC hospital structure [3.1] was tested in E-Defense for both the base-isolated and fixed-base cases. To replicate the furniture behavior on the fourth floor of the hospital structure, the fourth floor responses, JMA_BI and JMA_BF (for the base-isolated and fixed-base cases, respectively), when subjected to JMA ground motion (Kobe earthquake in 1995, recorded at JMA station) and SAN_BF (for the fixed-base case) when subjected to Sannomaru ground motion (an long-period artificial ground motion [3.1]) input motions were chosen. For comparison, the JMA ground motion itself was also adopted. In addition to those non-stationary motions, a variety of sinusoidal waves with different frequencies and amplitudes were selected to examine the accuracy of the motion capture technique in measuring large amplitude responses. The adopted frequencies ranged from 0.5 Hz to 5 Hz. The frequency of 0.5 Hz was similar to the dominant floor response frequencies for the base isolation case. The highest frequency of 5 Hz was chosen to examine the capacity of the motion capture technique to trace higher frequencies. In addition to those input motions, a manually driven test was also conducted by hard-pushing the furniture sequentially in various directions by hand to create large displacements. Table 3.1 summarizes the information of the chosen input motions.

Table 3.1 Input ground motions

| Input motions | Direction | PGA($m/s^2$) |
|---|---|---|
| JMA_BI | XY | 1.6/1.6 |
| JMA_BF | XY | 9.5/6.3 |
| SAN_BF | XY | 4.0/2.9 |
| JMA | X | 8.2 |
| Sin0.5Hz | X | 2.7 |
| Sin0.6/0.3Hz | X/Y (X: 0.6 Hz, Y: 0.3Hz) | 2.8/0.7 |
| Sin1Hz | X | 6.0 |
| Sin5Hz | X | 9.0 |
| Manually driven[(a)] | XY | Not applicable |

[(a)] Furniture pushed by hand

(3) *Instrumentations and markers*

The distances between the cameras and targets were from 2.5 to 4.5 m dependent on the position of the moving furniture as well as the position of respective cameras. The recording speed of the cameras was 30 frames per second (fps). All cameras were equipped with a CMOS image sensor and were able to capture 1,920 by 1,080 pixels resolution video. In the test, the horizontal field of view of the cameras was about 2.6 to 6.0 m for different camera locations so that "one pixel" represented about 1.5 to 3.0 mm. For all cameras, the shutter speed was set at 1/200. One or two cameras out of the five were selected to capture the furniture movement based on the motion capture technique described in Section 3.2.

To measure the true displacement of the furniture, fine grid lines were drawn on the wooden panel placed on the shaking table. The motion of the tested furniture was measured by tracking the item on the grid lines frame by frame in the video. The error of the results expected from the grid measurement was estimated to be at most ± 5 mm.

Figure 3.4 shows the adopted checker type marker.

Figure 3.4 Checker type maker

### 3.3.2 Discussion of test results

(1) *Camera angles*

In actual test conditions, the potential position for the cameras is likely limited because of various constraints in the setup. Figure 3.5 shows two different angles which may influence the results, i.e., the angle $\alpha$ between two cameras and the angle $\beta$ between the line from the camera to target and the horizontal plane.

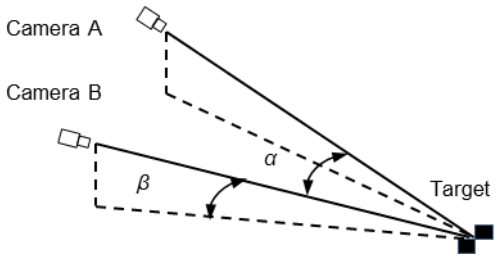


Figure 3.5 Angles between camera and horizontal plane

If the two cameras system is used, a relative position of the two cameras, i.e., the angle $\alpha$, is a concern. The differences in accuracy for four different angles were checked under the input motion Sin1Hz. The wagon was used for the test item. The difference between the maximum displacement measured by the motion capture technique and that estimated from the grid on the wooden panel was adopted as the index for comparison. The test results in Table 3.2 shows that the motion

capture technique was satisfactory for $\alpha$ ranging from 34˚ to 102˚ with similar differences not greater than 5 mm (relative to the maximum displacement of 373 mm). This brings a benefit to the test as it adds flexibility in the positioning of cameras.

As the furniture moved on the shaking table, angle $\beta$ varied from about 20˚ to 80˚ during the tests. The results show that there were no difficulties to accurately capture the target motions within this angle range.

Table 3.2 Influence of camera angles to measuring accuracy

| Angle | 34˚(No.1&5) | 49˚ (No.1&2) | 77˚ (No.1&3) | 102˚ (No.2&4) |
|---|---|---|---|---|
| Difference (mm) | 3 | 2 | 3 | 2 |

(2) *One camera system versus two cameras system*

The displacement histories measured using one camera or two cameras systems are compared in Figure 3.6 for the movement of the wagon under the Sin1Hz input motion. The results indicate that both methods maintained similar accuracy, with the difference not greater than 1 mm, for the displacement measurement. The one camera system has an advantage of significantly saving time in data processing as the two cameras system requires sensitive synchronization of the starting times of the two videos.

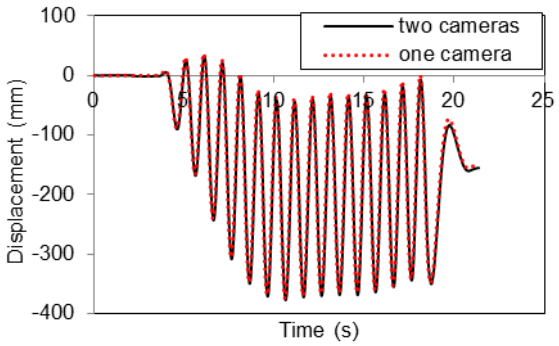


Figure 3.6 Difference between one camera and two cameras systems

Figure 3.7 shows an example of the effect of unsynchronization on measurement accuracy, in which the displacement history of the shake table itself under the Sin1Hz input motion and estimated by the two cameras system is plotted, one without a frame lag and the other with one frame lag of 1/200 s. The table's displacement was measured separately by the LVDT sensor attached to the table. The value was taken as the true displacement, and its history also is also plotted in Figure 3.7. The error remained not greater than 5 mm for the case without the frame lag when compared with the true displacement. In contrast, the results with one frame lag between the two cameras caused an error of about 20 mm.

The results indicate that the one camera system is equally accurate as and significantly handier than the two cameras system. Note, however, that this statement is applicable only for the

measurement of 2D motion and the two cameras system is a must for measuring 3D movement in reference to Equation (3.3).

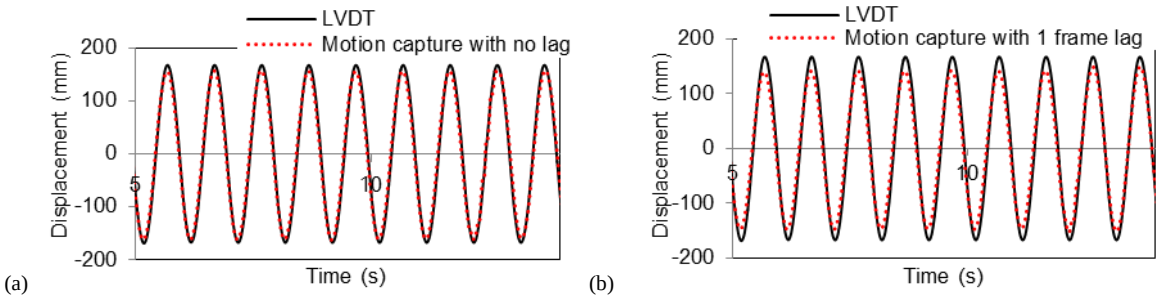


Figure 3.7 Influence of unsynchronization in two cameras system:
(a) with no lag; (b) with 1 frame lag

(3) *Recording speed of camera*

Typically, the recording speed of the commercial grade camera, i.e., the recording frame rate, is limited under one hundred frames per second (usually 24fps, 30fps or 60fps), which is much lower than the recording speed of industrial grade camera, which is up to hundreds or thousands fps. The accuracy of displacement measurement with the low recording speed camera is of concern, since the commercial grade cameras are cheaper than the industrial grade ones, and they are preferred for the use in our research domain.

Figure 3.8 shows two example cases of the movement of the unlocked wagon and locked CD under Sin1Hz input motion and JMA motion, respectively. The comparison shows accuracies to measure displacement using 30 fps and 60 fps cameras are nearly identical.

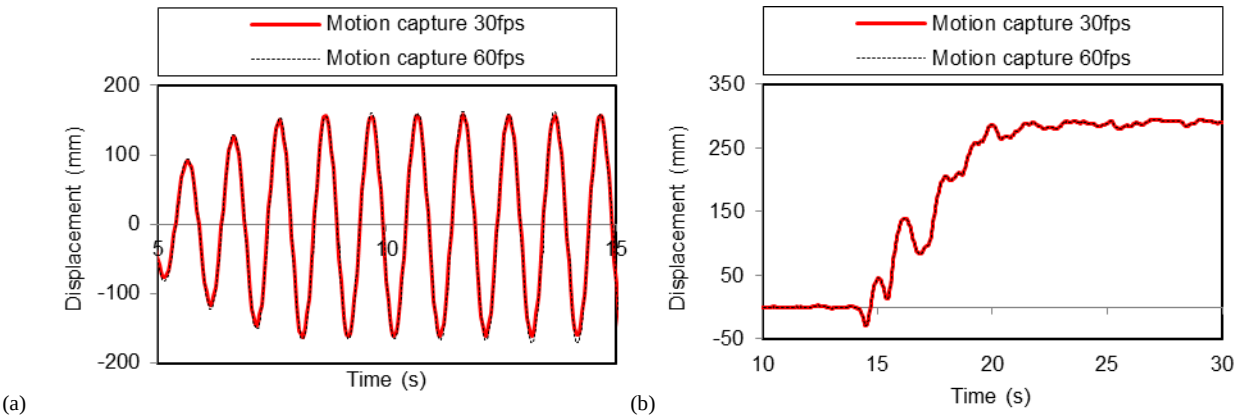


Figure 3.8 Measuring accuracy of camera with different recording speeds under:
(a) Sin1Hz; (b) JMA

### 3.3.3 Displacement measuring accuracy

The main source of the error in motion capture results is the misdetection of the marker from its true location in the image plane. The amplitude of the error is determined by the number of pixels dislocate from its true location and the image resolution *mmpp*, defined here as the real distance (in

millimeters) that a pixel represents.

The accuracy of displacement measurement was checked by comparing the results from the motion capture technique with those estimated by the grid on the shaking table. The motion of the shaking table itself was also estimated by the adopted motion capture technique. In that case, the displacement measured by the LVDT attached to the table was referred to as the true displacement. More than one hundred cases were examined for various combinations of furniture and caster conditions as well as input motions. Representative results are listed in Table 3.3. The table shows the maximum displacements obtained from the motion capture technique as well as their differences from the grid or LVDT measurement.

It was found that the differences between motion capture results and reference results (from grid reading or shaking table LVDT) were not greater than 10 mm regardless of the amplitudes of the movements (ranging from 8 mm to 3,125 mm). Considering the magnitude of errors caused by reading the grid, i.e., about ± 5 mm, the maximum displacement errors expected by the motion capture technique were estimated less than 3 times of the corresponding *mmpp*. When referring to the displacement errors associated with the motion of the shaking table itself, they never exceeded 5 mm (as shown in the bottom six rows of Table 3.3). Considering that the measurement using the LVDT attached to the shaking table was more accurate than what was obtained from the grid, the error level of less than 3 times of the corresponding *mmpp* is deemed reasonably conservative.

Figure 9 shows three examples of the moving orbits and displacement time history when the wagon was subjected to the Sin0.6/0.3Hz and manually-driven motion, and when shaking table was subjected to JMA_BF. It shows that the motion capture method was able to trace the motion satisfactorily.

Table 3.3 Difference of displacement between results from motion capture and true value

| Input motions | Target to track | *mmpp* | Maximum displacement (mm) | Difference (mm) |
|---|---|---|---|---|
| Sin0.6/0.3Hz | Wagon | 5 | 2071 | 10 |
| Sin1Hz | Wagon | 3 | 373 | 4 |
| SAN_BF | Wagon | 4 | 1833 | 7 |
| Manually | Wagon | 5 | 3150 | 6 |
| Sin5Hz | Wagon | 3 | 1570 | 6 |
| JMA | Wagon | 5 | 648 | 9 |
| JMA_BF | Wagon | 4 | 545 | 6 |
| Sin1Hz | Shaking table | 3 | 259 | 1 |
| Sin5Hz | Shaking table | 2 | 8 | 1 |
| JMA | Shaking table | 2 | 78 | 5 |
| JMA_BF | Shaking table | 4 | 97 | 0 |
| SAN_BF | Shaking table | 3 | 255 | 1 |

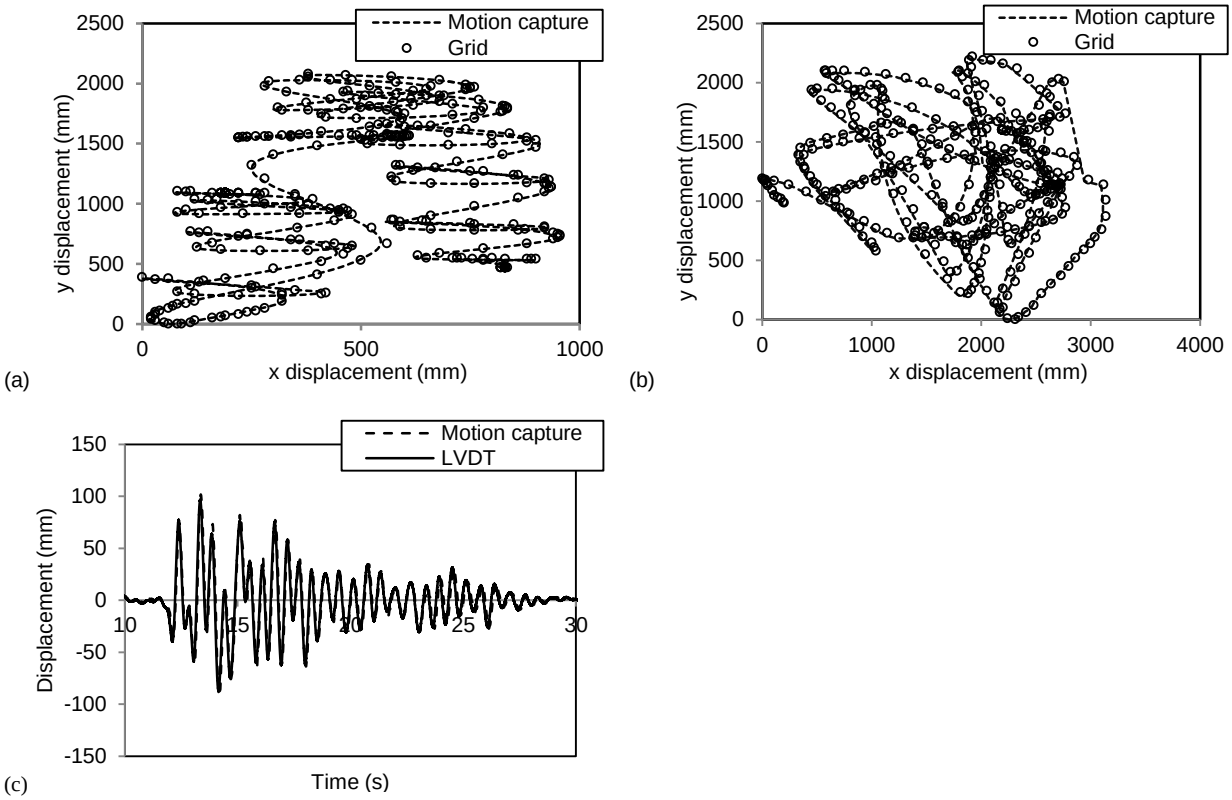


Figure 3.9 Motion capture displacement under: (a) Sin0.6/0.3Hz; (b) Manually-driven; (c) JMA_BF

### 3.3.4 Velocity estimation accuracy

The true velocity of the furniture was not available for the furniture tested. Therefore, only shaking table was used as the target for estimating the velocity and acceleration accuracies.

The velocity of the shaking table was obtained by differentiating the displacement from the motion capture technique. For the reference to compare the velocity and acceleration from motion capture, the velocity of shaking table was obtained by differentiating the displacement from the LVDT sensor installed in the shaking table.

Table 3.4 lists the comparison results in terms of the maximum velocity. This shows that the motion capture technique is able to estimate the velocity with a good accuracy (errors are less than 5%) for both low and high frequency (up to 5 Hz) movements.

Table 3.4 Difference of velocity and acceleration between results from motion capture and the true values

| Input motions | Maximum velocity (m/s) | Velocity differences (%) |
|---|---|---|
| Sin0.6/0.3Hz | 0.29 | 5% |
| Sin 0.5 Hz | 0.81 | 4% |
| Sin 1 Hz | 1.5 | 3% |
| Sin 5 Hz | 0.25 | 5% |
| JMA_BF | 0.83 | 1% |
| SAN_BF | 0.63 | 5% |

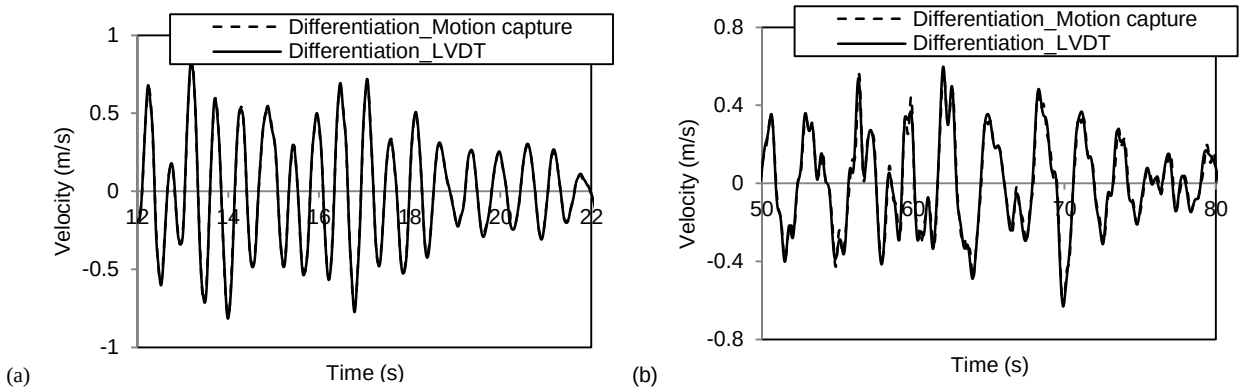


Figure 3.10 Motion capture velocity of shaking table under: (a) JMA_BF; (b) SAN_BF

## 3.4 Camera vibration and correction

### 3.4.1 Influence of vibration

In the test conducted in DPRI, the cameras were installed outside the shaking table, and they were relatively free from vibration induced by the shaking. However, in many realistic situations, such as the test conducted in E-Defense [3.1], cameras are most likely installed within the specimen, meaning that the cameras are inevitably subjected to vibration.

The vibration of the camera can cause the parameters that define the relative relationship between the camera and target to change. Consequently, the results will include non-negligible errors if the technique described in Section 3.2 is passively adopted. Depending on the severity of vibration as well as the camera's quality, the intrinsic parameters such as the focal length may also be subjected to change. In what follows, a technique to consider the vibration and correct the measured displacement is presented.

### 3.4.2 Correction method

To correct the error, the direct method (Method 1) is to calibrate the camera parameters $C_{ij}$ for every frame of the video using four reference markers that do not change their positions. However, this method may become unfeasible to find the four reference markers especially when the space is crowed and the items in the space are moving in a complex 2D pattern. An alternative method (Method 2) is proposed.

Figure 3.11 (a) shows a camera subjected to vibration. The camera is normally fixed to the wall with a support (usually a metal support to provide large stiffness). Vibrations in and around the $y$ axis, i.e., the translation and rotation along and around the camera's longitudinal direction, are deemed insignificant compared to the vibrations in other directions.

Assume there is no vibration at time $t_i$, and vibration occurred at time $t_i+\Delta t$. Figure 3.11 (c) and (d) show the translation and rotation movements of the camera caused by vibration. Translation movement of the camera will cause the angle $\alpha$ for the target to change by $\delta\alpha$ as shown in Figure

3.11(c). Angle $\theta$ is defined as the angle between the line from the center of the camera sensor and camera lens, and the moving plane. Rotation movement will cause the angle $\theta$ to change by $\delta\theta$ as shown in Figure 3.11 (d). The $u$ direction in the image coordinate is defined as the moving direction of the target in the image due to vibration; and its projection on the moving plane of the target is defined as $x$ direction for the world coordinate. The coordinate $u$ of the target in the image plane without vibration can be expressed as

$$u = f\tan(\alpha - \theta) \tag{3.5}$$

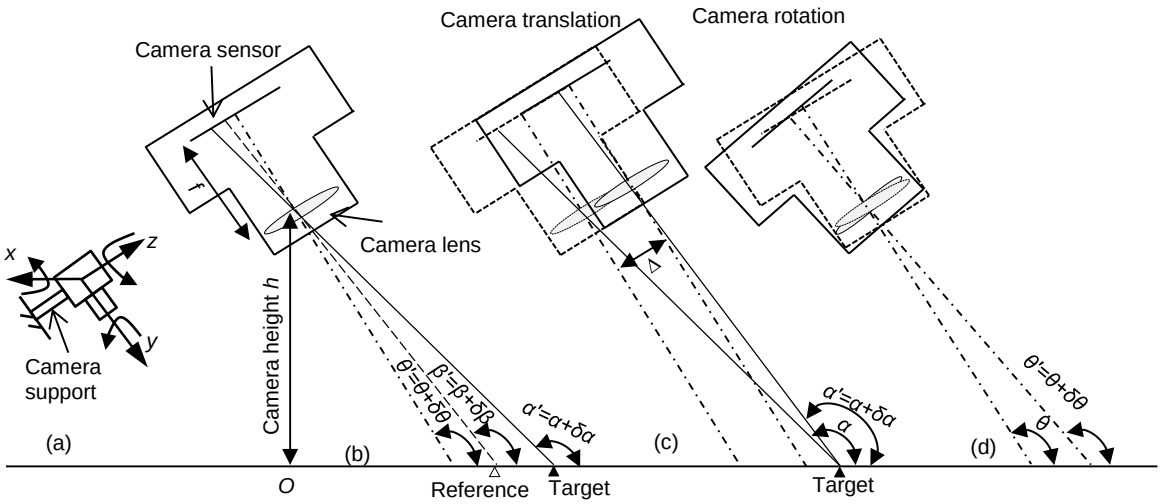


Figure 3.11 Influence of camera vibration: (a) camera vibration; (b) calculation of error; (c) camera translation; (d) camera rotation

The real displacement before vibration can be expressed in Equation (3.6) by assuming $y$=0 and $z$=0 in Equation (3.3)

$$x = \frac{u - C_{14}}{C_{11} - C_{31}u} \tag{3.6}$$

where $C_{11} = f/h$, $C_{14} = f/\tan\theta$, and $C_{31} = -\cos\theta/(h\sin\theta)$. $f$ is the camera focal length, and $h$ is the camera height as shown in Figure 3.11(b).

The new coordinate $u'$ of the target can be calculated as the sum of the original coordinate $u$ and the coordinate change $\Delta u$, which here is defined as the change of the relative position in the image plane of the target and a reference point, whose position does not change during the test

$$\Delta u = f\left(\left(\tan(\alpha' - \theta') - \tan(\beta' - \theta')\right) - \left(\tan(\alpha - \theta) - \tan(\beta - \theta)\right)\right) \tag{3.7}$$

where $\beta$ and $\beta'$ are the angles for the reference point before and after vibration as shown in Figure 3.11 (b). Assume there is no real movement for the target, $\Delta u$ should be 0. However, the vibration of camera causes the coordinate $u$ to change. The error in estimating the real displacement of target in the word coordinate is

$$\Delta x = \frac{(u+\Delta u)h\sin\theta - fh\cos\theta}{f\sin\theta + (u+\Delta u)\cos\theta} - \frac{uh\sin\theta - fh\cos\theta}{f\sin\theta + u\cos\theta} \tag{3.8}$$

With Equation (3.7), if $\Delta x$ in Equation (3.8) can be significantly suppressed, then the influence of vibration can be mitigated.

To prove this, two examples are shown in Figure 3.12 for the displacement results with correction Method 2, for a camera setting as: $h$=3000 mm, $\theta$=135º, $\delta\theta$=1º and $\Delta$=5 mm. This setting can guarantee the coving range of the camera of about 5 m for a camera with the angle of view of 40º, and it is suitable for the setting in the E-Defense test. Two $\alpha$ values, i.e., 145º and 130º, are used to examine the error for the target at different locations. Value $\beta$ is varied to examine the error with respect to the location of the reference. The dashed line shows the error without correction. By comparison, the error using the correction Method 2 could reduce the error to less than 4% of that without correction, when the angle $\beta$ is between 125 º to 145º, i.e., $\beta=\theta\pm10$º. For a camera with the angle of view of 40º, the reference point can be set at the location that its image point is in the central area of the image plane within half of the image size.

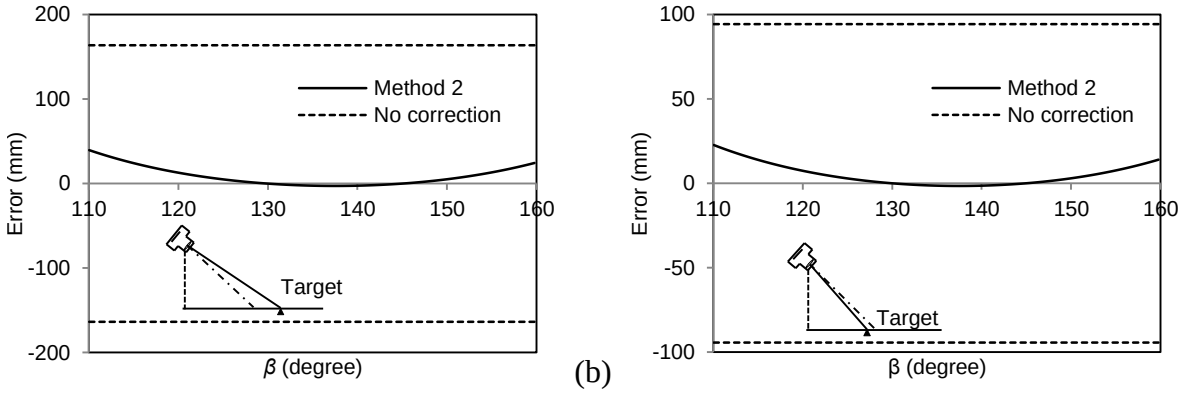


Figure 3.12 Comparison of the results with and without correction: (a) $\beta$=145º; (b) $\beta$=130º

### 3.4.3 Shaking table test result

Figure 3.13 (a) shows the moving orbit of an incubator obtained from the E-Defense test, which will presented in Chapter 4. The appliance is selected because it was placed in a room with only few appliances so that it was possible to set four markers to correct the results using Method 1. The appliance was subjected to JMA Kobe ground motion. The motion caused relatively large vibration of the camera and consequently the motion capture results included significant errors if no correction was

made. The two methods were used to correct the data. The corrected results show that the two methods gave nearly identical results over the duration of the motion. As for the accuracy, the uncorrected displacement in *y* direction was 403 mm, and the corrected displacements using both the two correction methods were 149 mm for a selected point for comparison, while the true value obtained from reading the grid on the floor was 150 mm. This indicates that the error was very small (not greater than 1% in this example) if corrected properly, which could be more than 100% otherwise.

(a)

(b)

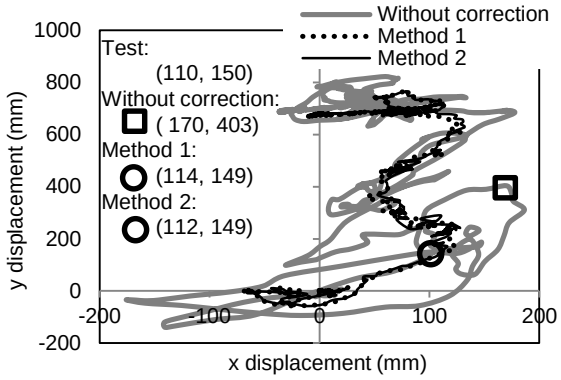


Figure 3.13 Correction of motion capture displacement: (a) incubator; (b) moving orbit

As for the comparison between Methods 1 and 2, Method 2 needs only one reference marker rather than a minimum of four makers needed for Method 1. Method 2 is computationally much faster (by more than ten times) than Method 1 in the real practice, making obvious the practical advantage of Method 2. This statement is more relevant particularly when many furniture items are to be measured.

## 3.5 Summary

A motion capture technique is presented for the measurement of the appliance's movement in shaking table test. The basic issues, including the influence of the angles between cameras, number of cameras needed, and accuracy in measuring displacements and estimating velocities, are examined through a series of shaking table test. The influence of camera vibration to the measuring accuracy is also discussed. The following conclusions are drawn from this chapter:

(1) Both the one camera and two cameras systems have similar accuracy in measuring the 2D movement. The one camera system is handier since it can save processing time and avoid errors that would occur in synchronizing the two videos.

(2) The test shows that it is promising to use motion capture to measure the large amplitude displacement. In addition, the captured displacement can also be used to estimate the velocity of the appliance through a differentiating process of the displacement. The error in measuring the displacement using motion capture is estimated of less than 3 times of the image resolution. Motion capture technique can estimate the velocity with an error of less than 5% of the maximum velocity.

(3) When the cameras are set inside of the testing environment, they are susceptible to vibration,

which is a source to promote errors. A simple method is proposed using a reference marker to calculate the relative change of the positions of the target marker and the reference marker, to obtain the actual displacement. Test results show that this method is effective.

# REFERENCES


[3.1] Sato E, Furukawa S, Kakehi A, Nakashima M. Full shaking table test for examination of safety and functionality of base-isolated medical facilities. *Earthquake Engineering and Structural Dynamics* 2011; 40: 1435-1453.

[3.2] Hudson DE. Reading and interpreting strong motion accelerograms, EERI engineering monographs on earthquake criteria, structural design, and strong motion records. Earthquake Engineering Research Institute, Berkeley, Calif ,1979.1.

[3.3] Mizuno T, Enoki S, Hayashi T, Asahina T, Shinagawa H. Extending the linearity range of eddy-current displacement sensor with magnetoplated wire. *IEEE TRANSACTIONS ON MAGNETICS* 2007; 43 (2): 543-547.

[3.4] Chang CC, Xiao XH. Three-dimensional structural translation and rotation measurement using monocular videogrammetry. *Journal of Engineering Mechanics* 2010; 136(7): 840-848.

[3.5] Ji YF. Nontarget image based technique for small cable vibration measurement. *Journal of Bridge Engineering* 2008; 13(1): 34-42.

[3.6] PV STUDIO 3D. LAB Corporation, Japan.

[3.7] Gongkang F, Adil GM. An optical approach to structural displacement measurement and its application. *Journal of Engineering Mechanics* 2002; 128(5): 511-520.

[3.8] Chang CC, Ji YF. Flexible Videogrammetric technique for three-dimensional structure vibration measurement. *Journal of Engineering Mechanics* 2007; 133(6): 656-664.

[3.9] Olaszek P. Investigation of the dynamic characteristic of bridge structures using a computer vision method. *Measurement* 1999; 25(3): 227-236.

[3.10] Poudel UP, Fu G, Ye J. Structural damage detection using digital video imaging technique and wavelet transformation. *Journal of Sound and Vibration* 2005; 286: 869-895.

[3.11] Hutchinson TC, Chaudhuri SR, Kuester F, Auduong S. Light-based motion tracking of equipment subjected to earthquake motions. *Journal of Computing in Civil Engineering* 2005; 1(3): 292-303.

[3.12] Hartley R, Zisserman A. Multiple view geometry in computer vision, 2nd Ed. Cambridge University Press, Cambridge, U. K., 2004.

[3.13] MATLAB 2012b. The MathWorks, Inc., Natick, Massachusetts, USA.

[3.14] Weng J, Cohen P, and Herniou M. Camera calibration with distortion models and accuracy evaluation. *IEEE Transactions on pattern analysis and machine intelligence* 1992; 14(10): 965-980.

# CHAPTER 4

# Full-scale shaking table test of base-isolated and fixed-base hospital

## 4.1 Introduction

### 4.1.1 Background

In urban society characterized by density, rapidity, globalization, among many others, how to ensure the business continuity is a critical concern. In Japan and many other earthquake-prone countries, large earthquakes are a major source that would impede the business continuity as evidenced by recent damaging earthquakes such as the 2011 Tohoku earthquake. It is also notable that critical emergency facilities such as fire stations and hospitals have to remain functional immediately after a damaging earthquake as they are the key stations critical for emergency responses. These facts clearly demonstrate that important structures must warrant not only safety (meaning no collapse) but continuing functionality as well even after most damaging earthquakes.

Base-isolation has been recognized as a solution for enhanced functionality of important structures, and applications have grown significantly for the past three decades. In Japan, the construction of base-isolated building structures started growing precipitously after the 1995 Kobe earthquake, and by 2010 over 2,500 such buildings have been in use. It is also notable that this technology has been accepted most popularly to medical facilities. However, the true benefit of base-isolation (in terms of the enhanced functionality of medical facilities) has not been fully calibrated yet as none of the built base-isolated medical facilities sustained very large earthquake motions whose magnitudes are equivalent to DBE or MCE levels in seismic design.

To better capture the true benefit of base-isolation, a series of large shaking table tests were conducted for a full-scale, four-story base-isolated hospital made of reinforced concrete [4.1]. The test was conducted using the E-Defense facility, known as the world largest shaking table. Major nonstructural components and plumbing systems were installed, and rooms were furnished with hundreds of furniture and equipment items to simulate the real hospital as close as possible. Both short-period ground motion and long-period long-duration motions were used in the test.

### 4.1.2 Organization

Section 4.2 introduces the design of the test specimen and the testing program. Information on the two

types of motions is presented. Section 4.3 and Section 4.4 discuss structural responses and medical appliances' responses in the base-isolated and fixed-base systems, respectively.

## 4.2 Design of test specimen and testing program

### 4.2.1 Specimen design

Figure 4.1 shows the base-isolated hospital specimen. The superstructure was designed with a base shear of 0.3 with respect to the level 1 (medium) design earthquake based on the current Japanese seismic code [4.2]. It was used as the fixed-base hospital specimen by fixing it to the shaking table directly. It is reasonable to do so because, according to the Japanese design practice both the elastic stiffness and maximum strength required for the superstructure of base-isolated building and fixed-base structure are nearly the same when the structure is low-rise and made of RC with walls.

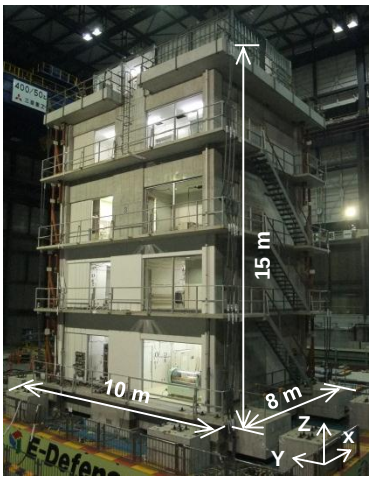


Figure 4.1 Base-isolated hospital specimen

The superstructure was a four-story RC structure with an 8 m by 10 m floor plan and 15 m in height. The total weight was 7470 kN, about 40% of which was the weight of the base floor. Figure 4.2 shows the elevation and plans of the specimen. Columns with section of 600 mm by 600 mm were arranged at the four corners, and the shear walls with section of 2100 mm by 300 mm were arranged at each bay to sustain both gravity and horizontal loads. The size of the beams was 250 mm by 1250 mm for the second floor and 250 mm by 900 mm for the upper floors. The base floor was stiffened with beams large enough to avoid damage when the specimen was lifted by cranes to set it down on the shaking table. The concrete with specified strength $F_c$ of 30 N/mm$^2$ was used for the base floor, and concrete with specific strength $F_c$ of 24 N/mm$^2$ was used for the rest.

The first mode natural period of the superstructure was 0.24 s in both the *X* and *Y* directions, identified with the white noise tests before the shaking table tests.

Two types of isolation systems commonly used in Japan were adopted for the base-isolated specimen. One system was natural rubber bearing combined with U-shaped steel dampers (designated as NRB+U hereafter) as shown in Figure 4.3 (a) and (b), in which the natural rubber

bearings exhibit linear behavior, while the U-shaped steel damper dissipate energy. The other was high-damping rubber bearing (designated as HDRB hereafter) as shown in Figure 4.3 (c), in which the bearing itself dissipated energy. Figure 4.2 (c) shows the arrangement of the base isolators. Consider the superstructure to be rigid, the period of NRB+U system was estimated as 2.56 s and the period of HDRB system was 2.41 s with respect to the secant stiffness measured for the bearing displacement of 300 mm. The major properties of the two types of isolators and the U-shaped steel damper are shown in Table 4.1.

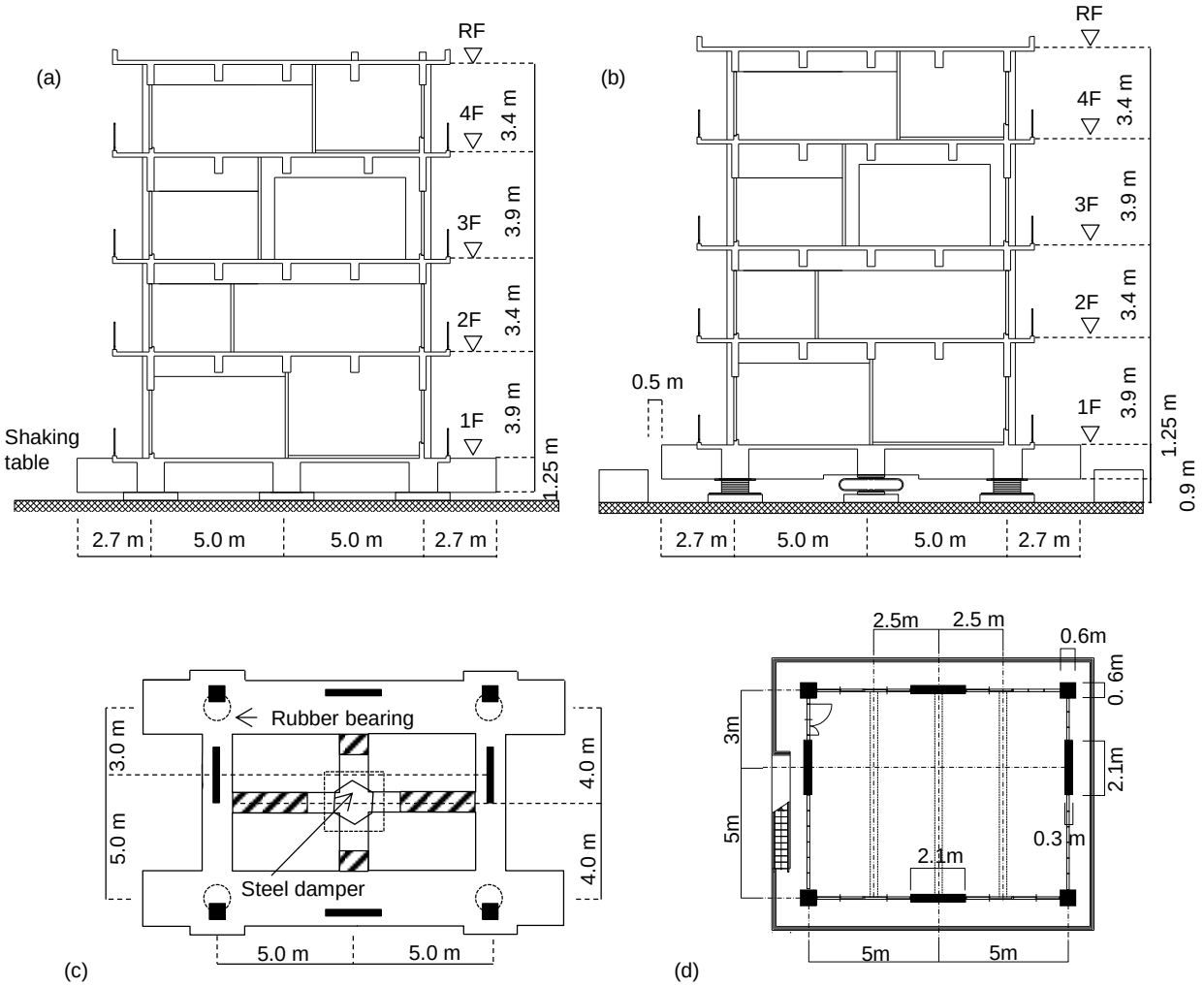


Figure 4.2 Specimen plan: (a) YZ elevation for fixed-base case; (b) YZ elevation for base-isolated case; (c) base floor plan and base isolators arrangement; (d) second to fifth floor plan


Figure 4.3 Base isolation system: (a) U-shaped steel damper; (b) natural rubber bearing; (c) high damping rubber bearing

Table 4.1 Mechanical and material properties of the base isolation devices

| Property | NRB | HDRB | Property | U-shaped steel damper |
|---|---|---|---|---|
| Diameter (mm) | 1000 | 750 | Number of rods | 6 |
| Thickness of rubber (mm) | 285 | 200 | Thickness of rod (mm) | 40 |
| Primary shape factor $S_1$[(a)] | 37.31 | 36.75 | Yield strength (kN) | 348 |
| Secondary shape factor $S_2$[(b)] | 3.51 | 3.75 | Yield displacement (mm) | 28 |
| Shear stiffness (kN/m) | $0.81\times10^3$ | $1.37\times10^3$[(c)] | Initial stiffness (kN/m) | 12,500 |
| Equivalent damping ratio | | 0.24 | Second stiffness (kN/m) | 216 |

[(a)] Primary shape factor defined as sectional area divided by circumferential area of each rubber layer.

[(b)] Secondary shape factor defined as diameter divided by total height of rubber.

[(c)] shear stiffness and equivalent damping ratio estimated for 200 mm displacement.

### 4.2.2 Arrangement of furniture and medical equipment

There were two rooms at each floor as shown in Figure 4.4, following the current hospital design practice.

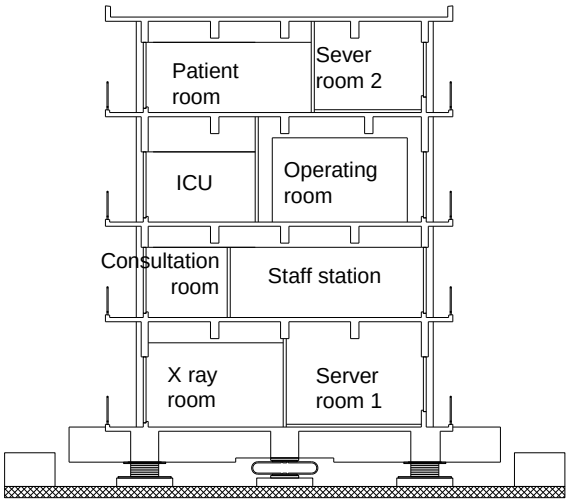


Figure 4.4 Room arrangement

A total of 191 pieces of furniture and medical equipment were installed to the superstructure. They can be categorized into multiple groups in terms of their different behavior under earthquake excitation. (i) easy sliding items, (ii) free standing items, (ii) fixed items, and (iv) suspended items.

(i) Easy sliding items. In the hospital facility, medical equipment and furniture items are commonly supported by casters which enable easy movement. For those items with unlocked caster, the equivalent sliding friction was small (about 0.04). Hence, they were very mobile and flexible and would move with large displacement. Whether the casters of each applicant were locked or unlocked was determined following the advice of medical experts. It was found that about 70% of furniture and medical equipment were supported by casters and about 85% of them were in the caster unlocked condition. (ii) Free standing items. The casters fully locked items and those free standing items

without casters belong to this group. The friction coefficient was about 0.3~0.6. Therefore, their response accelerations were expected to be larger. For those items, large acceleration was a threat to their functionality. Free standing items included medical shelves, patient beds and some heavy appliances such as the operation table, which took about 15% of all the furniture items and medical equipment. (iii) Fixed items. Those items that are easy to topple and fall down during the earthquake, were clamped or mounted to the floor or wall with anchors. Accelerations of those items were close to the floor. This group included some of the medical shelves and furniture items. (iv) Suspended items. Such items were also common in the hospital, including ceiling pendants and surgical lights.

To realize realistic environment as a medical facility, glass bottles, plastic chemical containers and small equipment such as tweezers were stored in shelves and drawers. Mannequins were placed on the operating table (adult) and in the incubator (infant) which had sizes and mass distributions identical to real human bodies. In addition to furniture items and medical appliances, miscellaneous medial related items, wall systems and piping were installed.

Among the rooms (Figure 4.5) arranged with a variety of medical appliances, the operation room disclosed the most impressive behavior, and this was primarily because many medical appliances were equipped with unlocked casters. This chapter focuses on the behavior of the medical appliances in this room. Figure 4.5 shows an overview of the operation room. The operation room was installed on the third floor with the room area of 5 m by 7 m.

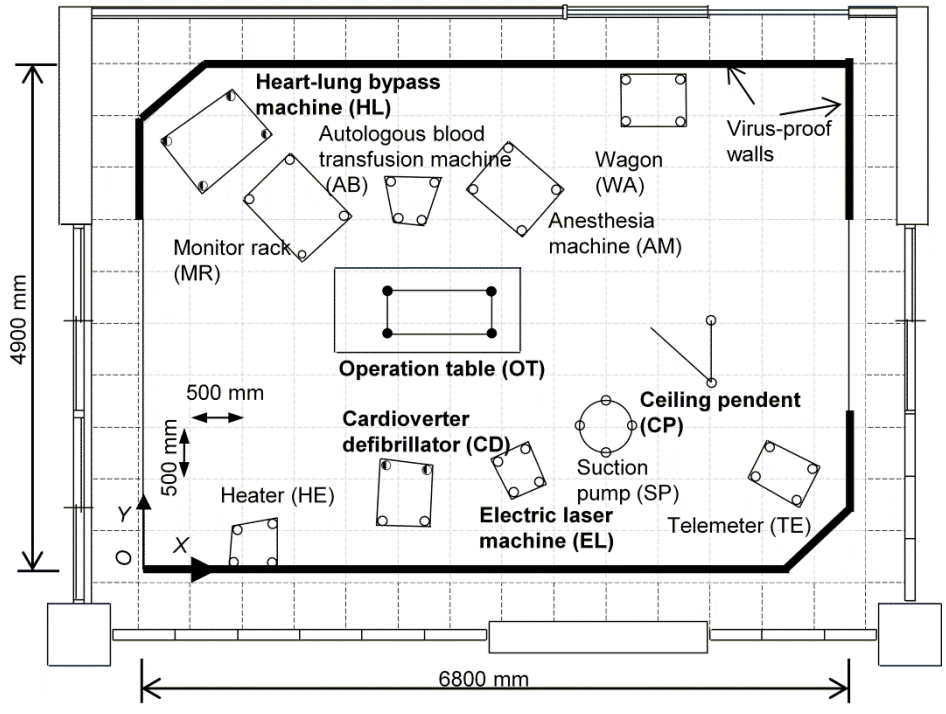


(a)

(b)

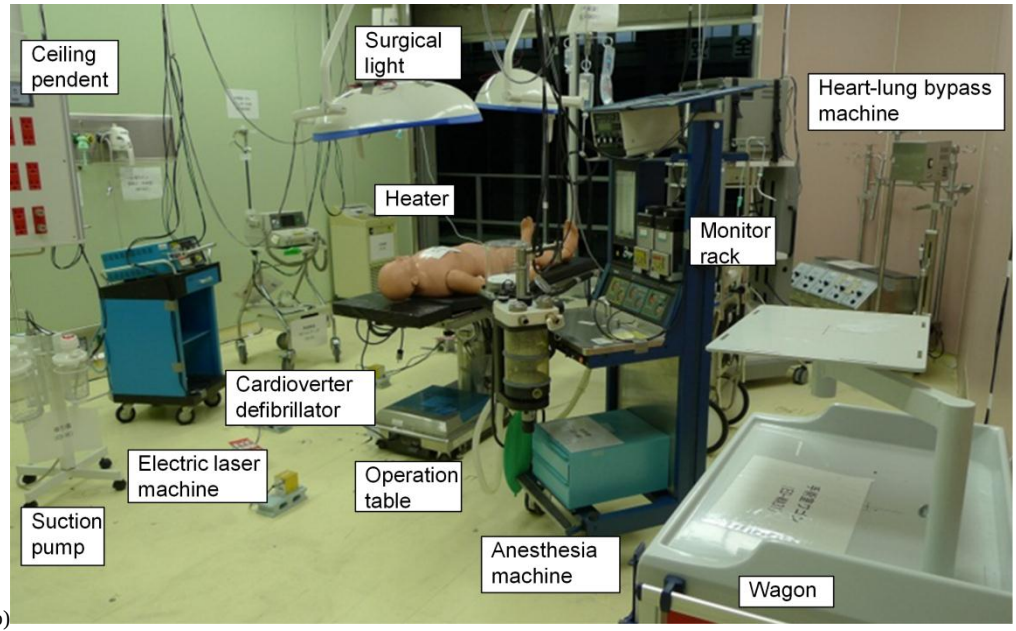


Figure 4.5 Schematic and photos of operation room: (a) layout; (b) photo

Twelve medical appliances were installed in the operation room with the majority of them equipped with casters. The distances between each other were as close as 500 mm. Note that the installed appliances were actual ones (not modeled) and the room arrangement was made realistic by consultation of medical professionals. In Figure 4.5 (a), the appliances tested with locked conditions are marked with black circles, and those tested with unlocked conditions are marked with blank circles. HL and CD were tested in both the unlocked and locked conditions and are marked with half-filled circles.

Among the twelve appliances, five appliances were chosen for detail examination: an operation table (OT), an electric laser machine (EL), a heart-lung bypass machine (HL), a cardioverter defibrillator (CD), and a ceiling pendant (CP). Details about the five appliances are presented in Table 4.2 and Figure 4.6. They are chosen as they represent three typical types of appliances in the operation room, i.e., free standing items (caster locked), easily sliding items with unlocked caster, and pendulum items. Other appliances in the room were all easily sliding items with unlocked casters and had similar behaviors.

OT represented the free standing furniture item. The friction coefficient of OT was 0.63 according to the calibration tests and it was chosen to compare with the other appliances that were equipped with casters. A mannequin having the size and mass distributions similar to a real human body was placed on OT to mimic the patient. Both EL and HL were easily sliding items with unlocked casters. Their friction coefficients were 0.05 and were much smaller than the coefficient of OT, a free standing appliance. HL was also tested with its four casters locked (EL did not have locking devices), having the friction coefficient larger than 0.6. CD had four casters and only the front two had the locking devices, which is common for convenience in busy hospitals. Both the unlocked and locked conditions were tested for CD. CP had two arms (see Figure 4.6 (e)), which could be rotated easily around the joints in horizontal directions with a small force not greater than 30 N. This type of device

was commonly used in the hospital to supply medical gases, electricity, etc.

Table 4.2 Information of typical furniture and equipment in the operation room

| Appliance | Width × Depth × Height (mm) | Weight (N) | Aspect ratio [(a)] | Notable features |
|---|---|---|---|---|
| Operation Table (OT) | 560×2100×830 | 2,560 | 1.5 | Casters locked, $\mu$ [(b)] = 0.63. |
| Electric laser machine (EL) | 410×480×830 | 330 | 2.0 | Casters unlocked, $\mu$ = 0.05. |
| Heart-lung bypass machine (HL) | 900×600×650 | 2,220 | 1.1 | When casters unlocked, $\mu$ = 0.05; when locked, $\mu$ > 0.6. |
| Cardioverter defibrillator (CD) | 350×500×800 | 300 | 2.3 | When casters unlocked, $\mu$ = 0.03; when front two casters locked, $\mu$ = 0.4. |
| Ceiling pendant (CP) | 1770×270×2250 | 243 | Not applicable | Forces to rotate two arms = 30 N and 12 N. |

[(a)] Aspect ratio= height/minimum of width and depth.

[(b)] $\mu$ = friction coefficient.

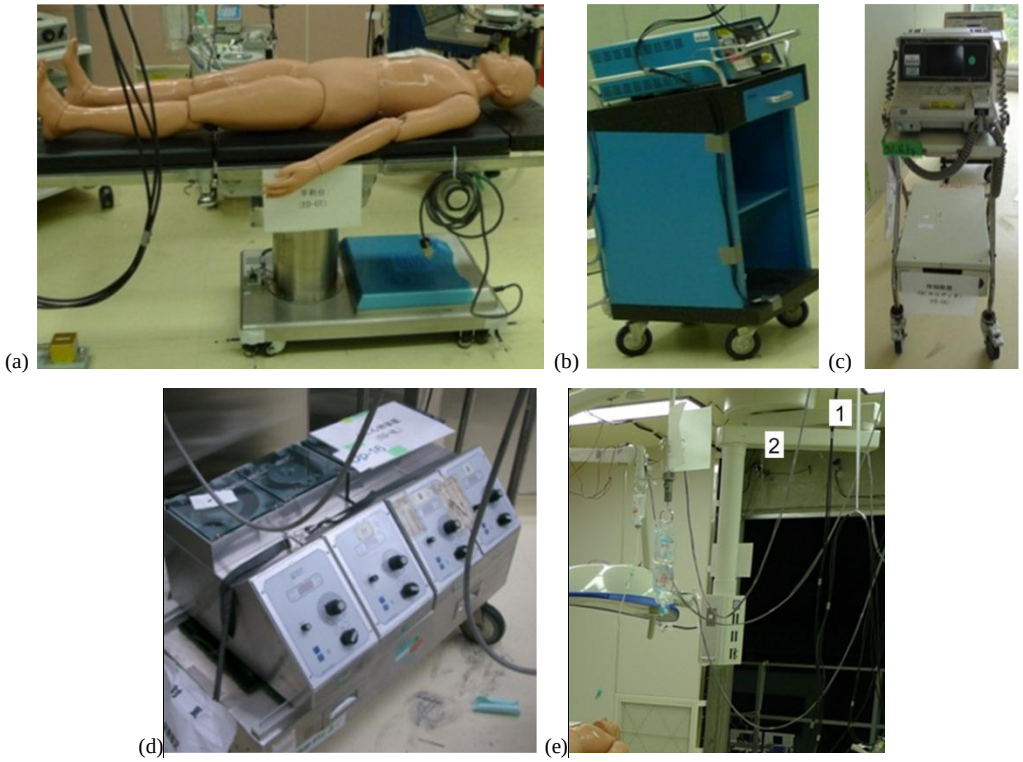


Figure 4.6 Representative medical appliances: (a) OT; (b) EL; (c) CD; (d) HL; (e) CP (with two arms, 1 and 2).

### 4.2.3 Measurement

A total of about 750 channels were used for measuring the responses; Accelerometers were installed at each floor to measure the structural accelerations in three directions. Story displacements were obtained by measuring the difference in displacement between two points: one belonging to the concerned floor and the other belonging to the floor upper to the concerned floor.

For the furniture items and medical equipment, accelerometers were installed to measure the acceleration response, while displacement time histories were measured by the motion capture technique described in Chapter 3. Five cameras were installed in the operation room and clamped on the wall with a height of 3.5 m from the floor so that they could cover all the appliances. The image resolution of those cameras was about 2 to 3 mm per pixel. In light of the preliminary test results, the estimated maximum error in displacement was not greater than 10 mm (3 times the image resolution). As discussed later in this Chapter, the maximum displacement and velocity observed in the concerned appliances were 3.6 m and 2 m/s. The associated maximum errors in displacement and velocity were deemed more than acceptable to evaluate the motion of the appliances and calculate the impact force.

### 4.2.4 Ground motions

Various ground motions with multiple levels of shaking were adopted in the shaking table test [4.1]. They were categorized into two types: short-period ground motion and long-period ground motion. Among those, the following two ground motions disclosed most notable behavior and damage on the tested appliances, i.e., JMA Kobe, a short-period ground motion recorded during the 1995 Hyogoken-Nanbu (Kobe) earthquake, and Sannomaru, a synthesized long-period ground motion, which has been developed for a scenario of simultaneous ruptures of Tokai and Tonankai troughs. In the meantime, those troughs ruptured repeatedly with a frequency of about 100 to 150 years, and Japan is most likely to suffer the next one by the middle of this century [4.1]. This paper presents the results obtained from those two ground motions.

In the test, JMA Kobe was scaled down to 80% to avoid excessive damage to the superstructure. The scaled PGA of JMA Kobe was 4.94 m/s$^2$ and 6.54 m/s$^2$ in the *X* and *Y* directions, respectively. Sannomaru had its dominant frequency at 2.5 to 3.5 s, which was close to the natural periods of the base-isolated structure. The PGA of this motion in the *X* and *Y* directions was 1.86 m/s$^2$ and 1.66 m/s$^2$, respectively. Figure 4.7 shows the acceleration time histories, acceleration response spectra, and velocity response spectra with 5% damping. Clear differences in the frequency content between JMA Kobe and Sannomaru can be observed in Figure 4.7 (c) and (d).

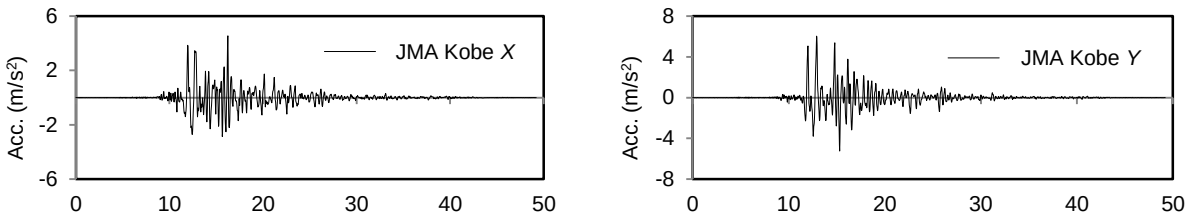

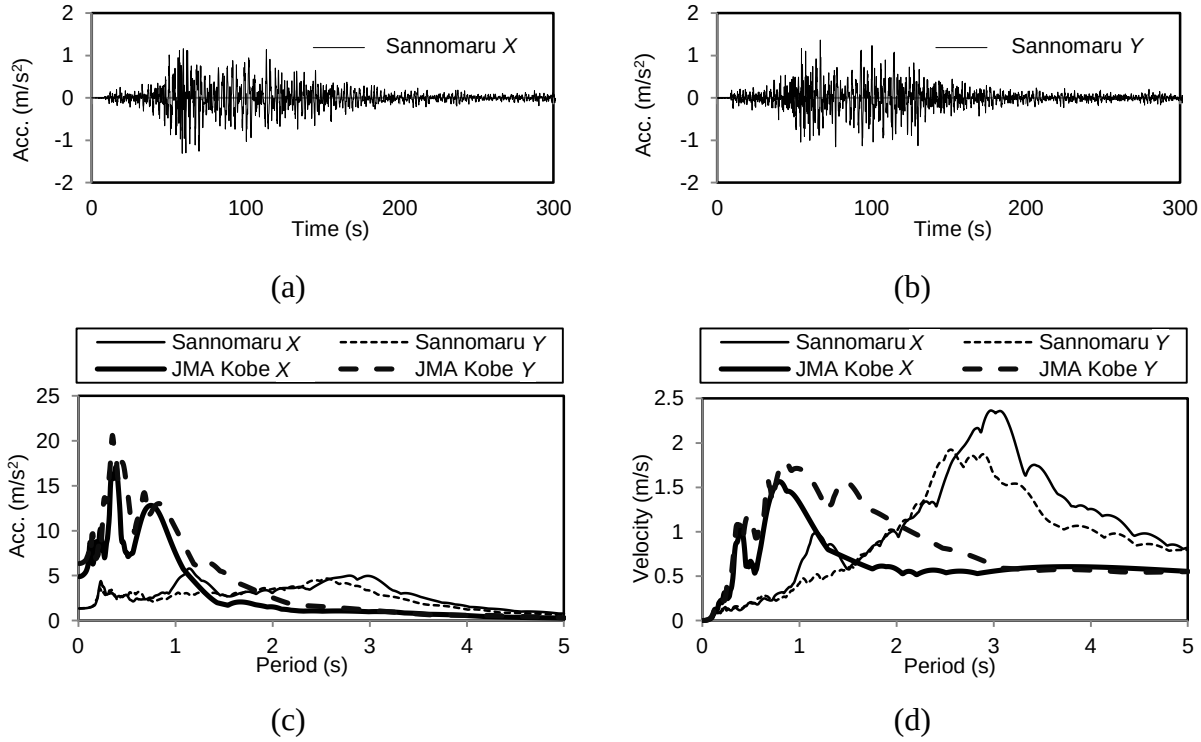


Figure 4.7 Input ground motions: (a) *X* direction acceleration time histories; (b) *Y* direction acceleration time histories; (c) acceleration response spectra; (d) velocity response spectra

The shaking table test was conducted with the E-Defense shaking table, which has a dimension of 15 m by 20 m and can accommodate a specimen up to 12 MN in weight. Details of this facility are presented elsewhere [4.3, 4.4]. Two base-isolated systems, NRB+U and HDRB, were tested first because the damage to the structure was insignificant, and then the fixed-base system was anchored to the shaking table and tested.

## 4.3 Structural response

The structure responses are of great importance to evaluate the functionality of the structure. On one side, the floor responses including the acceleration, displacement and story drift are directly used to evaluate the safety of the structure. One the other hand, the acceleration of the floor influences the furniture and medical appliances' behavior most significantly. Reducing the acceleration response of the structure is regarded as an effective way to reduce the responses of the contents inside the structure.

### 4.3.1 Performance of base-isolators

The test results show that the two types of isolation systems were stable throughout the shaking. Figure 4.8 shows the shear force-base floor displacement in *X* direction for two motions. There is no obvious stiffness deterioration in horizontal direction for both rubber systems after many rounds of shaking.

Figure 4.8 clearly shows that larger displacement responses occurred for the isolation systems under Sannomaru motion than with the short-period motion JMA Kobe. The performance of the U shaped steel damper was of great concern. The cumulative displacements of the U shaped steel damper reached 81 m without degradation in the stiffness after many rounds of shakings, of which 46 m was for Sannomaru shaking, without rupture. Figure 4.9 shows the U-shaped steel damper after all shakings.

Therefore, the performance of the isolators and U-shaped damper is satisfactory in large earthquake. No damage was observed through the testing program.

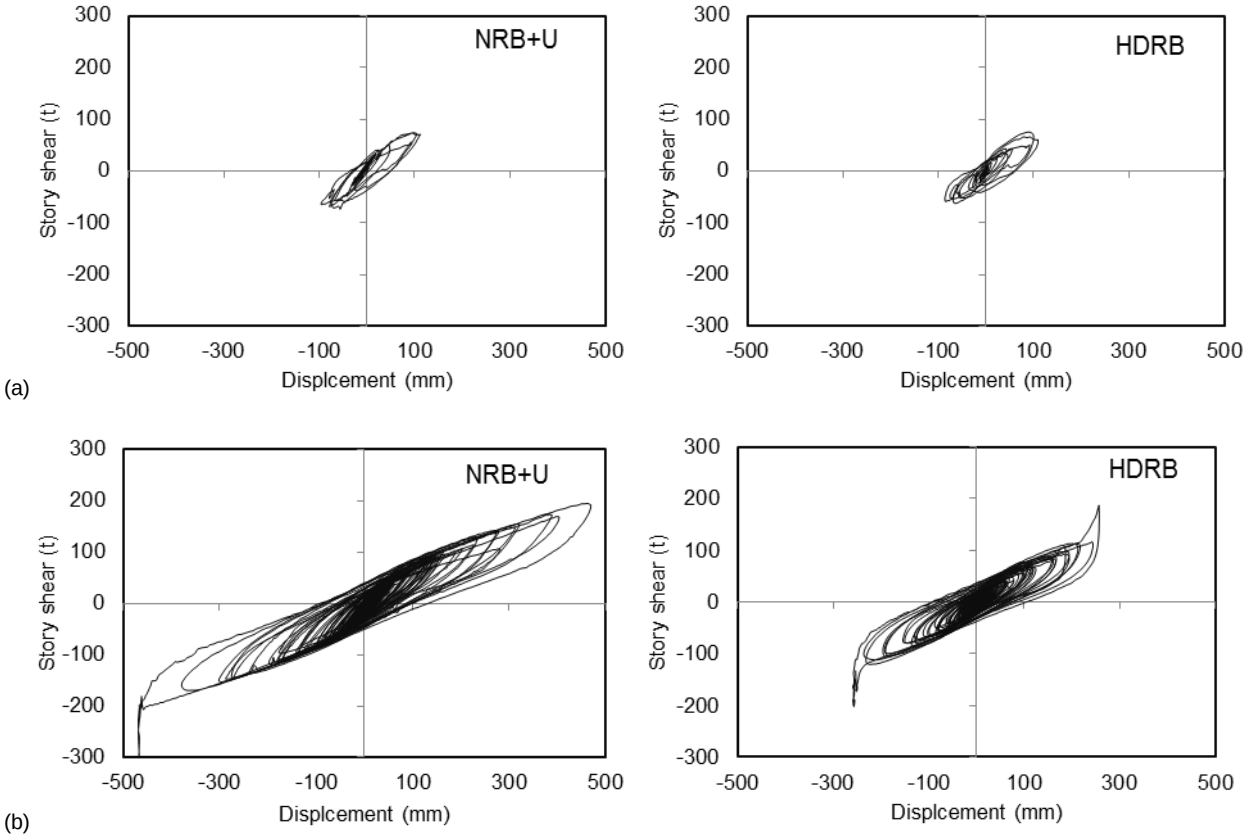


Figure 4.8 Performance of base isolation layer under: (a) JMA Kobe; (b) Sannomaru

Figure 4.9 U-shaped damper after all shakings

### 4.3.2 Base-isolated system versus fixed-base system

Table 4.3 listed the maximum acceleration responses of the shaking table input, each floor and the roof, for all the major shakings in horizontal directions. The vertical direction tests discussion are out of the scope of this dissertation. Information on the relevant research can refer to [4.5]. The results under the typical short-period motion, JMA Kobe, and the typical long-period motion, Sannomaru, are extensively used for discussion.

Table 4.3 Maximum acceleration and displacement responses under horizontal directions shaking

| | Wave | JMA Kobe | | | | Sannomaru | | | |
|---|---|---|---|---|---|---|---|---|---|
| | Response | Abs acc. ($m/s^2$) | | Abs vel. (m/s) | | Abs acc. ($m/s^2$) | | Abs vel. (m/s) | |
| | Direction | *X* | *Y* | *X* | *Y* | *X* | *Y* | *X* | *Y* |
| NRB+U | RF | 2.48 | 2.82 | 0.42 | 0.69 | 2.54 | 2.12 | 1.11 | 0.86 |
| | 4F | 1.99 | 2.45 | 0.41 | 0.67 | 2.54 | 2.10 | 1.10 | 0.86 |
| | 3F | 1.26 | 1.79 | 0.40 | 0.66 | 2.48 | 2.07 | 1.09 | 0.86 |
| | 2F | 1.49 | 1.98 | 0.39 | 0.65 | 2.45 | 2.04 | 1.08 | 0.85 |
| | 1F | 1.67 | 2.15 | 0.38 | 0.64 | 2.44 | 2.03 | 1.07 | 0.85 |
| | Table | 5.83 | 6.78 | 0.57 | 0.60 | 2.09 | 1.61 | 0.44 | 0.44 |
| HDRB | RF | 2.05 | 2.08 | 0.36 | 0.58 | 2.02 | 2.07 | 0.93 | 0.75 |
| | 4F | 1.68 | 1.95 | 0.35 | 0.57 | 1.99 | 2.05 | 0.89 | 0.75 |
| | 3F | 1.36 | 1.79 | 0.34 | 0.56 | 1.94 | 2.05 | 0.86 | 0.75 |
| | 2F | 1.28 | 1.79 | 0.33 | 0.55 | 1.93 | 2.03 | 0.87 | 0.74 |
| | 1F | 1.47 | 1.85 | 0.33 | 0.55 | 1.90 | 2.03 | 0.89 | 0.74 |
| | Table | 6.05 | 7.33 | 0.61 | 0.60 | 1.99 | 1.59 | 0.44 | 0.45 |
| Fixed-base structure | RF | 17.22 | 21.30 | 1.12 | 1.19 | 2.73 | 2.66 | 0.48 | 0.45 |
| | 4F | 13.38 | 13.69 | 1.01 | 1.08 | 2.31 | 2.13 | 0.47 | 0.45 |
| | 3F | 14.58 | 21.49 | 0.72 | 0.91 | 1.88 | 1.62 | 0.46 | 0.45 |
| | 2F | 12.68 | 19.78 | 0.57 | 0.75 | 1.82 | 1.49 | 0.45 | 0.44 |
| | 1F | 10.19 | 17.84 | 0.57 | 0.73 | 1.96 | 1.43 | 0.45 | 0.44 |
| | Table | 7.47 | 11.03 | 0.56 | 0.60 | 1.92 | 1.43 | 0.44 | 0.45 |

Figure 4.10 graphically shows the maximum acceleration response, velocity response and story drift ratio of each floor in *X* direction, for motions JMA Kobe and Sannomaru. To examine the amplification of acceleration and velocity responses from the input to each floor, the maximum acceleration and velocity of each floor are normalized by the maximum acceleration and velocity of the shaking table. Absolute values of those responses are listed in Table 4.3.

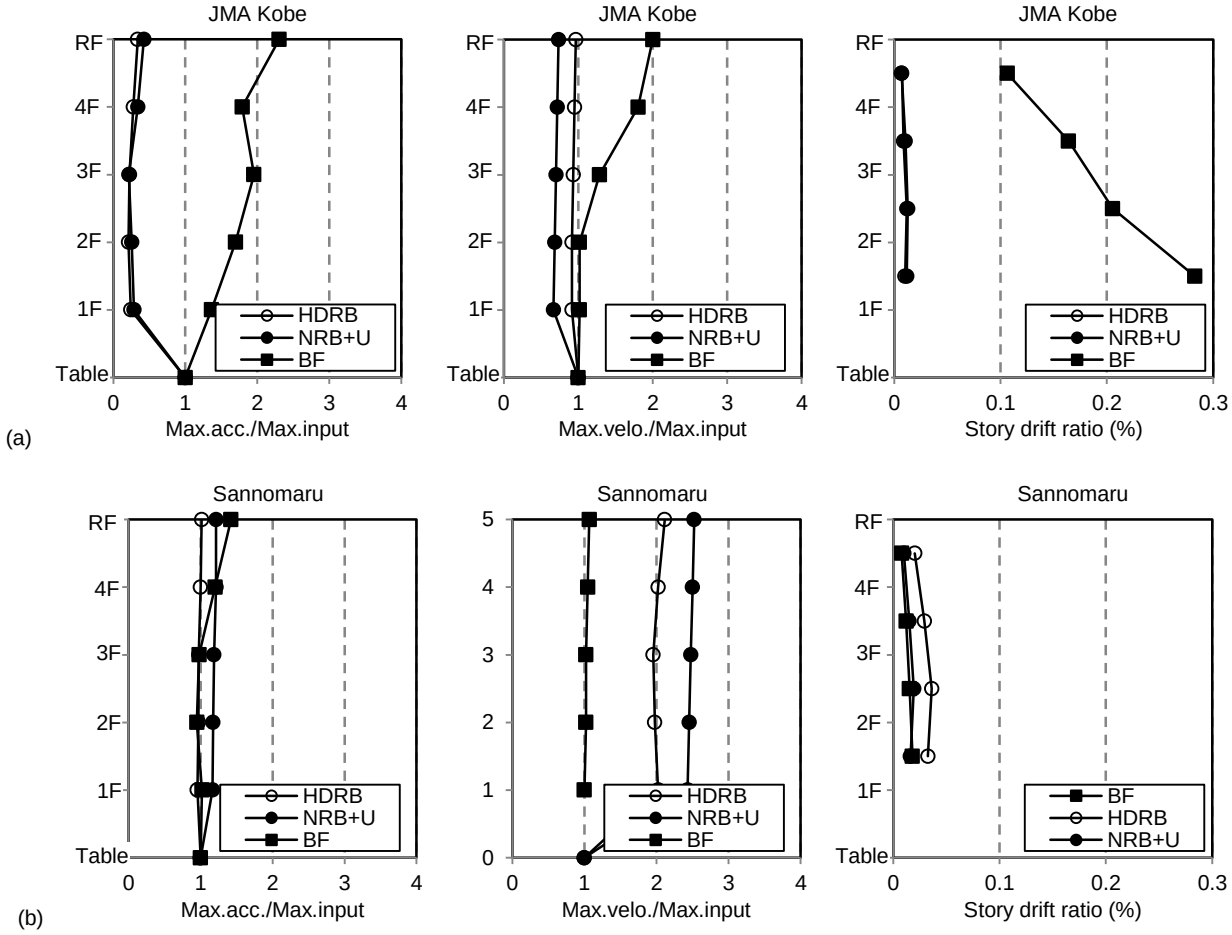


Figure 4.10 Normalized acceleration and velocity, and drift ratio in *X* direction under: (a) JMA Kobe; (b) Sannomaru

(1) Short-period motion JMA Kobe

For the base-isolated system, the acceleration and velocity responses of each floor including the roof were similar, with the reduction ratio from the shaking table of 0.2 to 0.4 for the acceleration, and 0.5 to 0.8 for the velocity. This indicates that the isolation system was very effective in reducing the floor responses, especially the acceleration. Smallest and largest responses occurred on the third floor and roof, respectively. The largest story drift occurred in the first floor and remained less than 0.1%. Therefore, the shakings did not cause damage to the structure. Both the NRB+U and HDRB systems exhibited similar performances.

For the fixed-base system, the acceleration and velocity responses increased significantly from the shaking table to the roof. The responses of the roof reached the maximum of 17.22 m/s$^2$ and 21.30 m/s$^2$ in two directions, which were of 2.3 and 1.9 times of the shaking table motions. In addition, the velocities were increased by two times from the shaking table. Compared with the base-isolated system, the maximum acceleration and velocity responses of the roof were about 7 and 2 times of those of the base-isolation system. The maximum story drift ratio of the floor reached 0.28% for the first floor, which was about 30 times that from the base-isolated system.

(2) Long-period motion Sannomaru

For the base-isolated systems, the acceleration and velocity responses were similar for different floors. The amplification factors of the responses from the shaking table to each floor were about 1.3 and 2, for the acceleration and velocity, respectively. This indicates that the base isolation could maintain the acceleration relatively close to the input motion. It is notable that the amplification factor of velocity was large, caused mainly by the large displacement demand of the isolator under this long-period motion.

For the fixed-base system, the acceleration and velocity were also amplified, but with smaller amplification numbers of about 1.4 and 1.1for acceleration and velocity, respectively, compared to the case with the short-period motion. Compared with the base-isolated system, most of the acceleration and velocity values of each floor were smaller, except for the acceleration response of the roof (amplification factor 1.4 for fixed-base vs. 1.2 for base-isolated). The reason that the fixed-base structure performed better was that its natural frequency was far away from the dominant frequency of the input motion, while resonance happed in the base-isolated structure.

In summary, no damage occurred for both the short- and long-period large earthquakes. In terms of the floor response, the base isolation system worked effectively in reducing the acceleration, velocity and story drift under the short-period motions. Under the long-period motion, although the displacement demand was large, the isolators worked without damage. The acceleration and velocity of the floors were only slightly amplified from the input motion. For all the cases tested, the story drift was much smaller than 0.5%, which was the level 1 design criterion.

For the fixed-base structure, its performance under the long-period motion was satisfactory. However, the short-period motion caused significantly larger responses of the floors compared with the base-isolated structure. Although the structure was still safe, such large response would influence the behavior of the medical appliances significantly.

## 4.4 Response of medical appliances

### 4.4.1. Behavior of medical appliances in base-isolated structure

During shaking, all medical appliances shown in Figure 4.5 (a) moved in the horizontal plane. Their behavior was evaluated according to the relative displacement and velocity responses with respect to the floor, and the absolute acceleration response.

Table 4.4 presents the maximum horizontal responses of the five medical appliances listed in Table 4.2 and the third floor. Since the direction of motion continuously changed during shaking, the displacement was defined as the maximum of the distances between any two points on the moving orbit. The maximum vector sum of the horizontal responses was used to estimate the accelerations and velocities of the respective appliances and the floor. Note that the displacement and velocity were absolute values for the floor, and relative values with respect to the floor for the medical appliances. Note also that the HL and CD were tested twice, once with the locked condition

and once with the unlocked condition, using the same input motions.

Table 4.4 Maximum horizontal responses of floor and typical appliances in base-isolated structure.

| | Displacement (mm) | Velocity (m/s) | Acceleration (m/s$^2$) |
|---|---|---|---|
| | JMA Kobe | | |
| Third floor | 461 | 0.72 | 1.94 |
| EL (unlock) | 439 | 0.45 | 2.69 |
| HL (unlock) | 135 | 0.13 | -[(a)] |
| CD (unlock) | 547 | 0.61 | 1.94 |
| CP (unlock) | 396 | 0.25 | 1.06 |
| OT (lock) | 0 | 0 | 2.29 |
| HL (lock) | 0 | 0 | 2.32 |
| CD (lock[(c)]) | 321 | 0.53 | 2.65 |
| | Sannomaru | | |
| Third floor | 970 | 1.05 | 2.51 |
| EL (unlock) | 1,474 | 1.61 | 63.5 (1.9[(c)]) |
| HL (unlock) | 3,602 | 1.92 | -[(a)] |
| CD (unlock) | 2,428 | 1.96 | 99.0 (2.0[(c)]) |
| CP (unlock) | 1,468 | 0.60 | 16.3 (1.3[(c)]) |
| OT (lock) | 0 | 0 | 56.5 (2.6[(c)]) |
| HL (lock) | 0 | 0 | 2.95 |
| CD (lock) | 602 | 0.43 | 2.43 |

[(a)] No accelerometer mounted on HL when unlocked.

[(b)] Two front casters locked.

[(c)] Peak acceleration excluding collision effect in parenthesis.

(1) *Short-period ground motion JMA Kobe*

*Behavior of unlocked appliances*

The maximum floor displacement, velocity, and acceleration were 461 mm, 0.72 m/s, and 1.94 m/s$^2$, respectively, and the dominant period of the response was about 2 s. The maximum displacement and velocity of the unlocked appliances were respectively 547 mm and 0.61 m/s, which were relatively close to the maximum displacement (1.2 times) and velocity (0.85 times) of the floor. Such coincidence can be explained in reference to the equivalent natural periods of these appliances.

Prior to the main shaking table test, a separate shaking table test was conducted with a series of random noise shakings. Figure 4.11 shows the amplification of the acceleration responses of the CD and EL relative to the input acceleration in the frequency domain. There is a notable peak at the frequency of 0.18 Hz (5.5 s) for both appliances, with the damping ratio of about 2%. This suggests that the tested appliances with unlocked casters have equivalent natural periods of about 5.5 s. This

period was about three times the dominant period (2 s) of the floor response under JMA Kobe. Figure 4.12 (a) shows the maximum displacement and velocity of an elastic SDOF system with 2% damping when it was subjected to the third floor's acceleration response obtained from JMA Kobe, plotted for various natural periods. The vertical axis, labeled "Amplification", denotes the maximum response of the SDOF system relative to the maximum of the input (i.e., the floor response), and the horizontal axis denotes the natural period of the SDOF system. The displacement and velocity amplifications are 1.3 and 0.9, respectively, for the natural period of 5.5 s. These amplifications are reasonably close to the experimental amplifications, 1.2 for the displacement and 0.85 for the velocity. The match between them indicates that the response of the appliance with unlocked casters can be estimated approximately by assuming it as an SDOF system having a long natural period such as 5.5 s in this study. As the maximum displacements of respective appliances were not greater than 550 mm, no collision was observed between the medical appliances or between an appliance and the surrounding wall.

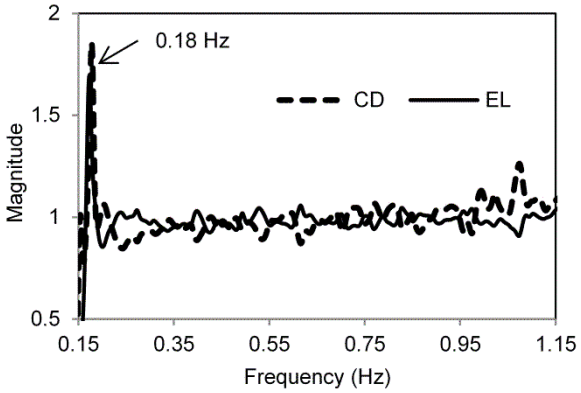


Figure 4.11 Equivalent natural period of unlocked appliances

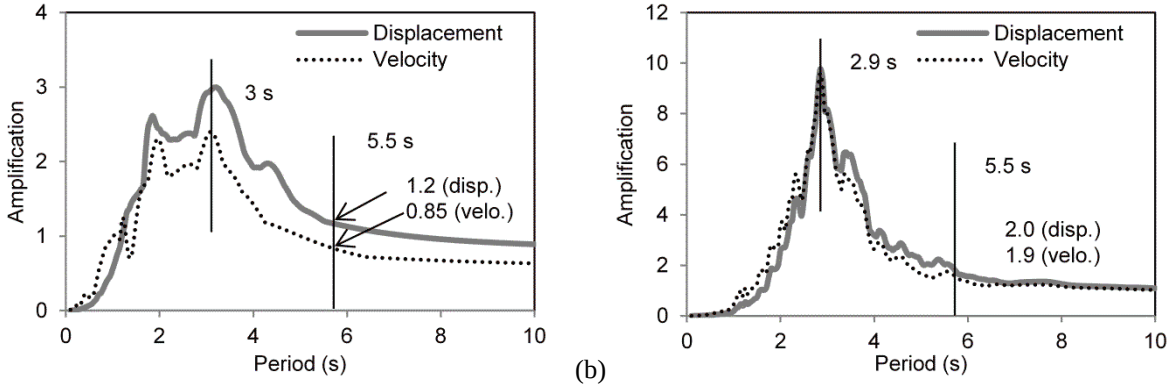


Figure 4.12 Response amplifications under floor's accelerations: (a) JMA Kobe; (b) Sannomaru

Although the accelerations in the sliding direction remained small because of the small friction coefficients (not greater than 0.05), the acceleration in the orthogonal direction was large, because the appliances behaved like rigid bodies in that direction as in the free-standing condition. Furthermore, when the appliances suddenly changed their direction of motion during the complex

2D motion, the casters were temporarily stuck, which also provided a locked condition. As a result, the accelerations of the unlocked appliances (1.3 to 2.0 m/s$^2$) were relatively close to the acceleration of the floor (2.51 m/s$^2$).

*Behavior of locked appliances*

The appliances with locked casters (OT and HL) did not move because of the large friction coefficient of over 0.6. An exception was the CD, in which the casters were partially locked and the friction coefficient was about 0.4. Although the maximum floor acceleration (1.94 m/s$^2$) was still significantly smaller than the force to slide the appliance, eccentricity of the mass center with respect to the two locked casters caused movement to a degree similar to what was observed for the appliances with unlocked casters. For the acceleration, the appliances with locked casters had the maximum accelerations (1.06 to 2.69 m/s$^2$) relatively close to the acceleration (1.94 m/s$^2$) of the floor, as they did not move and behaved almost as rigid bodies.

(2) *Long-period ground motion Sannomaru*

*Behavior of unlocked appliances*

Figure 4.13 shows the dislocation of the medical appliances, which was measured after shaking. Note that the dislocation was not the maximum movement during the entire shaking. The combination of a dashed line and italic font shows the original position, and the combination of a solid line and non-italic font shows the dislocated position. In the figure, all appliances except the OT were in the unlocked condition. The blank circles show unlocked casters, while the black circles indicate locked casters (for the OT). Figure 4.14 shows the moving orbits of the mass centers of respective medical appliances, all of which were recorded by the motion capture technique.

The maximum floor displacement, velocity, and acceleration were 970 mm, 1.05 m/s, and 2.51 m/s$^2$, respectively, and the dominant period of the response was about 3 s. The long-period motion caused wild movement of the appliances in the unlocked condition. The moving ranges of the appliances were 1.4 to 2.4 m (except for the HL), which were about an order of two with respect to the floor displacement. The HL exhibited the most notable movement of 3.6 m, moving from one side of the operation room to the other. This large motion was due to a serious collision between the HL and the virus-proof wall. The maximum velocity of the appliances reached 1.96 m/s, which was also about twice the maximum floor velocity. Figure 4.12 (b) shows the maximum displacement and velocity of an elastic SDOF system when it was subjected to the third floor's acceleration response under Sannomaru. The experimental amplification factors for the displacement and velocity were close to what was obtained from the simulation, i.e., about two, as shown in Figure 4.12 (b)).

From Figure 4.14, it is notable that the displacement histories of the unlocked appliances were very complicated, and their orbits were different, despite the fact that the appliances were subjected to the same input floor excitation. One reason was the effect of collision, which will be discussed in the next section, and another was the sensitivity of the motion to the properties of the appliances such as the caster configuration, caster direction, and mass eccentricity, among others.

The maximum accelerations given in parentheses in Table 2 were the maximum accelerations when excluding the very large accelerations amplified by collisions. For the appliances in the unlocked condition, these accelerations remained close to the maximum floor acceleration. Although these appliances were equipped with casters, they behaved like rigid bodies in the locked condition in the direction orthogonal to the sliding direction, and furthermore, they were temporarily stuck at the instant of a sudden change in direction. These observations were similar to what was observed for JMA Kobe, the near-fault ground motion.

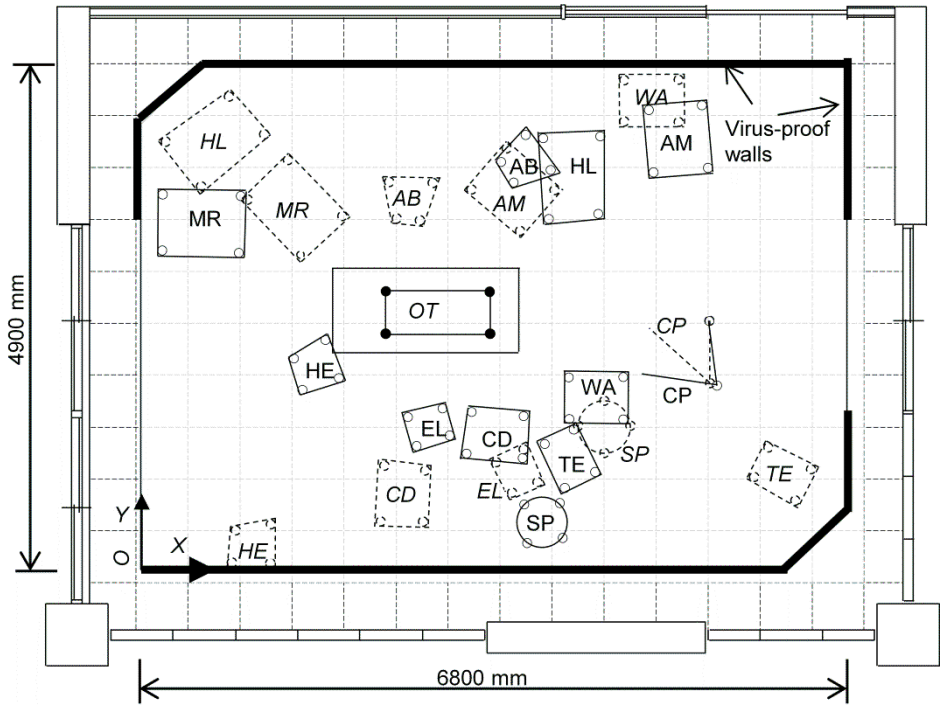


Figure 4.13 Dislocation of appliances measured after shaking

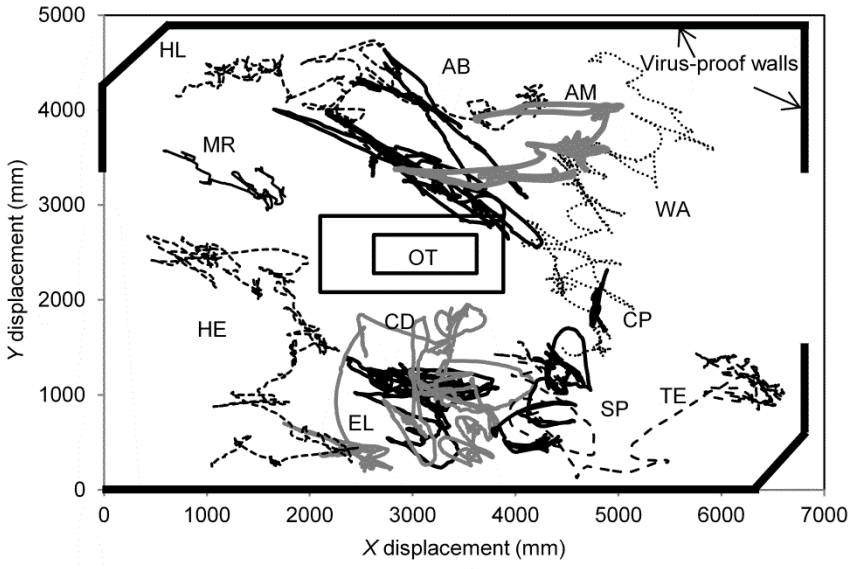


Figure 4.14 Moving orbit of representative appliances in operation room

*Behavior of locked appliances*

The maximum floor accelerations were reduced to no more than 2.51 m/s$^2$ by base isolation; hence, the locked appliances (OT and HL) did not move at all. The partially locked CD moved during the shaking but only slightly (not more than 25% of the motion in the unlocked condition). The maximum accelerations of those locked appliances (2.43 to 2.95 m/s$^2$) were close to the maximum floor acceleration as the appliances behaved as rigid bodies.

*Disorder and damage*

Effects of wild responses of appliances in terms of the inconvenience and disorder introduced to medical activities and damage to the appliances were discussed with medical professionals, and the following concerns were disclosed.

First, it was believed that there was a high possibility that electric plugs attached to appliances would be disconnected or torn off by excessive displacements. This would lead to malfunction of the appliance and might consequently cause serious disorder of the operation. In the worst case, it might cause the patient's loss of life.

Second, collision between appliances and between an appliance and the surrounding walls might seriously lessen the functionality of the appliances. As shown in Figure 4.14, the orbits of appliances overlapped, and collision occurred in many instances. Note that the CP (the ceiling pendant) was not at the same altitude as other appliances, and therefore, there was no collision between CP and the other appliances on the floor. Serious collisions occurred between the CD and EL, the CD and OT (locked) the EL and the virus-proof wall, the HL and the virus-proof wall, and the CP and the surgical light (shown in Figure 4.5 (b). Although the OT was locked and did not move, other appliances nearby collided against it.

Figure 4.15 gives several examples of collision and the resulting damage. Figure 4.15 (a) and (b) show that the CD crashed into the OT, and the CP crashed into the surgical light. The collision between the CD and OT caused uplifting and rocking of both (Figure 4.15 (c)). The collision between the HL and the virus-proof wall brought damage to the wall. Figure 4.15 (d) shows the breakage of the wall caused by the HL. Such damage would threaten power or medical gas supply systems embedded in or behind the wall.

The collision force $F$ depends on the relative velocity $\Delta v$ between the appliances upon collision and the elapsed time $dt$ during collision. It can be calculated as [4.6].

$$F = \frac{2m_1 m_2}{m_1 + m_2} \frac{\Delta v}{dt} \tag{4.2}$$

where $m_1$ and $m_2$ are the masses of the two appliances that collide.

Figure 4.16 shows the acceleration time histories of the CD, EL and OT during collision. Note that the plots shown in the figure are the vector sums of the $X$ and $Y$ accelerations. The figure indicates that the collisions lasted for about 0.01 s. The relative velocity between the CD and EL was 0.35 m/s when the two appliances collided. According to Equation (4.2), the collision force was 1.2 kN ($dt$ = 0.009 s). When the CD crashed into the OT, the relative velocity between them was 1.5

m/s, and the collision force was 8 kN ($dt$ = 0.01 s). In another case, the HL crashed into the wall at a velocity of 1.6 m/s. With $dt$ taken as 0.01 s, the collision force was 36 kN. This large force was speculated to be the source of the damage to the wall shown in Figure 4.15 (d).

According to the injury criteria developed for automotive restraint systems [4.7], tolerable compression and tension loads for the neck and femur are respectively 3.6 and 10 kN. A person is thus likely to be seriously hurt on the head or leg once hit by the moving appliances.

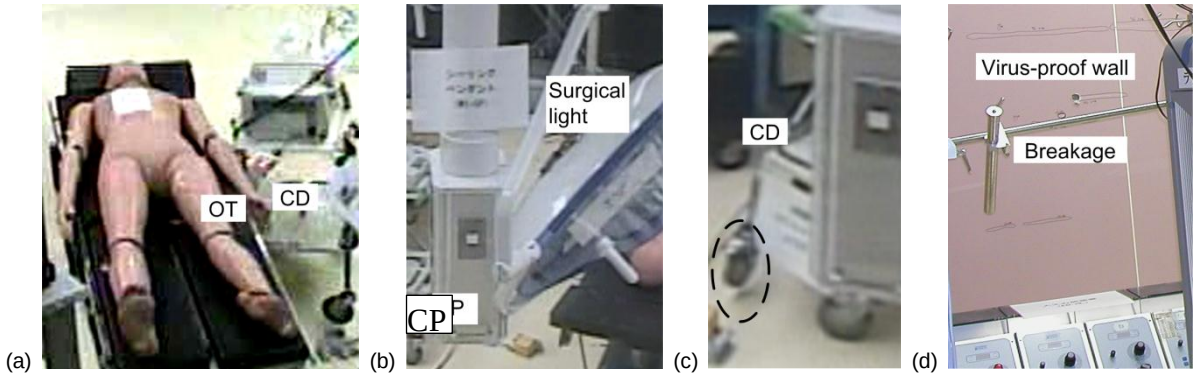


Figure 4.15. Examples of collision and resultant damage: (a) collision between the CD and OT; (b) collision between the CP and a surgical light; (c) uplifting of the CD after collision; (d) damage to a wall caused by the collision with HL

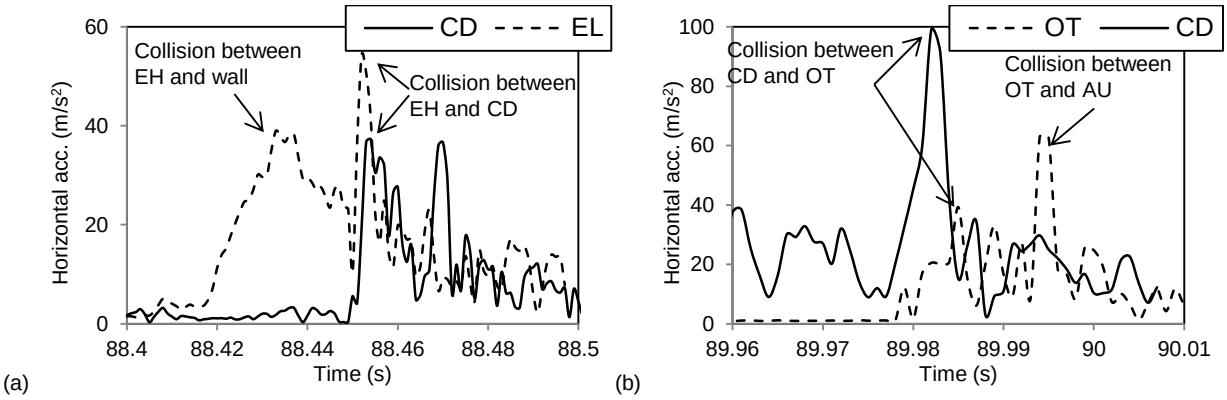


Figure 4.16 Horizontal accelerations of appliances: (a) CD and EL; (b) CD and OT

Serious collision also caused larger displacements of the appliances. As shown in Table 4.4, the maximum displacement of the HL was about twice the maximum displacements of other unlocked appliances. Such enlarged displacement was attributed primarily to the serious collision between the HL and the virus-proof wall. Furthermore, large accelerations that occurred upon collision were found to be a serious threat to the safety and functionality of acceleration-sensitive appliances, such as those having electronic components [4.8]. According to Table 4.4, the accelerations caused by collision approached 10 g, which is far beyond the accelerations tolerated by acceleration-sensitive appliances. Japan's Industrial Standards (JIS) [4.9] stipulate 2 g for the accelerations that the appliances shall tolerate without malfunction.

The above observations indicated that medical facilities in the base-isolated structures may not

be invincible against ground motions characterized by long-period because of likely vehement motion of medical appliances equipped with casters.

*Performance improvement by locking casters*

Both the OT and HL were tested in fully locked conditions (all casters locked) in the test. The friction coefficients of the two appliances in the locked condition exceeded 0.6. Since the maximum floor acceleration was reduced to at most 2.51 m/s$^2$ by base isolation, the appliances did not move. Considering that the maximum accelerations of both the OT (not including the accelerations caused by collision) and HL remained close to the maximum floor acceleration, the appliances would remain safe and functional once casters are fully locked.

Figure 4.17 shows the moving orbits of the CD in the unlocked and partially locked (with the two front casters out of the four casters locked) conditions. When the front two casters were locked, the level of motion was reduced to about one-quarter, from 2,428 mm and 1.96 m/s to 602 mm and 0.43 m/s in terms of maximum displacement and velocity. Note that the acceleration response increased but only slightly, from 2 to 2.4 m/s$^2$. According to medical professionals, it would be impractical for medical staff in a busy hospital to spend extra time for securely locking all casters, particularly those located at the back. Locking the casters is no doubt a simple and the best solution to avoid inconvenience, disorder, and damage following an earthquake, but simply asking the medical staff to exercise it is not feasible. In this context, the effectiveness of partial locking (locking just the two casters at the front) is deemed to provide a practical solution.

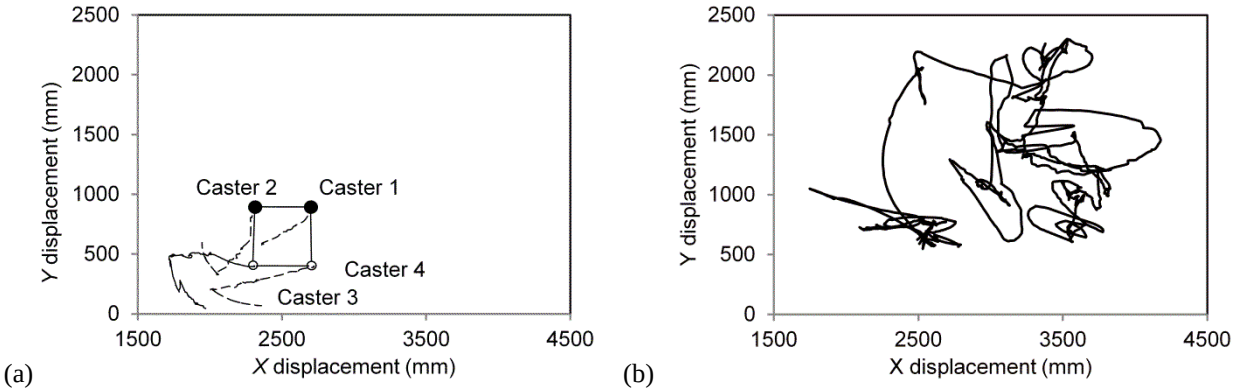


Figure 17 Comparison of moving orbit of CD under different locking conditions: (a) two front casters locked; (b) all casters unlocked

### 4.4.2. Behavior of medical appliances in fixed-base structure

For comparison, the hospital specimen was also tested in the fixed-base condition by clamping the superstructure directly to the shaking table. The same ground motions were used as for the base-isolated structure. Table 4.5 gives the maximum horizontal responses of the five medical appliances and the third floor. Note that the displacement and velocity are absolute values for the third floor, and relative values for the medical appliances with respect to the floor.

Table 4.5 Maximum horizontal responses of third floor and typical appliances in fixed-base structure

| | Displacement (mm) | Velocity (m/s) | Acceleration (m/s$^2$) |
|---|---|---|---|
| | JMA Kobe | | |
| Third floor | 350 | 0.99 | 25.10 |
| EL (unlock) | 172 | 0.62 | 7.80 |
| CD (unlock) | 383 | 0.89 | 7.20 |
| CP (unlock) | 415 | 0.57 | 10.37 |
| OT (lock) | 388 | 1.36 | 18.86 |
| CD (lock) | 740 | 1.48 | 32.78 |
| | Sannomaru | | |
| Third floor | 410 | 0.56 | 2.10 |
| EL (unlock) | 1014 | 1.11 | 2.38 |
| CD (unlock) | 1091 | 0.61 | 1.86 |
| CP (unlock) | 465 | 0.16 | 1.39 |
| OT (lock) | 0 | 0 | 3.07 |
| CD (lock) | 453 | 0.23 | 3.06 |

(1) *Behavior under different ground motions*

*Near-fault ground motion of JMA Kobe*

The maximum floor displacement, velocity, and acceleration were 350 mm, 0.99 m/s, and 25.1 m/s$^2$, respectively, and the dominant period of the response was about 0.4 s. The maximum displacement and velocity of the unlocked appliances were 415 mm and 0.89 m/s, which were close to the displacement and velocity of the floor. This appears reasonable considering a large difference between the dominant period of 0.4 s for the floor response and the equivalent natural period of 5.5 s for the unlocked appliances. The floor acceleration was large enough to break the friction force for the appliances with either locked or partially locked casters and caused them to move. The maximum displacement and velocity reached 740 mm and 1.48 m/s, and were larger (by a factor of about 1.5) than those for the unlocked appliances.

The appliances in the unlocked condition had the maximum accelerations close to the product of the friction coefficient in the locked condition (above 0.6) and gravity. This occurred because the appliances behaved like rigid bodies in the locked condition in the direction orthogonal to the sliding direction. The direction of motion of the appliances suddenly changed in the complex 2D motion, and the casters were temporarily stuck, which also increased the instantaneous friction coefficient. For the appliances in the locked condition, on the other hand, the accelerations (18.86 to 32.78 m/s$^2$) were of the same order as the maximum floor acceleration (25.1 m/s$^2$), but were significantly larger (by a factor of 3 to 5) than the product of the friction coefficient and gravity. This was attributed to the uplifting and rocking of the appliances due to the large floor accelerations.

*Long-period ground motion of Sannomaru*

The maximum floor displacement, velocity, and acceleration were 410 mm, 0.56 m/s, and 2.10 $m/s^2$, respectively, and the dominant period of the response was about 3 s. The maximum displacement and velocity of the unlocked appliances were about 1 m and 1.1 m/s, and about 2.7 and 2 times the displacement and velocity of the floor response. The dynamic amplifications from the responses of the floor to responses of the unlocked appliances, with an SDOF system whose natural period is 5.5 s, were 2.9 and 1.9 respectively for the displacement and velocity. These values are close to the amplifications obtained experimentally. The maximum displacement and velocity were more than 50% less for the locked appliances than for the unlocked appliances. This indicates that locking the casters was also effective in reducing the motion of appliances in the fixed-base structure subjected to long-period ground motion. For the acceleration, it was close to the floor acceleration for both unlocked and locked appliances. Overall, the test results show that, for the fixed-base structure, the long-period motion did not cause serious motion of the floor and medical appliances with either locked or unlocked casters.

*Disorder and damage*

No collision was observed for either the JMA Kobe or Sannomaru motions. However, the large floor acceleration of 25.1 $m/s^2$ for JMA Kobe caused serious uplifting and rocking of the locked appliances. Figure 4.18 shows photos of the OT during the shaking. The large accelerations of the OT nearly resulted in the mannequin placed on the OT sliding onto the floor. If there had been no belt used to fix the mannequin by the leg, the mannequin would have fallen off. The uplifting and rocking effect consequently caused large horizontal acceleration responses (as large as 32.78 $m/s^2$) of the appliances with locked casters as shown in Table 3. Acceleration-sensitive appliances in fixed-base structures would most likely sustain fatal malfunction under such near-fault ground motions. On the other hand, no serious damage was observed when appliances were subjected to the long-period ground motion of Sannomaru.

(a)  (b) 

Figure 4.18 Behavior of OT: (a) before shaking; (b) uplifting

(2) *Comparison with base-isolated structure*

Under the near-fault ground motion of JMA Kobe, the appliances in the unlocked condition had

maximum velocities and accelerations that were respectively about two and four times greater in the fixed-base structure than in the base-isolated structure. However, the maximum displacements in both structures were similar. The appliances with locked or partially locked casters had maximum displacements, velocities and accelerations that were respectively two, three and twelve times larger in the fixed-base structure than in the base-isolated structure. Such a notable increase in the response of locked appliances was attributed to the significant difference (a factor of 13) in the maximum floor acceleration; i.e., 25.1 m/s$^2$ for the fixed-base structure compared with 1.94 m/s$^2$ for the base-isolated structure.

Under the long-period ground motion of Sannomaru, the maximum accelerations of the floor and appliances were similar between the fixed-base structure and the base-isolated structure. However, the displacements and velocities of the appliances were notably decreased in the fixed-base structure. Figure 4.19 (a) compares the moving orbits of the CD in the unlocked condition between the two different structures. The CD moved with significantly smaller displacement (only 45%) in the fixed-base structure than in the base-isolated structure. This was attributed to the differences in the frequency characteristics of the floor response. Figure 4.19 (b) compares the floor accelerations obtained by FFT. The values in a frequency band lower than 0.5 Hz were significantly larger for the base-isolated structure than for the fixed-base structure, which resulted in larger displacements and velocities of the appliances.

To summarize, wild movement of the appliances took place in two cases. The most serious case was when the fixed-base structure was subjected to JMA Kobe ground motion, in which there was serious damage in both caster locked and unlocked conditions. This was clearly due to the very large floor response with the maximum acceleration of 25.1 m/s$^2$. The other case, although milder than the first case, was when the base-isolated structure was subjected to Sannomaru ground motion, in which all appliances stayed calm except for those with unlocked casters. The appliances with unlocked casters moved large distances. Note, however, that such large motion can be reduced significantly once the casters are locked.

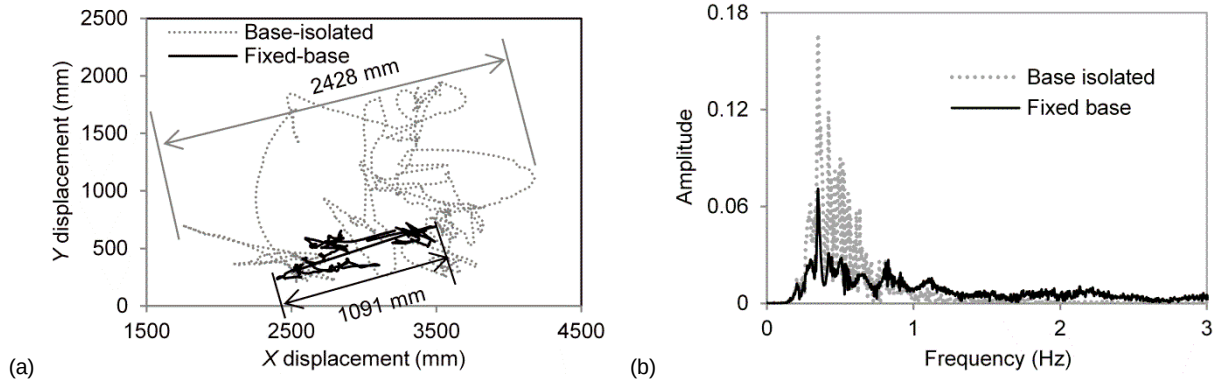


Figure 4.19 Comparison of base-isolated and fixed-base structures: (a) orbit of CD; (b) FFT of floor acceleration

### 4.4.3. Summary of behavior of medical appliances

Medical appliances were tested in both locked and unlocked conditions in base-isolated and fixed-base structures, using a near-fault ground motion of JMA Kobe and a long-period ground motion of Sannomaru. The test revealed that the performance of medical appliances could be classified according to the following categories, i.e., unlocked versus locked, near-fault ground motion versus long-period ground motion, and base-isolated structure versus fix-based structure. The behavior of appliances can be summarized as follows.

First is about unlocked appliances. Unless they were subjected to long-period ground motions in the base-isolated structure, those unlocked appliances were much more flexible with respect to the dominant period of the floor response; hence, the maximum displacement and velocity were similar to those of the floor response. When the base-isolated structure was subjected to long-period motions, the maximum displacement and velocity of unlocked appliances were about twice those of the floor (in this study), because the dominant component in the long-period motion matched the period of the appliances. Despite the fact that the unlocked appliances were equipped with mobile casters, their friction coefficients were large in the direction orthogonal to the sliding direction, and the casters were stuck temporarily when the moving direction changed suddenly. Therefore, they behaved like rigid bodies at least in some instances, and the maximum acceleration was similar to the maximum floor acceleration or the acceleration that corresponded to the breaking of friction; i.e., the product of the friction coefficient and acceleration of gravity.

Second is about locked appliances. In the base-isolated structure, the floor accelerations were greatly reduced; hence, there was no movement of locked appliances. They behaved as rigid bodies, and therefore, the maximum accelerations of the appliances were similar to the maximum floor accelerations. Even in the fixed-base structure, the response when subjected to long-period ground motions remained very small thanks to the small floor response, which was due primarily to a significant difference between the natural period of the structure (0.24 s in this study) and the dominant period of the long-period ground motion (3 s in this study). The exception was the case when the fix-based structure was shaken with strong near-fault ground motions. In such a case, the floor acceleration was promoted significantly (to as much as 2.6 g), and the appliances exhibited serious sliding and rocking. Among various combinations, the case when locked appliances were installed in a fixed-base structure and subjected to near-fault ground motions was by far the most damaging.

## 4.5 Summary

This chapter describes the evaluation of the responses of structure and medical appliance in a full scale four story RC hospital appliance through a series of shaking table test. Two different types of ground motions, i.e., short-period and long-period, were adopted in the test. The major objective of the test is to examine the performance of the base-isolate system under different types of motions, and check the behavior of appliance installed in the structure. Major findings can be summarized as follows:

**For base-isolated system,**

(1) The isolator exhibited stable performance in all the shakings for both the short-period and long-period motions. The cumulative displacement under the long-period and long-duration motion Sannomaru was over 46 m, which was much larger than 5 m under the short-period motion JMA Kobe. The U-shaped damper for the isolation system to dissipate energy eventually sustained 81 m without degradation in the stiffness after many rounds of shakings.

Under the short-period motion JMA Kobe, the acceleration and velocity responses of each floor, were reduced from the shaking table with the factor of 0.2 to 0.4 for acceleration, and 0.5 to 0.8 for velocity. The story drift ratio was much smaller than 0.1%. Under long-period motion Sannomaru, the acceleration and velocity were amplified from the shaking table to each floor by 1.2 and 2 times, respectively. The story drift ratio was also much smaller than 0.1%.

(2) The performance of medical appliances with locked and unlocked conditions under the short-period ground motion was promising. However, under the long-period motion, the base-isolated structure was not necessarily invincible in terms of the behavior of the appliances which were mobile. The displacement of the appliances with unlocked conditions was more than 3 meters while the velocity was up to 2 m/s.

(3) The wild movement of the appliances with unlocked condition under the long-period motion caused a series of problems including tearing the electric plugs for the appliances, serious collisions between appliances which caused uplifting, rocking of appliances, breakage of wall, and large acceleration which would cause malfunction of appliances. Such behaviors would significantly disorder the activity of the hospital and influence its functionality during and immediately after an earthquake.

(4) By fully or partially locking the casters of the appliances in the base-isolated structure, the displacement and velocity were significantly reduced (to only one-quarter) from those with unlocked condition.

**For fixed-base system,**

(5) Under the short-period motion JMA Kobe, the amplification factors of acceleration and velocity from the shaking table to the roof were 2.25 and 1.75, which were 6 and 2.5 times of those in base-isolated system. The maximum story drift ratio of the first floor reached to 0.45%, which was 8 times of that in base-isolated system. Under long-period motion, the amplification factors were about 1.7 and 1.2 for acceleration and velocity.

(6) Under the short-period motion, the accelerations of the appliances in fixed-base structure were about 3~20 times of those in the isolation system. This is attributed to the significantly larger acceleration of floor isolation compared with in the base-isolated system (by a factor of 13). The free standing appliances with locked casters were excited to move about 500 mm. Under long-period motion, the acceleration and displacement responses of the appliances were similar of those in the base-isolated system.

(7) In the fixed-base structure test, the behavior of the mobile appliances was better than in the base-isolated structure under the long-period ground motion. However, the large floor acceleration in fixed-base structure under the short-period ground motion caused significantly larger velocity (three times) and acceleration (twelve times) of the appliances than in the base-isolated structure, which

would threat the safety of the appliances and human's life. There was no effective way by changing the locking condition of the appliances to improve the performance of the appliances.

**Estimation of appliance's response,**

(8) For unlocked appliances, the relative displacement and velocity were close to the absolute displacement and velocity of the floor except for the case when the base-isolated structure was subjected to the long-period ground motion. In that case, the displacement and velocity were somewhat amplified. The level of amplification can be roughly estimated using the equivalent natural period of unlocked appliances.

# REFERENCES


[4.1] Sato E, Furukawa S, Kakehi A, Nakashima M. Full shaking table test for examination of safety and functionality of base-isolated medical facilities. *Earthquake Engineering and Structural Dynamics* 2011; 40: 1435-1453.

[4.2] Building Center of Japan. Structural provisions for building structures-2007 Edition (2007), Tokyo. (in Japanese)

[4.3] Ogawa N, Ohatani K, Katayama T, Shibata H. Construction of a three-dimensional, large-scale shaking table and development of core technology. *Philosophical Transactions of the Royal Society* 2001; 359: 1725-1751.

[4.4] Nakashima M. Roles of large structural testing for the advancement of earthquake engineering. *The Fourteenth World Conference on Earthquake Engineering* 2008. Beijing, China.

[4.5] Furukawa S. Performance of structures and equipment in base-isolated medical facilities subjected to severe earthquake motions (2011). Doctor dissertation.

[4.6] Muthukumar S, Desroches R. A Hertz contact model with non-linear damping for pounding simulation. Earthquake Engineering and Structural Dynamics 2006; 35: 811-828.

[4.7] Kleinberger M, Sun E, Eppinger R, Kuppa S, Sul R. Development of improved injury criteria for the assessment of advanced automotive restraint systems. NHTSA, September 1998.

[4.8] IBM. POWER7 information: Vibration and shock. Systems hardware information; 2010.<http://publib.boulder.ibm.com/infocenter/powersys/v3r1m5/index.jsp?topic=/p7ebe/p7ebevibrationandshock.htm>.

[4.9] JIS T 0601-2-24:2005 Medical electrical equipment-Part 2-24: particular requirements for the safety of infusion pumps and controllers. Japanese Standards Association.

# CHAPTER 5

# Development of semi-active controlled floor isolation system

## 5.1 Introduction

### 5.1.1 Background

Base isolation is one of the most successful and widely-applied techniques [5.1] to protect the structure. It is also designed to protect the important contents inside so as to maintain the functionality of the structure during and immediately after the earthquake [5.2-5.3]. However, the base isolation technique of the entire building may not be practical or economical in some cases, including for retrofit purpose. In such a situation, a floor isolation system which is designed for one floor or room of the structure is a cost-effective alternative to protect valuable non-structural equipment [5.4-5.8]. Unlike the equipment isolation system [5.4, 5.9] which works for a particular piece of equipment; or the base isolation which works for an entire building [5.2-5.3, 5.4], the floor isolation system serves for a group of equipment, such as the important and expensive medical appliances in a hospital [5.7].

For the floor isolation system, the load on the floor isolation system may be changed, when the equipment placed on the floor is moved in or moved out. This will cause significant changes in the system property, such as the damping ratio. The previous studies shown in Chapter 2 indicate that the semi-active controlled base isolation is more effective than the passive controlled base isolation. To take the best features of semi-active control, a semi-active controlled floor isolation system is designed utilizing a rolling pendulum system and an MR damper. To design the semi-active strategy, the properties of the rolling pendulum system, such as the natural period and friction force on the pendulum surface need to be validated. To this end, system identification tests were performed.

A new proposed semi-active control algorithm is shown in Chapter 6. Simulation work is necessary to develop the algorithm with an MR damper model. A series of dynamic loading tests were conducted to quantify the MR damper property. The Bouc-Wen model discussed in Section 2 was adopted to describe the MR damper behavior.

On the other hand, to realize the designed force calculated from the semi-active strategy, it is necessary to build up the inverse dynamic model, which calculates the input signal to the MR damper. However, since the MR damper is essentially a nonlinear device, it is difficult to design an inverse dynamic model directly. Instead, a PI controller with feedback of the actual force was designed and

applied to the semi-active control in this study.

### 5.1.2 Organization

This chapter describes the development of the semi-active controlled floor isolation system. The design of the floor isolation system and the specimen for the shaking table test is presented in Section 5.2. Section 5.3 introduces the system identification results of the system's natural period and friction. Dynamic loading test is performed to validate the property of MR damper in Section 5.4. A Bouc-Wen model is adopted to describe the MR damper behavior. To track the designed force, a PI controller is designed in Section 5.5 to calculate the control signal to the MR damper.

## 5.2 Design of floor isolation system

### 5.2.1 Floor isolation system

Figure 5.1 shows a schematic of the proposed unidirectional semi-active floor isolation system, located on the top floor of a fixed-base RC building. It includes a rolling pendulum isolation system used to create a long natural period to decouple the raised floor (the floor on which the equipment is placed) from the structure floor, and a semi-active control device to apply the control force. In this configuration, the input motion to the floor isolation system is the response of the top floor and is distinct from the ground motion input to the structure.

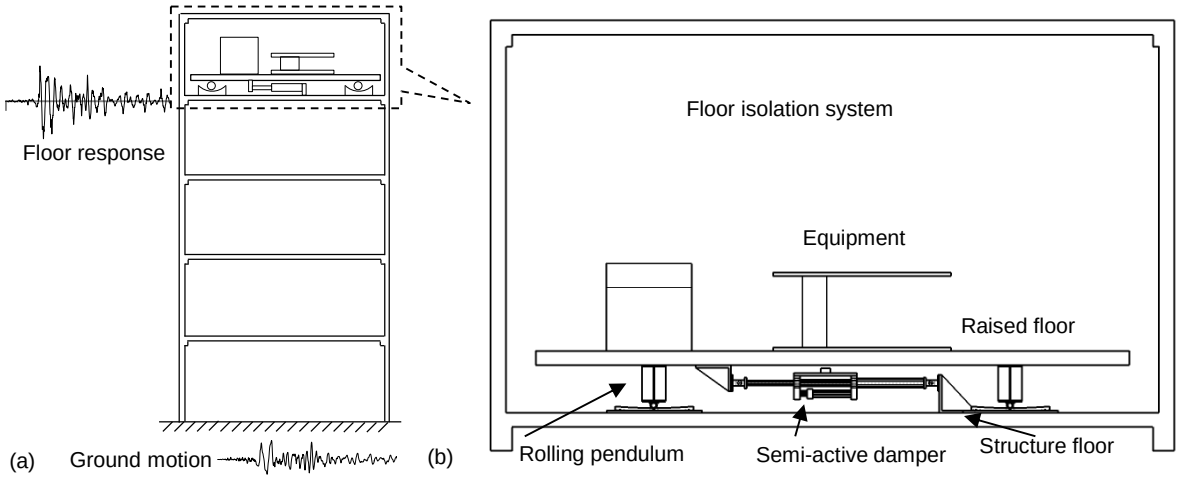


Figure 5.1. Schematic of proposed unidirectional floor isolation system: (a) floor isolation system in fixed-base structure; (b) semi-active floor isolation system.

### 5.2.2 Input motion characteristics

With the configuration of floor isolation system shown in Figure 5.1, the input motion to the floor isolation system is the response of the top floor, which is distinct from the ground motion to the structure. When the ground motion is transferred from the ground to the floor where the floor

isolation is installed, the ground motion is physically filtered by the structure.

When the ground motion dominated by a high frequency (short period) attacks the structure, it will result in the input motion to the floor isolation with the dominant frequency close to the predominant frequency of the structure. The input motion can also be amplified several times from the ground motion because of the resonance effect with the structure. This kind of motion tends to cause large acceleration due to the large magnitude. When the ground motion dominated by a low frequency (long period), here defined as a motion whose dominant frequency is 0.2 to 0.5 Hz (2 to 5 s), attacks the structure, the low frequency component will be transferred through the structure. Although the low frequency is not amplified from the ground, it will still cause large response, especially the displacement, due to the resonance with the floor isolation system.

In summary, the structure significantly filters out frequency components in the ground motion higher than the predominant frequency of the structure, mainly leaving frequency components that are close to or lower than the predominant frequency of the structure. The most critical frequency components of the input motion are those that are close to the predominant frequency of the structure and to the natural frequency of the floor isolation.

### 5.2.3 Test specimen of floor isolation system

To study the effectiveness of the proposed semi-active floor isolation system, a series of shaking table tests were conducted. Figure 5.2 (a) shows the test setup of the floor isolation specimen with a plan of 2.5 m by 2.5 m. Four sets of unidirectional rolling pendulum isolators were installed under the floor isolation system. Figure 5.2 (b) to (d) shows one of the rolling pendulum system used in the test. Assume that floor and contents on the floor are rigid, the natural period of the system will only depend on the geometry (radius) of the pendulum, and the load change on the floor will not influence the natural period [5.5]. Another feature of the pendulum system is that the friction coefficient of it is normally very small. It will benefit the design of semi-active control since it is not easy to account the friction in a linear control theory, such as the LQR control [5.10].

An MR damper, which has damping properties dependent on the applied magnetic field, was chosen to supply the semi-active control. MR dampers have been demonstrated to be very promising for civil engineering applications in both analytical and experimental studies. More detail properties of the rolling pendulum and MR damper are shown in Section 5.3 and 5.4. A steel frame was used to represent the weight of the isolated floor and equipment on the floor.

At the top of the steel frame, a raised floor made of wood panels was erected to simulate a real floor. The raised wooden floor was supported by a steel frame made by steel angles, to provide enough out-of-plan stiffness. Two different furniture items, one table without casters and one table with casters as shown in Figure 5.2, were used to represent the equipment used in a real floor isolation system. The characteristics of the two tables are shown in Table 5.1.

To prevent that the furniture items from falling off the raised floor, a fence was built around the edges of the raised floor. The total weight including the weight of the rollers, connection between roller and steel frame, steel frame, extra weight, raised floor, fence and the furniture items were 62.5

kN. By increasing or reducing the extra weight, it was possible to simulate the load change in real situations in which the furniture items were moved in or moved out.

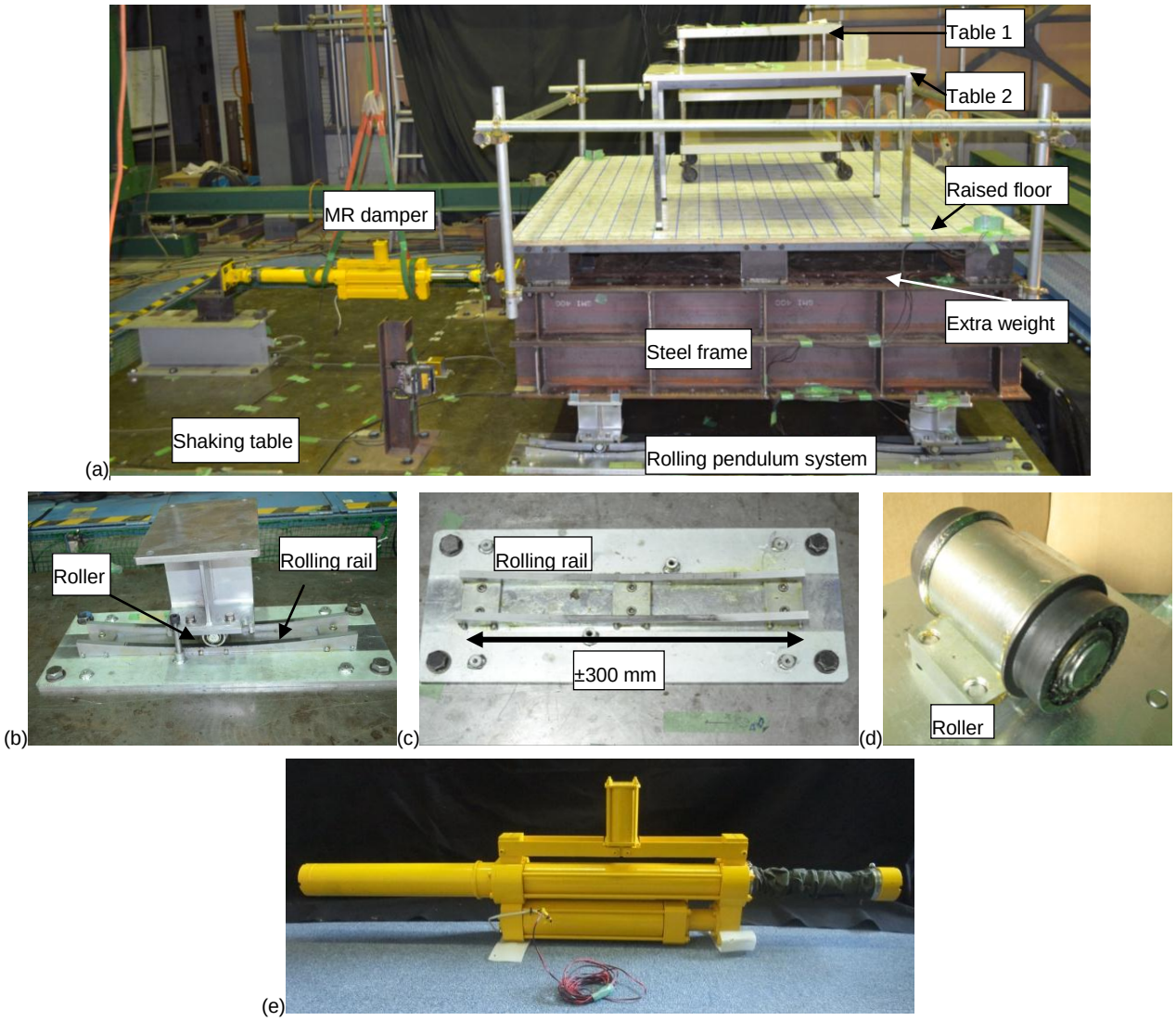


Figure 5.2 Specimen photos: (a) test setup for semi-active controlled floor isolation system; (b) rolling pendulum system; (c) rolling rail; (d) roller; (e) MR damper

Table 5.1 Characteristics of the furniture items

| Furniture items | Sizes (mm) | Mass (kg) | Friction coefficient |
|---|---|---|---|
| Table 1 with casters | 900×600×880 | 19 | 0.03 |
| Table 2 without casters | 1,200×750×700 | 12 | 0.42 |

The assemble of the floor isolation follows the following procedure: (1) locate the rolling pendulums on the shaking table and accurately align them as designed, and fix them on the shaking table; (2) setup the steel frame and extra mass on top of the rolling pendulum system without tightening the connection bolts to allow the slight adjustment in the next step; (3) pull and push the isolated floor for several rounds so the rollers can align with the slider accurately, and the system can run smoothly; (4) tighten the connection bolts; and (5) install the damper and setup the raised floor system and the fence.

In the procedure, Step (1) and (3) are of most impertinence. Misalignment of the pendulum system would result in a change of the natural period, and extra resistance in addition to the friction which was not controllable in semi-active strategy.

For comparison purpose, a floor isolation system shown in Figure 5.3 by replacing the MR damper into an oil damper was also designed to check the performance of passive controlled system. The oil damper and MR damper are designed to have the same maximum load capacity.

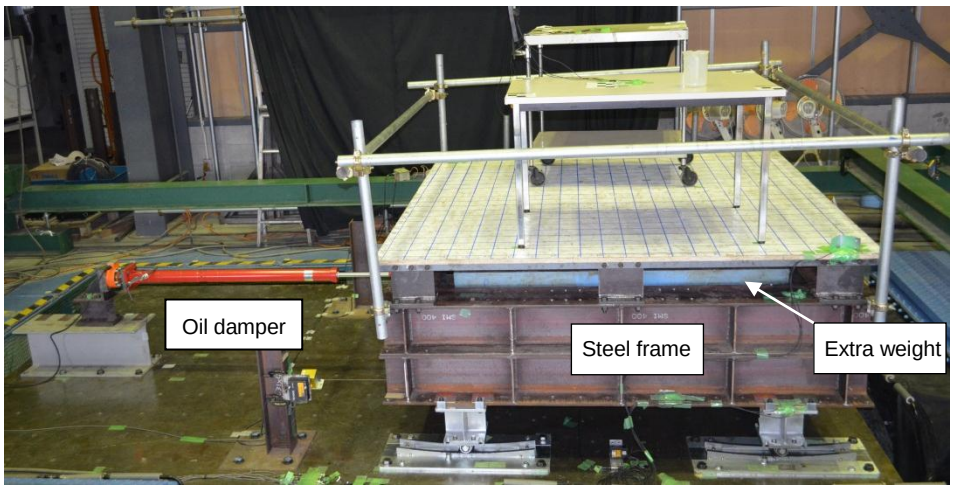


Figure 5.3 Passive floor isolation system with oil damper

## 5.3 Property of rolling pendulum

### 5.3.1 Friction

Static pull/push test was performed to evaluate the static force that would move the floor isolation system smoothly. The friction coefficient was obtained by normalizing the force by the weight of the floor isolation system. The test results show that the friction ratio was 0.01. Dynamic friction of the pendulum could be obtained by Equation (5.1), referring to Figure 5.4. The displacement-force and velocity-force relationships under Sannomaru input motion are shown in Figure 5.5. Also drawn in Figure 5.5 (b) is the friction calculated with the friction ratio of 0.012 obtained from the pull/push test. The figure shows that the friction behavior was complicated and the friction force was dependent on the displacement and velocity. The friction obtained from pull/push test (750N) was close to the maximum of the dynamic friction force.

$$f = \frac{1}{\cos\theta}\left(\left(\frac{m\dot{x}^2}{R} + mg\cos\theta\right)\sin\theta + m\ddot{x}\right) \tag{5.1}$$

$$\theta = \arcsin\left(x / R\right)$$

Since the friction on the rolling pendulum surface was small and did not influence the isolation behavior significantly, especially when the excitation amplitude was large, the static friction

coefficient of 0.012 was adopted for the design the semi-active control presented in Chapter 6.

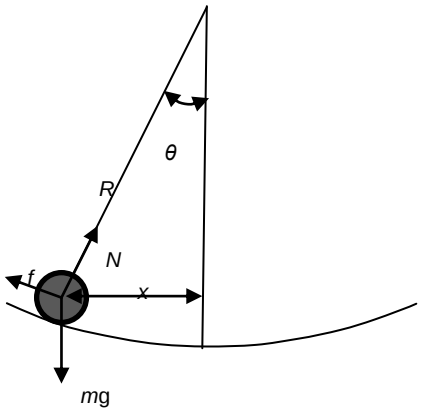


Figure 5.4 Calculation of friction

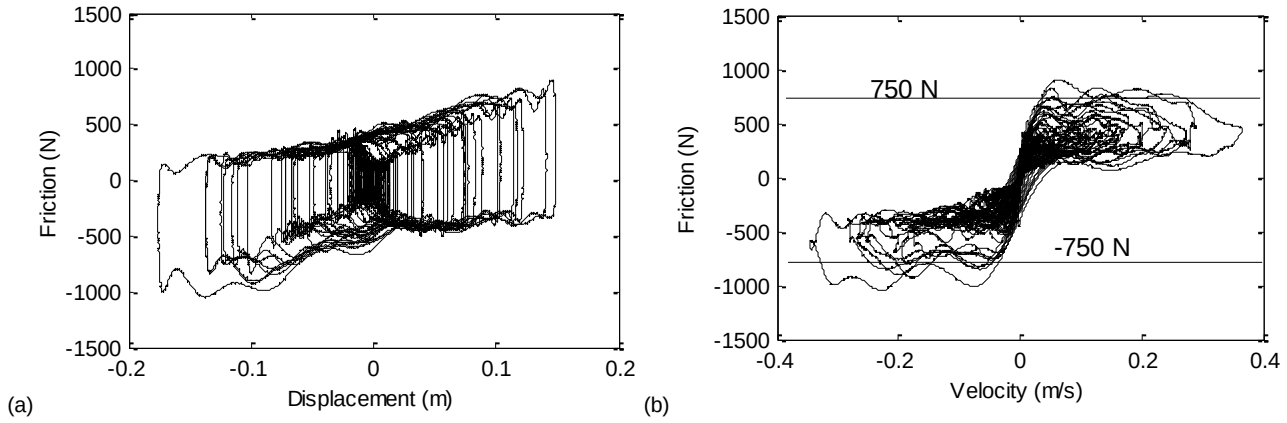


Figure 5.5 Dynamic friction force behavior: (a) Friction-Displacement; (b) Friction-Velocity

### 5.3.2 Natural period

With the assumption that the floor isolation is a SDOF system, the natural period is calculated in Equation (5.2) [5.5]

$$T = 2\pi\sqrt{R_{\mathrm{p}}/g} \tag{5.2}$$

where $R_{\mathrm{p}}$ is the radius of the slider as shown in Figure 5.4, and $g$ is the gravity. The equation indicates that the natural period is dependent only on the geometry of the slider.

The rolling pendulum designed for the prototype floor isolation is with a radius of 2.25 m, which results in a 3.0 s natural period. System identification test with a white noise excitation was carried out to examine the natural period of the rolling pendulum system. The white noise excitation used has the amplitude of 3 m/s$^2$ with frequency band of 0.05 to 15 Hz, and lasted 200 s. A frequency domain curve-fitting algorithm was employed to extract the modal parameters from the transfer function [5.10]. Figure 5.6 shows the curve fitting results of the transfer function magnitude that indicates the natural period of the rolling pendulum was 3.03 s. The identified natural period was

very close to the results calculated from Equation (5.2) of 3.0 s.

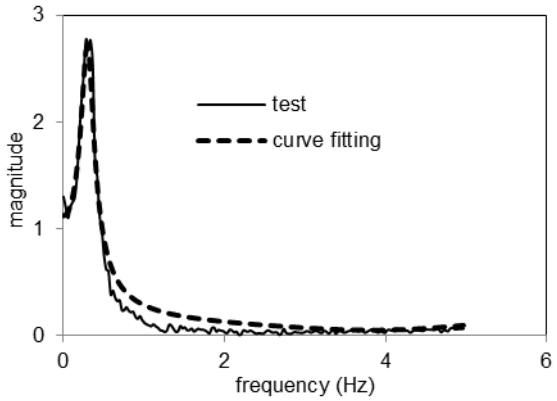


Figure 5.6 Natural period of friction pendulum system

## 5.4 Property of MR damper

Figure 5.7 shows the configuration of the MR damper used for the test and its configuration. The MR damper is a fixed orifice damper with magnetorheological fluid. The fluid has a density of 3,490 kg/m$^3$. When a magnetic field is applied to the fluid by the coil, particle chains form and the fluid becomes a semisolid and exhibits viscoelastic behavior. Transition to rheological equilibrium can be achieved in a few milliseconds [5.11]. The MR damper was designed to have a 10 kN load capacity and ± 200 mm stroke capacity. The total length is 1,549±200 mm as shown in Figure 5.8. The peak power required is 142 watts with a resistance of 16Ω. The current to the electromagnet coil of the MR damper can vary from 0 to 3A, which is supplied by a current driver manufactured by KEPCO, Inc.

In order to develop the control algorithms in Chapter 6, simulation work is necessary. A model must be developed for the simulation that can well describe the relationship between the input current to MR damper and the output force. Hence, dynamic loading test is necessary to validate its properties. Figure 5.8 shows the test setup for the dynamic loading test. One end of the MR damper was connected to the shaking table, and the other end to the frame fixed outside the shaking table. The shaking table acted as an actuator to input different motions to drive the MR damper.

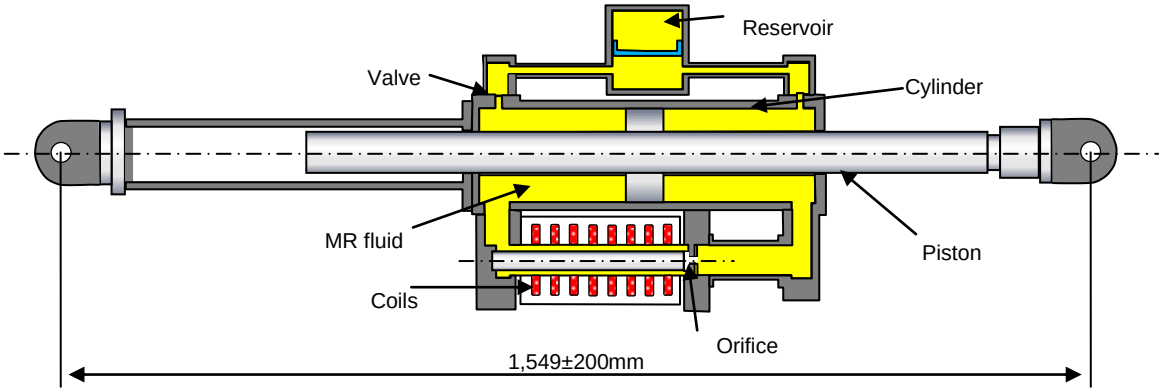


Figure 5.7 MR damper configuration

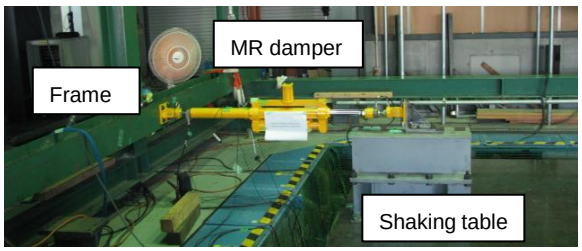

Figure 5.8 Test setup for MR damper property test

Figure 5.9 shows the schematic of the control system designed for validating the MR damper property. Digital control was carried out by using a Texas Instruments TMS320C6701 DSP chip and I/O boards with 16-bit A/D and D/A converters. Discrete-time controller was implemented in the software based on C code programming. The sampling frequency of the control signals from DSP was set to be 1,000 Hz. A displacement transducer was mounted to the damper to measure the displacement of the piston of MR damper. In addition, a load cell was attached to the end of the MR damper to measure the actual force output by the MR damper.

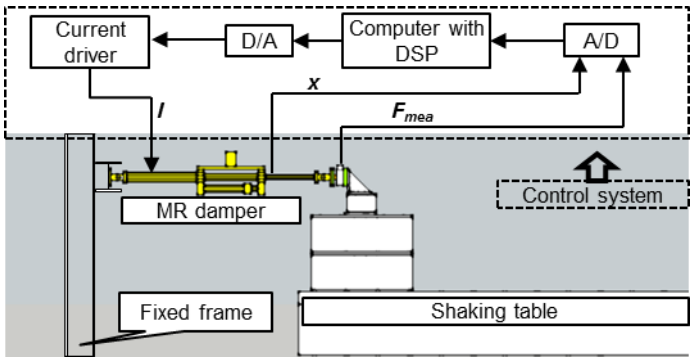

Figure 5.9 Schematic of control system

### 5.4.1 Dynamic loading program

A sinusoid motion was input to the shaking table to drive the MR damper, and the current applied to the MR damper was held at a constant level. In order to investigate the performance of MR damper at different amplitudes of displacement and velocity, a wide range of frequencies and displacement amplitudes of the input motions were considered. The input motions to the shaking table and the currents to the MR damper are listed in Table 5.2.

Table 5.2 Input motion and current

| Displacement (mm) | Frequency (Hz) | Velocity (mm/s) | Current (A) |
|---|---|---|---|
| 20 | 0.12 | 15 | 0, 0.5, 1, 1.5, 2, 2.5, 3 |
| 20 | 0.4 | 50 | 0, 0.5, 1, 1.5, 2, 2.5, 3 |
| 20 | 1.6 | 200 | 0, 0.5, 1, 1.5, 2, 2.5, 3 |
| 100 | 0.64 | 400 | 0, 0.5, 1, 1.5, 2, 2.5, 3 |
| 100 | 0.96 | 600 | 0, 0.5, 1, 1.5, 2, 2.5, 3 |
| 100 | 1.28 | 800 | 0, 0.5, 1, 1.5, 2, 2.5, 3 |

### 5.4.2 Test result

As an example, the response of the MR damper subjected to 1.28 Hz sinusoid motion with the maximum displacement of 100 mm (with the maximum velocity of 0.8 m/s) is shown in Figure 5.10 for seven different levels of current.

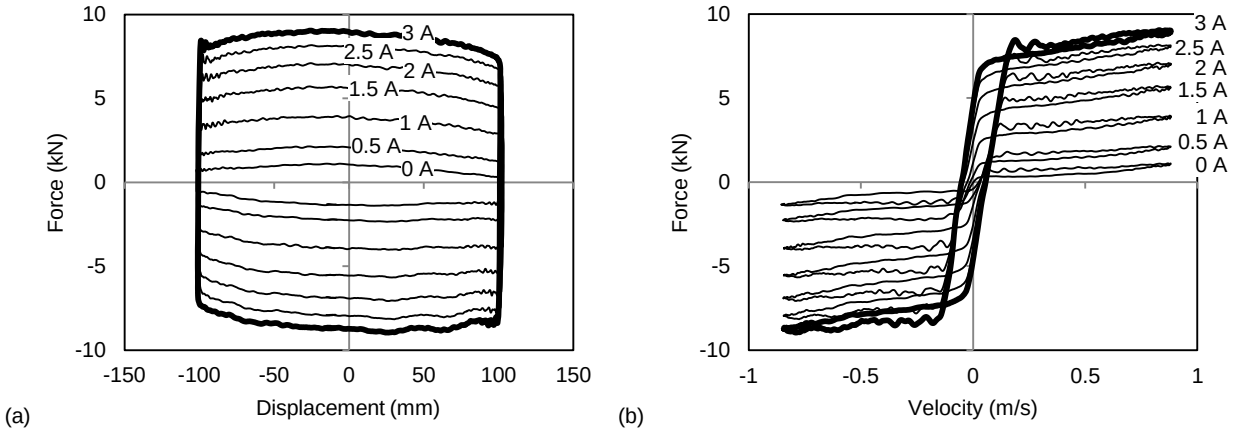


Figure 5.10. MR damper behavior with 1.28 Hz sinusoid motion and different levels of constant current: (a) force-displacement curve; (b) force-velocity curve.

As observed from Figure 5.10 (b), the force of the MR damper is a function of the input current. The maximum capacity of the MR damper reaches to 9 kN at the velocity of 0.88 m/s with a 3 A current input. The force of the MR damper without input current is about 1 kN at the velocity of 0.88 m/s. Also the force is influenced by the velocity. Taking the bolded curve as an example, the relationship between the force and velocity is not linear. At small velocities, the force varies linearly with velocity; however, at large velocities the rate at which the force increases with respect to the velocity decreases significantly. Moreover, it is notable that the relationship between the force and velocity is not one-to-one.

### 5.4.3 Dynamic model

The Bouc-Wen model [5.12, 5.13] was adopted to describe the MR damper behavior. The schematic of this model is shown in Figure 5.11. Using the Bouc-Wen model, the equation governing the MR damper force $F$ is given by

$$\begin{aligned} F &= c_0\dot{x} + k_0(x - x_0) + \alpha z \\ z &= -\gamma\left|\dot{x}\right| z \left|z\right|^{n-1} - \beta\dot{x}\left|z\right|^{n} + A_0\dot{x} \end{aligned} \tag{5.3}$$

where $z$ is an evolutionary variable. Parameters $k_0$, $x_0$, $\beta_0$, and $n$ are assumed constant and $c_0$, $\alpha_0$, $\gamma_0$ and $A_0$ are assumed to depend on the current applied to the MR damper. The following relationships are adopted for the damper used in this study [5.14]:

$$c_0 = c_{01}I + c_{02},\ \alpha_0 = \alpha_{01}I + \alpha_{02},\ \gamma_0 = \gamma_{01}/(\chi_1 I + \chi_2),\ A_0 = A_1/(\chi_1 I + \chi_2) \tag{5.4}$$

where $I$ is the input current to the MR damper. There are twelve parameters in the Bouc-Wen model that need to be calibrated. Using numerical simulation, the parameters were chosen to be $c_{01}$=200 N·s/m/A, $c_{02}$=600 N·s/m, $k_0$=-3,000 N/m, $x_0$=0 m, $\alpha_{01}$=9,900 N/A/m, $\alpha_{02}$=1,300 N/m, $\gamma_{01}$=10,000 $m^{-2}$, $\chi_1$=0.66 $A^{-1}$, $\chi_2$=0.25, $n$=2, $\beta_0$=2,000 $m^{-2}$, and $A_1$=1,000.

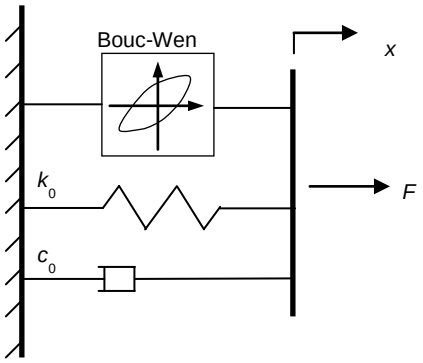


Figure 5.11 Schematic of Bouc-Wen model

Figure 5.12 shows the comparison between the predicted responses using the Bouc-Wen model and the corresponding experimental data, for the sinusoidal input motion with 1.28 Hz frequency and input current to the MR damper of 2 A. The comparison shows that the Bouc-Wen model can reasonably reproduce the MR damper behavior.

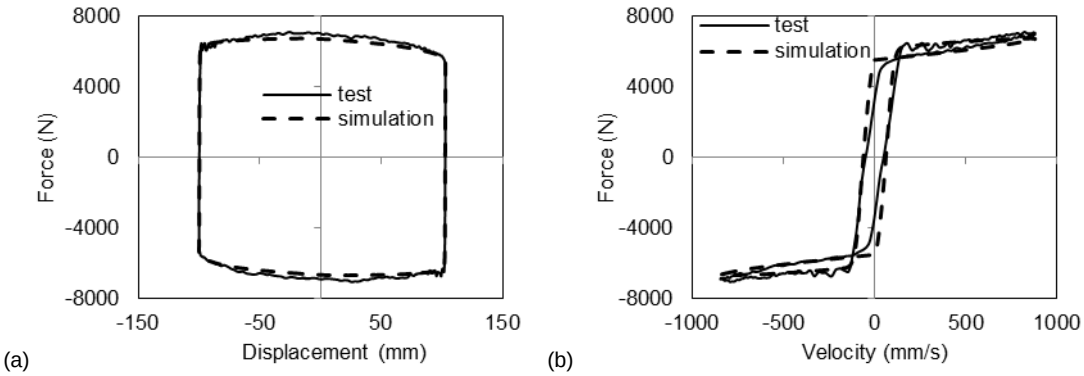


Figure 5.12 Comparison between predicted and experimentally obtained responses for the Bouc-Wen model: (a) force-displacement; (b) force-velocity

To check the performance of the Bouc-Wen model with a real ground motion, an example result is shown in Figure 5.13. The real ground motion is JMA Kobe. The error corresponding to the maximum force of 9,415 N is 318 N which indicates that the Bouc-Wen model can accurately simulate the MR damper behavior for real ground motion.

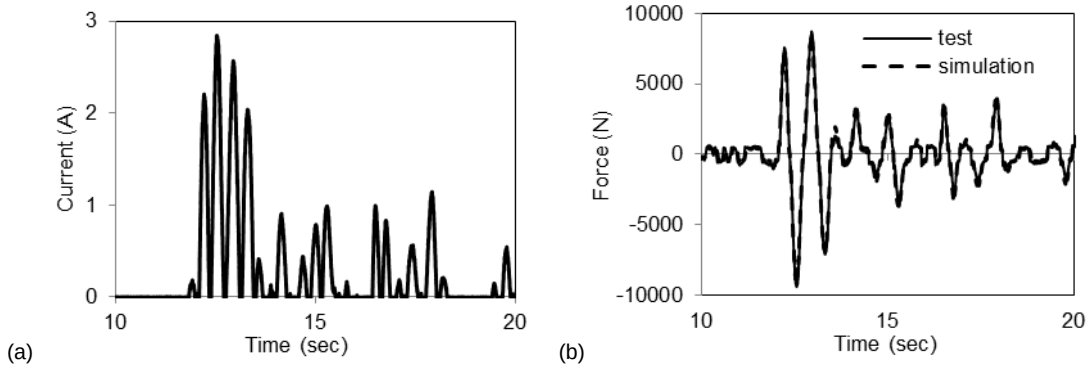


Figure 5.13 Time history of: (a) input current; (b) force comparison between predicted and experimentally obtained responses for Bouc-Wen model under JMA Kobe motion

In order to design an inverse dynamic mode, a Bingham model which is essentially a bilinear model is also proposed as shown in Figure 5.14. The control force is calculated as

$$u = \text{sign}\left(\dot{x}\right) f_c + c_0 \dot{x} + f_0 \tag{5.5}$$

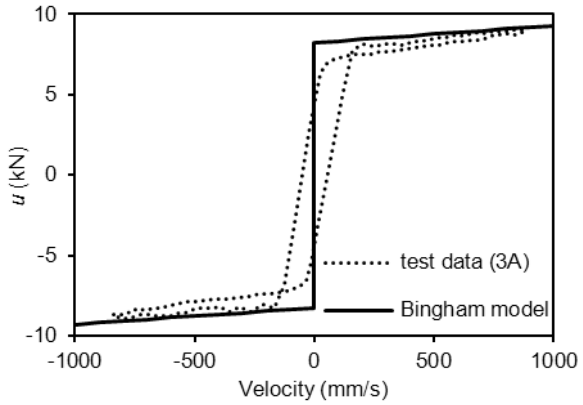


Figure 5.14 Bingham model

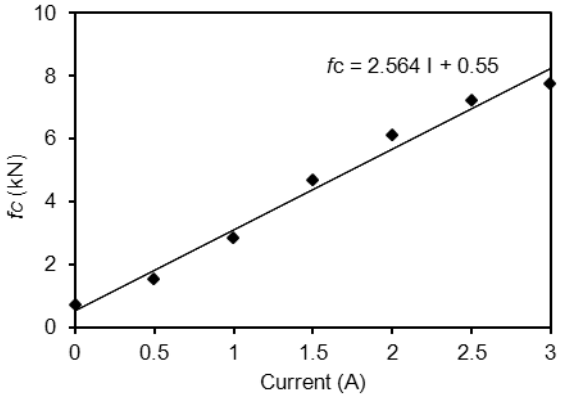


Figure 5.15 Relationship between $f_c$ and $I$

Test results show that the parameter $f_c$ ($N$) has a linear relationship with current $I$ as shown in Figure 5.15, and

$$f_c = 2564\, I + 550,\ c_0 = 1060,\ f_0 = 0 \tag{5.6}$$

## 5.5 PI controller design

Due to the complicated nonlinear behavior of MR damper, it is not easy to build a simple yet effective inverse dynamic model from the dynamic model, e.g., the Bouc-Wen model, directly. To overcome this difficulty, a clipped-optimal controller [5.15] has been developed and extensively used. The current to the MR damper based on this controller switches between zero and the maximum, which may cause large structural response as describe in Chapter 2. In this research, a PI

controller is proposed to calculate the current signal [5.16]. The PI controller is designed with the transfer function from the input current to the output force of the MR damper.

### 5.5.1 Dynamic loading program

A triangular type motion was used as the input to drive the MR damper at a constant velocity. Limited by the loading system capacity, the velocities tested were relatively low (40mm/s and 75 mm/s). The input current to the MR damper was a sinusoid signal at a wide range of frequencies, including 1 Hz, 2 Hz, 3 Hz, 4 Hz, 5 Hz, 6 Hz, 8 Hz, 10 Hz, 15 Hz, 20 Hz, 30 Hz and 40 Hz. The amplitudes of the current were 1 A and 3 A. Figure 5.16 shows the time histories of input displacement, velocity, current and the measured MR damper force.

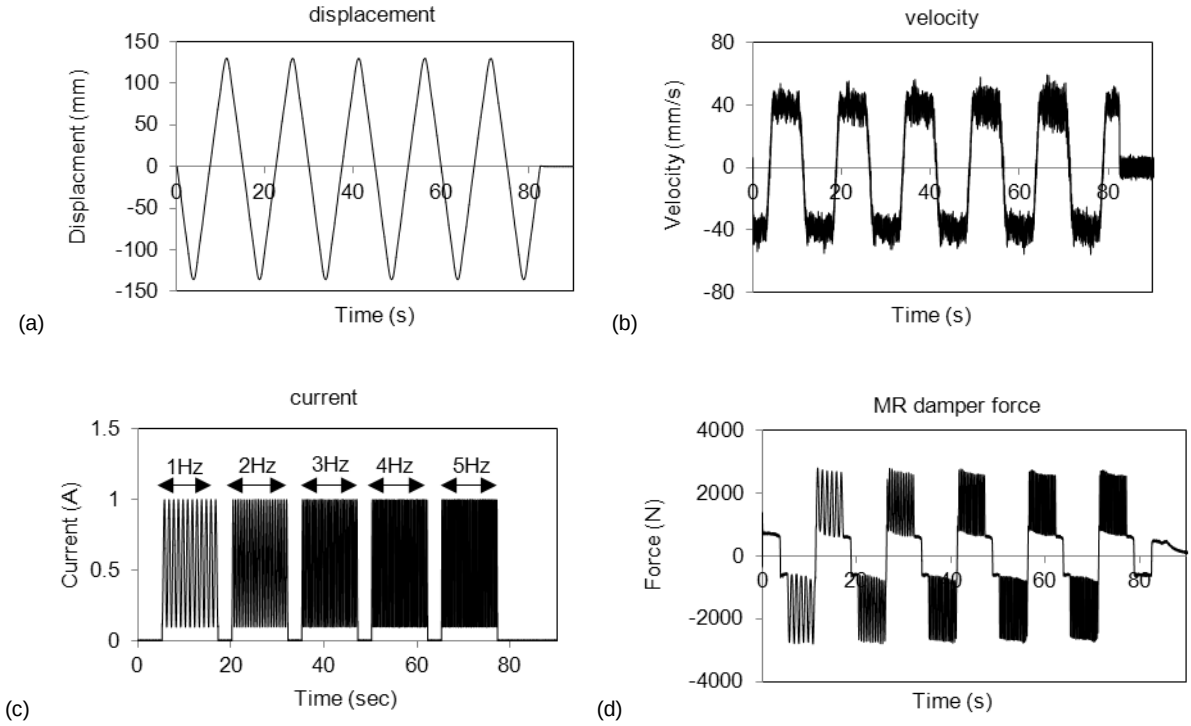


Figure 5.16 Time histories: (a) displacement; (b) velocity; (c) current; (d) MR damper force

### 5.5.2 Transfer function of MR damper

The transfer function $T_{cf}$ of the MR damper from the input current to output force, can be estimated as the quotient of the cross power spectral density ($P_{cf}$) of the current and force, and the power spectral density ($P_{cc}$) of current as shown in Equation (5.7):

$$T_{cf} = P_{cf}/P_{cc} \tag{5.7}$$

In the test the transfer function was obtained by checking the amplitudes and phases at different current frequencies tested. The obtained amplitudes and phases were used to form the complete transfer function in a discrete form. As an example, Figure 5.17 shows the magnitude and phase data

of $T_{cf}$ with the input current amplitude of 1 A and frequency of 1 Hz. The data at the particular location of 1 Hz, which was the same as the input current, was chosen as the amplitude and phase of $T_{cf}$. Consequently, the data for the transfer function at other frequencies were also calculated and are drawn in Figure 5.18 with square markers. The transfer functions of the MR damper tested at other three conditions are also shown. It should be pointed out that the transfer functions were different at either different loading velocities or current input amplitudes, which is evident in Figure 5.18, due to the nonlinear characteristics of the MR damper. The magnitude of the transfer function decreased as the current frequency increased rather than remains at a constant value.

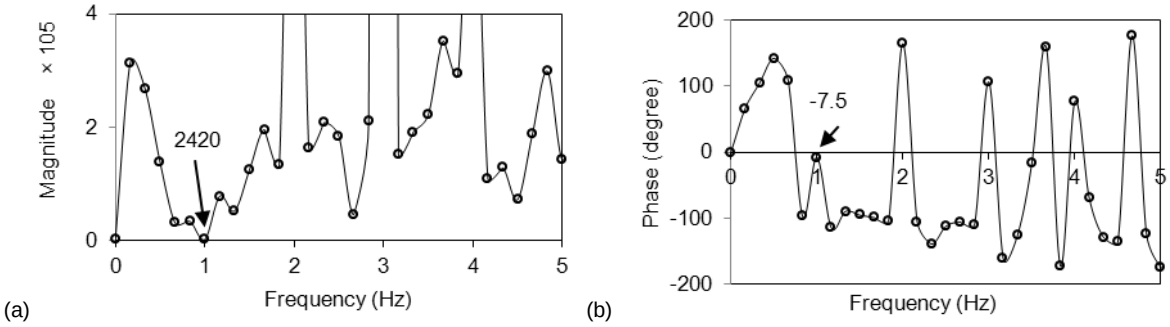


Figure 5.17 Magnitude and phase of the transfer function: (a) magnitude; (b) phase

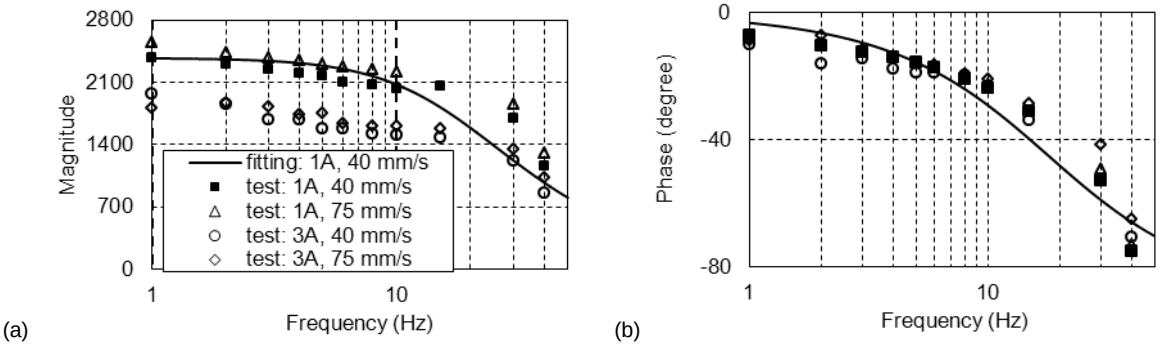


Figure 5.18 Transfer function for MR damper: (a) magnitude; (b) phase

Since the transfer function obtained from the test was in a discrete form, it was difficult to use it in designing the PI controller. A first order low-pass filter was used to fit the test transfer function with testing condition of 1A, 40 mm/s as shown in Equation (5.8), and was used to design the PI controller in next section.

$$T_{cf} = \frac{2375 \times 18 \times 2\pi}{s + 18 \times 2\pi} \tag{5.8}$$

### 5.5.3 PI controller

The PI controller was designed using the transfer function from the input current to output force shown in Equation (5.8). Figure 5.19 shows the block diagram of the PI controller for the MR

damper and the controller can be expressed in Equation (5.9) by employing a high-pass filter to eliminate the influence of low frequency on the integration part of the PI controller.

$$I=s/(s+\omega_1)/(K_p+K_i/s)e \tag{5.9}$$

in which $\omega_1$ is the cut off frequency=0.1 Hz; $K_p$=0.0002 and $K_i$=0.05 were determined by trial and error with the diagram shown in Figure 5.19, in which the MR damper was represented with the transfer function shown in Equation (5.9). Use of the transfer function instead of an MR damper model such as Bouc-Wen model would significantly save simulation time by trial and error. Symbol $e$ was the error force between the absolute value of designed force $f_{des}$ and the absolute value of actual measured force $f_{mea}$. Figure 5.20 shows the transfer functions of the PI controller from $f_{des}$ to $f_{mea}$, and from $e$ to $f_{mea}$. As a comparison, the PI controller with $K_p$=0.005 and $K_i$=0.05 was also designed. Although the PI controller with $K_p$=0.005 was more effective than the controller with $K_p$=0.0002 in reproducing the design force since it had a smaller phase change and the magnitude at frequencies larger than 10 Hz was closer to 1. However, the magnitude of the transfer function from $e$ to $f_{mea}$ had a much larger value than that of the system with $K_p$=0.0002 at frequencies larger than 1 Hz. This stiffer design might cause large errors due to the noise in high frequency band.

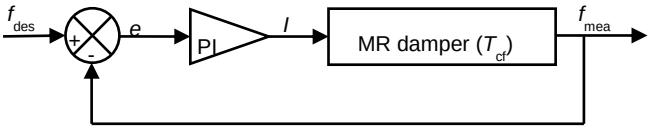


Figure 5.19 Block diagram of PI controller

An inverse Bingham model calculated from Equations (5.5) and (5.6) was also built for comparison purpose [5.16]

$$I=\left(f_{des}-550-1060\dot{x}\right)/\left(2564\text{sign}\left(\dot{x}\right)\right) \tag{5.10}$$

where $f_{des}$ is the design force determined from the control algorithm adopted; and $\dot{x}$ is the velocity of the MR damper. The main disadvantage of this model is that it reproduces a one-to-one relationship between current and velocity, and therefore it does not reproduce the hysteretic behavior observed at low frequency zone [5.16].

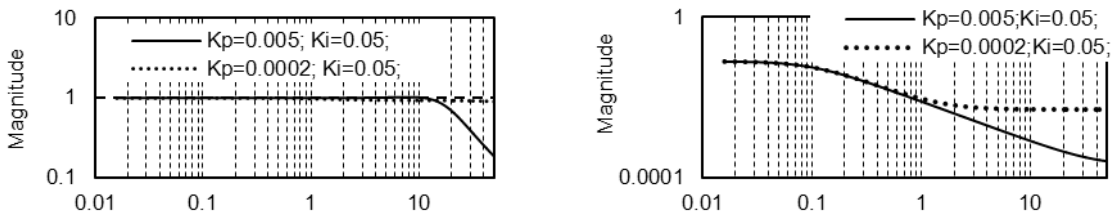

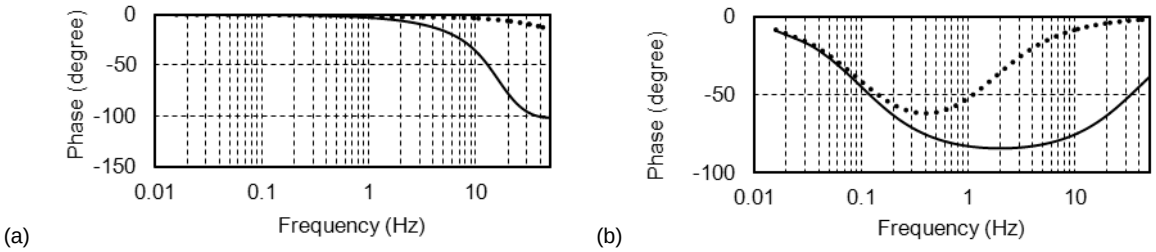


Figure 5.20 Transfer functions: (a) from $f_{des}$ to $f_{mea}$; (b) from $e$ to $f_{mea}$

A series of dynamic loading test was conducted to validate the PI controller efficiency. A sinusoidal type signal varying from 0.3 to 10 Hz (see Figure 5.21 (a)) was used as the designed force to be tracked. The MR damper piston moved in a constant velocity of 40 mm/s. In addition to the PI controller and inverse Bingham model, a clipped optimal controller without a low pass filter [5.15] was also tested.

Figure 5.21 shows the comparison of accuracies for the three different models. The comparison shows that the PI controller (with $K_p$=0.0002 and $K_i$=0.05) had smallest errors among the three at frequencies smaller than 3 Hz, and the maximum error was under 15% of the target force to track. The results also show that the PI controller with $K_p$=0.005 had larger errors than with $K_p$=0.0002, which proves that the noise would cause significant errors for the stiff controller design.

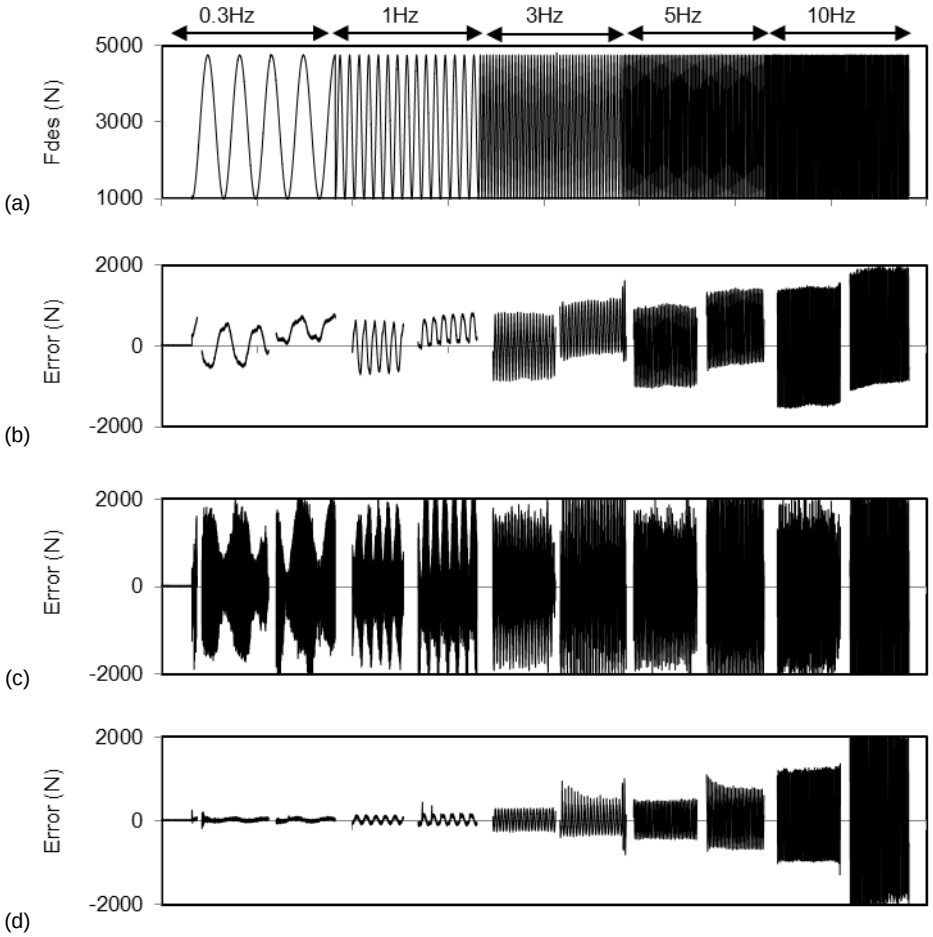

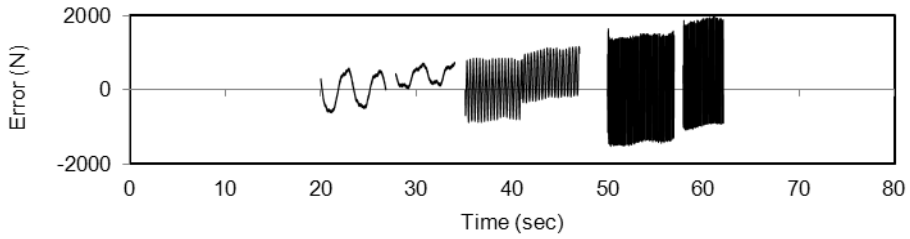


(e)

Figure 5.21 Comparison of the accuracies: (a) designed force; (b) Bingham model; (c) PI controller ($K_p$=0.005); (d) PI controller ($K_p$=0.0002); (e) clipped optimal

## 5.6 Summary

In Chapter 5, a unidirectional prototype floor isolation system with semi-active control is proposed to protect a group of important and expensive appliances. The floor isolation system should minimize the acceleration to protect equipment; however, displacement must also be limited to save floor space, especially with long-period motion. Major findings can be summarized as follows:

(1) The designed floor isolation system contains a rolling pendulum to ensure the flexibility, and a MR damper to supply the semi-active control force. The natural period of the system is 3 s, and the friction coefficient on the pendulum rolling surface is 0.01.

(2) The designed floor isolation is installed on the top floor of a five story RC building. When the ground motion is transferred through the structure to the input motion of the floor isolation, the structure significantly filters out frequency components in the ground motion higher than the predominant frequency of the structure, mainly leaving frequency components that are close to or lower than the predominant frequency of the structure.

(3) A series of dynamic loading tests were performed to evaluate the properties of the MR damper. The MR damper is essentially a nonlinear device. The force of the MR damper is a function of the input current and velocity. A Bouc-Wen model was adopted to describe the MR damper behavior. Comparison with dynamic loading test results shows that the Bouc-Wen model can accurately match the test results, and reasonably describes the hysteretic behavior at small velocity zone.

(1) A PI controller is designed to calculate the current to the MR damper based on the designed force using the transfer function of the MR damper operating at velocity of 40 mm/s. Test results show that the proposed PI controller could effectively track the target force with frequency lower than 3 Hz. The maximum error was under 15% of the target force to track.

## REFERENCES

[5.1] Skinner RI, Robinson WH, McVerry GH. An introduction to seismic isolation. Wiley: Chichester, England, 1993.

[5.2] Sato E, Furukawa S, Kakehi A, Nakashima M. Full shaking table test for examination of safety and functionality of base-isolated medical facilities. *Earthquake Engineering and*

*Structural Dynamics* 2011; 40: 1435-1453.

[5.3] Furukawa S, Sato E, Shi Y, Becker T, Nakashima M. Full-scale shaking table test of a base-isolated medical facility subjected to vertical motions. *Earthquake Engineering and Structural Dynamics*.

[5.4] Fujita T. Earthquake isolation technology for industrial facilities-research, development and applications in Japan. *Bulletin of the New Zealand National Society for Earthquake Engineering* 1985; 18(3): 224-249.

[5.5] Lambrou V, Constantinou MC. Study of seismic isolation systems for computer floors. *Rep*. No. NCEER-94-0020, State University of New York at Buffalo, Buffalo, N.Y., 1994.

[5.6] Shook D, Lin PY, Lin TK, Roschke PN. A comparative study in the semi-active control of isolated structures. *Smart Materials and Structures* 2007; 16: 1433-1446.

[5.7] Cui S, Bruneau M, Kasalanati A. Behavior of bidirectional spring unit in isolated floor systems. *Journal of Structural Engineering* 2010; 136(8): 944-952.

[5.8] Liu S, Warn GP. Seismic performance and sensitivity of floor isolation systems in steel plate shear wall structures. *Engineering Structures* 2012; 42: 115-126.

[5.9] Nagarajaiah S, Sun X. Response of base-isolated USC hospital building in Northridge earthquake. *Journal of structural engineering* 2000; 126: 1177-1186.

[5.10] Preumont A. Vibration control of active structures: an introduction. Kluwer Academic Publishers: England, 2002.

[5.11] Bossis G, Khuzir P, Lacis S, Volkova O. Yield behavior of magnetorheological suspensions. *Journal of Magnetism and Magnetic materials* 2003; 258-259: 456-458.

[5.12] Wen YK. Method of random vibration of hysteretic systems. *Journal of Engineering Mechanics Division ASCE* 1976; 102 (2): 249-263.

[5.13] Spencer BF, Dyke SJ, Sain MK, Carlson JD. Phenomenological model of magnetorheological damper. *Journal of Engineering Mechanics* 1997; 123(3): 230-238.

[5.14] Sahasrabudhe SS, Nagarajaiah S. Semi-active control of sliding isolated bridges using MR dampers: an experimental and numerical study. *Earthquake Engineering and Structural Dynamics* 2005; 34: 965-983.

[5.15] Dyke SJ, Spencer BF, Sain MK, Carlson JD. Modeling and control of magnetorheological dampers for seismic response reduction. *Smart Materials and Structures* 1996; 5: 565-575.

[5.16] Shi Y, Becker T, Kurata M, Nakashima M. Design of a PI controller for MR dampers using damper force feedback. *International Symposium on Earthquake Engineering* 2012.

# CHAPTER 6

# Control strategies for floor isolation system

## 6.1 Introduction

### 6.1.1 Background

Floor isolation is an alternative to base isolation for protecting a specific group of equipment installed on a single floor or room in a fixed-base structure. The acceleration of the isolated floor should be mitigated to protect the equipment, and the displacement needs to be suppressed, especially under long-period motions, to save more space for the floor to place equipment.

The design of a floor isolation system should consider the high variability of input motions. Long-period (low frequency) motions, defined here as motions having a predominant period close to or longer than the natural period of the floor isolation system (typically about 2 to 5 s), can be produced by subduction faults or soft soil conditions [6.1] and may result in large displacements in the isolation system due to resonance. Large displacements necessitate large clearances between the floor isolation system and the surrounding walls, decreasing useable area. Thus, the displacement of floor isolation systems under long-period motions should be limited. To reduce the displacements of floor isolation systems in long-period motions, high values of passive damping can be used, but at the expense of increased floor accelerations, especially for short-period (high frequency) motions [6.2]. As the primary function of a floor isolation system is to protect the equipment on the floor from damage, the acceleration of the floor system should be minimized. Thus, a system that can alter its response based on the input is desired.

In this study, semi-active control is investigated for use in floor isolation systems. The effectiveness of semi-active control relies significantly on the control algorithm design. In designing a semi-active floor isolation system that is effective in reducing acceleration for both short- and long-period motions while still limiting displacements, it is necessary to consider the frequency characteristics of different excitations. LQR control has been widely used in structural control [6.3-6.6]. The control gains used in LQR control are determined ignoring the input motion characteristics, and the calculated control gains remain constant.

In light of this, one method termed as the LQR control with frequency-dependent scheduled gain (LQRSG) method is proposed in this research for the floor isolation system in which the influence of excitation is considered in the time domain. The controller is designed based on the

traditional LQR control, with additional feedforward information of the excitation, monitored by acceleration sensors. Preliminary simulation results reveal that the determination of the control gain in the control is related to the dominant frequency of input motion. A window method is proposed to monitor the excitation and detect the dominant frequency in "real time" with a slight time delay in the time domain.

$H_\infty$ control is a frequency domain control method that allows the designer to directly deal with the input motion characteristics by implementing an input motion filter, and specify the disturbance attenuation over a desired frequency range [6.7, 6.8]. The real input motion is represented by a Gaussian white noise process passed through the input motion filter. With such a method, the control strategy can reasonably describe the excitation features over an entire class of excitation. It is adopted in this study to compare with the LQRSG method.

In addition, passive control is also designed. Shaking table testing program is outlined in this chapter to validate the semi-active control with different control algorithms.

### 6.1.2 Organization

This chapter describes the formulation of different control methods, including the passive control, traditional LQR control, LQRSG control, and $H_\infty$ control. Section 6.2 introduces the equation of motion of the floor isolation system based on a SDOF system. Simplification is carried out to simplify the nonlinear system to be linear. The passive control using oil damper is described in Section 6.3. Section 6.4 presents the formulation of the LQR control, which is the base of the new LQRSG method. Section 6.5 presents the development of the LQRSG method to consider the characteristics of input excitation in the time domain. The $H_\infty$ control which considers the characteristics of the input motion in the frequency domain is introduced in Section 6.6.

## 6.2 Equation of motion

Consider the isolated floor and the equipment on top to be a rigid body, the dynamic equation of motion of the SDOF floor isolation system shown in Figure 6.1 can be expressed as

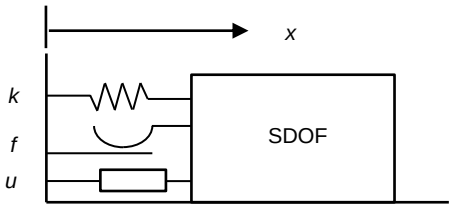


Figure 6.1 SDOF model

$$\ddot{x} + 2\zeta\omega\dot{x} + \omega^2 x + f_p / m + u / m = -\ddot{x}_{in} \tag{6.1}$$

where $x$ is the relative displacement of the floor isolation system with respect to the structure floor, $\zeta$ and $\omega$ are the viscous damping ratio and the natural frequency of the system respectively, $f_p$ is the friction on the contact surface of the rolling pendulum, $u$ is the control force of the MR damper, $\ddot{x}_{in}$ is the input acceleration, and $m$ is the total mass of the floor isolation system. For the floor isolation system with rolling pendulums considered in this study, the viscous damping ratio $\zeta$ is very small and can be assumed to be 0.

The system described in Equation (6.1) is a nonlinear system due to the characteristic of friction force. In order to apply the linear design method of semi-active control, a simple procedure is taken to consider the optimal control force by combining the friction force and MR damper control force together as follows

$$\ddot{x} + 2\zeta\omega\dot{x} + \omega^2 x + u^* / m = -\ddot{x}_{in} \tag{6.2}$$

where $u^*=f+u$. Equation (6.2) can readily be transferred into the state space form

$$\dot{\mathbf{X}} = \mathbf{A}\mathbf{X} + \mathbf{B}u^* + \mathbf{H}\ddot{x}_{in} \tag{6.3}$$

where

$$\mathbf{X} = \begin{bmatrix} x \\ \dot{x} \end{bmatrix}, \quad \mathbf{A} = \begin{bmatrix} 0 & 1 \\ -\omega^2 & -2\zeta\omega \end{bmatrix}, \quad \mathbf{B} = \begin{bmatrix} 0 \\ -1/m \end{bmatrix}, \quad \mathbf{H} = \begin{bmatrix} 0 \\ -1 \end{bmatrix} \tag{6.4}$$

## 6.3 Passive control

To compare with the semi-active controlled floor isolation system, passive control floor isolation system is also designed by using an oil damper.

Figure 5.3 shows the test setup for the floor isolation system with oil damper. The oil damper used in this research was designed to have the same load capacity of 10 kN with the MR damper, when the moving velocities of both the oil damper and MR damper are 1m/s and the input to the MR damper is set at the maximum current of 3 A. The oil damper properties were validated by a series of dynamic loading tests with sinusoidal motions using the same setup as shown in Figure 5.8 (by replacing the MR damper into the oil damper). Figure 6.2 shows the force-displacement and force-velocity relationships of the oil damper tested under the sinusoidal motion with a 150 mm amplitude and 1 Hz frequency. The responses of the damper under different test conditions show that the damper force $f_{oil}$ is proportional to the velocity of the oil damper $\dot{x}$,

$$f_{oil} = C\dot{x} \tag{6.5}$$

where $C$=10 kN·s/m is the constant damping coefficient.

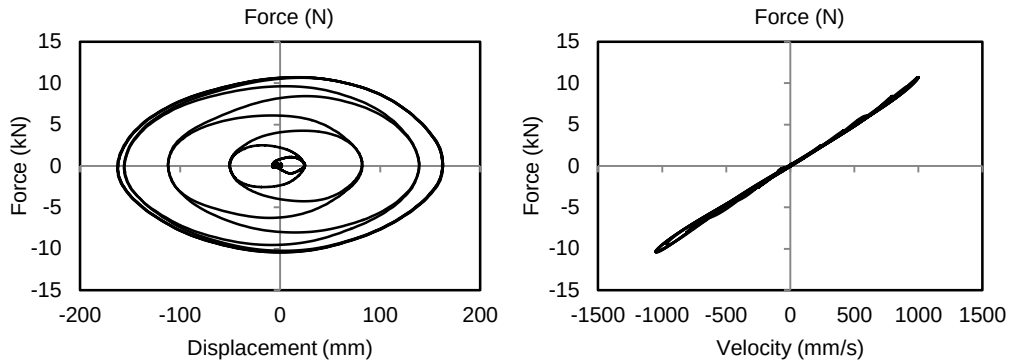


Figure 6.2 Oil damper behavior under 150 mm and 1 Hz sine wave

To validate the performance of passive control for load changes on the floor, three different floor isolation systems were designed by placing different weights on the steel frame shown in Figure 5.3. The standard total weight was 62.5 kN. The weight of 35 kN was used to represent the situation that some of the equipment was taken out, while the weight of 82.5 kN was used to represent that new equipment was moved in. The corresponding damping ratios to the three weights are shown in Table 6.1.

Table 6.1 Damping ratio of floor isolation system FOR different weights

| Weight (kN) | 35 | 62.5 | 82.5 |
|---|---|---|---|
| Damping ratio | 0.68 | 0.38 | 0.29 |

The damping ratios shown in Table 6.1 are relatively high which can benefit the reduction of the displacement in the floor isolation and help save more usable spaces to place equipment.

## 6.4 LQR control

### 6.4.1 Semi-active control strategy

Figure 6.3 shows the block diagram of the controller design for the floor isolation system. The desired control force is calculated firstly based on the controller from the active control theory, such as the LQR and $H_\infty$ controls. The force tracking system using PI controller (see Chapter 5) will calculate the control signal to the MR damper so that the actual force can trace the desired force as close as possible. Because calculation of the current from the PI controller uses the differences of the absolute value of the desired and actual forces, the direction of the designed force is very important. Typically the semi-active control devices including the MR damper are intrinsically energy dissipation devices, and therefore they cannot add mechanical energy to the controlled system. If the desired force obtained from the controller pushes the structure to move, the force is not achievable with the MR damper due

to the damper's energy dissipation feature. If this desired force is sent to the PI controller, an incorrect current will be obtained because that the PI controller cannot sense the direction of the force. In order to consider this feature of the MR damper and feed the correct desired force information to the PI controller, a secondary controller is designed with the governing Equations (6.6) to (6.7) to link the active control theory and the semi-active control device. The positive direction is defined as the tension force and velocity in the elongation of the MR damper.

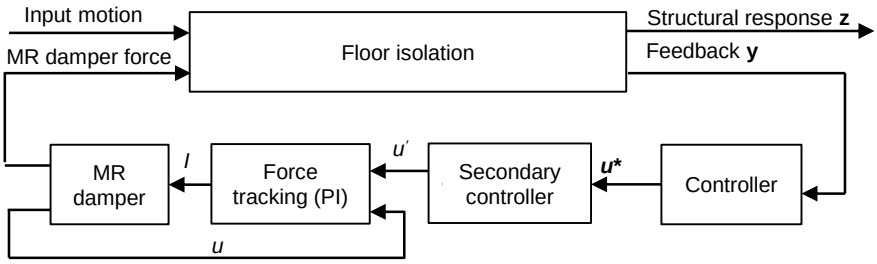


Figure 6.3 Block diagram of controller design

$$u^{'} = u^{*} - f \tag{6.6}$$

$$u = \begin{cases} u^{'} & \left(u^{'} \cdot \dot{x} > 0\right) \\ u_{\min}^{'} & \left(u^{'} \cdot \dot{x} \le 0\right) \end{cases} \tag{6.7}$$

where $u_{\min}^{'}$ is the minimum force of the semi-active device when the input current is zero.

The available feedback signals for the feedback **y** for the controller includes the displacement and velocity. The structural response **z** to be suppressed by the controller includes the absolute acceleration and displacement.

$$\mathbf{y} = \mathbf{C}_{\mathrm{y}}\mathbf{X} + \mathbf{D}_{\mathrm{y}}u^{*} + \mathbf{E}_{\mathrm{y}}\ddot{x}_{\mathrm{in}} \tag{6.8}$$

$$\mathbf{z} = \mathbf{C}_{\mathrm{z}}\mathbf{X} + \mathbf{D}_{\mathrm{z}}u^{*} + \mathbf{E}_{\mathrm{z}}\ddot{x}_{\mathrm{in}} \tag{6.9}$$

Where

$$\mathbf{C}_{\mathrm{y}} = \begin{bmatrix} 1 & 0 \\ 0 & 1 \end{bmatrix},\ \mathbf{D}_{\mathrm{y}} = \mathbf{0},\ \mathbf{E}_{\mathrm{y}} = \mathbf{0},\ \mathbf{C}_{\mathrm{z}} = \begin{bmatrix} -\omega^{2} & -2\zeta\omega \\ 1 & 0 \end{bmatrix},\ \mathbf{D}_{\mathrm{z}} = \begin{bmatrix} -1/m \\ 0 \end{bmatrix},\ \mathbf{E}_{\mathrm{z}} = \mathbf{0} \tag{6.10}$$

### 6.4.2 LQR control and weighting matrices

LQR control is widely used in the active and semi-active control [6.3-6.6]. Assuming the

independence of the input excitation and measurement noises, the optimal control force is designed by minimizing the performance function *J*, which weights the displacement and velocity [6.3-6.5]

$$J = \int_0^t \left( \mathbf{X}^T \mathbf{Q} \mathbf{X} + u^{*T} R u^* \right) dt \tag{6.11}$$

where **Q** is a 2×2 semi-positive definite weighting matrix for the structure responses, i.e., displacement and velocity, and *R* is a positive weighting scalar for the control force.

The resulted optimal control force

$$u^* = -\mathbf{G}\mathbf{y} = -\mathbf{G}\begin{bmatrix} x & \dot{x} \end{bmatrix}^T \tag{6.12}$$

where **G** is the feedback gain (i.e., the controller in Figure 6.4). It can be solved in the MATLAB [6.9] environment by computing the unique solution **P** of the algebraic Riccati equation [6.10]

$$\begin{aligned} &\mathbf{A}^T\mathbf{P} + \mathbf{P}\mathbf{A} - \mathbf{P}\mathbf{B}R^{-1}\mathbf{B}^T\mathbf{P} + \mathbf{Q} = 0 \\ &\mathbf{G} = R^{-1}\mathbf{B}^T\mathbf{P} \end{aligned} \tag{6.13}$$

The selection of **Q** and *R* plays an important role in designing the control gain. The assigned values for the elements of **Q** and *R* represent the relative importance of the reduction of the displacement, velocity and control. As of yet there is no systematic approach for selecting **Q** and *R*. An oft-used method is to assume **Q** to be a diagonal matrix [6.5, 6.6], such as

$$\mathbf{Q} = \begin{bmatrix} q_{11} & 0 \\ 0 & q_{22} \end{bmatrix} \tag{6.14}$$

A second type of diagonal matrix for **Q** [6.3, 6.4] is

$$\mathbf{Q} = q \begin{bmatrix} m\omega^2 & 0 \\ 0 & m \end{bmatrix} \tag{6.15}$$

where $q_{11}$, $q_{22}$ and $q$ are parameters to be assigned, reflecting the importance of the reduction in the state vector **X** (i.e., displacement and velocity) or the control force vector $u^*$; the relative importance between controlling displacement and velocity is reflected by the two diagonal elements in the **Q** matrix. The optimal selection of **Q** and *R* is found by trial and error through simulation.

Weighting **Q** and R are designed to be constant for the system considered in most previous researches. As the example of few exceptions, a time varying weighting matrix **Q** is proposed for the

instantaneous optimal control designed [6.11], by a Lyapunov direct method to guarantee the stability of the controlled structure. However, it is found that using such a time varying matrix requires much time to compute the control gain in real time.

### 6.4.3 Acceleration and displacement based performance function

The performance function shown in Equation (6.11) does not explicitly weight the acceleration response, which is of a major interest in the floor isolation system. A performance function shown in Equation (6.16), that directly weights the absolute acceleration, relative displacement and control force is adopted in this study [6.3],

$$\bar{J} = \int_0^t \left( \alpha \left( \ddot{x} + \ddot{x}_{\text{in}} \right)^2 + \beta x^2 + \gamma u^{*2} \right) dt = \int_0^t \left( \mathbf{X}^T \bar{\mathbf{Q}} \mathbf{X} + 2\mathbf{X}^T \mathbf{S} u^* + u^{*T} \bar{R} u^* \right) dt \tag{6.16}$$

where $\alpha$, $\beta$, and $\gamma$ are the weighting coefficients for the acceleration, displacement and control force, respectively. Using Equations (6.4) and (6.16), $\bar{\mathbf{Q}}$, **S,** and $\bar{R}$ can be found as

$$\bar{\mathbf{Q}} = \begin{bmatrix} \alpha\omega^4 + \beta & 2\alpha\zeta\omega^3 \\ 2\alpha\zeta\omega^3 & 4\alpha\zeta^2\omega^2 \end{bmatrix}, \mathbf{S} = \begin{bmatrix} \alpha\omega^2 / m \\ 2\alpha\zeta\omega / m \end{bmatrix}, \bar{R} = \alpha / m^2 + \gamma \tag{6.17}$$

By minimizing Equation (6.17), the optimal control force $u^*$(t) can be obtained

$$u^* = -\bar{\mathbf{G}}\mathbf{y} = \begin{bmatrix} \bar{g}_1 & \bar{g}_2 \end{bmatrix} \begin{bmatrix} x & \dot{x} \end{bmatrix}^T \tag{6.18}$$

where $\bar{\mathbf{G}}$ is the feedback gain. It can be solved by computing the solution $\bar{\mathbf{P}}$ of the algebraic Riccati equation [6.10]

$$\begin{aligned} &\mathbf{A}^T \bar{\mathbf{P}} + \bar{\mathbf{P}} \mathbf{A} - \left( \bar{\mathbf{P}} \mathbf{B} + \bar{\mathbf{S}} \right) \bar{R}^{-1} \left( \mathbf{B}^T \bar{\mathbf{P}} + \bar{\mathbf{S}}^T \right) + \bar{\mathbf{Q}} = 0 \\ &\bar{\mathbf{G}} = \bar{R}^{-1} \left( \mathbf{B}^T \bar{\mathbf{P}} \mathbf{E} + \bar{\mathbf{S}}^T \right) \end{aligned} \tag{6.19}$$

Substituting Equation (6.19) into Equation (6.1), it yields

$$\ddot{x} + \left( 2\zeta\omega + \bar{g}_2 / m \right) \dot{x} + \left( \omega^2 + \bar{g}_1 / m \right) x = -\ddot{x}_{\text{in}} \tag{6.20}$$

The equivalent natural period and damping ratio of this system is

$$
\begin{aligned}
T_e &= 2\pi/\omega_e \\
\omega_e &= \sqrt{\omega^2 + \bar{g}_1/m} \\
\zeta_e &= \left(2\zeta\omega + \bar{g}_2/m\right)/\left(2\omega_e\right)
\end{aligned}
\tag{6.21}
$$

where $\omega_e$ is the equivalent natural frequency. Thus, the LQR controlled system is equivalent to a passive controlled system with an equivalent natural frequency $\omega_e$ and damping ratio $\zeta_e$ as shown in Equation (6.22)

$$
\ddot{x} + 2\zeta_e\omega_e\dot{x} + \omega_e^2 x = -\ddot{x}_{in} \tag{6.22}
$$

### 6.4.4 Strategy to accommodate load changes

The floor isolation is designed to isolate a group of equipment. The live load on the floor is subjected to changes due to the rearrangement of the equipment. Therefore, the semi-active is sought to accommodate to the live load changes. Substituting Equations (6.4) and (6.18) into Equation (6.19), the control gain can be explicitly expressed as

$$
\begin{aligned}
\bar{g}_1 &= -m\omega^2 + \sqrt{m^2\omega^4 - \bar{R}^{-1}\left(\alpha\omega^4 - \beta\right)} \\
\bar{g}_2 &= -2m\zeta\omega + \sqrt{4m^2\zeta^2\omega^2 + 2\alpha\bar{R}^{-1}\omega^2\left(1 - 2\zeta^2\right) + 2m\bar{g}_1}
\end{aligned}
\tag{6.23}
$$

For $\bar{R} = \alpha/m^2 + r$, if $\alpha/m^2 \geq r$, then

$$
\bar{R} \approx \alpha/m^2 \tag{6.24}
$$

Therefore, the control gain

$$
\begin{aligned}
\bar{g}_1 &= m\left(\sqrt{\beta/\alpha} - \omega^2\right) \\
\bar{g}_2 &= m\left(\sqrt{2}\left(\beta/\alpha\right)^{1/4} - 2\zeta\omega\right)
\end{aligned}
\tag{6.25}
$$

Equation (6.25) indicates that the control gain is proportional to the mass of the floor isolation system. With this relationship, the semi-active control is able to adjust the control gain linearly to deal with the load change on the floor problem.

### 6.4.5 Selection of weighting parameters

Equation (6.23) indicates that the control gain $\bar{\mathbf{G}}$ depends on the weighting parameters, $\alpha$, $\beta$ and $\gamma$. Consequently, the selection of these parameters significantly affects the performance of the control

algorithm. Using numerical simulation, a method was developed to select the weighting parameters for a specific input motion. The following methodology places the main focus on reducing accelerations of the floor isolation system.

The three weighting parameters represent the relative importance of the reduction of acceleration, displacement, and control force in the system, as seen in Equation (6.16). Thus, it is their values relative to each other, rather than their absolute values, that have primary significance. Therefore, the value of $\gamma$ is set to one, and focus is placed on selecting the values for $\alpha$ and $\beta$.

Numerical simulation of the floor isolation system was conducted using the control system shown in Figure 6.3 with the Bouc-Wen model described in Chapter 5. The peak acceleration and displacement responses of the floor system were found for a range of $\alpha$ and $\beta$ combinations. Figure 6.4 (a)-(d) show the peak acceleration and displacement of the floor system as functions of $\log_{10}\alpha$ and $\log_{10}\beta$, under the short-period JMA and long-period SAN motions (i.e., JMA Kobe and Sannomaru in Chapter 4). As shown Figure 6.4 (a) and (c), when $\alpha$ is small, the trends for peak acceleration response are very different. However, at larger values of $\alpha$, the peak acceleration response of the two motions exhibit similar troughs, marked with a bold line in the figures.

Figure 6.4 (e) plots the acceleration response under the SAN motion in a 2D contour. There are numerous combinations of $\alpha$ and $\beta$ which result in the smallest accelerations, which occur along the bold line indicating the minimum acceleration response equal to 1.05 m/s$^2$. However, the displacements resulting from these combinations may differ (Figure 6.4 (b) and (d)). The relationship between the acceleration and displacement responses as a function of $\log_{10}\alpha$ is investigated in Figure 6.4 (f) for two constant values of $\beta$, $10^0$ and $10^{12}$ for the long-period SAN motion. At these values of $\beta$, $\alpha=10^{8.5}$ and $\alpha=10^{11.3}$ result in the smallest accelerations, respectively. The weighting combination $\alpha=10^{8.5}$ and $\beta=10^0$ results in displacements 16% larger than the combination $\alpha=10^{11.3}$ and $\beta=10^{12}$. Designating $\beta$ as larger than $10^{12}$ gives no further reduction in displacement responses. In light of the secondary benefit of displacement reduction, especially under long-period motions, the $\beta$ value is selected as $10^{12}$ in this study.

Once $\beta$ is fixed, the optimal weighting $\alpha$ to minimize acceleration response depends on the motion. The value of $\alpha$ that results in the minimum acceleration is referred to as the optimal weighting for the specific motion. A non-optimal selection of $\alpha$ may result in a much larger acceleration response. For example, setting $\alpha=10^{11.3}$ results in the smallest acceleration under SAN. When the same weighting is applied with JMA, it increases the maximum acceleration from 1 m/s$^2$ (obtained using the optimal $\alpha$ value of $10^{12.7}$ for JMA) to 1.4 m/s$^2$. Therefore, the selection of the optimal weighting significantly improves system performance, and it is beneficial to develop a relationship between optimal weightings and excitation characteristics.

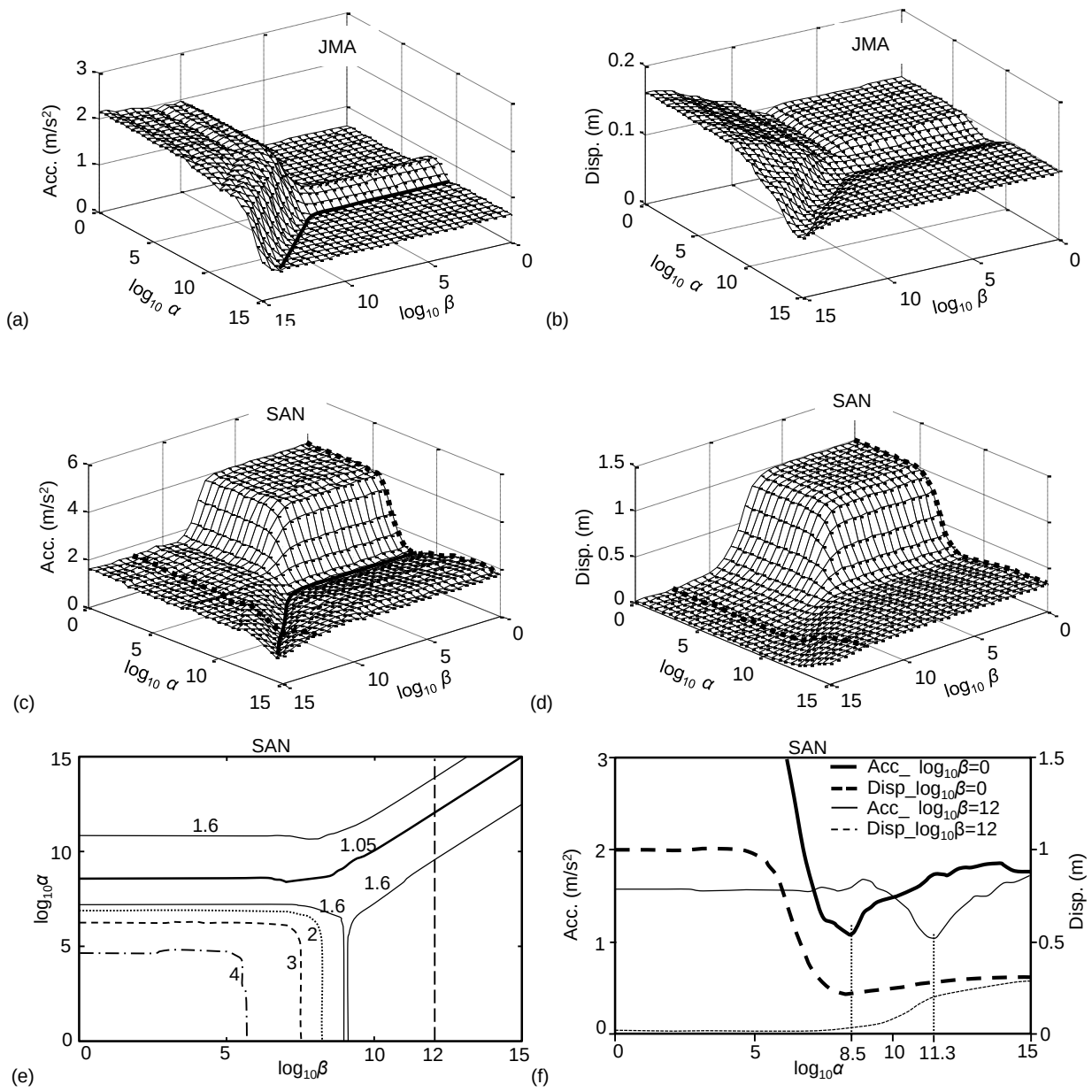


Figure 6.4 Selection of $\alpha$ with $\gamma$=1: (a) acceleration under JMA; (b) displacement under JMA; (c) acceleration under SAN; (d) displacement under SAN; (e) contour curve of acceleration (m/s$^2$) under SAN; (f) acceleration and displacement ($\beta$=10$^0$ and $\beta$=10$^{12}$) under SAN

### 6.4.6 Test parameters

Three different control gains were designed based on the simulation work with the Bouc-Wen model and PI controller designed in Chapter 5. Table 6.2 shows the weighting parameters used for those three different control gains. Two motions, JMA_R and SAN_R, were used in the simulation. They were from the roof responses of the four story RC structure shown in Chapter 4, with the input ground motions of JMA Kobe and Sannomaru. Gain 1 was obtained aiming at reducing the acceleration response of the short-period motion JMA Kobe; Gain 2 was effective in reducing acceleration response for the long-period motion, SAN_R. Gain 3 was calculated by averaging Gain 1 and Gain 2, in an attempt to reduce accelerations in both short- and long-period motions.

Table 6.2 LQR testing program

| Gain | Gain 1 | Gain 2 | Gain 3 |
|---|---|---|---|
| $\alpha$ | $10^{14}$ | $10^{11.3}$ | $10^{12.7}$ |
| $\beta$ | $10^{12}$ | $10^{12}$ | $10^{12}$ |
| $\gamma$ | 1 | 1 | 1 |

## 6.5 LQR control with frequency-dependent scheduled gain

To design an algorithm that effectively minimizes the acceleration response for all motions, while suppressing the displacement when subjected to long-period motion, a method using LQR control with frequency-dependent scheduled gain (LQRSG) is proposed. The scheduled gain method generally refers to a method by which the controller gains are varied according to the current value of scheduling signals [6.12]. Nagashima et al. [6.6] proposed a scheduled gain method for LQR control to adjust the control performance with the variation in the intensity level of the excitation. In their methods the control gain was calculated with a time-varying weighting matrix which indicated a tradeoff between the structural response and control effort. However, this design did not consider different choices of weightings between earthquakes having different frequency characteristics. Basu and Nagarajaiah [6.13] proposed a wavelet-based adaptive LQR algorithm for near fault motions to reduce the displacement. In this method, the weighting matrices of the LQR control were updated by using a scalar multiplier according to the energy in different frequency bands, which was obtained from the wavelet analysis of the structural response.

The proposed LQRSG method attempts to use the dominant frequency of the excitation as the scheduling signal, which can distinguish short- and long-period ground motions. Using the weighting selection method described in Section 3, with $\beta$ and $\gamma$ fixed the LQR control gain **G** depends on only $\alpha$. A relationship between the dominant frequency and control gain that results in the smallest acceleration is sought by examining the relationship between the weighting $\alpha$ and dominant frequency. Using this relationship, the gain-scheduling scheme can be established.

### 6.5.1 Relationship between weighting $\alpha$ and dominant frequency

A suite of motions, listed in Table 6.3, was selected to investigate the relationship between the weighting $\alpha$ and dominant frequency. The suite includes recorded ground motions (JMA, CHI, SAF, TAK, EMO, and ELC), two synthetic motions (HOG and SAN), and a recorded floor response (YOK_K) from the full scale RC structure shown in Chapter 4 [6.14]. Those motions were selected because their dominant frequencies span the range of interest. This frequency band of interest was defined as extending from the low frequency of 0.35 Hz, close to the natural frequency of the floor isolation system, to the high frequency of 1.9 Hz, close to the first mode frequency of the structure in which the floor isolation system was supposed to be installed. The optimal $\alpha$ values for the selected motions are listed in Table 6.3. Motions EMO and ELC and motions HOG and SAN have similar dominant frequencies respectively, and thus were used to check the consistency

of $\alpha$ with respect to the dominant frequency.

Table 6.3 Motions used for developing relationship between weighting parameter $\alpha$ ($\beta$=$10^{12}$ and $\gamma$=1) and dominant frequency

| Notation | Record Information | Amplitude ($m/s^2$) | Dominant frequency $f$ (Hz) | $\log_{10}\alpha$ |
|---|---|---|---|---|
| JMA | Kobe earthquake, 1995, JMA, EW, short-period | 6.2 | 1.00 | 12.7 |
| CHI | Chi-Chi earthquake, 1999, T102, NS, long-period | 1.7 | 0.40 | 11.0 |
| SAF | San Fernando earthquake, 1971, Pacoima Dam, NS, short-period | 12.0 | 0.96 | 11.9 |
| TAK | Kobe earthquake, 1995, Takatori, NS, short-period | 6.4 | 0.79 | 12.0 |
| EMO | Imperial Valley earthquake, 1979, 5155 EMO, NS, long-period | 3.1 | 0.48 | 11.5 |
| ELC | Imperial Valley earthquake, 1940, 117 El Centro, EW, long-period | 3.1 | 0.45 | 11.5 |
| HOG | Higashiougijima motion [(a)], synthetic, long-period | 1.8 | 0.34 | 11.2 |
| SAN | Sannomaru motion, synthetic, long-period | 2.2 | 0.35 | 11.3 |
| YOK_R | Roof response of the RC structure [6.14] under Yokohama ground motion [(c)], short-period | 10.0 | 1.90 | 14.0 |

[(a)]Higashiougijima is a synthetic long-period ground motion for Kawasaki site, Japan, assuming the rupture of the Tokai troughs.

[(b)]Yokohama is a synthetic short-period ground motion of a hypothetical Kanto earthquake expected to hit Tokyo.

As shown in Table 6.3, the optimal control gain to achieve a minimum acceleration response of the floor isolation system varies for excitations with different dominant frequencies. The relationship between the dominant frequency $f$ and $\log_{10}\alpha$ is plotted in Figure 6.5, which shows an approximate linear relationship between the two quantities. The relationship derived using linear interpolation can be expressed in Equation (6.26)

$$\alpha = 10^{1.8f + 10.6} \tag{6.26}$$

In Equation (6.26), $\alpha$ decreases for long-period (low-frequency) input motions, resulting in an increase in the ratio of $\beta/\alpha$ ($\beta$=$10^{12}$). Thus, while Equation (6.26) is derived with the aim of reducing accelerations for all motions, the increased relative importance of reducing displacement at low-frequency input helps reduce displacement under these motions.

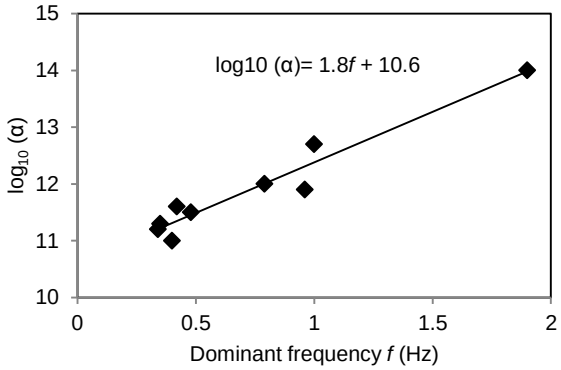


Figure 6.5 Relationship between dominant frequency $f$ and weighting parameter $\alpha$ for proposed floor isolation system, assuming $\beta$ and $\gamma$ are held constant

Substituting Equation (6.26) for Equation (6.18), the control gain $\bar{\mathbf{G}}$ is determined by

$$\bar{\mathbf{G}} = -m\left[10^{-0.9f+0.7} - \omega^2 \quad 10^{-0.45f+0.5} - 2\zeta\omega\right] \tag{6.27}$$

The equation schedules the control gain $\bar{\mathbf{G}}$ with respect to the dominant frequency of the input motion $f$ (Hz) for the proposed LQRSG method. The central idea of LQRSG method is to update the control gain of LQR control in the time domain. Note that the formulation of the relationship between the dominant frequency $f$ and weighting $\alpha$ in Equation (6.26) was designed for the floor isolation system and MR damper used in this study. In the general practice, numerical simulation should be performed for a specific isolation system equipped with a semi-active damper to create the relationship between $\alpha$ and $f$.

### 6.5.2 Detection of the dominant frequency in real time

As it is impracticable to predict the earthquake motion, the control gain $\bar{\mathbf{G}}$ to achieve the smallest acceleration response cannot be calculated *a priori*. To resolve this, a window method was proposed to detect the dominant frequency in "real time". The window method adopted the Fast Fourier Transform (FFT) method to analyze the frequency content of the input acceleration over a specific time window. Since the calculation of dominant frequency and control gain was performed after each time window, the control gain was obtained not in real time but as close to real time as possible.

Figure 6.6 shows how the necessary data are acquired using the window method. The length of each window, $\Delta t$ (=$\Delta t_1$+$\Delta t_2$), is assumed constant. To calculate the control gain $\bar{\mathbf{G}}_k$ at time instant $t_k$, the dominant frequency $f_k$ analyzed from the data in the time window $k$ from time $t_k - \Delta t$ to $t_k$ is used. The data used in window $k$ overlaps with the data recorded in window $k$-1 by a time $\Delta t_2$, and is used to reduce the time for updating the control gain. Increasing the overlap time will reduce the updating interval $\Delta t_1$ of the control gain. The control gain $\bar{\mathbf{G}}_k$ calculated based on the data in window $k$ is used for the control from $t_k$ to $t_{k+1}$ (=$t_k$+$\Delta t_1$), for a time $\Delta t_1$. The same procedure is

repeated to detect the dominant frequencies and calculate the corresponding control gains for each subsequent window.

The number of acceleration data points that can be acquired, $N_{\text{fft}}$, is determined by

$$N_{\text{fft}}=Samp\times\Delta t \tag{6.28}$$

where *Samp* is the sampling rate of the acquisition of acceleration data. The sampling rate determines the shortest possible updating time $\Delta t_1$ (=1/*Samp*). The resolution frequency, $\Delta f$, of the FFT is determined by $\Delta t$, as $\Delta f = 1/\Delta t$.

Figure 6.7 summarizes the proposed semi-active control for the floor isolation system using the LQRSG method with a feed-forward loop to detect the dominant frequency.

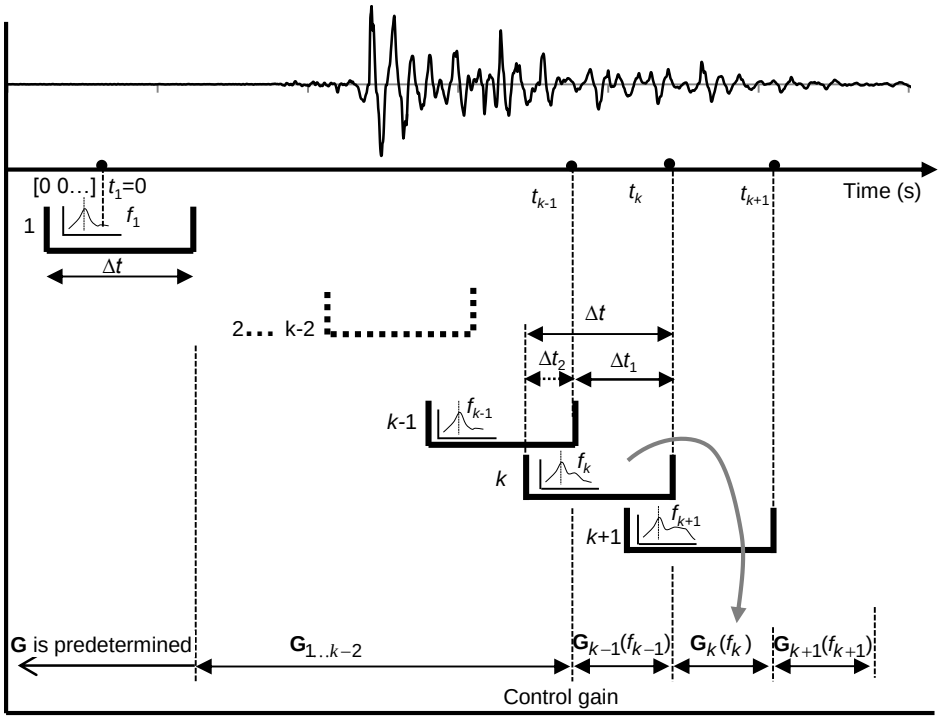


Figure 6.6 Detection time windows for updating control gains of LQRSG method

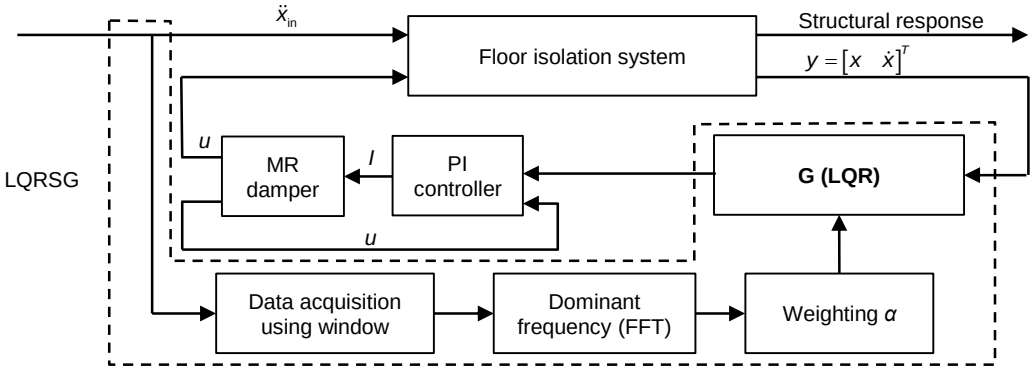


Figure 6.7 Control diagram of LQRSG method

### 6.5.3 Time windows for LQRSG method

As the resolution frequency of the FFT used to detect the dominant frequency of the input motion is equal to the inverse of length of the time window, $\Delta t$ cannot be too short. For example, if $\Delta t$=0.5 s, the resolution frequency $\Delta f$ is only 2 Hz. This design means that only multiples of 2 Hz are detectable, and the error in estimating the dominant frequency is large. The window should be long enough to enable detection of the dominant frequencies of long-period input motions, as well as frequencies close to the natural frequency of the system, which can cause resonance. On the other hand, if $\Delta t$ is too long, the frequency calculated will not represent the current characteristics of the excitation. There is a tradeoff on selecting the window length.

Three different time window schemes were designed as shown in Table 6.4 with window lengths of 2.048 s, 5.12 s and 20.48 s. Window 2 was designed to have a resolution frequency of roughly 0.2 Hz, which would be capable of capturing dominant frequencies for motions up to 5 s in period. This resolution frequency is smaller than the natural frequency of the floor isolation system (0.33 Hz) so frequencies close to the system can be detected. To compare the importance of using only most current frequency information with the importance of fine frequency detection resolution, Window 1 and Window 3 were designed. Window 1 had a shorter window length than Window 2. Therefore, the dominant frequency calculated reflected only current excitation frequency characteristics. As a tradeoff, the resolution frequency (0.5 Hz) was relatively higher than that of Window 2. Window 3 had a much longer window length than the other two windows. The data in the window represented a significantly longer sample, during which the ground motion characteristics may have changed. The benefit of using a long window length is that it gave a significantly finer FFT resolution of 0.05 Hz.

The determination of the lower bound of *Samp* should consider the accuracy of the FFT calculation results. Based on the Nyquist rate, the lower bound of sampling rate can be set as two times the highest frequency of interest to be detected. For the floor isolation system the highest frequency of interest is the first-mode frequency of the structure in which the floor isolation is installed. In order to design a control gain that can fit the current time excitation, the frequency information should be updated frequently, necessitating a large value of *Samp*. The upper bound of *Samp* should consider the acceleration data recording and processing capacities of the DSP. Based on the calculation speed of the DSP in this study, a maximum of 512 points of acceleration data in each window could be recorded to calculate the dominant frequency. *Samp* was determined for each window using Equation (6.28) and as shown in Table 6.4. All windows were designed to have the shortest possible control gain updating time, i.e., $\Delta t_1$=1/*Samp*.

Table 6.4. Time window scheme for use in validation test

| Parameters | Window 1 | Window 2 | Window 3 |
|---|---|---|---|
| Window length: $\Delta t$ (s) | 2.048 | 5.12 | 20.48 |
| Resolution: $\Delta f$ (Hz) | 0.5 | 0.2 | 0.05 |
| Updating time: $\Delta t_1$ (s) | 0.004 | 0.01 | 0.04 |
| Overlap time: $\Delta t_2$ (s) | 2.044 | 5.11 | 20.44 |
| Data sampling: *Samp* (Hz) | 250 | 100 | 25 |

## 6.6 $H_\infty$ control

Optimal linear control methodologies based on linear quadratic form of performance index (LQR) are the core of control theory. Such methodologies ignore the characteristics of the input excitation and do not allow regulation of the structural responses by directly modifying the transfer function in the frequency domain. And the control efforts on the response corresponding to high frequency excitation that do not significantly influence the overall behavior are normally overestimated. Frequency domain optimal control strategies allow the designer to directly deal with the characteristics of the input excitation and specify disturbance attenuation over a desired frequency range, as well as to roll off the control action at high frequencies that will not influence the overall behavior significantly [6.15].

As discussed in Chapter 5, the structure significantly filters out frequency components in the ground motion higher than the predominant frequency of the structure, mainly leaving frequency components that are close to or lower than the predominant frequency of the structure. Therefore, it is reasonable to describe this information in the frequency domain. To this end, the $H_\infty$ control, which is designed in the frequency domain [6.7, 6.8] is adopted in this study.

### 6.6.1 Design target

Figure 6.8 shows the transfer functions from the input acceleration to the floor acceleration and displacement for a passive control system with viscous damping. Two different damping ratios (0 and 40%) were adopted in the simulation. The floor acceleration transfer function shows that when the ratio $\omega_{in}/\omega$ between the input acceleration frequency and the natural frequency of the system is larger than $\sqrt{2}$, the smaller is the damping, the smaller is the acceleration; when $\omega_{in}/\omega$ is smaller than $\sqrt{2}$, the larger is the damping, the smaller is the acceleration. The floor displacement transfer function shows that larger damping is always more effective in reducing displacement, but the difference in the displacement response using different damping ratios is negligible for high frequency inputs ($\omega_{in}/\omega > 2$).

As indicated in Chapter 5, the most critical frequency components of the input motion are the high frequency components that are close to the predominant frequency of the structure because of the high amplitude, and those low frequency components that are close to the natural frequency of the floor isolation because of the resonance with the floor isolation. For high frequency input, low damping is preferred, while high damping is preferred for low frequency input. An optimal control design for the floor isolation system should satisfy both of these requirements. The $H_\infty$ control tries to design a system that has similar responses as a passive system with very low damping for the input motion with frequencies close to the predominant frequency of the structure. However, when the input motion is dominated by frequency components close to the natural frequency of the floor isolation system, the designed system uses higher damping to prevent resonance.

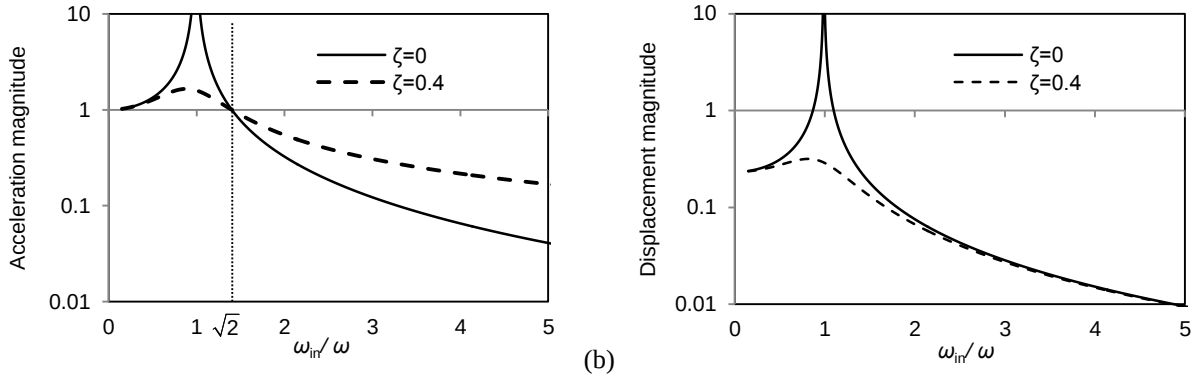


Figure 6.8 Transfer function of passive floor isolation system: (a) acceleration; (b) displacement

### 6.6.2 Formulation of $H_\infty$ control

The block diagram of $H_\infty$ control is shown in Figure 6.9. A frequency-dependent filter $W_1$ was designed to characterize the input motion $\ddot{x}_{\text{in}}$, considering the characteristics of the input motion to the floor isolation system, i.e., mainly the frequency components of the ground motion that are close to or lower than the predominant frequency of the structure, remain after the filtering effects of the structure. Filter $W_1$ can be considered as the transfer function, with the white noise $w$ as the input and the real earthquake excitation as the output. In addition, a filter $W_2$ was also designed to regulate the control on acceleration and displacement:

$$\ddot{x}_{\text{in}} = W_1 w \tag{6.29}$$

$$\mathbf{z} = W_2 \mathbf{C}_\mathbf{z} \mathbf{X} + \mathbf{D}_\mathbf{z} u^* \tag{6.30}$$

where

$$\mathbf{C}_\mathbf{z} = \begin{bmatrix} -\omega^2 & -2\zeta\omega \\ 1 & 0 \end{bmatrix}, \quad \mathbf{D}_\mathbf{z} = \begin{bmatrix} -1/m \\ 0 \end{bmatrix}$$

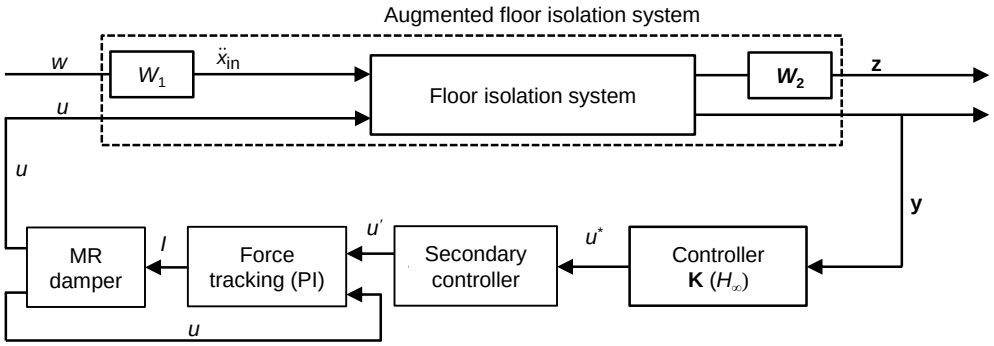


Figure 6.9 Block diagram of $H_\infty$ control design

By appending the filters to the floor isolation system, it results in a typically higher order augmented

system as shown in Figure 6.9. **K** is the designed $H_\infty$ controller. In this system, the measurement output **y** for the controller includes the displacement and velocity, i.e., **y** = **X**.

With the designed controller **K**, the control force $u^*$ can be obtained as:

$$u^* = \mathbf{K}\mathbf{y} \tag{6.31}$$

The central idea of $H_\infty$ control is to design a controller **K** that minimizes the $\infty$ norm of the transfer function of the augmented floor isolation system from the input $w$ to the regulated response **z**, $\mathbf{H}_{zw}$:

$$\left\|\mathbf{H}_{zw}\right\|_\infty = \sup\left[\bar{\sigma}\left(\mathbf{H}_{zw}(s)\right)\right] < \gamma \tag{6.32}$$

where sup denotes the supremum, $\bar{\sigma}$ stands for the maximum singular value of the transfer function, and $\gamma$ is a positive bound for the norm. The transfer function can be expressed as:

$$\mathbf{H}_{zw} = \left(W_2\mathbf{C}_z + \mathrm{D}_z\mathbf{K}\right)\left(s\mathbf{I} - \mathbf{A} - \mathbf{B}\mathbf{K}\right)^{-1}\mathbf{H}W_1 \tag{6.33}$$

The solution methods for the $H_\infty$ controller have been established [6.15, 6.16]. The solution of the optimal control gain **K** can be implemented with the aid of MATLAB [6.9].

### 6.6.3 Design of filters $W_1$ and $W_2$

The order of the augmented system shown in Figure 6.9 depends on the order of the additional filters. Generally, it is easier to implement control for a lower order system than a higher order system. It is therefore desirable to employ low order models for the two filters.

Filter $W_1$ can be designed with different shapes [6.15-6.17] depending on the frequency characteristics of the input motion. Considering the characteristics of the input motion for the floor isolation system, the frequency component close to or lower than the predominant frequency of the structure is most influential. A second order shaping filter is designed:

$$W_1 = \frac{4\zeta_\mathrm{f}\omega_\mathrm{f}s + \chi\omega_\mathrm{f}^2}{s^2 + 2\zeta_\mathrm{f}\omega_\mathrm{f}s + \omega_\mathrm{f}^2} \tag{6.34}$$

where $\zeta_\mathrm{f}$ = 0.3 [6.16, 6.17]. The filter is designed to have the frequency peak corresponding to the predominant frequency of the structure $\omega_\mathrm{p}$, i.e., $\omega_\mathrm{f} = \omega_\mathrm{p}$. The $\chi$ parameter adjusts the control effort on different frequency bands. When the $\chi$ parameter is larger, the filter has a larger power spectrum density (PSD) at a lower frequency region. With this setting, more control effort is shifted to lower frequency region.

Figure 6.10 shows the magnitude of $W_1$ for two different $\chi$ values (0 and 0.3). $\omega_\mathrm{f}$ is chosen as 13.2 rad/s (2.1 Hz). The PSD drops off sharply on the high frequency side, indicating that the

frequency content of the input motion higher than the predominant frequency of the structure is significantly filtered out. $W_1$ with $\chi = 0$ has a much lower amplitude in the low frequency region than when using $\chi = 0.3$. The setting $\chi = 0$ is found not able to cover the possible low frequency components around the natural frequency of the floor isolation. By increasing the value of $\chi$, more control effort is shifted to the low frequency region and it will achieve better performance for low frequency input motion.

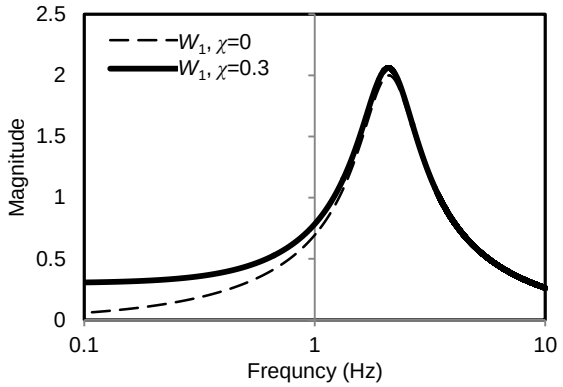


Figure 6.10 Filter $W_1$ with different values of $\chi$

When more control effort is placed on the reduction of displacement in the low frequency region, relative importance on the reduction of acceleration in the high frequency region becomes low. Therefore, $\chi$ is also an indicator for the adjustment of control effort on the acceleration and displacement.

The state space expression of $W_1$ is shown in Equation (6.35):

$$\begin{aligned} \dot{\mathbf{X}}_{\mathbf{W1}} &= \mathbf{A}_{\mathbf{W1}}\mathbf{X}_{\mathbf{W1}} + \mathbf{B}_{\mathbf{W1}} w \\ \ddot{x}_{\text{in}} &= \mathbf{C}_{\mathbf{W1}}\mathbf{X}_{\mathbf{W1}} \end{aligned} \tag{6.35}$$

where $\mathbf{X}_{\text{W1}}$ is a state variable and $w$ is the white noise excitation. $\mathbf{A_{W1}}$, $\mathbf{B}_{\mathbf{W1}}$and $\mathbf{C}_{\mathbf{W1}}$ are system matrices:

$$\mathbf{A}_{\text{w}} = \begin{bmatrix} 0 & 1 \\ -\omega_{\text{f}}^2 & -2\zeta_{\text{f}}\omega_{\text{f}} \end{bmatrix},\ \mathbf{B}_{\text{w}} = \begin{bmatrix} 0 \\ 1 \end{bmatrix},\ \mathbf{C}_{\text{w}} = \begin{bmatrix} \chi\omega_{\text{f}}^2 & 4\zeta_{\text{f}}\omega_{\text{f}} \end{bmatrix} \tag{6.36}$$

Filter $W_2$ is designed to weight the control targets as:

$$W_2 = \begin{bmatrix} \kappa & 0 \\ 0 & (1-\kappa)W_3 \end{bmatrix} \tag{6.37}$$

where $\kappa$ is a scalar weighting corresponding to the absolute acceleration of the floor isolation excluding the portion caused by the damper force $u^*/m$, as shown in Equation (6.30). $(1\text{-}\kappa)W_3$ is a

frequency-dependent filter corresponding to the displacement. $W_3$ is designed as a first order filter with a roll off frequency of 0.4 Hz. It is used to regulate the displacement under motions with frequencies close to or lower than the natural frequency (0.33 Hz) of the floor isolation system.

$$W_3 = \frac{0.4 \times 2\pi}{s + 0.4 \times 2\pi} \tag{6.38}$$

### 6.6.4 Transfer function analysis

Figure 6.11 shows the transfer functions of the floor isolation system from input acceleration to floor acceleration and displacement. Two passive control results with damping ratios of 0 and 0.4, and three $H_\infty$ control results are presented. For $H_\infty$ control, $\omega_f$ is chosen as 13.2 rad/s (2.1 Hz) for filter $W_1$. By simulation, the parameters $\chi$ and $\kappa$ in filter $W_1$ and $W_2$ are tuned to be 0.3 and 0.98, respectively. This allows the $H_\infty$ control with the two filters to have a similar acceleration and displacement with the passive control using a damping of 0, at the frequency that is close to the predominant frequency $\omega_p$ of the structure; while the response around the natural frequency of the floor isolation is close to or lower than those obtained for passive control using high damping of 0.4. The figure also shows that using two filters more effectively reduces acceleration rather than using either $W_1$ or $W_2$, or without using any of them.

Figure 6.12 shows the transfer function of the designed $H_\infty$ controller **K** (it has two inputs, i.e., displacement and velocity of the floor isolation). It is notable that the magnitude of the transfer function from the input displacement to the output force is relatively constant, and the one from the input velocity to the output force varies according to the input velocity frequency. When the input velocity dominates with the frequency close to the natural frequency of the floor isolation, the force magnitude is large, indicating a large damping in the system. When the input velocity dominates with a frequency close to the predominant frequency of the structure (2.1 Hz), the force magnitude is low, which indicates a low damping in the system.

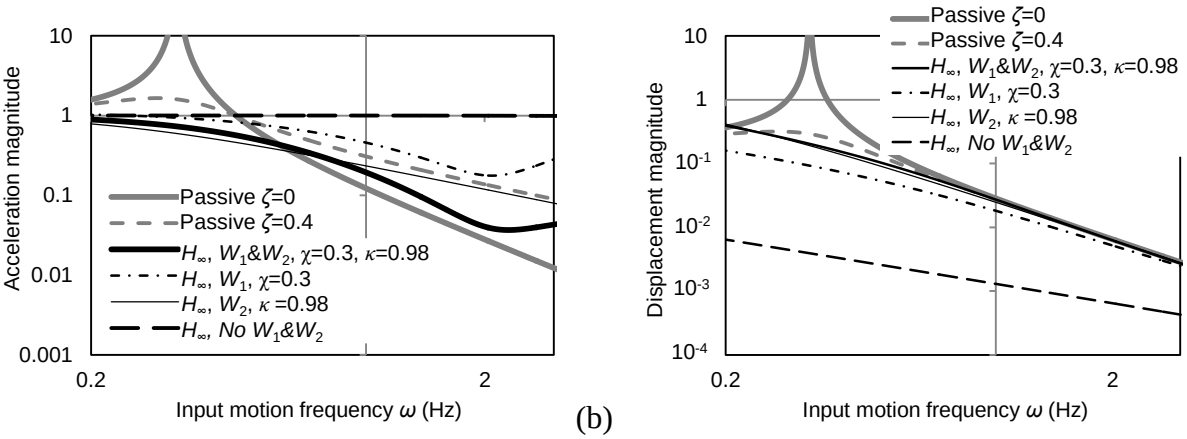


Figure 6.11 Transfer function of floor isolation system with different controls: (a) acceleration; (b) displacement

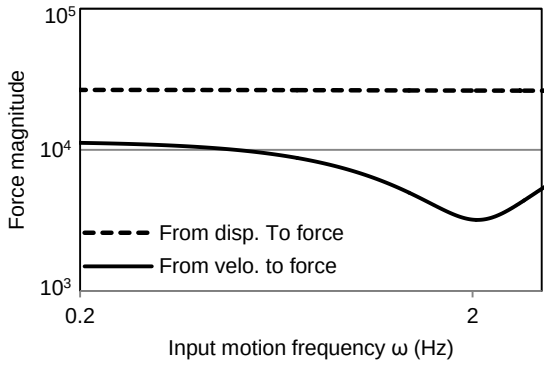


Figure 6.12 Transfer function of the designed $H_\infty$ controller **K** ($W_1$&$W_2$, $\chi$=0.3, $\kappa$=0.98)

### 6.6.5 Test parameters

As describe earlier, there are three variables to be determined, $\omega_f$, $\chi$ and $\kappa$. With the control target for the floor isolation system discussed in Section 6.6.1, the parameters $\chi$ and $\kappa$ in filter $W_1$ and $W_2$ were tuned to 0.3 and 0.98, respectively. $\omega_f$ was selected to be the same with the predominant mode frequency $\omega_p$ of the superstructure. The $\omega_p$ was different for different ground motions due to different degrees of damages after the shaking in the test [6.14]. To examine the effect of different $\chi$ values for input filter $W_1$ on balancing the reduction of acceleration and displacement, a $\chi$ value of 0.4 was also used. In addition, the controller designed without the weighting filters were also included in the test.

## 6.7 Summary

Different control strategies are designed, including passive control with oil damper, and semi-active control using LQR, and $H_\infty$ control algorithms. A new control method named LQR control with schedule gain (LQRSG) is proposed based on the traditional LQR control. The traditional LQR control designs a constant control gain and cannot account for the characteristics of the input motion. The $H_\infty$ control implements additional filter to deal with the input motion characteristics. On the other hand, the proposed LQRSG method aims at explicitly considering the influence of the input motion features to the control gain design in the time domain. Major findings and results can be summarized as follows:

(1) In order to validate the influence of load change on the floor to the performance of floor isolation system, a passive controlled system with three different weight values (by varying the steel plates on the floor) are designed. The resulted damping coefficients for the three systems with passive control are 0.68, 0.38 and 0.29.

(2) The traditional LQR control designs the control gain based on three selected weighting parameters, $\alpha$, $\beta$ and $\gamma$, representing the importance of minimizing floor acceleration, floor displacement and damper control force, respectively. It does not consider the characteristics of the excitation. A linear relationship was found through simulation between the dominant frequency of the input motion and the log of the optimal weighting parameter $\alpha$. Base on this relationship, an LQRSG method was proposed which updates the control gain based on the dominant frequency

of the input motion detected in real time. The LQRSG method enables the semi-active control to account the input motion characteristic in the time domain.

(3) A window method is proposed to monitor the dominant frequency of the excitation in "real time". It detects the acceleration data of the excitation in a time window and analyzes the dominant frequency using a FFT method. Consequently, the control gain is updated based on the dominant frequency of the input motion, without knowing any information of the input motion *a priori*.

(4) A second order input shaping filter is designed to account for the input motion characteristic for the $H_\infty$ control in the frequency domain. The input shaping filter covers two critical frequency components of the input motion that are close to the predominant frequency of the structure and to the natural frequency of the floor isolation. Transfer function analysis shows that with the newly designed shaping filter for the input motion, the $H_\infty$ control result in similar acceleration and displacement at frequencies close to the predominant frequency of the structure with the passive control using viscous damping ratio of 0, while the acceleration and displacement around the natural frequency of the floor isolation is close to or lower than the passive control using a viscous damping ratio of 0.4.

# REFERENCES


[6.1] Hall JF, Heaton TH, Halling MW, Wald DJ. Near-source ground motion and its effects on flexible buildings. *Earthquake Spectra* 1995; 11(4): 569-605.

[6.2] Alhan C, Gavin HP, Aldemir U. Optimal control: basis for performance comparison of passive and semiactive isolation systems. *Journal of Engineering Mechanics* 2006; 132(7): 705-713.

[6.3] Sadek F, Moharaz B. Semiactive control algorithms for structures with variable dampers. *Journal of Engineering Mechanics* 1998; 124(9): 981-990.

[6.4] Li H, Ou J. A design approach for semi-active and smart base-isolated buildings. *Structural Control and Health Monitoring* 2006; 13: 660-681.

[6.5] Kurata N, Kobori T, Takahashi M, Niwa N, Midorikawa H. Actual seismic response controlled building with semi-active damper system. *Earthquake Engineering and Structural Dynamics* 1999; 28: 1427-1447.

[6.6] Nagashima I, Maseki R, Asami Y, Hirai J, Abiru H. Performance of hybrid mass damper system applied to a 36-storey high-rise building. *Earthquake Engineering and Structural Dynamics* 2001; 30: 1615-1637.

[6.7] Yang JN, Lin S, Jabbari F. H∞-based control strategies for civil engineering structures. *Structural Control and Health Monitoring* 2004; 11: 223-237.

[6.8] Narasimhan S, Nagarajaiah S. Smart base isolated buildings with variable friction systems: H∞ controller and SAIVF device. *Earthquake Engineering and Structural Dynamics* 2006; 35: 921-942.

[6.9] MATLAB 2010b. Natick, Massachusetts: The MathWorks Inc., 2010.

[6.10] Arnold WF, Laub AJ. Generalized eigenproblem algorithms and software for algebraic Riccati equations. *proc. IEEE* 1984; 72: 1746-1754.

[6.11] Yang JN, Li Z, Liu SC. Control of hysteretic system using velocity and acceleration feedbacks, *Journal of Engineering Mechanics* 1992; 118(11):2227-2245.

[6.12] Rugh WJ, Shamma JS. Research on gain scheduling. *Automatica* 2002; 26: 1401-1425.

[6.13] Basu B, Nagarajaiah S. A wavelet-based time-varying adaptive LQR algorithm for structural control. *Engineering Structures* 2008; 30: 2470-2477.

[6.14] Sato E, Furukawa S, Kakehi A, Nakashima M. Full shaking table test for examination of safety and functionality of base-isolated medical facilities. *Earthquake Engineering and Structural Dynamics* 2011; 40: 1435-1453.

[6.15] Spencer BF, Suhardjo J, Sain MK. Frequency domain optimal control strategies for aseismic protection. *Journal of Engineering Mechanics* 1994; 120(1): 135-158.

[6.16] Packard A, Zhou K, Pandey P, Becker G. A collection of robust control problems leading to LMI's. Proceedings of the 30th Conference on Decision Control, Brighton, England.

[6.17] Suhardio J, Spencer BF. Feedback-feedforward control of structures under seismic excitation. *Structural safety* 1990; 8:69-89.

# CHAPTER 7

# Shaking table test for floor isolation system

## 7.1 Introduction

### 7.1.1 Background

To protect the important and valuable equipment such as the medical appliances, in earthquake events, a semi-active floor isolation system is designed in Chapter 5 and 6. In this system, either passive or semi-active damping device can be used.

Similar with the medical appliances in Chapter 4, the equipment placed on the floor isolation can be categorized into different types according to their different fixing conditions, including fixed, free standing and sliding with casters. The equipment with fixed condition behaves like a building constructed on the ground and is sensitive to the acceleration of the floor, which. Free standing equipment includes the equipment without casters and the equipment with casters but locked. The response of this kind of equipment depends on the friction force and input accelerations. For those two types of equipment, the displacement movement is not a critical issue but to reduce the acceleration is of most importance. The third type of equipment is the one installed with casters to ensure the mobility in the daily use. This kind of equipment is very mobile and the sliding displacement is a threat to the safety of itself and the neighboring equipment because of the potential impact between equipment items or to the surrounding walls, as shown in Chapter 4. The input motion amplitude and frequency characteristics influence the equipment behavior significantly.

Since it is difficult to apply control to equipment directly considering the number of equipment items, the most possible and effective way is to control the structural responses, which subsequently influence the behavior of the equipment. As for those three types of equipment, acceleration influences all of them significantly. Therefore, it is important to control the acceleration response of the floor isolation system. Meanwhile, the displacement of the floor needs to be controlled to maximize the usable space to place more equipment items. To validate the semi-active control designed in Chapter 6, a series of shaking table tests were conducted.

### 7.1.2 Organization

This chapter describes the results of the shaking table tests for the floor isolation system with different control strategies. The responses of the floor isolation and the equipment (simulated by furniture items) on it are presented. Section 7.2 describes the testing program with details of the setup, instrumentation, evaluation indices and the input motions. The test results are discussed in Section 7.3 to7.6, for the floor system without isolation, and floor isolation system with passive control, LQR control, $H_\infty$ control, and the newly developed LQRSG control, respectively. The performance of the proposed PI controller is also examined.

## 7.2 Testing program

### 7.2.1 Control system setup

The test specimen is shown in Chapter 5 (Figures 5.2 and 5.3). A displacement restraint that represented the surrounding wall was installed under the steel frame to prevent the floor isolation system from moving over 200 mm (which was the displacement capacity of the adopted MR damper). Figure 7.1 shows the control system used in the test. Digital control of the MR damper was performed using a Texas Instruments TMS320C6701 DSP chip and I/O boards with 16-bit A/D and D/A converters. The sampling frequency of the control signals from the DSP was 1,000 Hz.

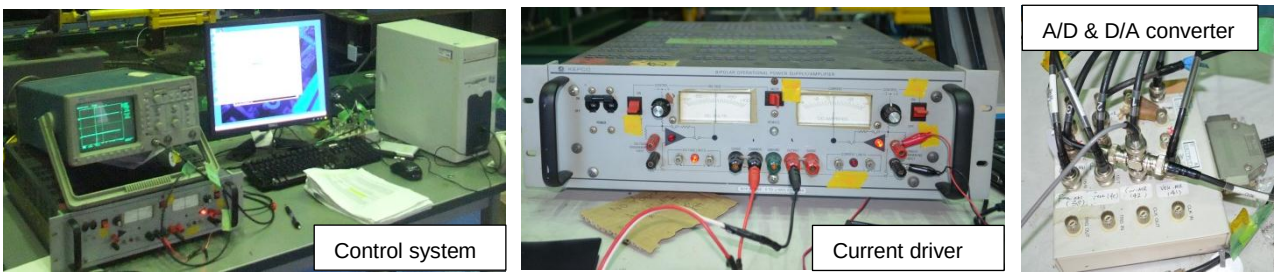


Figure 7.1 Control system used in semi-active control

### 7.2.2 Instrumentation

Various kinds of sensors were installed to monitor the floor isolation system responses, and the motion capture system presented in Chapter 3 was built to measure the behavior of the furniture, which was used to represent the equipment on the floor isolation system. Figure 7.2 shows part of the sensors installed for the specimen.

(1) *Displacement sensors*

The feedback signals for the semi-active control methods shown in Chapter 6 were the displacement and velocity. The displacement was measured with a magnetostrictive displacement transducer mounted on the MR damper as shown in Figure 7.3. The velocity was calculated by passing the displacement data through a second-order Butterworth filter with a cut-off frequency of 30 Hz.

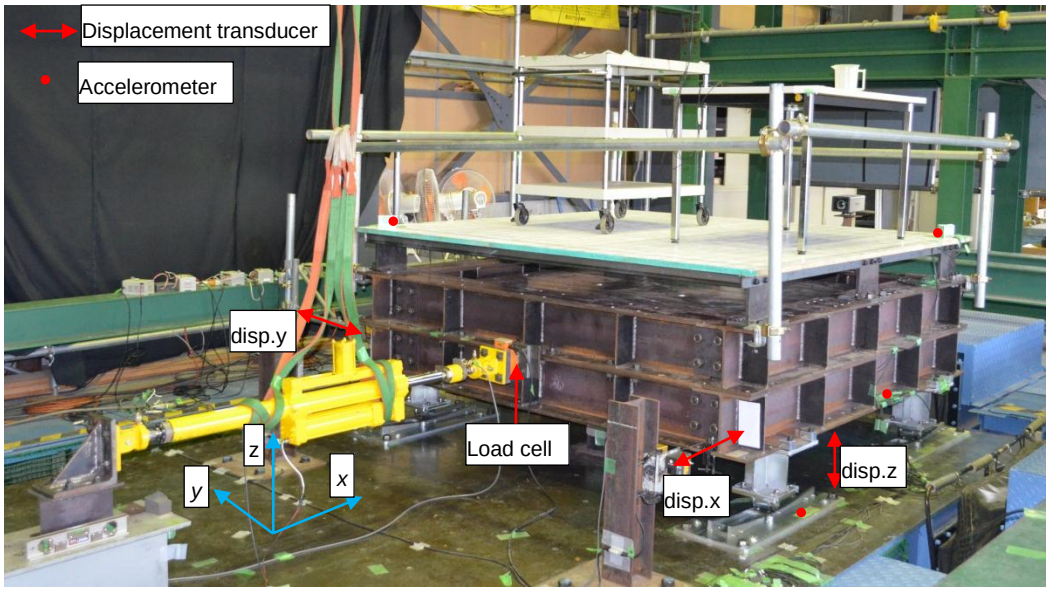


Figure 7.2 Instrumentation for the shaking table test

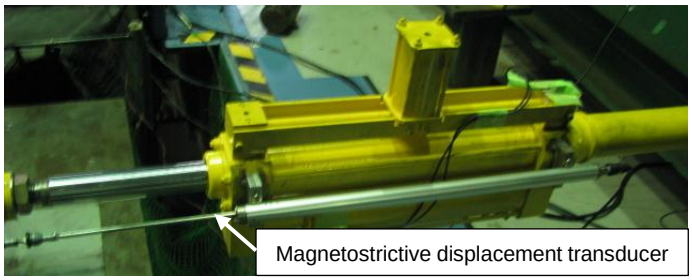


Figure 7.3 Displacement transducer mounted on MR damper

(2) *Acceleration sensors*

Accelerometers were installed to monitor the floor response. To measure the input motion acceleration used to analyze the dominant frequency and to update the control gain in the LQRSG method, one accelerometer in the direction of the input excitation was installed directly on the shaking table.

Accelerometers were installed at the center of each furniture item's top surface as shown in Figure 7.4. Since that the moving direction of the furniture kept changing during the shaking, the horizontal acceleration was quantified with the following equation

$$acc_{xy} = \sqrt{acc_x^{\,2} + acc_y^{\,2}} \tag{7.1}$$

where $acc_x$ and $acc_y$ are the absolute accelerations of the furniture in the $x$ and $y$ directions.

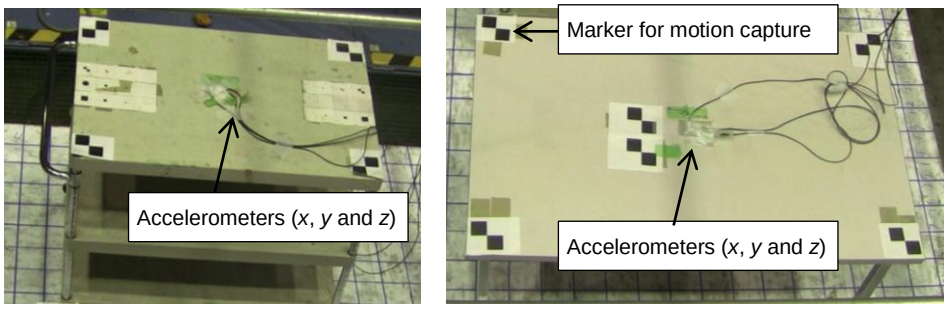


Figure 7.4 Accelerometers installed on furniture and markers used for motion capture

(3) *Load cell*

A load cell with 50 kN capacity was attached to the end of the MR damper (see Figure 7.2) to measure the actual force output of the MR damper. The measured force was used as a feedback signal for the PI controller (see Chapter 5) to calculate the current signal.

(4) *Motion capture system*

The motion capture system was setup to measure the displacement and calculate the velocity of the furniture items. Two cameras were used and placed at a height of 3 m from the raised floor as shown in Figure 7.5. The cameras were set outside the shaking table, thus they were free from vibration. Checker type markers were attached to the surface of the furniture items and the floor.

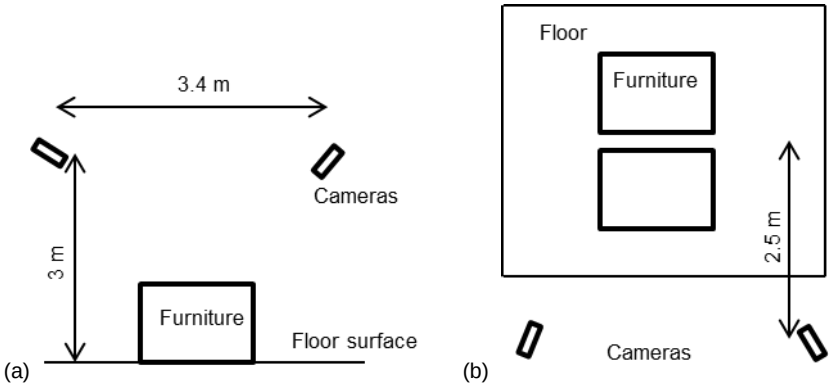


Figure 7.5 Locations of cameras: (a) elevation; (b) layout plan

### 7.2.3 Input motions

Both short- and long-period ground motions were used, including recorded ground motions, a synthetic motion, and recorded roof responses from the full scale RC structure shown in Chapter 4. Table 7.1 lists the characteristics of the motions, including the dominant frequency $\bar{f}$ and the peak acceleration $\ddot{x}_{in}$. Figure 7.6 shows the acceleration time histories and FFT analysis results of the acceleration records, as well as the velocity spectra. The motions JMA_R, SAN_R and JMASAN_R used in the tests were those not included in the simulation used to obtain the

relationship between the dominant frequency and weighting parameters in Chapter 6. The magnitudes of the input accelerations were scaled, with the scale values shown in Table 7.1. The scales were chosen based on the limitation of the shaking table loading capacity and to limit excessive displacements in the floor isolation system.

The FFT results of accelerations in Figure 7.6 reveal that the motions of roof responses were dominated at high frequency around 1.4-2 Hz, which was the predominant mode frequency of the base-fixed structure (Chapter 4) and far from the natural frequency of the floor isolation system. Because the structure tested sustained damage after many rounds of shakings, the predominant mode frequency of the structure varied when those roof responses were recorded. The predominant mode frequency of the structure decreased from 2.1 Hz at the shaking of SAN, to 1.4 Hz at the shaking of JMA. The frequency components beyond the predominant mode frequency of the structure were significantly filtered out for motions of JMA_R, YOK_R and ELC_R. For the long-period motion of SAN_R, the low frequency components from the ground motion of SAN were not filtered out and more high frequency components around 2.1 Hz were added in. The frequency of the roof response was more dominant while the ground motion was distributed in a wider band (JMA vs. JMA_R, ElC vs. ElC_R in Figure 7.6 (b)). The ground motions of JMA, SAN, CHI, and ELC were also included to check the effectiveness of the control strategies, when the floor isolation system was installed at the first floor.

JMASAN_R was a synthetic motion created by running JMA_R and SAN_R motions one after the other, going from high-frequency dominant to low-frequency dominant motion. In real situation, the change in dominant frequency could occur for a floor isolation system if the structure in which it is installed sustains significant damage or if the ground below the building liquefies during the excitation. The motion was used to provide direct evidence of the performance of the LQRSG method in dealing with motions having different frequency characteristics.

JMA, JMA_R, SAN and SAN_R were used as the main shaking excitations for different control strategies. To validate the newly proposed LQRSG strategy to deal with different types of motions, all motions in Table 7.1 were adopted.

Table 7.1 Input motions

| Notation | Description | $\bar{f}$ (Hz) | $\ddot{x}_{in}$ (m/s$^2$) | Scale |
|---|---|---|---|---|
| JMA | Kobe, 1995, JMA, NS, ground motion, short-period | 1.0 | 4.7 | 80% |
| CHI | Chi-Chi, 1999, T102, NS, ground motion, long-period | 0.4 | 1.7 | 100% |
| JMA_R | Roof response under JMA, short-period | 1.4 | 10.5 | 80% |
| YOK_R | Roof response under Yokohama ground motion, short-period | 1.9 | 10.0 | 60% |
| SAN | Sannomaru ground motion, long-period | 0.35 | 1.7 | 80% |
| SAN_R | Roof response under SAN, long-period | 0.35 | 2.7 | 80% |
| ELC | Imperial Valley, 1940,117 El Centro, EW, ground | 0.45 | 3.1 | 100% |

| | | | | |
|---|---|---|---|---|
| | motion, wide band | | | |
| ELC_R | Roof response under ELC, short-period | 1.75 | 8.7 | 60% |
| JMASAN_R | JMA_R and SAN_R in series | 1.4 | 10.5 | 80% |

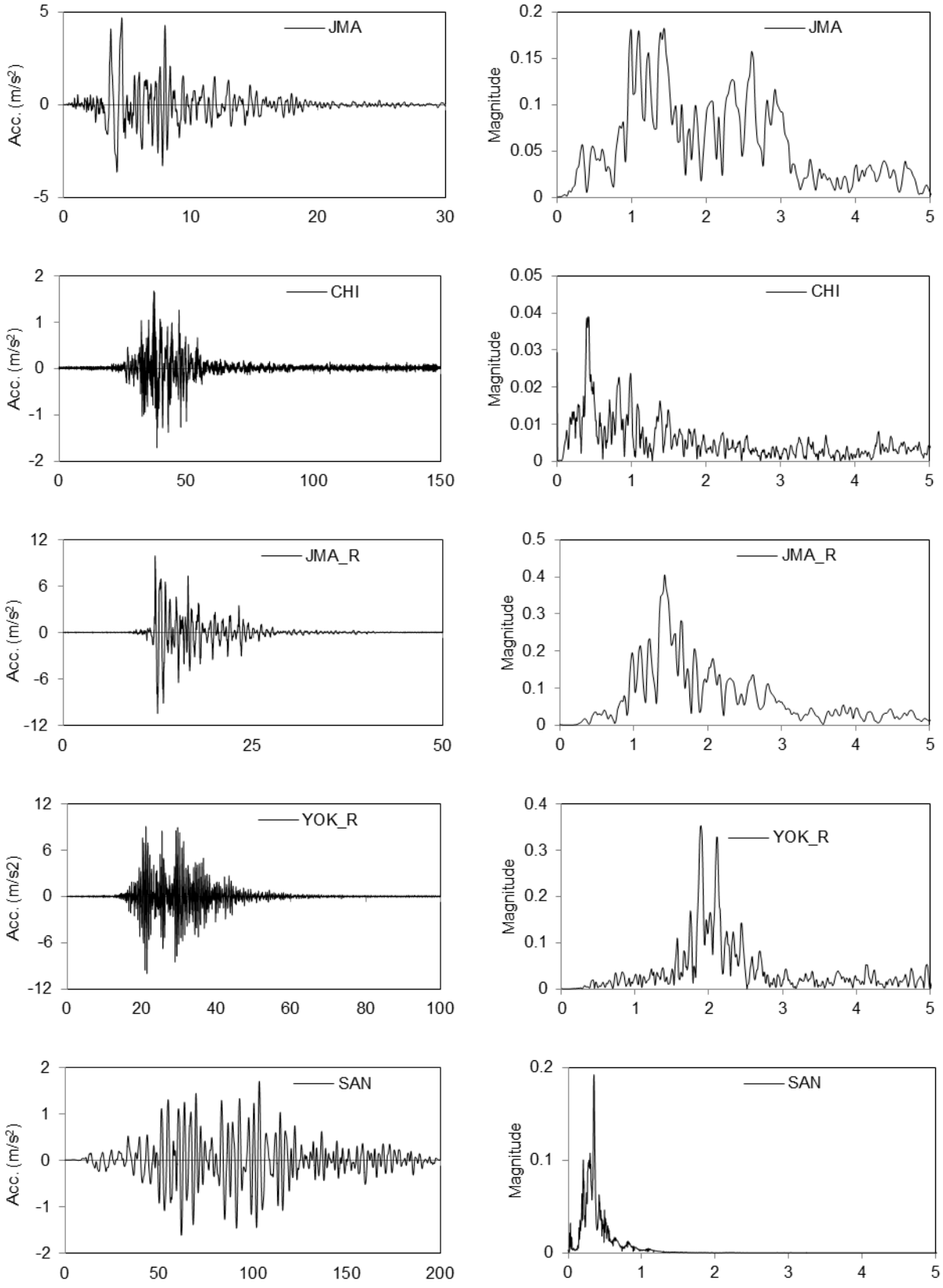

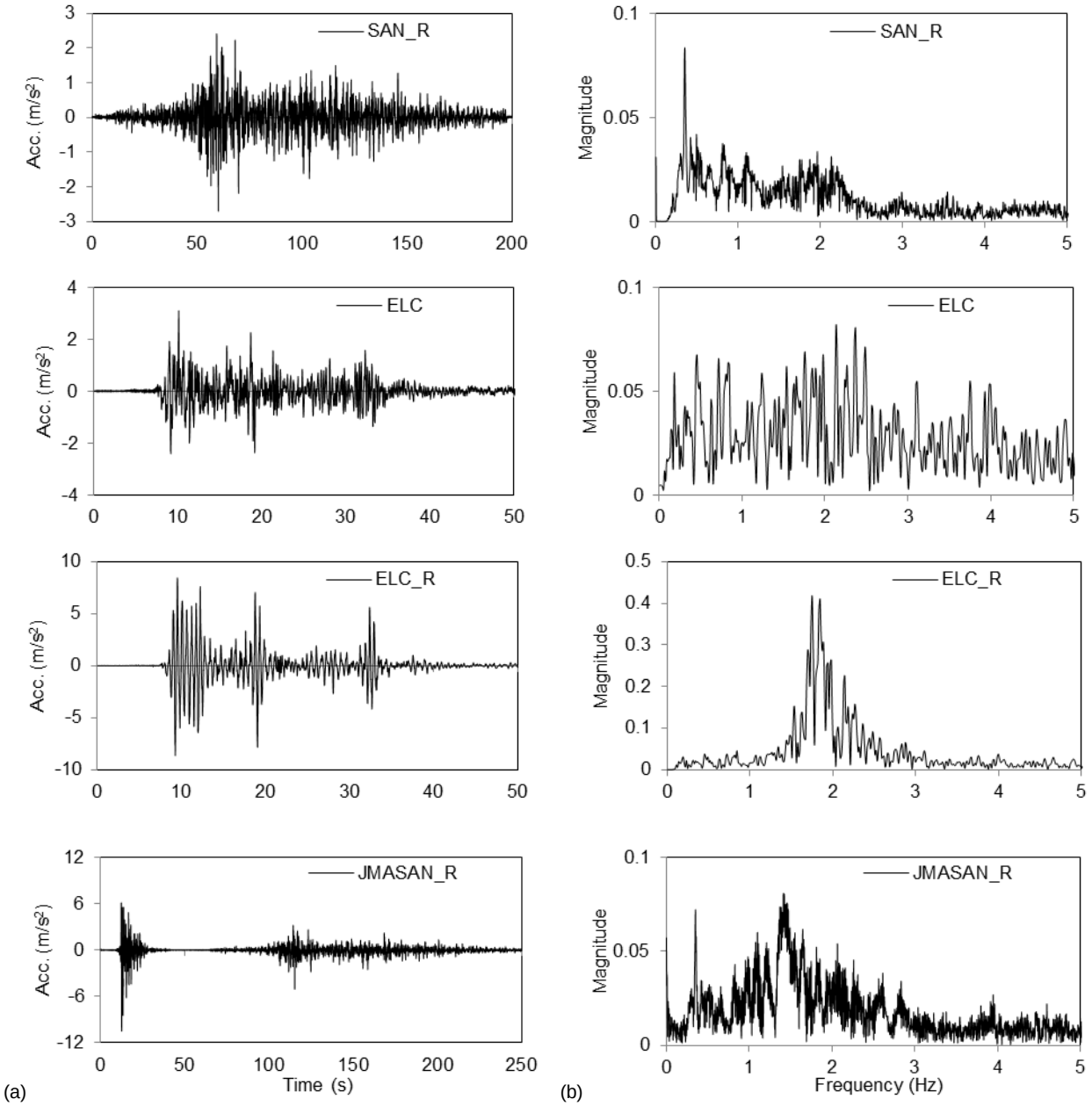


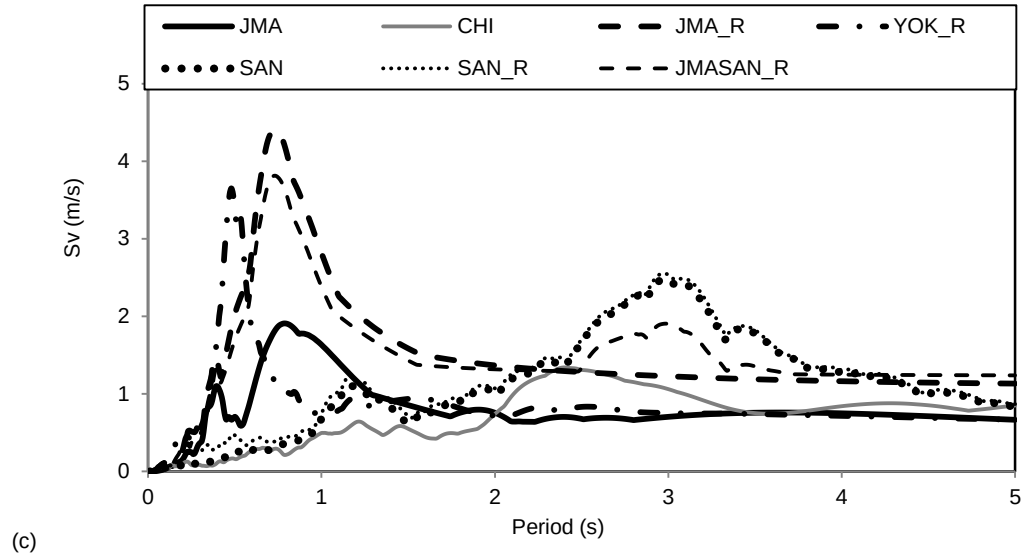


Figure 7.6 Input motions: (a) acceleration time history; (b) FFT of acceleration; (c) velocity spectra

### 7.2.4 Performance indices

The comparison results were quantified by performance evaluations of the floor isolation system in terms of six performance indices $J_1$ (m/s$^2$), $J_2$ (m/s$^2$), $J_3$ (mm), $J_4$ (m/s$^2$), $J_5$ (mm) and $J_6$ (m/s). The indices $J_1$ and $J_3$ represent the peak acceleration and the peak displacement responses of the floor isolation, while index $J_2$ represents the root mean square (RMS) acceleration response. $J_4$, $J_5$ and $J_6$ are the peak acceleration of the furniture estimated from Equation (7.1), peak relative displacement of furniture detected by the motion capture technique, and peak relative velocity of the furniture calculated from Equation (7.2)

$$J_4 = \max\left(\sqrt{velo_x{}^2 + velo_y{}^2}\right) \tag{7.2}$$

where $velo_x$ and $velo_y$ are the velocities of the furniture estimated by the displacement results obtained from the motion capture.

$J_1$ and $J_2$ were adopted to assess the acceleration response of the floor that can influence the behavior of the furniture, especially those with fixed and free standing condition. The peak displacement response was also an important index to evaluate whether the control was effective for suppressing the displacement to a safe level so as to reduce the clearance and save usable space.

## 7.3 Floor isolation system with passive control

An oil damper controlled passive floor isolation system with different weights (35 kN, 62.5 kN and 82.5 kN) were constructed and tested. The floor response and furniture responses are shown in Table 7.2 and are also plotted in Figure 7.8 to Figure 7.9.

The responses varied much for different weights systems. With the damping in the passive system increased which represents that the furniture (equipment) items are moved out in real practice, the acceleration response $J_1$ of the floor increased for the short-period motions JMA and JMA_R while decreased for the long-period motions SAN and SAN_R; on the other hand, the displacement $J_3$ decreased for all the four motions. Therefore, the passive control could not accommodate to the load change on the floor isolation; and it could not stay optimal for both short- and long-period motions.

For the caster locked furniture, the floor isolation did not excite it to move. The maximum acceleration was close to the input motion. Therefore, similar to the floor response, the furniture response also varied with respect to the weight of the floor isolation. For the caster unlocked furniture, the accelerations were lower than 2 m/s$^2$ and did not vary much regarding the weight of the system. However, the displacement and velocity were influenced in the same trend as the floor response. The largest displacement and velocity were about 800 mm and 0.8 m/s, which were lower than the values observed in the test shown in Chapter 4. This is attributed to that only unidirectional motion was tested in this test.

Figure 7.2 Floor and furniture responses of passive floor isolation system

| Input motions | Floor response | | | Caster unlocked furniture | | | Caster locked furniture | | |
|---|---|---|---|---|---|---|---|---|---|
| | $J_1$ (m/s$^2$) | $J_2$ (m/s2) | $J_3$ (mm) | $J_4$ (m/s$^2$) | $J_5$ (mm) | $J_6$ (m/s) | $J_4$ (m/s$^2$) | $J_5$ (mm) | $J_6$ (m/s) |
| | 35 kN system, $\zeta$=0.68 | | | | | | | | |
| JMA | 1.44 | 0.26 | 65 | 1.08 | 89 | 0.23 | 2.13 | 0 | 0 |
| JMA_R | 3.21 | 0.52 | 125 | 1.80 | 137 | 0.43 | 3.50 | 0 | 0 |
| SAN | 1.04 | 0.29 | 96 | 1.42 | 255 | 0.52 | 1.87 | 0 | 0 |
| SAN_R | 1.14 | 0.32 | 107 | 1.77 | 302 | 0.32 | 2.12 | 0 | 0 |
| | 62.5 kN system, $\zeta$=0.38 | | | | | | | | |
| JMA | 1.07 | 0.17 | 70 | 0.82 | 37 | 0.15 | 1.66 | 0 | 0 |
| JMA_R | 1.88 | 0.32 | 136 | 1.73 | 55 | 0.21 | 2.20 | 0 | 0 |
| SAN | 1.06 | 0.31 | 170 | 1.99 | 643 | 0.68 | 1.32 | 0 | 0 |
| SAN_R | 1.90 | 0.33 | 180 | 1.78 | 261 | 0.31 | 2.80 | 0 | 0 |
| | 82.5 kN system, $\zeta$=0.29 | | | | | | | | |
| JMA | 0.96 | 0.15 | 73 | 0.41 | 59 | 0.13 | 1.51 | 0 | 0 |
| JMA_R | 1.54 | 0.27 | 134 | 0.52 | 86 | 0.24 | 1.76 | 0 | 0 |
| SAN | 3.74 | 0.37 | 204 | 1.96 | 751 | 0.75 | 4.71 | 0 | 0 |
| SAN_R | 4.81 | 0.42 | 208 | 1.50 | 560 | 0.72 | 5.01 | 0 | 0 |

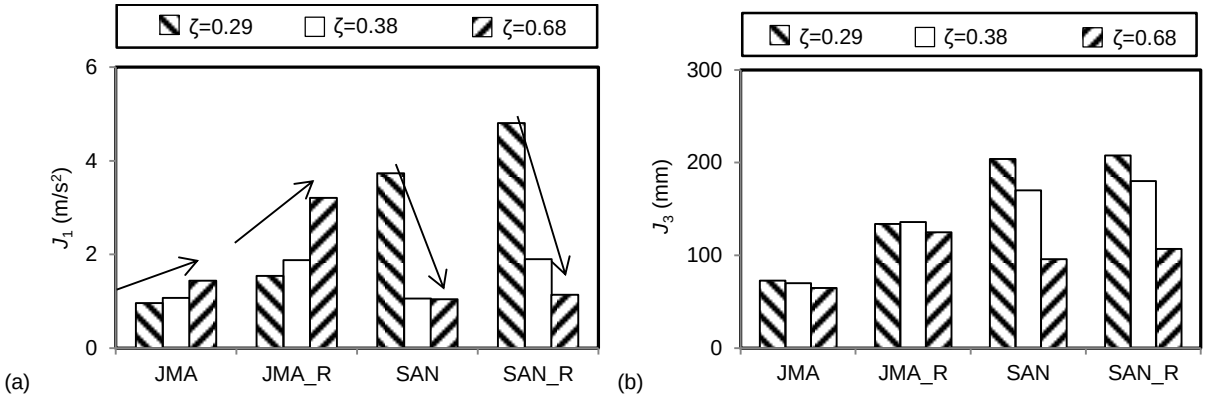


Figure 7.7 Floor responses for passive floor isolation system: (a) acceleration $J_1$; (b) displacement $J_3$

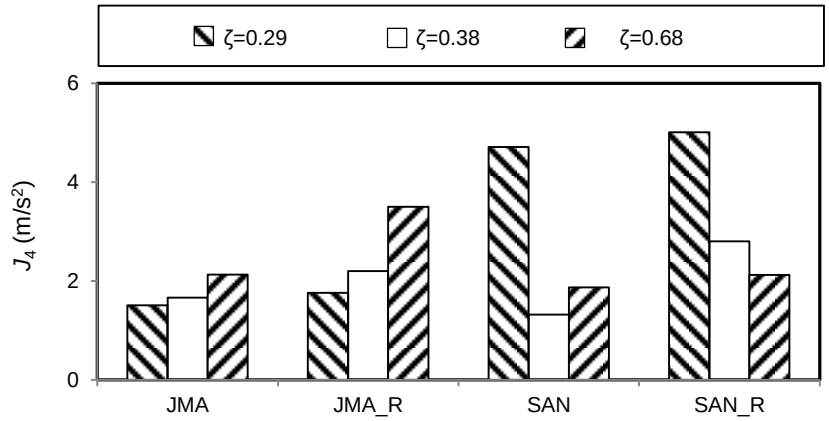


Figure 7.8 Acceleration response $J_4$ of caster locked furniture for passive floor isolation system

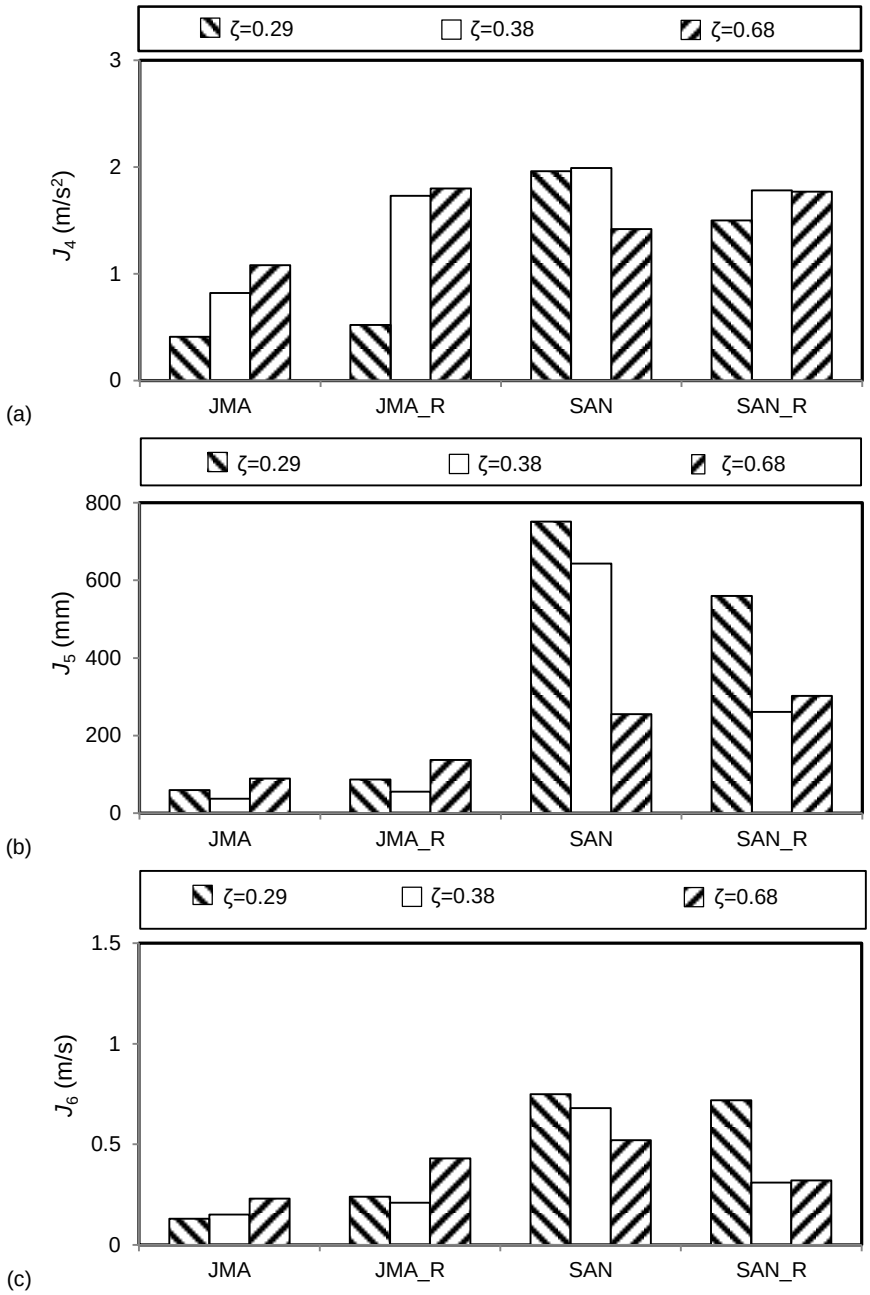


Figure 7.9 Responses of caster unlocked furniture for passive floor isolation system: (a) acceleration $J_4$; (b) displacement $J_5$; and (c) velocity $J_6$

## 7.4 Floor isolation system with LQR control

### 7.4.1 Floor responses

Three different gains were chosen for the LQR control. Gain 1 was designed to reduce the acceleration response for the short-period motion JMA_R; Gain 2 was designed to reduce the acceleration response for the long-period motion SAN_R; and Gain 3 was calculated by averaging Gain 1 and Gain 2, in an attempt to reduce accelerations in both short- and long-period motions.

The performance indices shown in Table 7.3 in bold font are from LQR control with the gain that resulted in the smallest acceleration. For each motion, the gain (among the three gains

designed) associated with the LQR control that resulted in the smallest acceleration responses was referred to as the optimal gain. The values of $J_1/J_1^{LQRop}$ and $J_2$ are shown graphically in Figure 7.10, where $J_1^{LQRop}$ is the $J_1$ performance index of the LQR control with the optimal gain. Note that the optimal gain differs from motion to motion.

The comparison among the three gains for the LQR control clearly indicates that the response of the floor isolation is dependent on the selection of control gain. For the short-period motions, JMA, JMA_R, YOK_R and ELC_R, the acceleration index $J_1$ was increased by 254%, 141%, 248%, and 80% respectively, compared with that using optimal gain, when non-optimal gains were used. However, the differences in displacement index $J_3$ were not significant. For all the long-period motions, CHI, SAN, and SAN_R, Gain 2 resulted in the optimal response; with Gain 1 or Gain 3, impact occurred and the displacement was increased by over 10% to 30% compared with that using Gain 2. Note that the displacement using Gain 1 or Gain 3 would be more than 200 mm if there was no restraint at 200 mm.

Under JMA, JMA_R, SAN, and SAN_R motions, the acceleration of the floor with LQR control using optimal gain was only 8%, 11%, 57% and 34%, respectively, of that without control. Therefore, the floor isolation system can be very effective in reducing the acceleration if an optimal gain is assigned to the semi-active control system, for different motions including ground motions, floor motions, and short-period and long-period motions.

It is apparent that choosing a non-optimal gain caused significant increases in acceleration and displacement compared with those using the optimal gain. However, such non-optimal selection of control gain is inevitable since it is impractical to know the excitation characteristics *a priori*.

Results show that the acceleration responses using LQR control with optimal gains could be effectively reduced from the passive control while not causing significant increase in displacement response.

Compared with passive control with a medium damping ratio (38%), the traditional LQR control with the optimal control gain could more effectively reduce the acceleration response of the floor isolation system by 35% to 90%, while not causing significant larger displacement. Smaller floor responses resulted in smaller (40% to 90%) acceleration of the furniture with locked caster.

Table 7.3 Floor responses of floor isolation system with LQR control

| Input motions | Gain 1: $\alpha=10^{14}$ | | | Gain 2: $\alpha=10^{11.3}$ | | | Gain 3: $\alpha=10^{12.7}$ | | |
|---|---|---|---|---|---|---|---|---|---|
| | $J_1$ (m/s$^2$) | $J_2$ (m/s2) | $J_3$ (mm) | $J_1$ (m/s$^2$) | $J_2$ (m/s2) | $J_3$ (mm) | $J_1$ (m/s$^2$) | $J_2$ (m/s2) | $J_3$ (mm) |
| JMA | **0.37** | **0.09** | **78** | 1.31 | 0.17 | 78 | 0.39 | 0.11 | 75 |
| JMA_R | **0.86** | **0.16** | **142** | 2.07 | 0.33 | 135 | 1.06 | 0.14 | 131 |
| SAN | 7.71 | 0.36 | Impact | **0.94** | **0.27** | **181** | 5.19 | 0.27 | Impact |
| SAN _R | 9.94 | 0.45 | Impact | **0.78** | **0.24** | **166** | 8.59 | 0.32 | Impact |
| CHI | 4.44 | 0.20 | Impact | **0.86** | **0.18** | **167** | 2.82 | 0.19 | Impact |
| ElC | 0.71 | 0.07 | 153 | **0.52** | **0.07** | **110** | 0.69 | 0.07 | 146 |
| YOK_R | 0.72 | 0.18 | 101 | 1.95 | 0.35 | 101 | **0.56** | **0.13** | **87** |
| ElC_R | 0.65 | 0.09 | 125 | 1.01 | 0.14 | 91 | **0.56** | **0.09** | **99** |

| | | | | | | | | | |
|---|---|---|---|---|---|---|---|---|---|
| JMASAN_R | 5.77 | 0.34 | Impact | 1.55 | 0.22 | 153 | **0.94** | **0.2** | **195** |

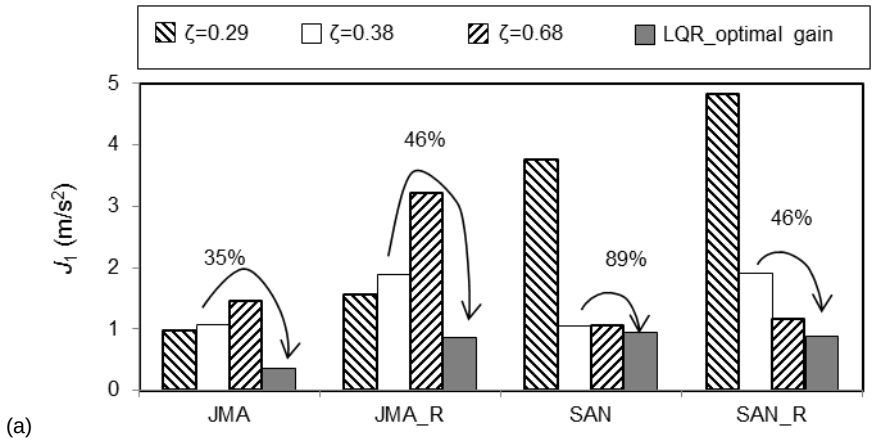


(a)

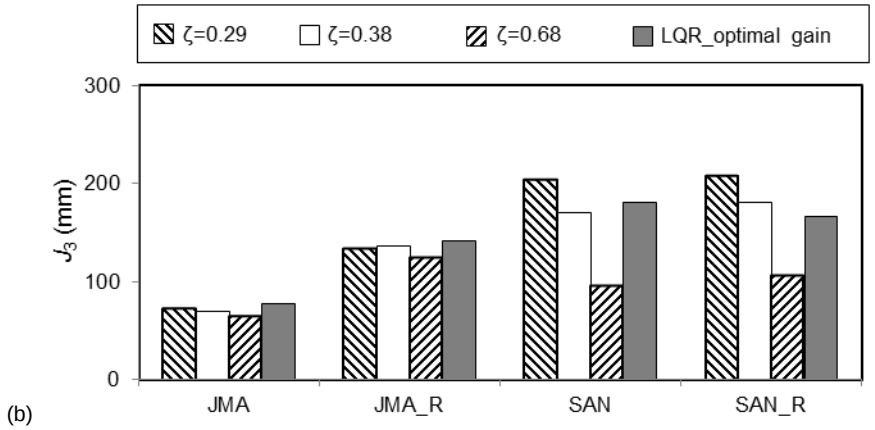


(b)

Figure 7.10 Comparison of passive control and LQR control using optimal gain: (a) acceleration $J_1$; (b) displacement $J_3$

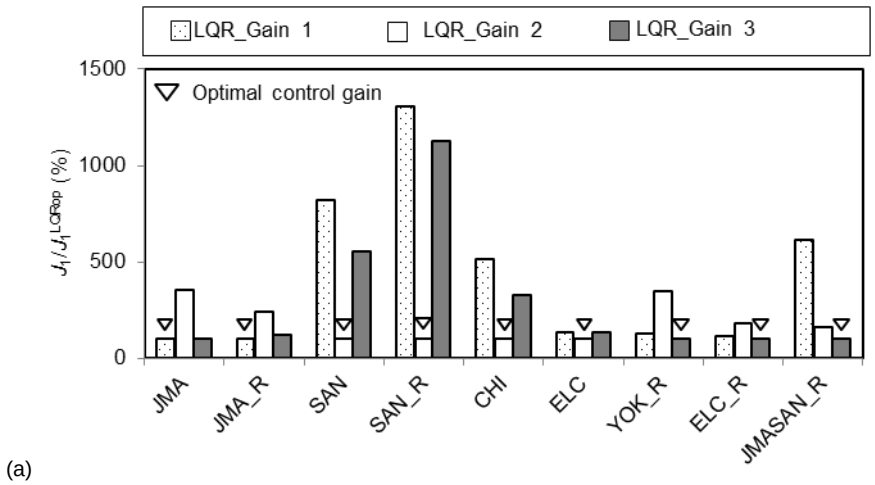


(a)

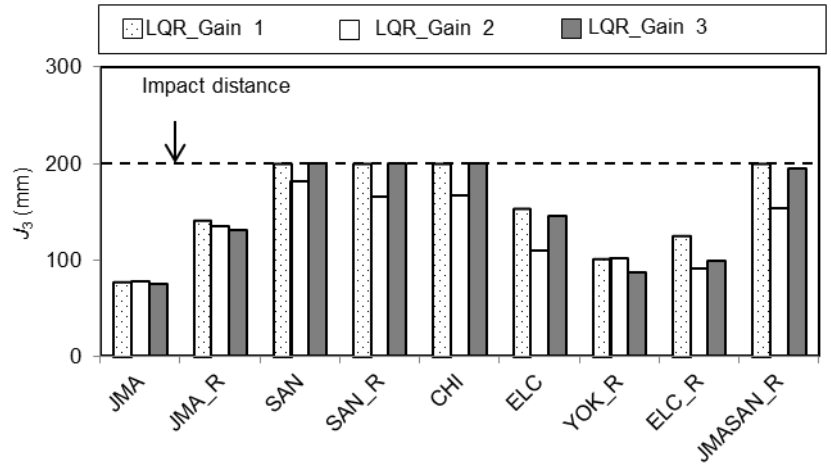


(b)

Figure 7.11 Floor responses for floor isolation system with LQR control: (a) normalized acceleration $J_1$; (b) displacement $J_3$

### 7.4.2 Furniture responses

The responses of the caster locked furniture under JMA, JMA_R, SAN and SAN_R are shown in Table 7.4. $J_4$ is graphically shown in Figure 7.12, as well as the results from the test with passive control. The responses of the caster unlocked furniture are shown in Table 7.5. Comparison between responses of caster unlocked furniture for the floor isolation system with traditional LQR control and those with passive control is plotted in Figure 7.13.

Generally, the non-optimal control gain caused larger acceleration, velocity and displacement of the furniture with both locked and unlocked conditions, which could be more than 2 times. Compared to the passive control, the LQR control with optimal gain resulted in smaller acceleration response (by 35% to 90%) of the caster locked furniture. However, it is notable from Figure 7.12 that the results with a non-optimal gain even resulted in larger acceleration responses (by 35%) than the results passive control. Compared with passive control, the LQR control with optimal gain could reduce the acceleration, displacement and velocity by about 30% to50%.

Table 7.4 Responses of caster locked furniture on floor isolation system with traditional LQR

| Input | Gain 1 ($\log_{10}\alpha$=14) | | | Gain 2 ($\log_{10}\alpha$=11.3) | | | Gain 3 ($\log_{10}\alpha$=12.7) | | |
|---|---|---|---|---|---|---|---|---|---|
| motions | $J_4$ (m/s$^2$) | $J_5$ (mm) | $J_6$ (m/s) | $J_4$ (m/s$^2$) | $J_5$ (mm) | $J_6$ (m/s) | $J_4$ (m/s$^2$) | $J_5$ (mm) | $J_6$ (m/s) |
| JMA | **0.64** | **0** | **0** | 1.18 | 0 | 0 | 0.60 | 0 | 0 |
| JMA_R | **1.40** | **0** | **0** | 3.01 | 0 | 0 | 1.51 | 0 | 0 |
| SAN | 4.96 | 0 | 0 | **1.18** | **0** | **0** | 4.11 | 0 | 0 |
| SAN_R | 5.31 | 0 | 0 | **1.42** | **0** | **0** | 5.10 | 0 | 0 |

Table 7.5 Responses of the caster unlocked furniture on the floor isolation system with traditional LQR

| Input | Gain 1 ($\log_{10}\alpha$=14) | | | Gain 2 ($\log_{10}\alpha$=11.3) | | | Gain 3 ($\log_{10}\alpha$=12.7) | | |
|---|---|---|---|---|---|---|---|---|---|
| motions | $J_4$ (m/s$^2$) | $J_5$ (mm) | $J_6$ (m/s) | $J_4$ (m/s$^2$) | $J_5$ (mm) | $J_6$ (m/s) | $J_4$ (m/s$^2$) | $J_5$ (mm) | $J_6$ (m/s) |

| | | | | | | | | | |
|---|---|---|---|---|---|---|---|---|---|
| JMA | **0.39** | **26** | **0.08** | 0.39 | 57 | 0.16 | 0.39 | 27 | 0.06 |
| JMA_R | **0.53** | **27** | **0.08** | 0.62 | 90 | 0.23 | 0.50 | 49 | 0.18 |
| SAN | 4.33 | 622 | 0.85 | **1.05** | **360** | **0.36** | 2.05 | 689 | 0.56 |
| SAN_R | 8.89 | 621 | 0.83 | **1.07** | **347** | **0.29** | 2.97 | 619 | 0.76 |
| CHI | 1.19 | 481 | 0.59 | **0.66** | **275** | **0.27** | 0.94 | 369 | 0.45 |
| ELC | 0.49 | 125 | 0.18 | **0.43** | **205** | **0.20** | 0.56 | 56 | 0.12 |
| YOK_R | 0.52 | 33 | 0.06 | 0.49 | 50 | 0.08 | **0.53** | **17** | **0.16** |
| ELC_R | 0.60 | 35 | 0.08 | 0.71 | 51 | 0.16 | **0.56** | **31** | **0.08** |
| JMASAN_R | 4.75 | 449 | 0.65 | 0.91 | 310 | 0.30 | **0.80** | **280** | **0.27** |

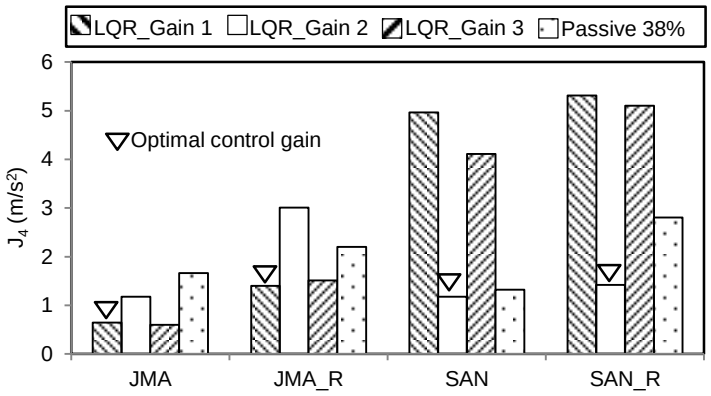


Figure 7.12 Acceleration response $J_4$ of caster locked furniture for floor isolation system with LQR control and passive control

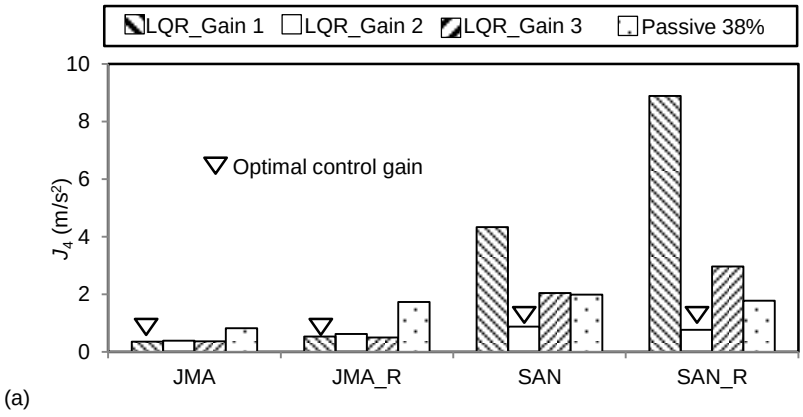


(a)

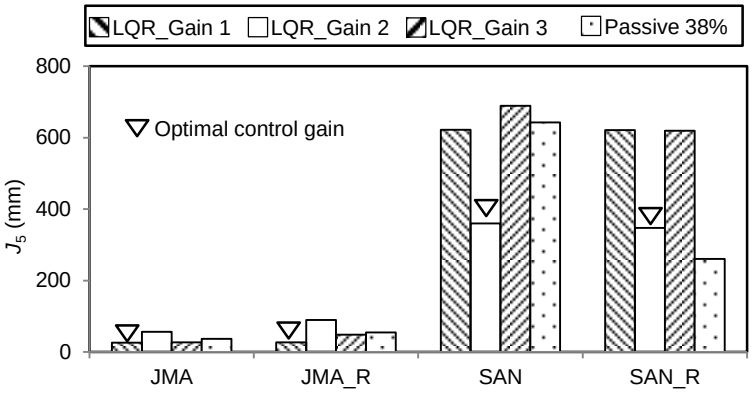


(b)

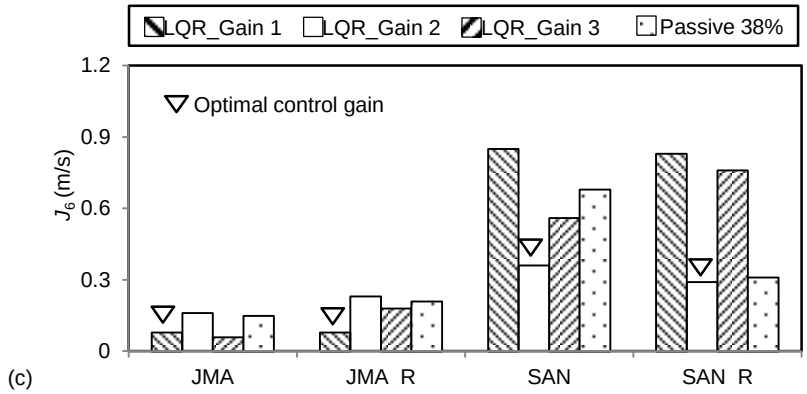


Figure 7.13 Responses of caster unlocked furniture for floor isolation system with LQR control and passive control: (a) acceleration $J_4$; (b) displacement $J_5$; (c) velocity $J_6$

The acceleration responses of the furniture with locked casters depended on the input acceleration significantly as shown in Figure 7.14. To reduce the furniture acceleration with locked casters, it is necessary to suppress the floor acceleration. On the other hand, the behavior of caster unlocked furniture is more difficult to predict. Only the unlocked furniture was tested for other control strategies including LQRSG control and $H_\infty$ control.

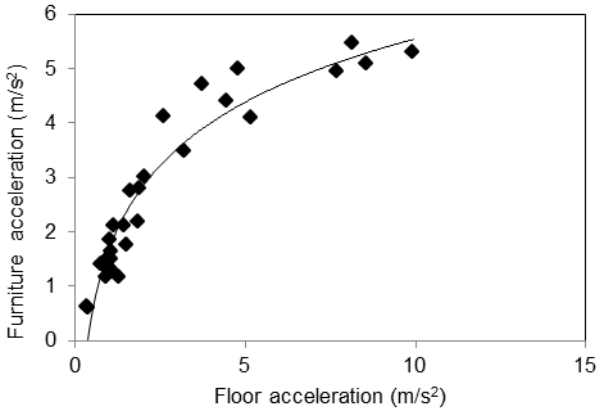


Figure 7.14 Relationship between floor acceleration and furniture acceleration

## 7.5 Floor isolation system with LQRSG control

### 7.5.1 Floor responses

Table 7.6 shows the floor responses of the floor isolation system with different windows. The values of $J_1/J_1^{\mathrm{LQRop}}$ and $J_3$ are shown graphically in Figures 7.15 and 7.16.

Table 7.6 Floor responses of floor isolation system with LQRSG control

| Input motions | $J_1$ (m/s$^2$) | $J_2$ (mm) | $J_1$ (m/s$^2$) | $J_2$ (mm) | $J_1$ (m/s$^2$) | $J_2$ (mm) |
|---|---|---|---|---|---|---|
| | LQRSG with Window 1 | | | | | |

| | | | | | | |
|---|---|---|---|---|---|---|
| JMA_R | 1.17 | 0.17 | 134 | | | |
| SAN_R | 3.90 | 0.24 | Impact | | | |
| | LQRSG with Window 2 | | | LQRSG with Window 3 | | |
| JMA | 0.37 | 0.08 | 65 | 0.55 | 0.08 | 62 |
| JMA_R | 0.90 | 0.17 | 135 | 0.95 | 0.18 | 135 |
| SAN | 0.74 | 0.21 | 168 | 0.66 | 0.21 | 150 |
| SAN_R | 0.85 | 0.24 | 178 | 0.77 | 0.24 | 168 |
| CHI | 0.66 | 0.14 | 171 | 0.67 | 0.14 | 160 |
| ELC | 0.69 | 0.07 | 150 | 0.68 | 0.07 | 149 |
| YOK_R | 0.55 | 0.13 | 91 | 0.57 | 0.13 | 93 |
| ELC_R | 0.60 | 0.09 | 117 | 0.59 | 0.09 | 117 |
| JMASAN_R | 0.85 | 0.21 | 161 | 1.35 | 0.21 | 150 |

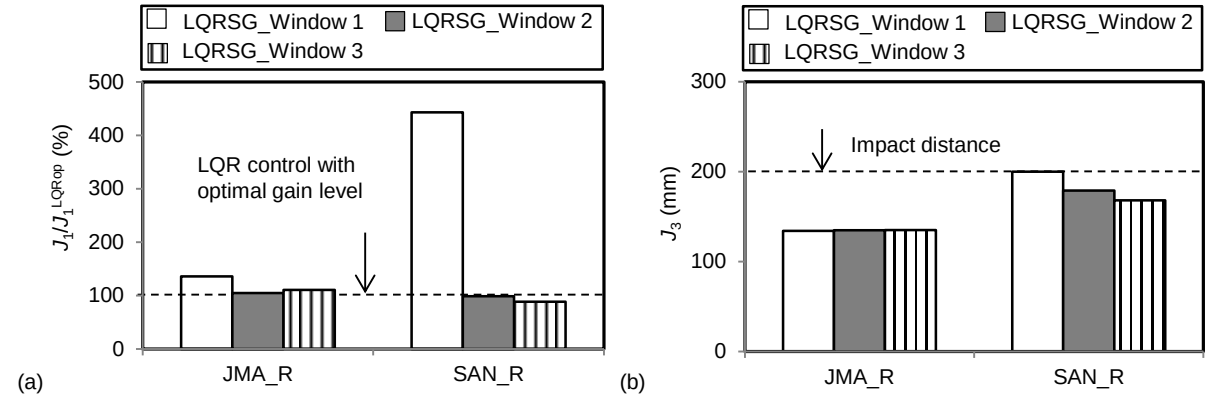


Figure 7.15 Floor responses of isolation system with LQRSG using three windows: (a) normalized acceleration $J_1$; (b) displacement $J_3$

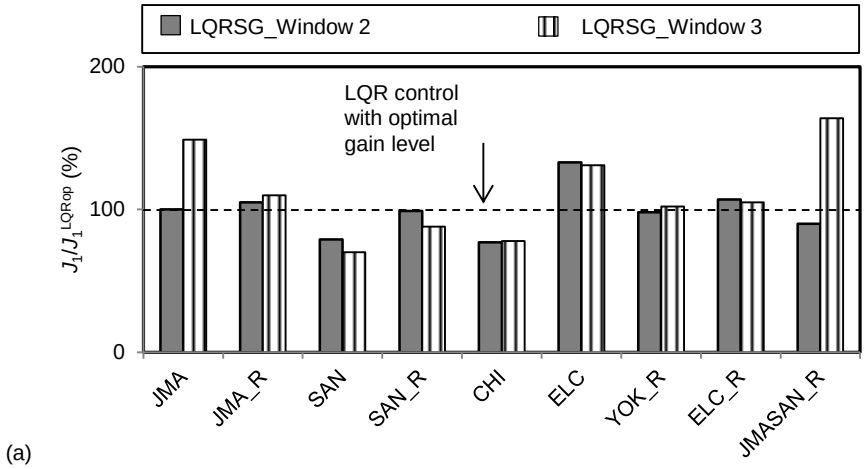

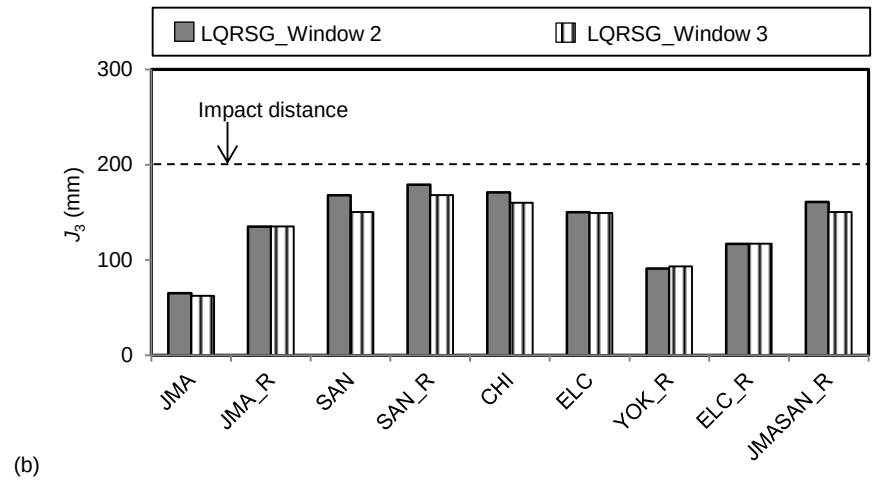


Figure 7.16 Floor responses of floor isolation system using LQRSG with Window 2 and Window 3: (a) normalized acceleration $J_1$; (b) displacement $J_3$

(1) *LQRSG method with different windows*

Figure 7.17 shows the dominant frequencies of the input motion SAN_R detected using the three windows. Window 1 has the shortest window length of 2.048 s and was designed to capture the most current frequency characteristics among the three windows. As a result of the limited resolution frequency of 0.5 Hz, the frequency detected switched between 0.5, 1 and 1.5 Hz. Using Window 1, under the long-period SAN_R motion, the displacement reached maximum displacement capacity of 200 mm. Under the short-period JMA_R motion, the maximum acceleration response ($J_1$) reached 1.17 m/s$^2$, which was 36% larger than that in the LQR control with the optimal gain. Although Window 1 was designed to capture the most current characteristics of the input motion to benefit the control gain determination, test results show that the effect of low resolution was more significant. Window 1 was not applied with other motions.

Window 2 had a medium window length of 5.12 s and resolution of 0.2 Hz, while Window 3 had a long window length of 20.04 s and resolution of 0.05 Hz. Test results from JMA_R and SAN_R motions in Table IV show that the responses using either Window 2 or 3 were lower than using Window 1. Window 3 was slightly more effective at controlling the displacements in all the long-period motions due to the small detection resolution frequency which was able to capture variation within the low-frequency content. The displacement using Window 3 was reduced by 5% to 10% compared to using Window 2. On the other hand, Window 2 was more effective than Window 3 in reducing the accelerations ($J_1$) for the short-period motions, which was of primary interest. This is likely due to the shorter window length which enabled Window 2 to capture only the current characteristics of the input motion. Window 2 reduced the index $J_1$ under JMA, JMA_R, YOK_R, and JMASAN_R by 23%, 5%, 4% and 37% compared to Window 3.

Comparing the experimental results from the three windows reveals that the resolution of the window is the most important factor in the determination of response. The resolution frequency should be capable of capturing a range of potential dominant input frequencies of long-period motions, as well as frequencies close to the natural frequency of the system, so that low-frequency

content causing resonance can be detected. Using even finer resolution reduces the error in detecting the dominant frequency and benefits the response control under long-period motions. However, for short-period motions the detected frequency may not reflect the current frequency characteristics accurately when longer windows are used.

The test results also show that the LQRSG method was effective for both ground motions (JMA, CHI and SAN) and floor response inputs (JMA_R, YOK_R and SAN_R). The reduction factors from the input motion to the response (index $J_1$) were 8% and 9% for motions JMA and JMA_R, and 44% and 32% for SAN and SAN_R, respectively, when using Window 2.

It is noted that although the detected dominant frequency switched suddenly between the adjacent windows in all three window schemes, there were no issues with stability in the tests.

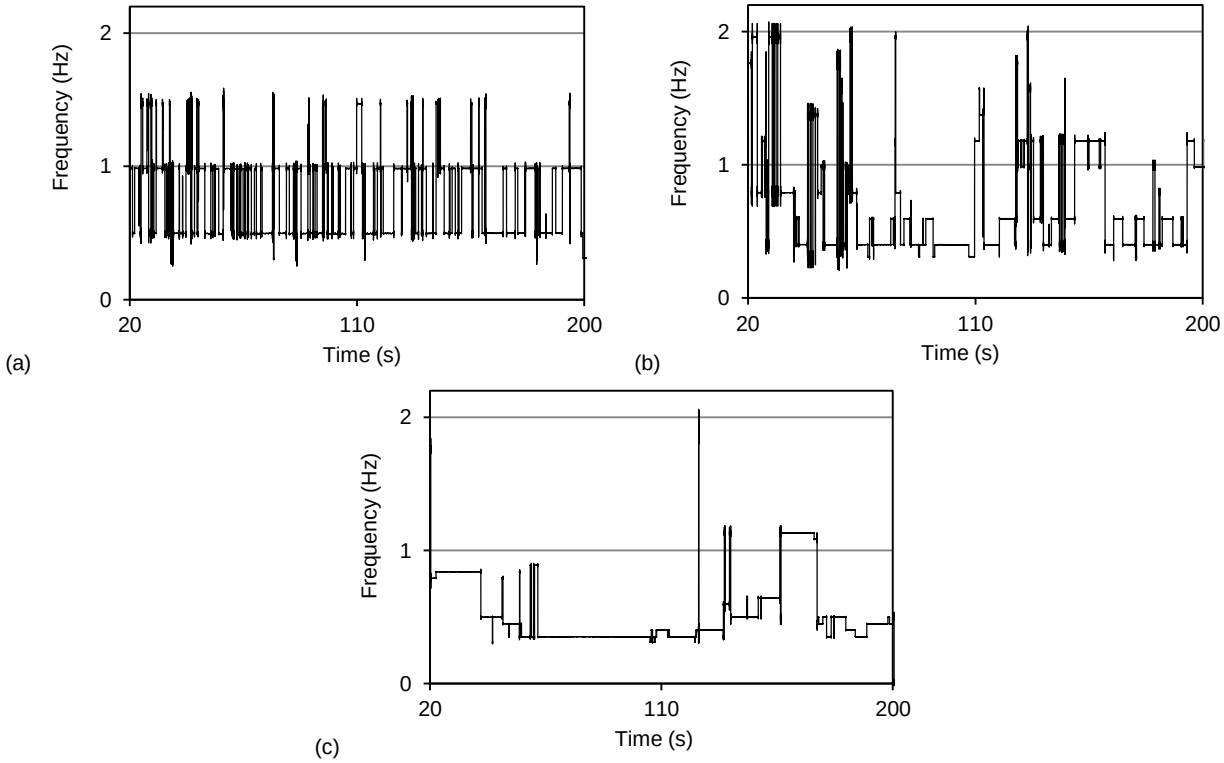


Figure 7.17 Dominant frequency of SAN_R using: (a) Window 1; (b) Window 2; (c) Window 3

(2) *Comparison between LQRSG and LQR*

The result using LQRSG with Window 2 was used to compare with that using LQR control. The problem of LQR control is that it was difficult to select the optimal gain. Using a non-optimal gain for LQR control, the acceleration under short-period motions and the displacement under long-period motions were significantly increased compared to when using the optimal gain.

The LQRSG method was effective when dealing with different types of earthquake excitations having different frequency characteristics. While the accelerations under short-period motions were effectively mitigated, the displacements under long-period motions were also reduced. With non-optimal gains for LQR control, the accelerations under short-period motion and displacements under long-period motion were increased by 55% to 250%, and 10% to 30%, respectively,

compared with the values using LQRSG (Table 7.7). Direct evidence of the advantage of using LQRSG came from the response under JMASAN_R, which had both low and high frequency content dominated at 0.35 Hz and 1.4 Hz. The LQRSG method was able to automatically adjust the control strategy based on the frequency change of the input motion. Since the weighting parameter on reducing the acceleration was lessened during low-frequency dominated portions of the motion, the LQRSG method was also effective in reducing the displacement. By comparison, the acceleration using LQR control with Gain 2 and the displacement using LQR control with Gain 1, were increased by 82% and 20% of those with the LQRSG method, respectively.

The result under ELC was relatively higher than that in the traditional LQR control (0.69 m/s$^2$ 0.43 m/s$^2$). Such difference may be caused by the frequency characteristic of the ELC motion, which is more distributed than other motions (see Figure 7.6).

When compared with the result of LQR control using the optimal gain, the $J_1$ index of the LQRSG method was smaller except for JMA_R and SAN_R (5% and 9% higher than that with LQR control, because of the data deviation in estimating Equation (6.26) from the simulation). This shows the effectiveness of LQRSG in searching for the optimal control gain based on the dominant frequency.

### 7.5.2 Furniture responses

The responses of the furniture with unlocked casters are shown in Table 7.8. The results with Windows 2 and 3 are compared graphically in Figure 7.18 with the traditional LQR control using both Gain 3 and the optimal gain.

The furniture responses with Windows 2 and 3 were slightly smaller than those with Windows 1. Figure 7.18 shows that furniture responses with LQRSG using Windows 2 and 3 did not vary much, mainly because the floor accelerations were similar and sufficiently small. Generally, the furniture responses including the acceleration, displacement and velocity under long-period motions were larger than those under the short-period motions.

The furniture responses with LQRSG control resulted in similar responses, with the traditional LQR control using optimal gain; but were much smaller than the results obtained with LQR control using Gain 3 for SAN, SAN_R and CHI motions.

Table 7.7 Responses of the caster unlocked furniture on floor isolation system with LQRSG

| Input motions | $J_4$ (m/s$^2$) | $J_5$ (mm) | $J_6$ (m/s) | $J_4$ (m/s$^2$) | $J_5$ (mm) | $J_6$ (m/s) |
|---|---|---|---|---|---|---|
| | Window 1 | | | | | |
| JMA_R | **0.66** | **68** | **0.18** | | | |
| SAN_R | 1.37 | 476 | 0.56 | | | |
| | Window 2 | | | Window 3 | | |
| JMA | 0.45 | 10 | 0.05 | 0.49 | 17 | 0.11 |
| JMA_R | 0.51 | 33 | 0.11 | 0.61 | 36 | 0.13 |
| SAN | **1.13** | **473** | **0.30** | 1.12 | 438 | 0.30 |

| | | | | | | |
|---|---|---|---|---|---|---|
| SAN_R | **1.07** | **361** | **0.33** | **1.10** | 413 | 0.39 |
| CHI | **0.88** | 277 | 0.30 | **0.83** | 308 | 0.34 |
| ELC | **0.60** | **134** | **0.20** | 0.55 | 105 | 0.19 |
| YOK_R | 0.56 | 17 | 0.06 | **0.59** | **25** | **0.08** |
| ELC_R | 0.57 | 31 | 0.09 | **0.48** | **27** | **0.07** |
| JMASAN_R | **1.08** | 229 | 0.24 | **0.98** | 450 | 0.34 |

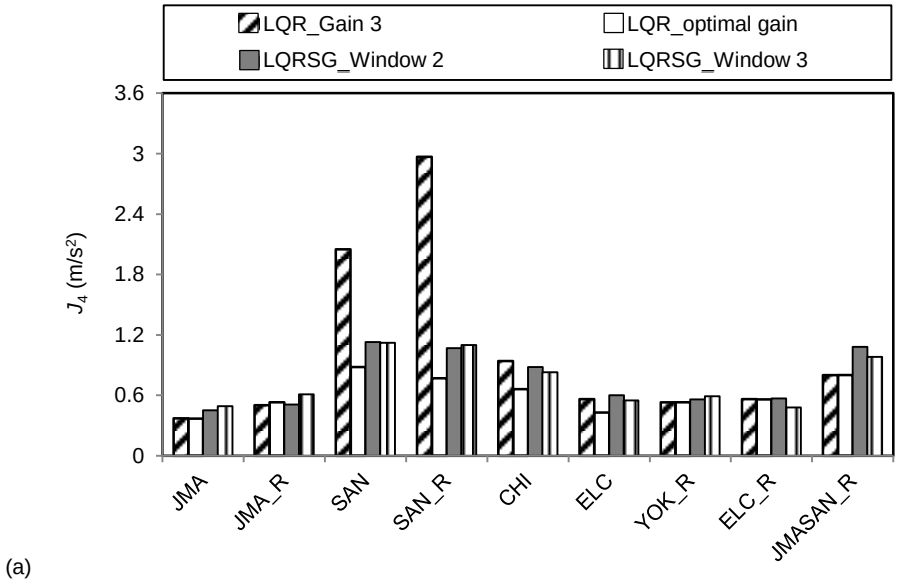


(a)

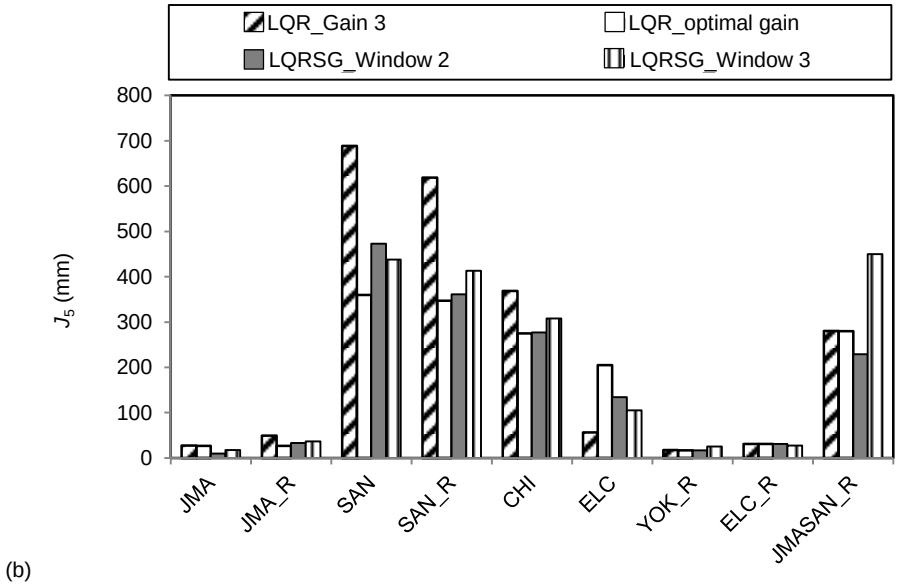


(b)

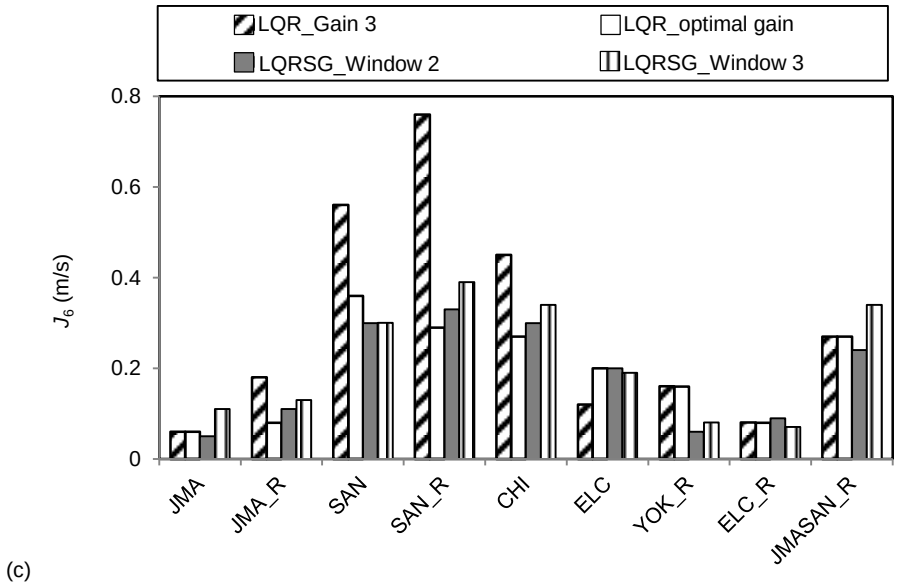


(c)

Figure 7.18 Responses of caster unlocked furniture for floor isolation system with LQR control and LQRSG control: (a) acceleration $J_4$; (b) displacement $J_5$; (c) velocity $J_6$

## 7.6 Floor isolation system with $H_\infty$ control

Because the $H_\infty$ control designed in this study is particularly for the floor isolation system installed in the structure, as shown in Chapter 5, the recorded roof responses, JMA_R, SAN_R, YOK_R and ELC_R from the structure [7.1] were used. In addition, ELC motion was also adopted in the attempt to compare the control on floor motion and ground motion.

### 7.6.1 Floor responses

The floor responses with $H_\infty$ control are shown in Table 7.8. The results are also graphically shown in Figure 7.19. LQRSG control using Window 2 is included in the figure for comparison.

Table 7.8 Responses of floor isolation system with $H_\infty$ control

| | $J_1$ (m/s$^2$) | $J_2$ (m/s$^2$) | $J_3$ (mm) | $J_1$ (m/s$^2$) | $J_2$ (m/s$^2$) | $J_3$ (mm) |
|---|---|---|---|---|---|---|
| | $H_\infty$, $\omega_f = \omega_p$[(a)], $\chi = 0.3$ | | | $H_\infty$, $\omega_f = \omega_p$, $\chi = 0.4$ | | |
| JMA_R | 0.87 | 0.15 | 124 | 1.13 | 0.17 | 122 |
| YOK_R | 0.57 | 0.14 | 108 | 0.55 | 0.13 | 92 |
| SAN_R | 0.66 | 0.20 | 196 | 0.66 | 0.22 | 136 |
| ELC_R | 0.71 | 0.20 | 89 | 0.82 | 0.22 | 88 |
| ELC | 0.43 | 0.10 | 109 | 0.52 | 0.11 | 82 |
| | $H_\infty$, $\omega_f$ = 13.2 (2.1 Hz), $\chi = 0.3$ | | | $H_\infty$, $\omega_f$ = 13.2 (2.1 Hz), $\chi = 0.4$ | | |
| JMA_R | 1.10 | 0.18 | 130 | 1.50 | 0.23 | 125 |
| | $H_\infty$, without filter $W_1$ | | | | | |

| | | | |
|---|---|---|---|
| JMA_R | 2.07 | 0.36 | 134 |
| YOK_R | 1.23 | 0.38 | 140 |
| SAN_R | 1.22 | 0.38 | 67 |

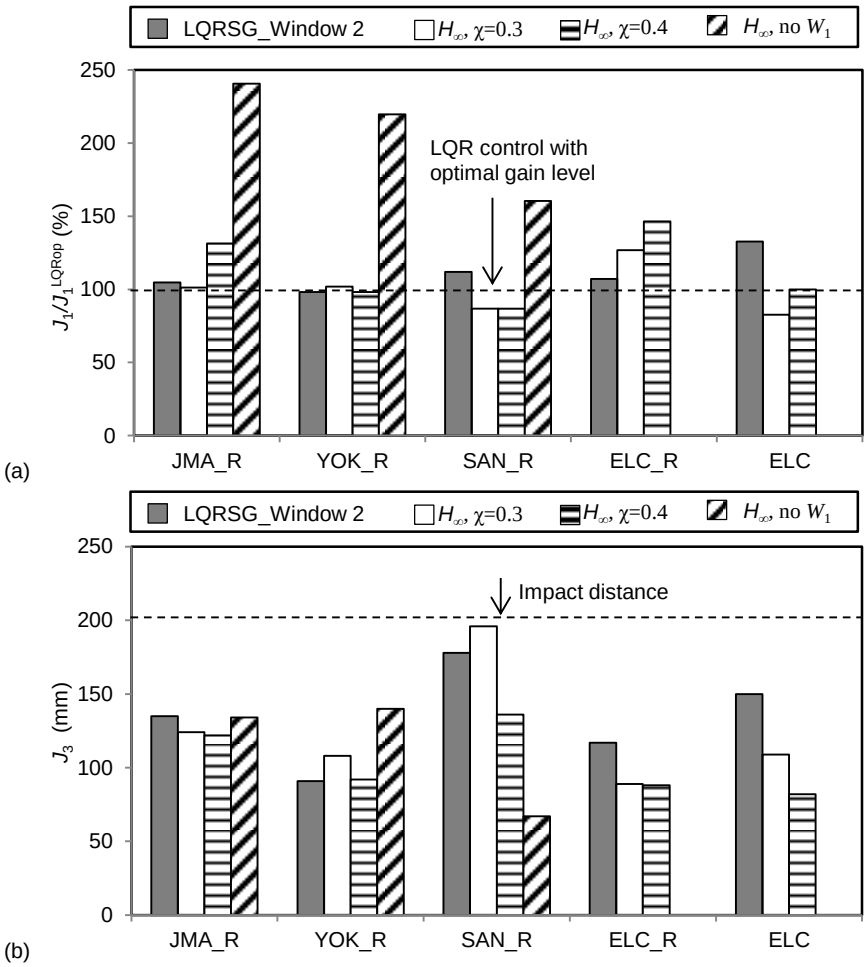


Figure 7.19 Floor responses of floor isolation system with $H_\infty$ and LQRSG controls: (a) normalized acceleration $J_1$; (b) displacement $J_3$

With the control target for the floor isolation system discussed in Chapter 6, the parameters $\chi$ and $\alpha$ in filter $W_1$ and $W_2$ were tuned to 0.3 and 0.98, respectively. To examine the effect of different $\chi$ values for input filter $W_1$ on balancing the reduction of acceleration and displacement, a $\chi$ value of 0.4 was also used.

When both the two filters $W_1$ and $W_2$ were adopted and the parameter $\omega_f$ was assigned as $\omega_p$, the $H_\infty$ control could effectively reduce the acceleration and displacement. Using $\chi$ = 0.3, the acceleration was reduced to 8% of the input for the short-period motions JMA_R and ELC_R, and 24% for the long-period motion SAN_R. The control was more effective on reducing acceleration at $\chi$ = 0.3 than at $\chi$ = 0.4 for the short-period motions JMA_R and ELC_R, as shown in Table 7.9 and Figure 7.19. This was primarily because the input filter $W_1$ at $\chi$ = 0.3 had a relatively lower PSD in the low frequency band, and a relatively higher PSD in the frequency band close to the predominant frequency of the structure. This is also the reason to the lower efficiency in reducing the displacement for the long-period motion SAN_R at lower $\chi$ values.

The input filter $W_1$ for the $H_\infty$ control was important for controlling the floor response. Without filter $W_1$, $H_\infty$ control was effective in reducing acceleration for the long-period SAN_R motion, but was ineffective for the short-period JMA_R motion. This was attributed to more focus given to controlling low frequency (long-period) components in the input motion. In this condition, the $H_\infty$ control aimed to reduce the response of the input motions with frequencies close to the natural frequency of the floor isolation. The long-period motion SAN_R dominated at 0.35 Hz and was close to the 0.33 Hz natural frequency of the floor isolation system. Therefore, the performance of the floor isolation under the long-period was better than the performance using the filter $W_1$.

However, compared to using $H_\infty$ control with the input filter $W_1$ ($\chi$ = 0.3), when the short-period motion JMA_R excited the floor isolation, the acceleration and displacement increased respectively by 135% and 37%. Figure 7.20 shows the displacement versus MR damper force relationships under JMA_R motion for the cases with and without the input filter $W_1$. This figure indicates that the control force of MR damper with $W_1$ was significantly smaller than when $W_1$ was not used. Without informing the controller of the input motion characteristics, control of the short-period motion tended to use larger forces in controlling the floor isolation response.

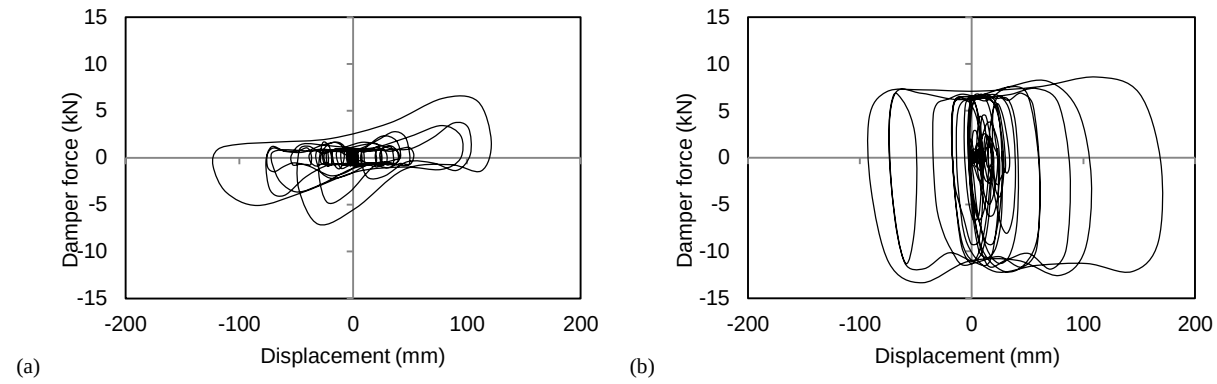


Figure 7.20 Displacement-damper force relationships under JMA_R: (a) with $W_1$; (b) without $W_1$

Compared with LQRSG control, $H_\infty$ control could result in similar responses as shown in Figure 7.19. However, $H_\infty$ control needed a good estimation of the predominant frequency of the structure so as to design the input motion filter $W_1$.

Figure 7.21 shows a comparison of the normalized maximum floor acceleration by the maximum input acceleration for different testing conditions. Two different $\omega_f$ values were assigned to filter $W_1$ under JMA_R motion. One of the $\omega_f$ values was the same as the predominant frequency of the structure $\omega_p$ (8.8 rad/s), and the other one was 13.2 rad/s. The comparison shows that when $\omega_f$ was adopted as $\omega_p$, $H_\infty$ control was more effective than when $\omega_f$ was adopted as the higher value.

Comparing the results between the input motion ELC (ground motion) and ELC_R (roof motion) shows that the designed $H_\infty$ control was more effective for ELC_R motion in terms of the normalized acceleration. The ratio between the floor acceleration and input motion were 22% and 8% for ELC and ELC_R respectively. The differences were attributed to the different input motion characteristics. Motion ELC_R was dominated at the frequency that was close to the predominant frequency of the structure. When the $H_\infty$ control was designed to have $\omega_f = \omega_p$, the filter $W_1$

correctly captured the frequency characteristics of the input motion, and $H_\infty$ control effectively reduced the floor response. However, the frequency of motion ELC was distributed over a wider frequency band and was not able to be captured by the input shaping filter. Therefore, when the $H_\infty$ control was used for the two motions, it was more effective for the ELC_R motion. This shows the effectiveness of using $H_\infty$ control for the floor isolation.

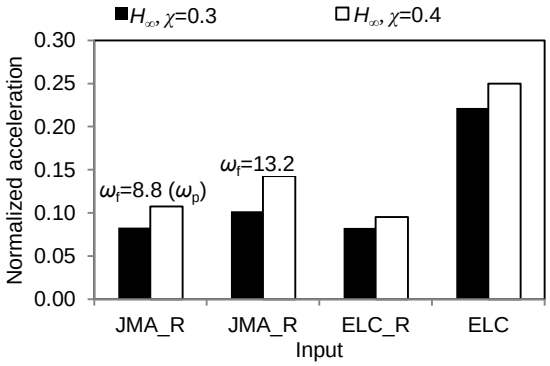


Figure 7.21 Normalized acceleration by input with $H_\infty$ control

### 7.6.2 Furniture responses

The responses of the furniture with unlocked casters using $H_\infty$ control are shown in Table 7.9 and graphically compared in Figure 7.22 with the LQRSG control using Windows 2 and 3.

The furniture responses with LQRSG control were smaller in most of cases. Nevertheless, the differences among the furniture behaviors with different control strategies (LQRSG and $H_\infty$) were not significant. All of them could protect the furniture from excessive responses as observed in the traditional LQR control with non-optimal gains, which caused impact between the isolation system and the stopper. It is notable that an incorrect $\omega_f$ for $H_\infty$ control increased the furniture behavior, as indicated by the results of JMA_R.

Table 7.9 Response of caster unlocked furniture with $H_\infty$ control

| | $J_4$ (m/s$^2$) | $J_5$ (mm) | $J_6$ (m/s) | $J_4$ (m/s$^2$) | $J_5$ (mm) | $J_6$ (m/s) |
|---|---|---|---|---|---|---|
| | $H_\infty$, $\omega_f = \omega_p$[(a)], $\chi$ = 0.3 | | | $H_\infty$, $\omega_f = \omega_p$, $\chi$ = 0.4 | | |
| JMA_R | 0.58 | 65 | 0.14 | 0.60 | 35 | 0.09 |
| YOK_R | 0.52 | 22 | 0.05 | 0.43 | 24 | 0.13 |
| SAN_R | 1.13 | 588 | 0.34 | 1.09 | 471 | 0.28 |
| ELC_R | 0.51 | 67 | 0.17 | 0.55 | 84 | 0.21 |
| ELC | 0.39 | 163 | 0.20 | 0.40 | 176 | 0.26 |
| | $H_\infty$, $\omega_f$ = 13.2 (2.1 Hz), $\chi$ = 0.3 | | | $H_\infty$, $\omega_f$ = 13.2 (2.1 Hz), $\chi$ = 0.4 | | |
| JMA_R | 0.96 | 98 | 0.20 | 0.89 | 123 | 0.24 |
| | $H_\infty$, without filter $W_1$ | | | | | |
| JMA_R | 0.61 | 90 | 0.27 | | | |
| YOK_R | 0.68 | 61 | 0.15 | | | |

| | | | |
|---|---|---|---|
| SAN_R | 1.18 | 468 | 0.47 |

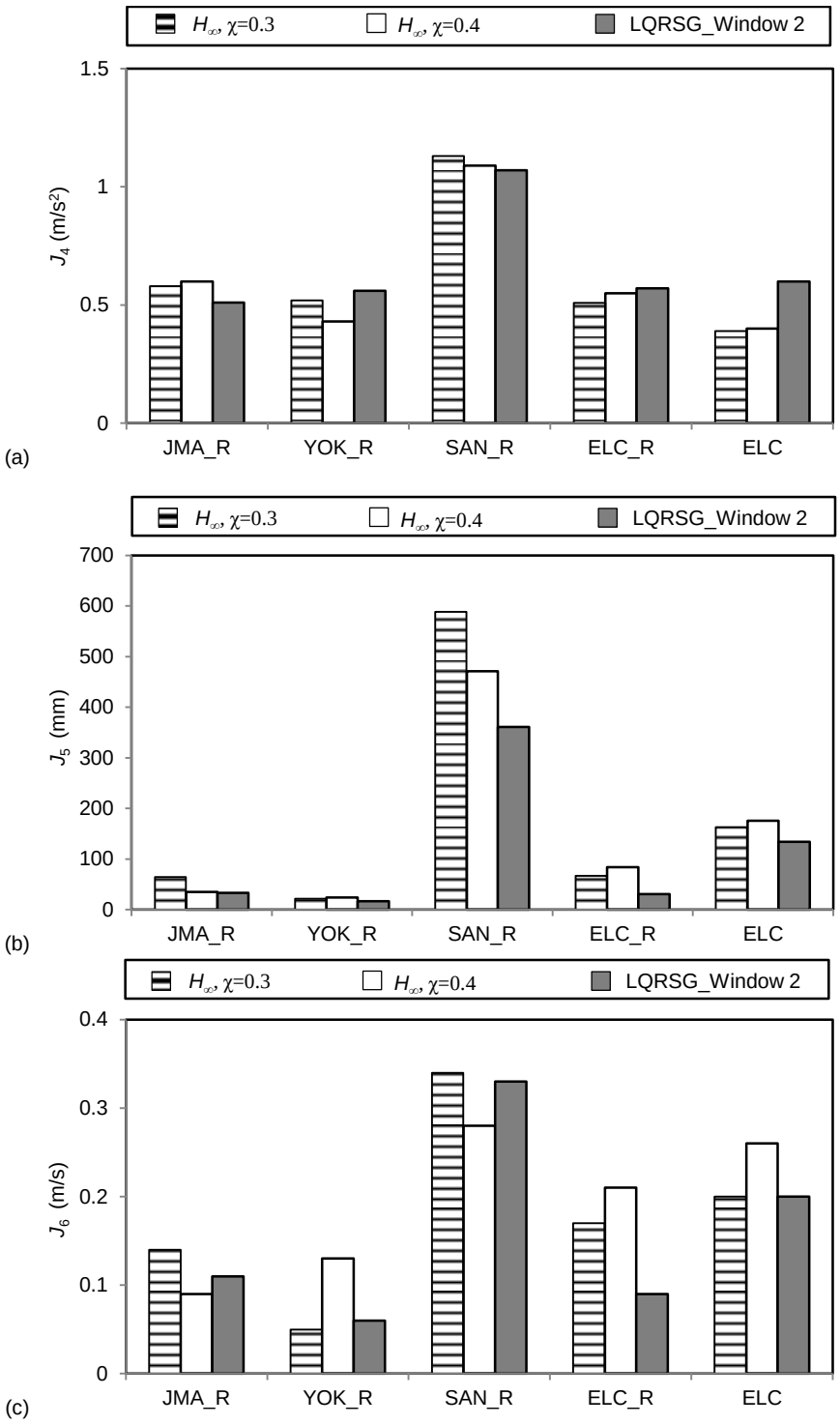


Figure 7.22 Responses of caster unlocked furniture for floor isolation system with $H_\infty$ control and LQRSG control: (a) acceleration $J_4$; (b) displacement $J_5$; (c) velocity $J_6$

## 7.7 Performance of PI controller

Because the MR damper is a nonlinear device, the transfer function from the input current to output force is not unique. The development of PI controller utilized a transfer function of MR damper

with the moving velocity of 0.04 m/s. To check the performance of the PI controller working at a much larger velocity is necessary. Figure 7.23 shows the velocity, designed force ($F_{des}$) and actual measured force ($F_{mea}$) in the LQR control with scheduled gain, under both JMA_R and SAN_R motions. Window 2 was adopted for determination of control gain in those example cases.

The maximum velocities were 1.1 m/s for JMA_R and 0.48 m/s for Sannomaru_R motions. The results show that the actual force matched the designed force with a good accuracy. The errors were 127 N and 76 N for the two cases, corresponding to their peak designed force of 4947 N and 6043 N, respectively. It is worth to note that disparity between the designed force and actual measured force existed in the bands of about ±700 N for JMA_R and ±1000 N for SAN_R. This is because designed force was closed to 0 when the responses were small and it was not practical to realize it due to the lower capacity of the MR damper, i.e., the force of MR damper when the current was 0.

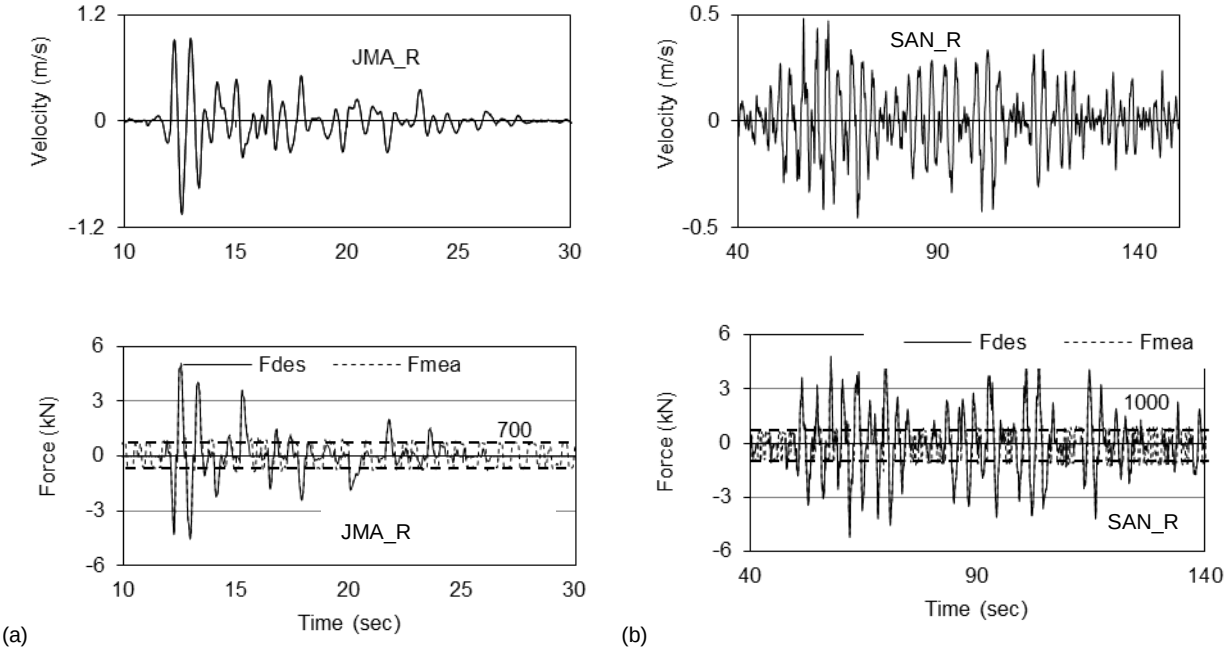


Figure 7.23 Velocity and force under: (a) JMA_R; and (b) SAN_R

## 7.8 Summary

A series of shaking table tests were conducted to validate the performance of the floor isolation system using semi-active control and passive control. Furniture was placed on top of the floor isolation to examine its behavior with different control methods. Major findings from the test can be summarized as follows:

(1) The passive controlled system could not accommodate the load change problem. The acceleration and displacement responses of the floor varied significantly for different load systems (different damping ratios). Also the furniture responses varied due to the different floor responses. It was difficult to adjust the damping level so that the passive controlled system could work effectively under both short-period and long-period motions.

(2) The selection of control gain in traditional LQR control is important. Compared with using an optimal gain, using a non-optimal gain resulted in more than two times the acceleration for the short-period input motions JMA, JMA_R, and YOK_R, and 20% larger displacement for the long-period motions CHI, SAN, and SAN_R. The non-optimal control gain also caused larger furniture acceleration, velocity and displacement, which could be more than 2 times.

Compared with passive control using a medium damping ratio (38%), the traditional LQR control with the optimal control gain could more effectively reduce the acceleration response of the floor isolation system by 35% to 90%, while not causing significant larger displacement. Smaller floor responses resulted in smaller (40% to 90%) acceleration of the furniture with locked caster. Also the traditional LQR control with the optimal control gain was more effective in reducing the acceleration, velocity and displacement of the furniture with unlocked casters by about 50%.

(3) For the LQRSG control, the length of the time window used to detect the dominant frequency of the input motion affects the performance of the control method. Test results show that the window length should be selected so that the resolution frequency is lower than 1) the lowest dominant input frequency expected in the system and 2) the natural frequency of the system. Using longer windows which allow for even finer resolution reduces the error in detecting the dominant input frequency and benefits displacement control under long-period motions but is not as quick to capture changes in frequency content, which decreases acceleration reduction benefits for short-period motions.

The LQRSG method was significantly more effective than LQR control over a range of short- and long-period motions, since it could update the control gain automatically using the window method without knowing the motion *a priori*. LQRSG method matched or further improved upon the performance of LQR control with optimal gain for both short- and long-period motions. The LQRSG method consistently reduced accelerations compared to passive control under both short- and long-period motions, while maintaining similar displacements.

The responses of the furniture with LQRSG were similar with those from the system with traditional LQR control using optimal gain.

(4) The $H_\infty$ control in the frequency domain need a good estimation of the predominant frequency the structure in which the floor isolation is installed so as to select the parameters for the input shaping filter. If this information was available, the $H_\infty$ resulted in the floor and furniture responses that were close to those from LQRSG.

Generally, it was difficult to control the displacement movement of the furniture with unlocked condition effectively without direct controlling of the furniture system. The results with different control methods including passive control, and semi-active control with LQR, $H_\infty$, and LQRSG algorithms show that locking the caster was an effective way to reduce the displacement and velocity of furniture without increasing its acceleration.

# CHAPTER 8

## Summaries and conclusions

A number of innovative control technologies have been developed to achieve enhanced functionality and operability of the structure. Those technologies include passive control, active control, hybrid control and semi-active control. Base isolation, a type of passive control system, is one of the most successful and widely-applied techniques. Base isolation can protect both the structure and non-structural elements and contents so as to maintain the functionality of the structure during and immediately after the earthquake. In Japan, there are over 2,500 base-isolated buildings at present, and the applications are extensively applied to hospitals and medical facilities, because these facilities are the first ones that need to function right after a damaging earthquake event. There are still several aspects worth investigating for the isolation system, including the behavior of both the structure and appliance inside the structure, under long-period motions. It is well known that the long-period motion is expected to cause large displacement response to the structure; however, there is little information on the appliance behavior under long-period motions. Especially, information is limited for appliances equipped with casters to promote the mobility in the daily use. Applying semi-active control to the isolation system to enhance the functionality of the system is another aspect worth investigating. Due to the complicity of control, it is still a challenging task to design a control system that can effectively deal with both the short-period and long-period ground motions.

This dissertation tries to examine the functionality of base-isolated and floor-isolated structures under both short-period and long-period motions. A series of full scale shaking table tests were conducted on a base-isolated hospital building, in which hundreds of non-structural elements, contents including furniture and medical appliance with different locking conditions were installed. Performance of the structure and the contents was observed and evaluated based on the test results. A more flexible solution to protect a group of appliance, i.e., a floor isolation system, was designed and studied. Semi-active control was applied to the floor isolation to improve the performance of structure and appliances under both short-period and long-period motions.

This dissertation consists of eight chapters. Chapter 1 is the background of this study, and Chapter 8 is the summary and conclusions. Chapters 2 to 7 constitute the main part of the dissertation. The respective focuses of those chapters are: (1) a literature review of the study focusing on the enhancement of functionality and operability of structures; (2) development of motion capture technique to trace the appliance behavior in the shaking table test; (3) the E-Defense full scale

shaking table test on base-isolated and fixed-base hospital conducted to study the behavior of structure and non-structural elements as well as the contents inside of the room; (4) development of control strategies for a semi-active controlled floor isolation system; and (5) shaking table test to evaluate the performance of the floor isolation system to protect the equipment. The contents of the six chapters are summarized as follows.

**Review of previous research**

Chapter 2 reviews the techniques to improve the structural functionality and the semi-active control for structure. The major contents are summarized as follows:

(1) The passive base isolation system can significantly reduce the acceleration response of the structure and improve the functionality of the building. However, the displacement response under long-period motions is large. Simply adding damping to the system will decrease the displacement but at the expense of increased acceleration. Active and semi-active base isolation systems have the potential to overcome the problem in passive isolation system under long-period motion. The effectiveness of the control design will depend on the device and control algorithms.

(2) Floor isolation system is an alternative to base isolation. It is necessary to reduce the acceleration to protect the appliance as well as to limit the displacement in order to maximize the usable floor isolation area. Different from the base isolation, the input motion to the floor isolation that is installed on a higher floor, is normally amplified from the ground motion, and filtered by the structure.

(3) In both the base isolation and floor isolation systems, there is little information from the past research on the behavior of appliance equipped with casters to enhance the mobility, under different types of earthquakes with different frequency characteristics.

(4) Different control algorithms, including LQR and $H_\infty$ have been reviewed. LQR cannot account for the frequency characteristic of the input motion. To extend its application, modification is needed. The $H_\infty$ consider the frequency characteristics of the input motion by implementing a shape filter to the controller in the frequency domain.

(5) A model to describe the MR damper behavior is necessary. Three different models, Bingham model, Bouc-Wen model and modified Bouc-Wen model are reviewed. The Bingham model is not able to describe the hysteretic behavior of the MR damper. Bouc-Wen mode can reasonably describe the MR damper behavior with less number of parameters than the modified Bouc-Wen model, although the latter one has higher accuracy. Force tracking system is needed to calculate the control signal to MR damper. The on-off type clipped optimal controller is widely used for MR damper, but the abrupt switch law has the potential to cause large response to the structure.

**Motion capture technique for measurement of furniture behavior**

The traditional displacement transducer has difficulties in measuring the movement with large amplitude and rotation, and covering multi targets. The motion capture technique can overcome those difficulties but normally expensive industry grade cameras are needed, and the measuring range is

limited in order to improve the measuring accuracy. When the cameras are set in an environment with vibration, motion capture results will contain errors. A series of shaking table test was conducted to validate the accuracy of motion capture in measuring large amplitude (up to meters) displacement using commercial grade cameras. A simple but effective method is proposed to correct the motion capture results when error is induced due to the camera vibration. The following conclusions are drawn from Chapter 3:

(1) Both the one camera and two cameras systems have similar accuracy in measuring the 2D movement. The one camera system is handier since it can save processing time and avoid errors that would occur in synchronizing the two videos.

(2) The test shows that it is promising to use motion capture to measure the large amplitude displacement. In addition, the captured displacement can also be used to estimate the velocity of the appliance through a differentiating process of the displacement. The error in measuring the displacement using motion capture is estimated of less than 3 times of the image resolution. Motion capture technique can estimate the velocity with an error of less than 5% of the maximum velocity.

(3) When the cameras are set inside of the testing environment, they are susceptible to vibration, which is a source to promote errors. A simple method is proposed using a reference marker to calculate the relative change of the positions of the target marker and the reference marker, to obtain the actual displacement. Test results show that this method is effective.

**Full-scale shaking table test of base-isolated and fixed-base hospital**

Chapter 4 describes the evaluation of the responses of structure and medical appliance in a full scale four story RC hospital appliance through a series of shaking table test. Two different types of ground motions, i.e., short-period and long-period, were adopted in the test. The major objective of the test is to examine the performance of the base-isolate system under different types of motions, and check the behavior of appliance installed in the structure. Major findings can be summarized as follows:

For base-isolated system,

(1) The isolator exhibited stable performance in all the shakings for both the short-period and long-period motions. The cumulative displacement under the long-period and long-duration motion Sannomaru was over 46 m, which was much larger than 5 m under the short-period motion JMA Kobe. The U-shaped damper for the isolation system to dissipate energy eventually sustained 81 m without degradation in the stiffness after many rounds of shakings.

Under the short-period motion JMA Kobe, the acceleration and velocity responses of each floor, were reduced from the shaking table with the factor of 0.2 to 0.4 for acceleration, and 0.5 to 0.8 for velocity. The story drift ratio was much smaller than 0.1%. Under long-period motion Sannomaru, the acceleration and velocity were amplified from the shaking table to each floor by 1.2 and 2 times, respectively. The story drift ratio was also much smaller than 0.1%.

(2) The performance of medical appliances with locked and unlocked conditions under the near-fault ground motion was promising. However, under the long-period motion, the base-isolated structure was not necessarily invincible in terms of the behavior of the appliances which were mobile.

The displacement of the appliances with unlocked conditions was more than 3 meters while the velocity was up to 2 m/s.

(3) The wild movement of the appliances with unlocked condition under the long-period motion caused a series of problems including tearing the electric plugs for the appliances, serious collisions between appliances which caused uplifting, rocking of appliances, breakage of wall, and large acceleration which would cause malfunction of appliances. Such behaviors would significantly disorder the activity of the hospital and influence its functionality during and immediately after an earthquake.

(4) By fully or partially locking the casters of the appliances in the base-isolated structure, the displacement and velocity were significantly reduced (to only one-quarter) from those with unlocked condition.

For fixed-base system,

(5) Under the short-period motion JMA Kobe, the amplification factors of acceleration and velocity from the shaking table to the roof were 2.25 and 1.75, which were 6 and 2.5 times of those in base-isolated system. The maximum story drift ratio of the first floor reached to 0.45%, which was 8 times of that in base-isolated system. Under long-period motion, the amplification factors were about 1.7 and 1.2 for acceleration and velocity.

(6) Under the short-period motion, the accelerations of the appliances in fixed-base structure were about 3~20 times of those in the isolation system. This is attributed to the significantly larger acceleration of floor isolation compared with in the base-isolated system (by a factor of 13). The free standing appliances with locked casters were excited to move about 500 mm. Under long-period motion, the acceleration and displacement responses of the appliances were similar of those in the base-isolated system.

(7) In the fixed-base structure test, the behavior of the mobile appliances was better than in the base-isolated structure under the long-period ground motion. However, the large floor acceleration in fixed-base structure under the near-fault ground motion caused significantly larger velocity (three times) and acceleration (twelve times) of the appliances than in the base-isolated structure, which would threat the safety of the appliances and human's life. There was no effective way by changing the locking condition of the appliances to improve the performance of the appliances.

Estimation of appliance's response,

(8) For unlocked appliances, the relative displacement and velocity were close to the absolute displacement and velocity of the floor except for the case when the base-isolated structure was subjected to the long-period ground motion. In that case, the displacement and velocity were somewhat amplified. The level of amplification can be roughly estimated using the equivalent natural period of unlocked appliances.

**Development of semi-active controlled floor isolation system**

In Chapter 5, a unidirectional prototype floor isolation system with semi-active control is proposed to protect a group of important and expensive appliances. The floor isolation system should minimize

the acceleration to protect equipment; however, displacement must also be limited to save floor space, especially with long-period motion. Major findings can be summarized as follows:

(1) The designed floor isolation system contains a rolling pendulum to ensure the flexibility, and a MR damper to supply the semi-active control force. The natural period of the system is 3 s, and the friction coefficient on the pendulum rolling surface is 0.01.

(2) The designed floor isolation is installed on the top floor of a five story RC building. When the ground motion is transferred through the structure to the input motion of the floor isolation, the structure significantly filters out frequency components in the ground motion higher than the predominant frequency of the structure, mainly leaving frequency components that are close to or lower than the predominant frequency of the structure.

(3) A series of dynamic loading tests were performed to evaluate the properties of the MR damper. The MR damper is essentially a nonlinear device. The force of the MR damper is a function of the input current and velocity. A Bouc-Wen model was adopted to describe the MR damper behavior. Comparison with dynamic loading test results shows that the Bouc-Wen model can accurately match the test results, and reasonably describes the hysteretic behavior at small velocity zone.

(4) A PI controller is designed to calculate the current to the MR damper based on the designed force using the transfer function of the MR damper operating at velocity of 40 mm/s. Test results show that the proposed PI controller could effectively track the target force with frequency lower than 3 Hz. The maximum error was under 15% of the target force to track.

**Control strategies for floor isolation system**

Different control strategies are designed, including passive control with oil damper, and semi-active control using LQR, and $H_\infty$ control algorithms. A new control method named LQR control with schedule gain (LQRSG) is proposed based on the traditional LQR control. The traditional LQR control designs a constant control gain and cannot account for the characteristics of the input motion. The $H_\infty$ control implements additional filter to deal with the input motion characteristics. On the other hand, the proposed LQRSG method aims at explicitly considering the influence of the input motion features to the control gain design in the time domain. Major findings and results can be summarized as follows:

(1) In order to validate the influence of load change on the floor to the performance of floor isolation system, a passive controlled system with three different weight values (by varying the steel plates on the floor) are designed. The resulted damping coefficients for the three systems with passive control are 0.68, 0.38 and 0.29.

(2) The traditional LQR control designs the control gain based on three selected weighting parameters, $\alpha$, $\beta$ and $\gamma$, representing the importance of minimizing floor acceleration, floor displacement and damper control force, respectively. It assumes that the input excitation is a Gaussian white noise process. Therefore, it does not consider the characteristics of the excitation. A linear relationship was found through simulation between the dominant frequency of the input motion and the log of the optimal weighting parameter $\alpha$. Base on this relationship, an LQRSG

method was proposed which updates the control gain based on the dominant frequency of the input motion detected in real time. The LQRSG method enables the semi-active control to account the input motion characteristic in the time domain.

(3) A window method is proposed to monitor the dominant frequency of the excitation in "real time". It detects the acceleration data of the excitation in a time window and analyzes the dominant frequency using a FFT method. Consequently, the control gain is updated based on the dominant frequency of the input motion, without knowing any information of the input motion *a priori*.

(4) A second order input shaping filter is designed to account for the input motion characteristic for the $H_\infty$ control in the frequency domain. The input shaping filter covers two critical frequency components of the input motion that are close to the predominant frequency of the structure and to the natural frequency of the floor isolation. Transfer function analysis shows that with the newly designed shaping filter for the input motion, the $H_\infty$ control result in similar acceleration and displacement at frequencies close to the predominant frequency of the structure with the passive control using viscous damping ratio of 0, while the acceleration and displacement around the natural frequency of the floor isolation is close to or lower than the passive control using a viscous damping ratio of 0.4.

**Shaking table test for floor isolation system**

A series of shaking table tests were conducted to validate the performance of the floor isolation system using semi-active control and passive control. Furniture was placed on top of the floor isolation to examine its behavior with different control methods. Major findings from the test can be summarized as follows:

(1) The passive controlled system could not accommodate the load change problem. The acceleration and displacement responses of the floor varied significantly for different load systems (different damping ratios). Also the furniture responses varied due to the different floor responses. It was difficult to adjust the damping level so that the passive controlled system could work effectively under both short-period and long-period motions.

(2) The selection of control gain in traditional LQR control is important. Compared with using an optimal gain, using a non-optimal gain resulted in more than two times the acceleration for the short-period input motions JMA, JMA_R, and YOK_R, and 20% larger displacement for the long-period motions CHI, SAN, and SAN_R. The non-optimal control gain also caused larger furniture acceleration, velocity and displacement, which could be more than 2 times.

Compared with passive control using a medium damping ratio (38%), the traditional LQR control with the optimal control gain could more effectively reduce the acceleration response of the floor isolation system by 35% to 90%, while not causing significant larger displacement. Smaller floor responses resulted in smaller (40% to 90%) acceleration of the furniture with locked caster. Also the traditional LQR control with the optimal control gain was more effective in reducing the acceleration, velocity and displacement of the furniture with unlocked casters by about 50%.

(3) For the LQRSG control, the length of the time window used to detect the dominant frequency

of the input motion affects the performance of the control method. Test results show that the window length should be selected so that the resolution frequency is lower than 1) the lowest dominant input frequency expected in the system and 2) the natural frequency of the system. Using longer windows which allow for even finer resolution reduces the error in detecting the dominant input frequency and benefits displacement control under long-period motions but is not as quick to capture changes in frequency content, which decreases acceleration reduction benefits for short-period motions.

The LQRSG method was significantly more effective than LQR control over a range of short- and long-period motions, since it could update the control gain automatically using the window method without knowing the motion *a priori*. LQRSG method matched or further improved upon the performance of LQR control with optimal gain for both short- and long-period motions. The LQRSG method consistently reduced accelerations compared to passive control under both short- and long-period motions, while maintaining similar displacements.

The responses of the furniture with LQRSG were similar with those from the system with traditional LQR control using optimal gain.

(4) The $H_\infty$ control in the frequency domain need a good estimation of the predominant frequency the structure in which the floor isolation is installed so as to select the parameters for the input shaping filter. If this information was available, the $H_\infty$ resulted in the floor and furniture responses that were close to those from LQRSG.

(5) Generally, it was difficult to control the displacement movement of the furniture with unlocked condition effectively without direct controlling of the furniture system. The results with different control methods including passive control, and semi-active control with LQR, $H_\infty$, and LQRSG algorithms show that locking the caster was an effective way to reduce the displacement and velocity of furniture without increasing its acceleration.

# Acknowledgement

I would like to first thank my advisor, Professor Masayoshi Nakashima, for his support, advice, and encouragement throughout my PhD in Kyoto University. His profound knowledge and enthusiastic working attitude inspired me to go through my PhD research. It is a great honor to work with him and I would keep those things I have learned in mind and take as my guideline for my future. The valuable things I have learned are not only the professional knowledge, but also the way to do a research through creative thinking, hardworking and try-to-be-perfect attitude.

Great thanks go to Professor Izuru Takewaki and Professor Hiroshi Kawase for their kindness to be the members of the dissertation committee, reading this dissertation and offering constructive comments.

I would like to thank Dr. Eiji Sato, a senior researcher of National Research Institute for Earth Science and Disaster Prevention (NIED, Japan), for sharing his experience in the field of control theory, the implementation of the control test, and for his inspiring discussions over the years.

Special thanks go to Professor Satish Nagarajaiah in Rice University (U.S). He has offered me a chance to work with him and provided many appreciated advices on the control theory during my visit to Rice University in April and May, 2012.

Also, special thanks go to Professor Yiyi Chen in Tongji University (China), my former supervisor, for his encouragement on my research over these years.

I would like to thank Dr. Masahiro Kurata, Dr. Xiaodong Ji, Dr. Dimitrios G. Lignos，Dr. Yao Cui, Dr. Sachi Furukawa, Dr. Becker Tracy, Dr. Ryuta Enokida, Dr. Yu-lin Chung, Dr. Yunzhen Tang, and Dr. Po-Chien Hsiao. We have been working in the same group in Professor Nakashima's Lab for very long time. Their suggestions to my research and help on my experiments are greatly appreciated. Also, I am grateful to Dr. Kohei Fujita, Dr. Kazuaki Hoki, Dr. Mai Ito, Dr. Kazuhiro Hayashi, Dr. Xuchuan Lin, Mr. Yunbiao Luo, Mr. Liusheng He, Mr. Xiaohua Li, Mr. Michitaka Inami, Mr. Ryusuke Enomoto, Yudai Taniguchi, Mayako Yamaguchi, for their help on my experiments. Without their help, I would not finish my experiment smoothly. Special thanks go to Mrs. Chisato Gamou and Miss Sumiko Motohashi who create a workplace where we can get support for our study and daily life.

Grateful acknowledgement is given to the Ministry of Education, Science, and Culture, Government of Japan (Monbusho) for granting me the scholarship which made this study possible.

Finally, I would like to thank my parents, brother, my wife and lovely daughters for their encouragement, support and love. This work would not have been possible without the love and support of them.

June 2013

Yundong Shi